



2809289157

REFERENCE ONLY

## UNIVERSITY OF LONDON THESIS

Degree PhD

Year 2006

Name of Author LIN TOTT

Christopher John

### COPYRIGHT

This is a thesis accepted for a Higher Degree of the University of London. It is an unpublished typescript and the copyright is held by the author. All persons consulting the thesis must read and abide by the Copyright Declaration below.

### COPYRIGHT DECLARATION

I recognise that the copyright of the above-described thesis rests with the author and that no quotation from it or information derived from it may be published without the prior written consent of the author.

### LOAN

Theses may not be lent to individuals, but the University Library may lend a copy to approved libraries within the United Kingdom, for consultation solely on the premises of those libraries. Application should be made to: The Theses Section, University of London Library, Senate House, Malet Street, London WC1E 7HU.

### REPRODUCTION

University of London theses may not be reproduced without explicit written permission from the University of London Library. Enquiries should be addressed to the Theses Section of the Library. Regulations concerning reproduction vary according to the date of acceptance of the thesis and are listed below as guidelines.

- A. Before 1962. Permission granted only upon the prior written consent of the author. (The University Library will provide addresses where possible).
- B. 1962 - 1974. In many cases the author has agreed to permit copying upon completion of a Copyright Declaration.
- C. 1975 - 1988. Most theses may be copied upon completion of a Copyright Declaration.
- D. 1989 onwards. Most theses may be copied.

*This thesis comes within category D.*

This copy has been deposited in the Library of \_\_\_\_\_ *UCL*

This copy has been deposited in the University of London Library, Senate House, Malet Street, London WC1E 7HU.



# Analyses of the early stages of star formation

Christopher John Lintott

Thesis submitted for the Degree of Doctor of Philosophy  
of the University of London

---

Department of Physics & Astronomy

UNIVERSITY COLLEGE LONDON

---

September 2006

UMI Number: U594402

All rights reserved

INFORMATION TO ALL USERS

The quality of this reproduction is dependent upon the quality of the copy submitted.

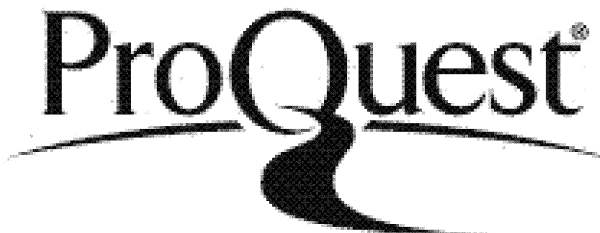
In the unlikely event that the author did not send a complete manuscript and there are missing pages, these will be noted. Also, if material had to be removed, a note will indicate the deletion.



UMI U594402

Published by ProQuest LLC 2013. Copyright in the Dissertation held by the Author.  
Microform Edition © ProQuest LLC.

All rights reserved. This work is protected against unauthorized copying under Title 17, United States Code.



ProQuest LLC  
789 East Eisenhower Parkway  
P.O. Box 1346  
Ann Arbor, MI 48106-1346

*[He] could never resist an old wine or a new idea*

Berthold Brecht

*The life of Galileo*

\*

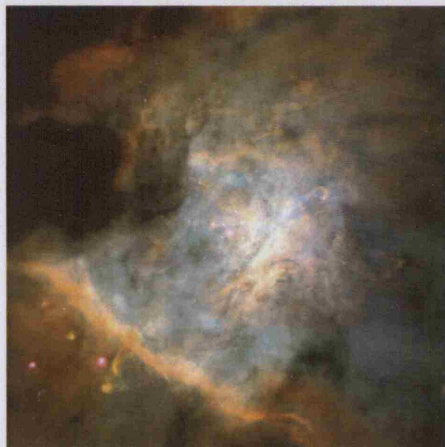
*When I heard the learned astronomer,  
When the proofs, the figures, were ranged in columns before me,  
When I was shown the charts and diagrams, to add, divide and measure them,  
When I sitting heard the astronomer where he lectured with much applause in the  
lecture-room.  
How soon unaccountable I became tired and sick,  
'Till rising and gliding out I wandered off by myself,  
In the mystical moist night-air, and from time to time,  
Looked up in perfect silence at the stars.*

Walt Whitman

\*

*I knew that even if I were second or third rate, it was astronomy that mattered.*

Edwin Hubble



From the Milky Way to high redshift: The central region of the Orion Nebula, as seen by HST; the starburst galaxy M82 in optical (HST, white) & H-alpha (WIYN, purple), which reveals the starburst-powered ‘superwind’ (Credit : Mark Westmoquette); the Hubble Ultra Deep Field reveals some of the most distant galaxies ever observed.

I, Christopher John Lintott, confirm that the work presented in this thesis is my own.  
Where information has been derived from other sources, I confirm that this has been  
indicated in the thesis.

11<sup>th</sup> September 2006

# ABSTRACT

---

This thesis presents a study of the physical and chemical properties of star forming regions, both in the Milky Way and in the distant Universe, building on the existing astrochemical models developed by the group at UCL. Observations of the nearby star-forming region, L134A, which were carried out with the James Clark Maxwell Telescope (JCMT) in Hawai'i are compared to the predictions of a model of star formation from gas rich in atomic (rather than molecular) hydrogen. A similar model is used to investigate the effect of non-equilibrium chemistry on the derivation of the cosmic-ray ionization rate, an important parameter in controlling both the chemistry and the physics of star forming clumps. A collapse faster than free-fall is proposed as an explanation for differences between the distribution of CS and N<sub>2</sub>H<sup>+</sup> in such regions. Moving beyond the Milky Way, JCMT observations of sulphur-bearing species in the nearby starburst galaxy, M82, are presented and compared with existing molecular observations of similar systems. M82 is a local analogue for star forming systems in the early Universe, many of which have star formation rates several thousand times that of the Milky Way. A model which treats the molecular gas in such systems as an assembly of ‘hot cores’ (protostellar cores which have a distinctive chemical signature) has been developed, and is used to predict the abundance of many species. An application of this model is used to explain the observed deviation in the early Universe from the otherwise tight relation between infrared and HCN luminosity via relatively recent star formation from near-primordial gas. Many of the stars formed in the early Universe must now be in massive elliptical systems, and work on the structure of these systems is presented. Data from the Sloan Digital Sky Survey is analysed to show that such galaxies have cores dominated by baryons rather than dark matter, and the dark matter profile is constrained by adiabatic contraction.

## Acknowledgments

Although it is conventional to present a thesis which represents a body of work carried out in isolation (presumably in an ivory tower, if the budget allows), the truth is that much of the work contained within is the result of collaboration and discussion with many people. My supervisors, Profs. Jonathan Rawlings and Ofer Lahav, have been both wise and tolerant, while Dr Serena Viti and Prof. David Williams have acted as supervisors in all but name. Dr Ignacio Ferreras played a valuable role in acting as the voice of extragalactic sanity for the work presented in chapter 6, and in collaborating on that in chapters 5 and 7. The thesis would have been much poorer without the opportunity for conversations with my fellow UCL students, particularly Tom Bell and Anaïs Rassat. Thanks are due to all of them, and to the other authors listed on individual papers on the next page. Funding for the research came from the Particle Physics and Astronomy Research Council.

On a more personal note, I would like to thank those who are responsible for my passion for astronomy and astrophysics. Graham Veale and Ian Walsh of Torquay Boys' Grammar School should be thanked for building a marvellous observatory and then letting me loose in it, and Stuart Clark deserves honourable mention for letting me see what research (and star formation) were all about. There are many from Cambridge who I should thank, but particular mention should be made of my director of studies, Jeremy Rawson (who will be delighted to see how much chemistry there is in the following pages), Nicky Farrer, Malcolm Longair and Sarah Bridle. Throughout this PhD, a part-time job on the BBC's 'Sky at Night' programme and other outreach activities have provided the most stimulating of distractions, and I should thank Sir Patrick Moore (who also proofread most of the text), Jane Fletcher, Robin Rees and Dr. Brian May for making this possible. Data included in chapter 5 was partially obtained while filming on location in Hawai'i. Finally, I would like to say thank you to Laura, without whom none of this would ever have happened. The mistakes remain mine, of course.

## List of published papers

Modern research waits for no man, and certainly for no thesis. The work here has already been published, therefore, in the following papers:

1. **Lintott, C. J.**; Viti, S.; Rawlings, J. M. C.; Williams, D. A.; Hartquist, T. W.; Caselli, P.; Zinchenko, I.; Myers, P., 2005, ApJ, 620, 795

*Molecular abundance ratios as a tracer of accelerated collapse in regions of high-mass star formation*

2. **Lintott, C. J.**; Viti, S.; Williams, D. A.; Rawlings, J. M. C.; Ferreras, I., 2005, MNRAS, 360, 1527

*Hot cores : probes of high-redshift galaxies?*

3. **Lintott, C.J.** & Rawlings, J.M.C., 2006, A&A, 448, 425

*Determining the cosmic ray ionization rate in dynamically evolving clouds*

4. **Lintott, C.J.**, Fererras, I. & Lahav, O., 2006, ApJ, 648

*Massive elliptical galaxies : From cores to haloes*

5. **Lintott, C.J.** & Viti, S., 2006, ApJL, 646, 37

*Rapid star formation in the presence of Active Galactic Nuclei*

# CONTENTS

---

<b>Frontispiece</b>	<b>3</b>
<b>Abstract</b>	<b>5</b>
<b>Acknowledgments</b>	<b>6</b>
<b>List of published papers</b>	<b>7</b>
<b>Table of Contents</b>	<b>8</b>
<b>List of Figures</b>	<b>12</b>
<b>List of Tables</b>	<b>14</b>
<b>1 Introduction</b>	<b>15</b>
1.1 Star Formation . . . . .	17
1.1.1 Turbulence in the ISM . . . . .	19
1.1.2 Collapse and ignition . . . . .	21
1.1.3 Bonnor-Ebert Spheres . . . . .	27
1.2 Role of dust grains . . . . .	28
1.3 Interstellar molecules and chemistry . . . . .	36
1.3.1 The role of deuterium . . . . .	39
1.3.2 Cooling in dense molecular clouds . . . . .	41
1.4 The history of star formation . . . . .	42
1.4.1 The first stars . . . . .	42
1.4.2 From population III to the present day . . . . .	46

1.5	Definition of common symbols . . . . .	50
<b>2</b>	<b>Astrochemical models : Determining the cosmic ray ionization rate</b>	<b>51</b>
2.1	Introduction . . . . .	51
2.2	Estimates of the cosmic ray ionization rate, $\zeta$ . . . . .	54
2.3	Chemical indicators of $\zeta$ in dark clouds . . . . .	61
2.4	The model . . . . .	62
2.5	Results . . . . .	64
2.5.1	Evolution with time . . . . .	64
2.5.2	Sensitivity to free parameters . . . . .	67
2.6	Discussion and conclusions . . . . .	71
<b>3</b>	<b>L134A: A young H-rich star-forming region?</b>	<b>74</b>
3.1	Introduction . . . . .	74
3.2	Observations . . . . .	76
3.3	Results . . . . .	79
3.3.1	Deriving column densities and fractional abundances . . . . .	80
3.4	Discussion . . . . .	83
3.4.1	Modelling . . . . .	87
3.5	Conclusions . . . . .	88
<b>4</b>	<b>Accelerated collapse in regions of high-mass star formation</b>	<b>92</b>
4.1	Introduction . . . . .	92
4.2	Observations . . . . .	95
4.3	Rapid collapse of cores in high-mass star forming regions . . . . .	97
4.3.1	Results . . . . .	100
4.4	Discussion and Conclusions . . . . .	102
<b>5</b>	<b>Extragalactic astrochemistry: sulphur in starbursts</b>	<b>105</b>
5.1	Introduction . . . . .	105
5.1.1	NGC253 . . . . .	106
5.1.2	Molecules and structure of M82 . . . . .	107
5.2	Observations of sulphur-bearing species . . . . .	110
5.2.1	Results . . . . .	111
5.3	Comparison with models . . . . .	113

5.4	Discussions and conclusions . . . . .	115
<b>6</b>	<b>Hot cores: Probes of star formation at high-redshift</b>	<b>118</b>
6.1	Introduction . . . . .	118
6.2	Modelling high-mass star formation in the early Universe . . . . .	120
6.2.1	How to observe distant star formation . . . . .	120
6.2.2	Methodology . . . . .	122
6.2.3	Results . . . . .	127
6.2.4	Conclusions . . . . .	131
6.3	Star formation in the presence of active galactic nuclei . . . . .	133
6.3.1	Introduction . . . . .	133
6.3.2	The effect of Active Galactic Nuclei . . . . .	135
6.3.3	Infrared excess or nitrogen under-abundance? . . . . .	138
6.3.4	Conclusions . . . . .	141
<b>7</b>	<b>Massive elliptical galaxies : From cores to haloes</b>	<b>144</b>
7.1	Introduction . . . . .	144
7.1.1	Dark matter in the Universe . . . . .	144
7.1.2	Galaxy formation in a CDM Universe . . . . .	147
7.2	The sample . . . . .	151
7.3	Stellar Mass . . . . .	152
7.4	Dynamical Mass . . . . .	155
7.5	Scaling relations . . . . .	159
7.6	Acceleration . . . . .	162
7.7	Spherical collapse in a $\Lambda$ CDM Universe . . . . .	164
7.8	The evolution of the dark matter profile . . . . .	169
7.8.1	Results . . . . .	171
7.8.2	Galaxy formation and cooling . . . . .	172
7.9	Conclusions . . . . .	177
<b>8</b>	<b>Summary and Future work</b>	<b>179</b>
8.1	Future Work . . . . .	181
8.2	Observations . . . . .	183
<b>A</b>	<b>Deriving column densities</b>	<b>185</b>

<b>Bibliography</b>	<b>189</b>
---------------------	------------

## LIST OF FIGURES

---

1.1	The dark cloud Barnard 68 . . . . .	17
1.2	Star formation in the Eagle Nebula . . . . .	26
1.3	The interstellar extinction curve . . . . .	29
1.4	A SCUBA galaxy . . . . .	33
1.5	Madau plot from Steidel <i>et al.</i> . . . . .	49
2.1	Evolution of abundances for key species . . . . .	65
2.2	Variation of $R_1$ and $R_2$ with time during phases II and III . . . . .	66
2.3	Evolution of $R_1$ from atomic initial conditions . . . . .	68
2.4	The effect of including freeze-out . . . . .	70
3.1	H <sub>I</sub> emission in L134 . . . . .	77
3.2	C <sup>17</sup> O in L134A . . . . .	81
3.3	HCN at position III . . . . .	82
3.4	HNC at the centre and position II . . . . .	83
4.1	C <sup>34</sup> S and N <sub>2</sub> H <sup>+</sup> in S255 . . . . .	96
4.2	Evolution of CS:N <sub>2</sub> H <sup>+</sup> during collapse . . . . .	102
4.3	Evolution of CS:N <sub>2</sub> H <sup>+</sup> during collapse in models with an increase in temperature at late times . . . . .	103
5.1	CS in M82 . . . . .	112
5.2	Evolution of the C <sub>3</sub> H <sub>4</sub> :NH <sub>3</sub> ratio . . . . .	116
6.1	SO:HCN ratio for Milky Way and low metallicity hot cores . . . . .	129
6.2	Change in HCN abundance with increasing ionization . . . . .	137

7.1	Stellar mass function of sample of galaxies . . . . .	153
7.2	Variation of model mass to light ratio with input parameters . . . . .	156
7.3	Dynamical to stellar mass ratio within $R_e$ . . . . .	158
7.4	Correlations between velocity dispersion and luminosity, stellar mass and dynamical mass . . . . .	160
7.5	Mass-to-light ratios as a function of velocity dispersion . . . . .	163
7.6	Acceleration of early and late type galaxies . . . . .	165
7.7	Mass/velocity dispersion relations . . . . .	167
7.8	Concentration of halos before and after adiabatic contraction . . . . .	173
7.9	Density-temperature diagram . . . . .	175
7.10	Virial vs initial radius . . . . .	176

## LIST OF TABLES

---

1.1	List of detected interstellar molecules . . . . .	37
1.2	Observed deuterium fractions . . . . .	40
2.1	Elemental abundances used in ionization model . . . . .	63
2.2	Rate coefficients for key reactions ( $\text{cm}^3\text{s}^{-1}$ ) . . . . .	63
3.1	Positions observed . . . . .	78
3.2	Frequencies observed . . . . .	79
3.3	Observed column densities and fractional abundances . . . . .	84
3.4	Logarithmic fractional abundances of CO, HCN, HNC and CS as a function of time for models A-F. See text for a description of the models . . . . .	89
4.1	Accelerated collapse run parameters . . . . .	101
4.2	Accelerated collapse model predictions for species behaviour . . . . .	104
5.1	Molecules observed toward M82 . . . . .	110
5.2	Column densities of selected species in M82 . . . . .	113
5.3	Observed abundance ratios for selected species . . . . .	113
6.1	Abundances from population III supernovæ models . . . . .	124
6.2	Calculated column densities for stars formed from material enriched by the supernova of a population III star with ZAMS mass of $80M_{\odot}$ . . . . .	128
6.3	As table 6.2, for a star with ZAMS mass of $150M_{\odot}$ . . . . .	128
6.4	As table 6.2, for a population III supernova which produces a total yield of $80M_{\odot}$ . . . . .	129
6.5	Major formation and destruction routes for HCN . . . . .	139

## CHAPTER 1

---

# Introduction

Across all areas of astrophysics our understanding has improved at unprecedented rates throughout the last century. These advances have been driven by technological progress, first by advances in observational equipment and technique (especially in the expansion of astronomical observation beyond the optical to its present coverage of the entire electromagnetic spectrum), and more recently by advances in the computing power available to theorists. To illustrate the progress made, it is sufficient to recall that in 1902 it was perfectly possible to write that ‘the idea of galaxies beyond our own Milky Way is a long forgotten and discredited hypothesis’ (Clerke, 1902).

On larger, cosmological scales, many different observational probes combine to produce a coherent description of the large-scale behaviour of the Universe, constrained by a set of parameters the values of which are now known in most cases to within a few percent. Progress in finding agreement between disparate and independent parameters has been such that the resulting solution has become known as the ‘concordance cosmology’, but the current end result is a Universe in which  $\sim 95\%$  of the energy density remains in the unknown forms of dark matter and dark energy. Although theoretical predictions of the nature of both of these components exist, they remain essentially mysterious. Equally, in the last ten years the first planets beyond our Solar System have been identified; yet it is fair to say that there is much still to be learned about the processes which must have formed our own Solar System. Many of the first extra-solar planets to be discovered (see Butler *et al.* (2006) for a recent catalogue) are much larger than Jupiter, and yet are closer to their parent star than the orbit of Mercury is to the Sun. This is to some extent the

result of observational bias, as techniques used for the necessarily indirect discoveries are most sensitive to large planets close to the studied star. None the less, traditional models of planet formation - which predicted rocky planets close to their parent stars accompanied by gaseous giants further out - require adjustment. Looking further back in the evolution of our Solar System, before planets can form, a star must do so, and understanding star formation is therefore key to understanding our own planet's origin. Less obviously, but no less importantly, an understanding of star formation is also fundamental to attempts to study and understand the larger problems of the formation and evolution of large-scale structure, and to the cosmological conclusions derived from observations of this structure in turn. For instance, attempts to constrain the structure and history of a particular galaxy often depend on the incorporation into the model of the galaxy's star formation history (SFH). Such attempts are remarkably successful in reproducing the observed properties of galaxies as they are observed today (see, for example, Bruzual and Charlot (2003)), but their foundations are not secure. The list of as yet unresolved questions about star formation is long, but those of particular importance include:

- is the Initial Mass Function (IMF) universal, and what physical or chemical processes determine the mass of a forming star?
- what triggers the formation of a star (or stars) from previous quiescent gas?
- the efficiency of star forming regions is unclear.
- there has been no unambiguous detection of a pre-stellar core in the process of collapsing.

Star formation is a subject ripe for investigation, and so in this thesis I present a series of analyses of the early stages of star formation. ‘Early’ should be interpreted as referring both to the ‘early’ stages of a single star’s formation and, in chapters 6 and 7, to the ‘early’ stages of the evolution of the Universe. I hope to demonstrate that the detailed understanding and intuition developed in studying star formation within the Milky Way is also relevant in exotic environments. Similar techniques to those used in studying star formation within the Milky Way can be used in nearby starburst galaxies which are forming stars at rates several orders of magnitude higher than in our own Galaxy (chapter 5) and as far back in time as the epoch of the formation of the second stars (the first generation to produce solar mass stars), a period spanning more than 13 billion years.

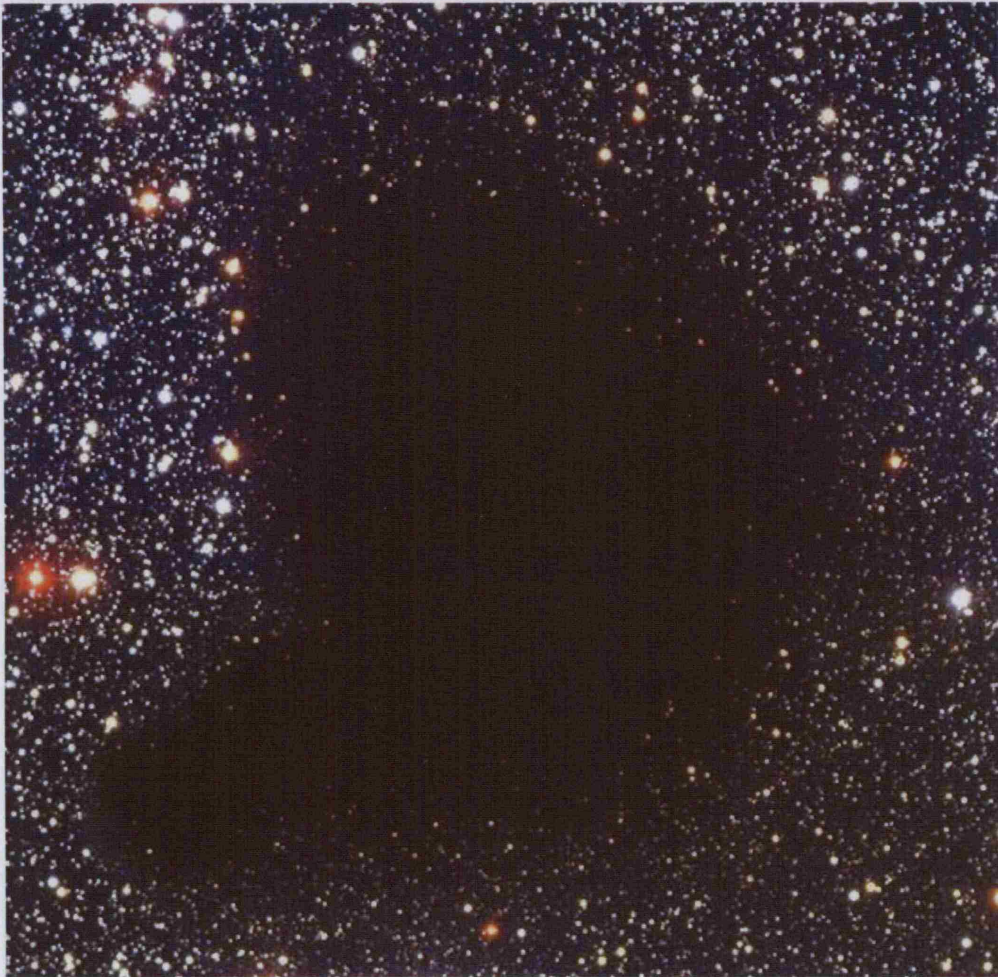


Figure 1.1: Barnard 68, a pre-collapse dark molecular cloud, seen in the optical by the Very Large Telescope.

## 1.1 Star Formation

It seems appropriate to begin with an overview of our knowledge of star formation. Stars form from dense and cool regions of the interstellar medium known as giant molecular clouds (GMCs). A simple comparison of the masses of the clouds with the sum of the masses of the stars produced within them, however, reveals that the majority of the material within the cloud is ‘sterile’. In other words, stars form from only a small fraction of the total material available; Leisawitz *et al.* (1989) give a ratio of stellar to total mass of  $\sim 1 - 2\%$ . GMCs themselves do not appear to be collapsing on large scales. Although they cannot be supported by thermal pressure (Goldreich and Kwan, 1974) the ionization is sufficient to allow magnetic support of these structures (McKee, 1989).

Magnetic support may also be important on the smaller scales associated with star

formation, as small clumps contained within the GMC (see section 1.1.2) collapse to form stars. The clumps are pervaded by the galactic magnetic field (which is observed via Zeeman splitting) which has its origin in a galactic dynamo, the origin of which is as yet not clearly established. A cloud with only thermal support will collapse when its mass exceeds the limit given by Jeans (1928):

$$M_J = \left( \frac{\pi k T_k}{\mu m_H G} \right)^{\frac{3}{2}} \rho^{-\frac{1}{2}} \quad (1.1)$$

where  $T_k$  is the kinetic temperature,  $\mu$  is the mean particle mass and  $\rho$  is the mass density. Collapse will then occur in free-fall time given by Spitzer (1978). As an example, consider a cold sphere of uniform density  $\rho(t)$ , at rest at time  $t = 0$  which has the equation of motion:

$$\frac{d^2r}{dt^2} = -\frac{GM(r_0)}{r^2} = -\frac{4\pi G\rho(0)r_0^3}{3r^2} \quad (1.2)$$

where  $M$  is the mass within an initial radius,  $r_0$ . Multiplying this equation by  $dr/dt$  and then integrating with respect to time gives

$$\frac{dr}{r_0 dt} = - \left[ \frac{8\pi G\rho(0)}{3} \left( \frac{r_0}{r} - 1 \right) \right]^{\frac{1}{2}}. \quad (1.3)$$

It is then possible to substitute  $r/r_0 = \cos^2 \beta$ , obtaining

$$\beta + \frac{1}{2} \sin 2\beta = t \left[ \frac{8\pi G\rho(0)}{3} \right]^{\frac{1}{2}} \quad (1.4)$$

In this simple picture, all shells reach the centre at the same time, when  $\beta = \pi/2$ , which corresponds to a free-fall time of

$$t_{ff} = \left( \frac{3\pi}{32G\rho} \right)^{0.5}. \quad (1.5)$$

The equation above will be valid for cases in which the initial density is a function of radius, although the free-fall time will be different for material that begins at different radii. As long as the density decreases outward, then the shells will not cross and the equations remain valid, providing a picture of an ‘inside-out’ collapse.

The Milky Way contains  $\sim 1 \times 10^9 M_\odot$  ( $1M_\odot$  = one solar mass) of molecular gas (Combes, 1991), most of which lies in large clouds with masses of  $\gtrsim 10^4 M_\odot$  (Elmegreen, 1985). If all the matter in such clouds really were simply collapsing at the rate determined by free-fall collapse, then the galactic star formation rate would be  $M_* \geq 200 M_\odot \text{yr}^{-1}$ , greatly in excess of that actually observed.<sup>1</sup> There must therefore be some means of support, and the main possibilities are support by magnetic fields, by turbulence or (more likely) by some combination of the two.

We will return to this issue, but it is important to establish the distinction which is often made between ‘low-mass’ and ‘high-mass’ star formation. Low-mass star formation is usually taken to refer to the formation of stars with masses lower than one solar mass, in isolated cores. This forms an ideal situation for modellers, but is relatively rare in observations. High-mass star formation, in contrast, usually refers to the formation of clusters of hot, massive stars (of spectral classes O and B) in what is known as an OB association. These are likely to be complex environments. High-mass stars form primarily in environments within which star formation has been triggered (by the passage of a shock wave, for example, which may result in the collapse of structures which were already gravitationally super-critical). In practice, low-mass stars also form in clusters, while high-mass stars may occasionally form in isolation, but the distinction between the two is nevertheless useful in seeking to model star forming phenomena and observations. I will follow the convention of defining any object for which the final stellar mass will be equal to or larger than a few solar masses as a ‘high-mass protostellar object’.

### 1.1.1 Turbulence in the ISM

In recent years the idea that star formation is triggered when shocks, driven by supersonic turbulent flows, form density enhancements from which new stars will form (Mac Low and Klessen, 2004) has become increasingly popular. Turbulence is defined simply as the flow resulting from the random motion of gas across many scales, and perhaps the most simple form is so-called ‘incompressible turbulence’. Here the rms velocities of the particles involved are subsonic, and the density remains constant throughout as a consequence of the assumption of incompressibility. Kolmogorov (1941) described this form of turbulence, assuming that turbulence is driven on a large scale ( $L$ ), forming eddies. In an astrophysical context, ‘large’ may be taken to be on the scale of giant molecular clouds. As these eddies

---

<sup>1</sup>This argument was first made by Zuckerman and Palmer (1974).

interact, they transfer some energy to smaller scales forming smaller eddies, until the dissipation scale  $l_{dis}$  is reached. The rate of energy transfer ( $\dot{E}$ ) is given by

$$\dot{E} = \frac{\nu v^3}{L} \quad (1.6)$$

where  $\nu$  is an empirically determined constant and  $v$  is the turbulent velocity. The kinetic energy is then distributed according to the power law  $E \propto v^2 \propto k^{-\frac{11}{3}}$  where  $k$  is the wave number.

Although this picture is simple and mathematically attractive, gas flows in the interstellar medium (ISM) do not match this ideal. First, these flows are extremely compressible. Second, the equation of state of the gas is dominated by radiative cooling, so that the pressure is strongly tied to the density and temperature. Finally the turbulence, driven by shock waves from supernovæ and other inhomogeneous processes, is not uniformly driven. In addition, density fluctuations in the ISM can be caused not only by the action of turbulence, but by thermal transition (Wolfire *et al.*, 1995) or gravitational collapse (Kim and Ostriker, 2001). Furthermore, supersonic turbulence offers additional routes for dissipation, as the local nature of the ‘cascade’ no longer applies; it has long been known (Zuckerman and Palmer, 1974) from observation that random motions in molecular clouds are indeed hypersonic.<sup>2</sup> Shock waves are able to dissipate large amounts of energy, but a substantial fraction always remains to be dissipated by vortices as described above (Porter *et al.*, 1992). Finally, the ISM is magnetized. Taking all of this into account, Ng and Bhattacharjee (1996) find that the best fit Kolmogorov-type spectrum is  $k^{(-\frac{5}{3})}$ .

How does this turbulence affect the evolution of the ISM? The first to discuss star formation triggered by compression were Elmegreen and Lada (1977), who modelled the evolution of turbulent compressions that appear in gas swept up by expanding HII regions. More recently, numerical models of highly compressible turbulence in self-gravitating turbulence (e.g. the 2D code of Ballesteros-Paredes *et al.* (1999), or the 3D low-resolution simulations of Vazquez-Semadeni *et al.* (1996), later extended by Klessen *et al.* (2000)) suggest that gravitational collapse does not in and of itself generate sufficient further turbulence to support the core. Furthermore, although on large scales turbulent support against gravitational collapse is possible, collapse is still possible on small scales. Simulations using full magneto-hydrodynamics (MHD) are important in quantifying and constraining

---

<sup>2</sup>Hypersonic motions are defined as those at more than five times the local speed of sound.

the rôle of magnetic fields. A model by Balsara *et al.* (2001), however, indicates that the presence of magnetic fields does not significantly extend the collapse time scale. This is partly due to the accretion of material down filaments which are aligned with field lines.

Van Loo *et al.* (2006) recently extended the model of Falle and Hartquist (2002) to produce a two dimensional magnetohydrodynamic (MHD) model capable of reproducing the formation of high-density structures. Their simulation does not include self-gravitation, but has an initial state of a uniform background which is then perturbed by a fast-mode wave. They obtain a series of structures which are ‘similar’ to observed embedded cores (despite the absence of gravity from the simulation), with the shape of the clump sensitive to the properties of the MHD waves. Such high density cores survive for much longer than those produced in one dimensional MHD simulations, and this work will have significant implications for models of chemistry associated with forming dense cores.

If the collapse of cores is triggered by turbulent motions, what regulates the efficiency of collapse? Vázquez-Semadeni *et al.* (2003) showed that one possibility is the amount of gas available to the collapsing core on scales where supersonic and subsonic turbulence meet. It appears that strong accretion on to the cores ceases long before the reservoir of observable gas has been fully depleted, with the mass fraction at which this happens dependent on the turbulent properties.

### 1.1.2 Collapse and ignition

Within the GMCs, most stars form in clusters (Testi *et al.*, 1999). However, theoretical understanding is most developed in the relatively rare regions in which (almost exclusively) low-mass stars are forming in isolation. Having already established that only part of the larger cloud collapses, we note that much effort has been devoted to the question of what might trigger the collapse of a small part of a larger cloud. Elmegreen and Lada (1977) suggested that the passage of a shock wave may trigger collapse (presumably of pre-existing overdense regions), while more recent work has focused on the decay of turbulence, or (see below) on ambipolar diffusion (Shu, 1977, 1983).

Whatever causes the collapse, it is clear that small regions of the cloud must indeed collapse; observations reveal dense regions a few tenths of a parsec across, known generically as ‘cores’, within the larger clouds in the form of high opacity regions which are also rich in NH<sub>3</sub> (Benson and Myers, 1989) and in other species (Butner *et al.*, 1995; Fuente *et al.*, 2005b). Molecules such as these are, as we shall see, of immense value in identifying

(or ‘tracing’) dense regions within which star formation may be occurring. Approximately half of such cores are associated with radiation detected by the InfraRed Astronomical Satellite (IRAS) (Beichman *et al.*, 1986) and the presence of such an infrared source at the centre of a dense core is assumed to indicate the presence of a newly-formed star. Their mean size as derived from molecular line maps is  $\sim 0.21 \pm 0.08$  pc (Bourke *et al.*, 1995). There is, however, some dependence on the choice of molecule, and Wang *et al.* (1995) find smaller sizes for cores which are mapped in C<sup>18</sup>O rather than in CS or NH<sub>3</sub>. These discrepancies also apply to estimated masses, but typically these cores appear to have masses of a few tens of solar masses (Onishi *et al.*, 1996). The last ten years of observation have made it clear that these objects have a large range in mass, composition and, of particular importance, in age. It is of more use to identify sub-classes which can be arranged in an evolutionary sequence.

In the process of low-mass star formation, it is believed that the earliest stages of star formation are represented by what are known as ‘starless cores’. These dense cores of gas, which do not include an IRAS source, are potential sites of future star formation (Myers and Benson, 1983). Ward-Thompson *et al.* (1994) identified a subset of these cores which have dust continuum emission visible at millimetre and/or submillimetre wavelengths as ‘preprotostellar cores’, or PPCs. It seems likely that some - not all - of these objects have already begun their collapse. Unlike the phases of low mass star formation which follow, these objects contain a disparate set of density profiles, including both sources which are strongly peaked and those which are almost uniform. They argue that these objects represent the earliest observed phase of star formation, are magnetically supported and may be undergoing ambipolar diffusion prior to collapse to form a protostar.

Ambipolar diffusion is defined as the drift of electrically charged particles within a plasma following their interaction with the magnetic field. Neutral particles within the plasma are obviously unaffected by the presence of the field, and hence by ambipolar diffusion. In an astrophysical context, the neutral particles are primarily hydrogen molecules, whereas the charged electrons and protons resist collapse due to support from the interstellar magnetic field. In reality, it is likely that some combination of magnetic and turbulent support operates in star forming regions. In fact, the lifetime of a pre-stellar core may be too short for significant ambipolar diffusion to take place, casting doubt on models which rely upon it as the sole means of support (Elmegreen, 2000).

Once accretion has produced a central source, the now protostellar object matches the

description of what Andre *et al.* (1993) define as class 0 sources. These clumps have strong sub-mm emission, and are identified by their low values of the ratio of bolometric to sub-millimetre (sub-mm) luminosity (i.e. a significant amount of the power remains in the sub-mm and millimetre regions of the spectrum). Lada (1987) classified young stellar objects which are slightly more advanced according to their spectral energy distributions; class I sources have spectral distributions which are much wider than a blackbody, class II sources correspond to classical T Tauri stars, while class III protostellar sources (corresponding to weak line T Tauri stars) show the reddened blackbody characteristic of a star approaching the zero age main sequence. Comparing the observed population density of class 0 and I sources suggests that the early phase is short-lived, perhaps lasting for only  $10^4$  years (Andre *et al.*, 2000). The lifetime of a class I source is perhaps an order of magnitude larger (e.g. Kenyon *et al.* (1990)). These results - which are all based on statistical population counts - have recently been challenged by Mouschovias *et al.* (2006). The authors use observations of star formation in external galaxies to derive a typical molecular cloud lifetime of  $10^7$  years, long enough for ambipolar diffusion to play an important role in the star-forming process.

Unambiguous observational signatures of collapse within these cores have proved to be elusive. The best attempts have been based on studies of the line profiles of abundant molecules. If the abundances are sufficient to cause self-absorption, then infall should result in a characteristic double-peaked profile in which the blue peak is stronger than that on the red side of the line (Evans, 1999). However, the shape of the line profile is also highly sensitive to many other parameters which may confuse the measurement hopelessly. Examples from models are given by Rawlings and Yates (2001) and Ward-Thompson and Buckley (2001). Redman *et al.* (2004a) have studied the effect of rotation on the molecular line profile, and they find that rotation can produce both red and blue asymmetric line profiles without the need for inflow or outflow, fitting a rotating model to the well-known pre-stellar core L1689B.

In the case of high-mass protostars, the situation is worse. The increased mass involved leads to a more rapid collapse, and so the opportunities for observation - and consequently the choice of objects for study - are, in the early stages of collapse at least, greatly reduced. Furthermore, the nearest regions in which massive stars are forming lie at kiloparsec distances, an order of magnitude more distant than the nearest low mass sources (De Buizer *et al.*, 2005). The percentage of both binary and multiple systems increases with

stellar mass (Larson, 2001), and the combination of these factors make detailed observation and modelling difficult. Most high mass protostellar objects (HMPOs) are seen only when they have reached what is known as the ‘hot core’ stage<sup>3</sup>, the distinctive signature of which is a consequence of interaction between the gas and dust grains. During the earlier stages of protostellar collapse, the low temperatures cause many molecules to ‘freeze-out’ from the gas phase on to the surface of dust grains (see section 1.2). Further reactions are then able to occur on the surfaces of these grains (both between molecules which are both adsorbed on to the grain surface and between a single adsorbed molecule and a molecule in the gas phase) until the ignition of the central protostar.

Despite work by Willacy *et al.* (1994), it is still believed that the vast majority of the reaction products remain on the surface of the grain until this point. The newly-formed star is able to heat the surrounding material rapidly (both directly and by the re-emission of radiation from surrounding dust) and the mantle ices quickly sublime, producing a complex but short-lived ‘soup’ of molecules in the gas phase. (It is still unclear whether the mantles are removed from the dust by direct thermal evaporation or by shocks; see Hatchell and Viti (2002) for a discussion.) These molecules form what is observed as a ‘hot core’, and this phase lasts approximately  $10^5$  years (Hatchell *et al.*, 1998).

Until recently, it was believed that the distinctive chemical signature associated with hot cores was exclusively linked to high-mass star formation. It was believed that only stars with masses greater than one solar mass would satisfy the requirement for ongoing infall at the moment of protostellar ignition which is required to provide material around the igniting star from which molecules may sublime. However, recent observations have identified hot core analogues around low-mass protostars (which the observers in question like to call ‘hot corinos’). Initially the evidence for these objects - defined as inner warm regions surrounding a central protostar within which grain mantle species have sublimated, and hence are visible in the gas phase - was based on observations with single dish millimetre telescopes (Ceccarelli *et al.*, 2000; Doty *et al.*, 2004). While these observations were of sufficient resolution to identify the link between the hot core-like signature and the dense central source, the size of the emitting region remained unknown until Maret *et al.* (2004) showed that these regions have typical sizes of a few tens of astronomical units (AU), and Bottinelli *et al.* (2004) presented detailed interferometric observations which were found to favour the presence of evaporated grain mantles.

---

<sup>3</sup>The term seems to have first been used in its modern context by Wootten *et al.* (1984).

Returning to the evolution of high-mass protostars, the hot core phase is believed to be followed by the development of an ultra-compact HII region (UCHII). These regions are essentially newly-formed stars which are still embedded in the surrounding molecular clouds, and are ultra-compact due to the presence of absorbing dust which reduces the size of the Stromgren sphere<sup>4</sup>. They are observable only in the sub-mm, in the infrared and, in the case of central stars which are of a spectral class hotter than B3, in the radio, although recent work by Hofner *et al.* (2002) has also detected hard X-rays ( $\geq 2.5\text{keV}$ ) from the well-known W3 star forming complex. As suggested by the name, ultra-compact HII regions are both compact, with diameters typically less than  $10^{17}\text{cm}$ , and dense; a typical density is in excess of  $10^4\text{cm}^{-3}$  (Churchwell, 2002). Observed at a wavelength of  $100\mu\text{m}$ , they are among the brightest and most luminous of Galactic sources, as the entire output of the nascent star is converted into infrared emission via absorption and re-emission by the surrounding dust. An additional typical feature of the UCHII environment is the presence of molecular masers. These appear almost ubiquitous, and are associated with several molecular species, the most common of which are  $\text{H}_2\text{O}$ , OH and  $\text{CH}_3\text{OH}$ , although masers associated with  $\text{H}_2\text{CO}$  and  $\text{NH}_3$  have also been observed (Churchwell, 2002). As these are associated with regions which have densities far above the minimum density required to excite any commonly observed molecular species ( $\geq 10^6\text{cm}^{-3}$ ), they are excellent probes of small scales which are otherwise inaccessible to observers.

I have discussed both ‘high-mass’ and ‘low-mass’ star formation, but what determines the mass of the final star? Surprisingly, this question is still open. Recent observations have suggested that the initial mass function is determined as early as the pre-stellar core stage. For example, Motte *et al.* (2001) present the results of a survey of two protoclusters within the Orion B star-forming region (NGC 2068 and 2071) and find a mass spectrum ‘reminiscent of the observed stellar initial mass function’. This work is, however, dependent on the assumption of spherical symmetry which must be made in order to convert from the two dimensional projection as seen on the plane of the sky to a three dimensional distribution.

These observational results also provide a strong argument against the previously well-supported competitive accretion theory of star formation (e.g. Zinnecker (1982); Larson (1992)), which suggests that stars are all initially much smaller than a typical stellar mass.

---

<sup>4</sup>The radius of the HII region is often referred to as the Stromgren radius and hence the Stromgen sphere is the ionized region within this radius.



Figure 1.2: This Hubble Space Telescope image of the Eagle Nebula, M16, clearly shows the evaporation of material from regions around newly formed stars.

The final stellar mass is then determined by the accretion onto the protostar of further unbound gas from the surrounding environment (or, in latter stages, by the collision and merging of separate protostellar objects), a view apparently supported by supercomputer simulations such as those carried out by Bonnell *et al.* (1998, 2001). This is in sharp contrast to the so-called ‘collapse’ models (discussed in the rest of this section) which suggest that the star does not accrete enough material to change its mass substantially (e.g. McKee and Tan (2003)), which is therefore set once collapse has begun. If the stellar IMF is determined by the mass of the pre-stellar cores, then it is clear that the collapse model must be favoured over competitive accretion. In addition to this observational evidence, Krumholz *et al.* (2005) present a theoretical study of the two competing models, and conclude that ‘no observed star forming region can undergo significant competitive

accretion, and that the simulations which show competitive accretion do so because the assumed properties differ from those determined by observation'. In this study, the process of building up a pre-stellar core is modelled by the accretion of non-self-gravitating gas on to a point particle (which is known as Bondi-Hoyle accretion) at a rate given by

$$\dot{m}_* = 4\pi\phi_{B-H}\bar{\rho}\frac{(Gm_*)^2}{(\sqrt{3}\sigma)^3} \quad (1.7)$$

where  $\bar{\rho}$  is the mean density and  $\phi_{B-H}$  is a function of  $\sigma$  (the velocity dispersion),  $m_*$  (the stellar mass) and a radius which represents the effects of turbulence. Using this formula and the assumption of virial equilibrium (appropriate as long as the effect of shocks is unimportant), the authors derive values for the fractional mass accreted in a dynamical time for a variety of star-forming regions, all of which are extremely small ( $< 0.005$ ). As mentioned above, this analysis leaves open the possibility that a forming star could still gain mass by capturing other bound cores. However, Krumholz *et al.* conclude that less than 1% of the total mass can be accreted per dynamical time.

### 1.1.3 Bonnor-Ebert Spheres

The simplest model of a star-forming core takes the form of a sphere, supported against gravity only by hydrostatic pressure (i.e. neglecting the possibility of both magnetic and turbulent support). Poisson's equation can then be written as

$$\frac{1}{r^2}\frac{\partial}{\partial r}\left(\frac{r^2}{\rho}\frac{\partial P}{\partial r}\right) + 4\pi G\rho = 0 \quad (1.8)$$

where  $r$  is the radius and  $\rho$  and  $P$  are the density and pressure respectively, both of which are assumed to be a function of the radius. If the core is assumed to be roughly isothermal, the equation of state is given by (Kirk *et al.*, 2005)

$$P = \rho\frac{kT}{m} + \frac{a}{3}\sqrt{T} \quad (1.9)$$

where  $a$  is the isothermal sound speed given by  $a^2 = kT/m$ ,  $k$  is the Boltzman constant,  $T$  the temperature and  $m$  the mean molecular mass.

Introducing dimensionless parameters

$$\xi = 2r/R_{flat} \quad (1.10)$$

and

$$\psi = -\ln(\rho/\rho_c) \quad (1.11)$$

where  $\rho_c$  is the central density and

$$R_{flat} = \sqrt{\frac{kT}{\pi m G \rho_c}} \quad (1.12)$$

where  $m$  is the mean particle mass, then equation 1.8 can be written as

$$\frac{1}{\xi^2} \frac{d}{d\xi} \left( \xi^2 \frac{d\psi}{d\xi} \right) - e^{-\psi} = 0 \quad (1.13)$$

which is the Lane-Emden equation. Following the treatment of Kirk *et al.* (2005), the solution to this equation can be parameterized by considering two radii.  $R_{flat}$ , defined above, is the point at which the profile steepens, while  $R_{edge}$  (the ‘truncation radius’) is the distance at which the core emission is indistinguishable from the background emission or at which the density profile becomes steeper than  $r^{-3}$ . Solutions with  $\xi_{max} = 2R_{edge}/R_{flat}$  correspond to the spheres which were first examined by Ebert (1955) and Bonnor (1956). It is commonly assumed that pre-protostellar cores take this form; any core with  $\xi_{max} > 6.5$  is unstable, and will collapse. Alves *et al.* (2001) find that, for the well-known starless core B68,  $\xi_{max} = 6.9 \pm 0.2$ , slightly in excess of the critical collapse criterion. However, it should be remembered that this derivation assumes an isothermal sphere. B68 is decidedly not spherical, and may not be isothermal and the model described in this section may therefore not apply. Instead of collapsing, it has been suggested that it may in fact be pulsating (Redman *et al.*, 2005).

## 1.2 Role of dust grains

The interstellar medium is essentially a mixture of gas and dust. Astronomers use the term ‘dust’ to refer to everything from molecules containing tens of atoms, up to micron-sized

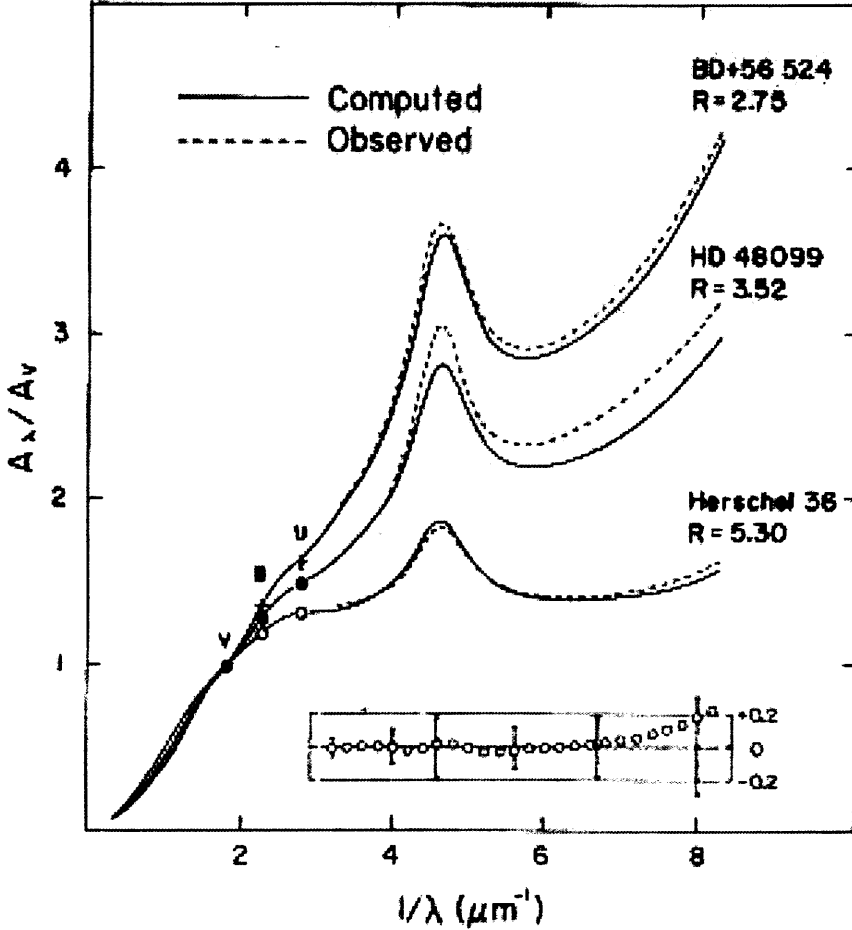


Figure 1.3: The interstellar extinction curve in the optical and the near-infrared from Cardelli *et al.* (1989) toward three lines of sight chosen to have different values of  $R_v$ .

particles. These particles play a critical role in determining the observational properties of star-forming regions and in controlling their associated chemical reactions.

The most obvious sign of the presence of interstellar dust is in the extinction of starlight (first studied in detail by Trumpler (1930)). As seen in figure 1.3, the extinction changes with wavelength, and this dependence strongly constrains the grain size distribution of the absorbing dust.

The extinction at a particular wavelength is defined by

$$A_\lambda = 2.5 \log_{10} \frac{F_\lambda^0}{F_\lambda} \quad (1.14)$$

where  $F_\lambda$  is the observed flux and  $F_\lambda^0$  is the flux in the absence of extinction (Draine,

2003). In the optical and ultraviolet regions of the spectrum, the parametrization of Cardelli *et al.* (1989) is often used, so that the normalized extinction curve is written as

$$\frac{A_\lambda}{A_I} \approx f(\lambda, R_V, C_1, C_2, C_3, C_4, \lambda_0, \gamma) \quad (1.15)$$

where the normalized extinction is some function,  $f$ , of

i  $R_v = \frac{A(V)}{E(B-V)}$ ,

ii at wavelengths greater than 3030 Å, the function  $f(\lambda)$  depends only on  $\lambda$  and  $R_v$ ,

iii  $C_3, \lambda_0, \gamma$  are parameters which produce the observed ‘bump’ in the spectrum at 2175 Å,

iv  $C_1, C_2$  and  $C_4$  determine the slope and curvature of the continuous extinction at  $\lambda \leq 3030$  Å.

If  $R_v$  is known, the other six parameters can be estimated, although the fit is, of course, improved by observations of the extinction at other wavelengths. Studies of the extinction of both stars (Fitzpatrick, 1999) and galaxies (Finkbeiner *et al.*, 2004) are consistent with a value of  $R_v \approx 3.1$  for an ‘average’ sight-line in the Milky Way. Lines of sight which have  $R_v$  larger than this mean are believed to intersect clouds which are undergoing grain growth by the twin mechanisms of accretion and coagulation (Draine, 2003).

In the infrared, diffuse clouds produce universal extinction, independent of  $R_v$ . Between 0.9 and 5.0 μm the power-law  $A_\lambda \propto \lambda^{-\beta}$  where  $\beta \approx 1.70$  (Rosenthal *et al.*, 2000). Beyond this point the data are less clear; Lutz *et al.* (1996) find a constant extinction between 4 and 8 μm, while Rosenthal *et al.* (2000) find a decline to a minimum at 6.5 μm. In dense clouds, the presence of ice due to the lower temperatures alters the extinction curve, but this is not a problem in more diffuse clouds.

Determining the extinction curve in external galaxies is obviously more of an observational challenge than in the Milky Way. However, Berlind *et al.* (1997) and Keel and White (2001a,b) find extinction laws similar to that of the Milky Way in nearby spiral galaxies. In more exotic systems, in which conditions are further removed from those in the solar neighbourhood, the situation may be different. Calzetti (2001) used the emission spectrum to investigate the extinction in starburst galaxies (those with star formation rates much larger than the Milky Way), and concluded that the extinction in the infrared

is relatively wavelength-independent compared with the Milky Way curve. In addition, no evidence was found for the 2175Å which may be due to problems in applying the radiative transfer to optically thick distributions of stars and dust. Similarly, the feature appears to be absent from quasar spectra (Pitman *et al.*, 2000).

Returning to the local Universe, direct evidence for the nature of interstellar dust comes from spectral features beyond those outlined in the extinction curve described above. I have mentioned already the feature at 2175Å discussed above, and it is believed to be associated with graphitic carbon, an identification first proposed by Stecher and Donn (1965). However, it is not clear that the variation in full-width half-maximum while  $\lambda_0$  is constant can be accounted for by graphite, and polycyclic aromatic hydrocarbon (PAH) molecules may prove to be the true carriers (Li and Draine, 2001). As the relative abundances of specific PAH vary between sightlines, so would the appearance of the spectral features.

A strong absorption feature at  $9.7\mu\text{m}$  indicates the presence of silicate minerals, and is interpreted as corresponding to the Si-O stretching mode, while the  $18\mu\text{m}$  feature may correspond to the O-Si-O bending mode (Smith *et al.*, 2000). These features are broad and do not show the detailed structure that is seen in laboratory studies of crystalline silicates (e.g. Scott and Duley (1996)) and the exact mix of crystalline and amorphous silicates present in the interstellar medium is, as yet, undetermined (e.g. Bowey and Adamson (2002)).

Small grains, which consist of anything from tens to hundreds of atoms and radii smaller than  $\sim 0.01\mu\text{m}$ , are also an important component of the interstellar medium. These grains have an average vibrational energy comparable to that of photons from the interstellar radiation field which heat the grains (Draine and Li, 2001). They therefore undergo short-lived episodes of stochastic heating which is followed by the reradiation of much of the energy in the infrared, a process first described by Greenberg (1968). Their importance became apparent when IRAS detected emission at 12 and  $25\mu\text{m}$  which was much greater than expected (Boulanger and Perault, 1988) from a population solely composed of large grains. Li and Draine (2001), identifying such small grains with the PAHs previously identified as the source of emission features in the diffuse interstellar medium (Allamandola *et al.*, 1985), propose a model in which the fraction of carbon in such molecules is  $6 \times 10^{-5}$ . Such a model is able to account both for the infrared excess and for the observed PAH emission features.

In addition to the features described above, the most infamous of all absorption spectral

features are the still essentially unidentified diffuse interstellar bands (DIBs). Discovered by Heger (1918), at least some of the bands are now believed to be due to individual PAHs; Desert *et al.* (1995) showed that a correlation between the strength of the 2175Å bump described above and several DIBs existed. In addition, fine structure has been detected (Kerr *et al.*, 1998) which supports the idea that the DIBs are associated with molecules which produce rotational bands.

It is clear from this evidence - and much more - that dust grains are important components of the interstellar medium. How, then, does the dust form? There exists strong evidence that one source of the dust lies in the outflows of old stars; infrared emission from dust is observed in outflows from red giants and carbon stars, and in planetary nebulae (Moseley, 1980). However, theoretical studies of grain destruction (e.g. Jones *et al.* (1994)) predict a mean lifetime of only  $3 \times 10^8$  years for dust produced in this way, and when this figure is compared with the production rate of old stars this leads to the conclusion that grains must also form elsewhere. Sugerman *et al.* (2006) present observations of the type-II supernova 2003gd and find a mid-infrared excess consistent with cooling dust, visible between 499 and 678 days after the peak in brightness following the initial explosion. The authors also present radiative-transfer models showing that  $0.02M_{\odot}$  of dust may have formed in the first 250 days after the outburst, concluding that the efficiency of such processes may be large enough to account for the observed dust content of high redshift galaxies (Morgan and Edmunds, 2003).

Understanding the production of dust in the early Universe is of especial interest following the discovery of a large class of sub-mm bright galaxies first seen by observers using the Submillimetre Common-User Bolometer Array (SCUBA) on the James Clerk Maxwell Telescope (JCMT). These so-called ‘SCUBA galaxies’, one of which is shown in figure 1.4, were first reported in observations made at a wavelength of  $850\mu\text{m}$  by Smail *et al.* (1997), and are faint or undetectable at other wavelengths.

For example, the lack of detection by the X-ray space telescope, XMM, (Waskett *et al.*, 2003) rules out the possibility that observers are confusing star forming sources with active galactic nuclei, and suggests that the SCUBA galaxies are genuine sites of star formation. In fact, they may represent the majority of star-forming systems at redshifts greater than 2. The spatial density of these sources is extremely high, perhaps as large as several orders of magnitude greater than that of present-day large galaxies with luminosities of  $L \sim 10^{13}L_{\odot}$  (Blain *et al.*, 2002). This result suggests that there has been significant evolution in the

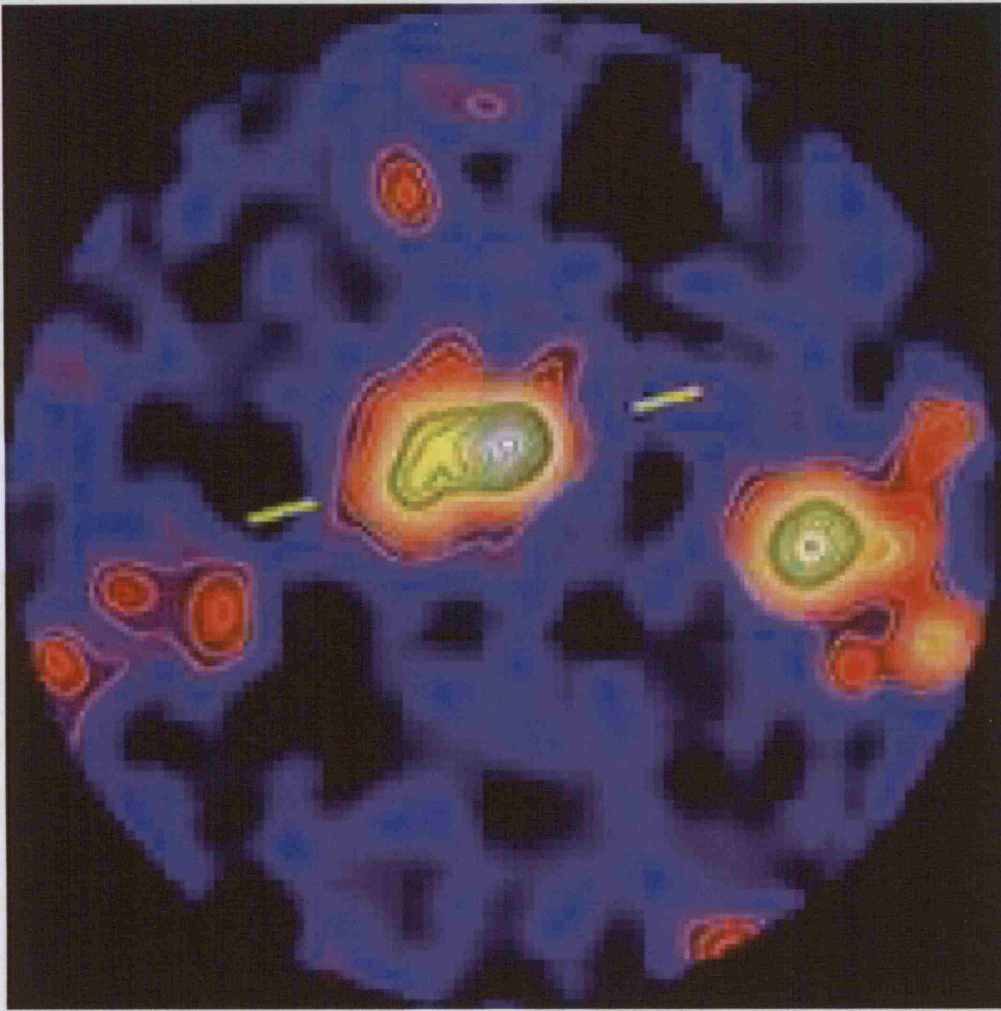


Figure 1.4: Detections of galaxies such as this by the Submillimetre Common-User Bolometer Array (SCUBA) indicate the presence of substantial dust-enshrouded star formation at redshifts greater than 2.

sub-mm galaxy population since  $z = 2$ . Indeed, the possibility remains that SCUBA galaxies may represent the progenitors of present-day ellipticals, which contain old, metal-rich stars (see chapter 7 for more details on these systems).

Dust grains are also important - regardless of their true composition - in influencing the development of interstellar chemistry, particularly in star forming regions. The clearest evidence for the importance of chemistry on the surface of these dust grains is the presence of vast quantities of molecular hydrogen in the interstellar medium.  $\text{H}_2$  is, in fact, the most common form of non-stellar baryonic matter in the Universe. Gas-phase reactions in the interstellar medium are not efficient enough to account for the observed abundance of  $\text{H}_2$ , and so its formation on dust grains is believed to dominate over the gas-phase

production (Gould and Salpeter, 1963). (Obviously, this is not true in the early Universe - see section 1.4). There are two primary mechanisms proposed for this crucial reaction: the Langmuir-Hinshelwood and the Eley-Rideal mechanisms. In the former, the hydrogen atoms adsorb on to the grain surface but diffuse along it. Upon their collision they react to form a hydrogen molecule, and the energy produced by the reaction may liberate the newly formed product from the surface. In the Eley-Rideal case, an incoming atom reacts directly with one already on the surface. Although the relative importance of these two mechanisms will, to some extent, depend on the conditions in which the grain is found, at least in diffuse clouds the dust grain should have only a few atoms stuck to it, making the Eley-Rideal mechanism less likely (Vidali *et al.*, 2005).

Of course, bare grain surfaces are not always exposed for hydrogen to adsorb onto. Particularly in dense clouds, such grains are usually covered in icy mantles (Whittet *et al.*, 1996; Gibb *et al.*, 2000) composed primarily of water and carbon monoxide (with water always the dominant partner). The structure of the ice is still unclear, and much observational and experimental effort is currently being expended on investigating the role of layered or mixed structures.

Further reactions on or in icy mantles are responsible for the production of many of the more complex species observed in the ISM. Such reactions may occur between molecules on the surface (see, for example, Aikawa *et al.* (2003a)), but are equally possible via the interaction of such molecules with photons or cosmic rays as the ice is processed (e.g Loeffler *et al.* (2005)). Material on the grains may then desorb by one of a variety of mechanisms, returning to the gas phase in doing so. Thermal desorption is possible, but the typical energy barrier against desorption for large species is 1000K, so that at the low temperatures common in star forming regions proceeds at such a slow rate as to be insignificant. The collision of cosmic rays with the dust grains, however, causes heating of the grain to around 70K on short timescales ( $\sim 10^{-5}$ s, Hasegawa and Herbst (1993)) which may result in desorption of material. Garrod *et al.* (2006a) have investigated the effect on abundances of introducing a third desorption mechanism in which the energy released by exothermic reaction allows the products to immediately desorb (rather than expending the energy in bulk heating of the grains which would, in any case, be insufficient to significantly increase the chances of any given molecule leaving the grain via thermal desorption). The authors show that, at least in the specific case of methanol in cold dark clouds, allowing a fraction ('typically under 0.10') of molecules to leave the grain

surfaces in just this way improves the fit of models to observation. This extra component in the modelling of astrochemistry of star forming regions will be the subject of further investigation in the near future.

Whatever happens in cold dark regions, heating of the cloud (most likely after the ignition of a protostar) will result in the sublimation of the ice and the return of the species to the gas phase where they are commonly observed in the sub-mm. The resulting rich gas chemistry (the ‘hot core’ phase) was, as we have seen, believed to be characteristic of high-mass star formation when material was still infalling during protostellar ignition. However, recent observations indicate similar features associated with low mass star formation (Bottinelli *et al.*, 2004).

The process of desorption that follows has been investigated by laboratory experiments utilising the technique of temperature programmed desorption (TPD, Collings *et al.* (2004)). Such experiments, which warm ices previously deposited on a substrate while monitoring the appearance in the gas phase of sublimated species, reveal a variety of separate desorption events, which - in order of increasing temperature - are listed below. Not all molecules will show all five of these phases of desorption on all substrates. In experiments, gold, for experimental ease, or (slightly more realistically) graphite are typically used.

1. Desorption of the pure species on the surface of the ice mantle.
2. Desorption of a monomolecular layer deposited on H<sub>2</sub>O ice.
3. Desorption of molecules during the conversion of H<sub>2</sub>O from amorphous to crystalline structural forms, also known as the ‘volcano’ effect.
4. Co-desorption along with the H<sub>2</sub>O ice.
5. Desorption of the pure species from the substrate .

Experiments which aim to identify the relative contributions of these five processes to the desorption of each species have been carried out, and the results can be incorporated in chemical models of star forming regions (Viti *et al.*, 2004a). For a broad overview, species are divided into those that behave as H<sub>2</sub>O (as described in Fraser *et al.* (2001)) and those that behave as CO (as described by Collings *et al.* (2003)), although in practice many are intermediate between these extremes of behaviour. The most striking difference between

star-forming regions and these experiments is the different time-scales; it is obviously impractical to run a TPD experiment for thousands of years. However, experiments such as these are important in understanding the conditions within which chemical reactions take place.

### 1.3 Interstellar molecules and chemistry

Interstellar chemistry is surprisingly complicated, with over a hundred molecular species participating in several thousand reactions. Of these molecules, the first to be identified (apart from molecular hydrogen) were detected via optical spectra: CH (McKellar, 1941; Adams, 1941),  $\text{CH}^+$  (Adams, 1949) and CN (Swings and Rosenfeld, 1937) in the spectra of reddened stars. The first molecule to be discovered via its radio emission was OH in 1963 (Weinreb *et al.*, 1963) and detections of ammonia ( $\text{NH}_3$ , Cheung *et al.* (1968)), water (Cheung *et al.*, 1969) and formaldehyde ( $\text{H}_2\text{CO}$ , Snyder *et al.* (1969)) followed before the end of the decade; it became clear that a complex chemsity was able to develop, at least in the dense regions of the interstellar medium. The majority of species are produced by addition reactions. The chemistry associated with dust is discussed in section 1.2; in the early stages of star formation and in the diffuse interstellar medium chemical reactions which occur in the gas phase are in any case dominant.

A list of species that have currently been identified in the ISM is given in Table 1.1, the majority of which have been identified in radio, sub-mm or infrared spectra.<sup>5</sup> From such a list it is difficult to identify those molecules that are important, such as those which act as reservoirs for substantial proportions of oxygen, carbon and nitrogen. Carbon monoxide - the most abundant species apart from molecular hydrogen - contains up to 20% and 40% of the interstellar available oxygen and carbon respectively. Much of the remaining oxygen is in the form of water ice, either in star-forming regions (Whittet *et al.*, 1993) or in quiescent clouds (Schutte *et al.*, 1996). Models predict that the majority of gas phase nitrogen should be in the forms of either atomic nitrogen or  $\text{N}_2$ , but only indirect limits (via detections of  $\text{N}_2\text{H}^+$ ) on the abundance of these two independent species can be obtained from observations; the amount in solid ice is similarly poorly constrained. The majority of carbon is locked up in solid carbanaceous material (see below) and the

---

<sup>5</sup>The table overleaf is a list of detected interstellar molecules as of November 2005. Those detections in italics are tentative or disputed. The data are primarily taken from the list maintained at NRAO.

H <sub>2</sub>	C <sub>3</sub>	c – C <sub>3</sub> H	C <sub>5</sub>	C <sub>5</sub> H	C <sub>6</sub> H	CH <sub>3</sub> C <sub>3</sub> N	CH <sub>3</sub> C <sub>4</sub> N	CH <sub>3</sub> C <sub>5</sub> N	HC <sub>9</sub> N
AlF	C <sub>2</sub> H	1 – C <sub>3</sub> H	C <sub>4</sub> H	C <sub>2</sub> H <sub>4</sub>	CH <sub>2</sub> CHCN	HCOOCH <sub>3</sub>	CH <sub>3</sub> CH <sub>2</sub> CN	(CH <sub>3</sub> ) <sub>2</sub> CO	CH <sub>3</sub> OC <sub>2</sub> H <sub>5</sub>
AlCl	C <sub>2</sub> O	C <sub>3</sub> N	C <sub>4</sub> Si	1 – C <sub>3</sub> H <sub>2</sub>	CH <sub>3</sub> CN	CH <sub>3</sub> COOH	(CH <sub>3</sub> ) <sub>2</sub> O	NC <sub>2</sub> O <sub>2</sub> H <sub>5</sub>	HC <sub>11</sub> N
C <sub>2</sub>	C <sub>2</sub> S	C <sub>3</sub> O	C <sub>3</sub> S	c – C <sub>3</sub> H <sub>2</sub>	CH <sub>3</sub> CN	C <sub>7</sub> H	CH <sub>3</sub> CH <sub>2</sub> OH	CH <sub>3</sub> CH <sub>2</sub> CHO	
CH	CH <sub>2</sub>				CH <sub>2</sub> CN	HCOCH <sub>3</sub>	H <sub>2</sub> C <sub>6</sub>		
CH <sup>+</sup>	HCN	C <sub>2</sub> H <sub>2</sub>	C <sub>2</sub> H <sub>2</sub> D	CH <sub>4</sub>	CH <sub>3</sub> OH	NH <sub>2</sub> CH <sub>3</sub>	CH <sub>2</sub> OHCHO		
CN	HCO		HCCN	HC <sub>3</sub> N	CH <sub>3</sub> SH	c – C <sub>2</sub> H <sub>4</sub> O	CH <sub>2</sub> CHCHO		
CO	HCO <sup>+</sup>		HCS <sup>+</sup>	HCNH <sup>+</sup>	HC <sub>3</sub> NH <sup>+</sup>	CH <sub>2</sub> CHOH			
CO <sup>+</sup>			HOC <sup>+</sup>	HNCO	HC <sub>2</sub> NC	HC <sub>2</sub> CHO			
CP				H <sub>2</sub> O	HCOOH	NH <sub>2</sub> CHO			
CSi				H <sub>2</sub> S	HNC	H <sub>2</sub> CHN	C <sub>5</sub> N		
HCl				3KCl	HNC	H <sub>2</sub> CO	HC <sub>4</sub> N		
NH				NH	HNO	H <sub>2</sub> CN	H <sub>2</sub> NCN		
NO				NO	MgCN	H <sub>2</sub> CS	SH <sub>4</sub>		
NS				NaCl	MgNC	H <sub>3</sub> O <sup>+</sup>	H <sub>2</sub> COH <sup>+</sup>		
				OH	N <sub>2</sub> H <sup>+</sup>	NH <sub>3</sub>			
				PN	N <sub>2</sub> O	SiC <sub>3</sub>			
				SO	NaCN	C <sub>4</sub>			
				SO <sup>+</sup>	OCS				
				SiN	c – SiC <sub>2</sub>				
				SiO	CO <sub>2</sub>				
				SiS	NH <sub>2</sub>				
				CS	H <sub>3</sub> <sup>+</sup>				
				HF	SiCN				
				SH	AINC				

remainder is in the form of CO. This most common of molecules (aside from H<sub>2</sub>) has been detected in the early Universe, at redshifts in excess of 6. As all but the lightest elements are produced in stars or supernovæ, and only added to the ISM at or near the end of the star's lifetime. The nucleosynthetic signature of supernovæ is evident in the observed abundance ratios of various elements, and stars too small to end their lives in supernovæ but large enough to leave the main sequence on relatively short timescales also contribute through mass loss as and after they leave the main sequence.

The first detailed study of the formation of molecules in the ISM was that of Bates and Spitzer (1951) who attempted to understand the abundances of the then recently-discovered molecules, CH and CH<sup>+</sup>. The kinetic temperature in regions in which molecules are forming is low, and so reactions must be exothermic and proceed without a significant activation energy barrier. Two-body reactions between positive ions and neutral species satisfy both of these criteria, and their importance was highlighted by, among others, Herbst and Klemperer (1973). In particular, the high relative abundance of H<sub>2</sub> means that polyatomic ions are built up via reactions of the form:



following initial ionization of a parent species ('A') by cosmic rays (see chapter 2). Less efficiently, an alternative route for the formation of ions is available via short lived collision complexes<sup>6</sup>:



These product ions primarily react rapidly with the most common species - H<sub>2</sub> and CO - or recombine with electrons in reactions which are exothermic enough to produce in fragmented, neutral products. Neutral-neutral reactions are also common between more reactive species (such as OH) and are believed to have produced further neutral species such as O<sub>2</sub> and N<sub>2</sub>. The most common neutral species (beyond H<sub>2</sub> and CO) are H<sub>2</sub>O and NH<sub>3</sub>. Although reactions of neutral species (and large ions) with hydrogen have large

---

<sup>6</sup>Excited states are denoted by \* throughout the text.

energy barriers, they can become significant in shocked gas. This route is particularly important in allowing the formation of water via the route provided by



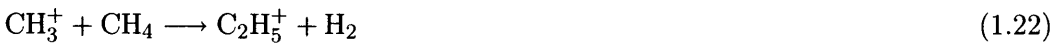
which is efficient above 230K (van Dishoeck and Blake, 1998).

The choice of rates for these reactions are crucial for those attempting to model the behaviour of the interstellar medium. At room temperature the rate coefficient for the exothermic reactions described above is typically near  $10^{-9}\text{s}^{-1}$  and the rate coefficients are expected to increase in interstellar conditions (Watson, 1978). Unless otherwise stated, the work presented in this thesis uses the UMIST database of rate coefficients (Le Teuff *et al.*, 2000) which collates data for 4113 gas-phase reactions involving 396 species composed of 12 elements. The freeze-out of molecules onto the grain surface and reactions upon the grains are also included where appropriate.

The list of species in table 1.1 includes many complex hydrocarbons; their production requires the presence of atomic carbon in a region shielded from the interstellar radiation field in order to avoid photodissociation. The dominant route for the production of unsaturated hydrocarbons (which are observed in star forming regions) is the insertion of carbon via reaction with  $\text{C}^+$  (e.g.



(Herbst, 1995)) but condensation reactions such as



or radiative association may also contribute.

### 1.3.1 The role of deuterium

One of the most distinctive features of the chemistry associated with molecular clouds is the high abundance of many deuterated species. Many species have a deuteration fraction of  $10^5$  the solar neighbourhood value (which Linsky (2003) found to be  $\sim 1.5 \times 10^{-5}$ ). As

Species	D/H	Reference
HCO <sup>+</sup>	0.045	Butner <i>et al.</i> (1995)
N <sub>2</sub> H <sup>+</sup>	0.1	Crapsi <i>et al.</i> (2004)
H <sub>2</sub> CO	~ 0.01 – 0.1	Bacmann <i>et al.</i> (2003)
HNC	0.02-0.09	Hirota <i>et al.</i> (2003)
CH <sub>3</sub> OH	0.014	Parise <i>et al.</i> (2004)
NH <sub>3</sub>	0.1	Roueff <i>et al.</i> (2000)

Table 1.2: Examples of observed deuterium fractions (N[deuterated species]/N(non-deuterated species]) for species in prestellar cores and low mass protostars. Several of the species have been observed in multiply deuterated forms. For example, both doubly and triply deuterated CH<sub>3</sub>OH are reported by Parise *et al.* (2004). A more extensive list is given by Roberts (2005)

an illustration, an incomplete survey of observed deuterium fractions is given in table 1.2, but in regions with atomic D/H ratios in excess of 0.1 even triply deuterated species such as CD<sub>3</sub>OH (Parise *et al.*, 2004) and ND<sub>3</sub> (van der Tak *et al.*, 2002) are observed.

In the dense, cold interstellar medium, most deuterium atoms will initially be found in the form of HD, while the most abundant ion will be H<sub>3</sub><sup>+</sup>, which can react via the reversible reaction



to form the positive ion H<sub>2</sub>D<sup>+</sup>. The reaction is exothermic in the forward direction, and so at low temperature the reverse reaction is not efficient. Once formed, H<sub>2</sub>D<sup>+</sup> is then able to produce further deuterated molecules (Phillips and Vastel, 2003) via reactions such as



and



D<sub>3</sub><sup>+</sup> could in fact be the dominant charge carrier in depleted cold, dark cores (Roberts *et al.*, 2003). These exothermic reactions are largely responsible for the observed enhancements in the abundances of deuterated species (Walmsley *et al.*, 2004). However, it has

long been known that the depletion of molecules on to the surface of dust grains is accompanied by the enhancement of the deuterium fraction in the material remaining in the gas phase (Dalgarno and Lepp, 1984). Without such depletion, the presence of molecules with high proton affinity (such as CO) ‘traps’ the deuterium in ions such as  $\text{DCO}^+$ , thus reducing the  $\text{H}_2\text{D}^+/\text{H}_3^+$  ratio and, as  $\text{H}_2\text{D}^+$  is the major route into the chemical network described above, also reducing the likelihood of further deuteration of other, more complex molecules. The lower ionization fraction in prestellar cores (as compared with dark clouds) also results in an increase in deuterium fractionization as the rate of recombination of deuterated ions is reduced. Models incorporating these effects (e.g. Phillips and Vastel (2003)) have been successful in reproducing the observed abundance of many deuterated species. In addition, as a result of their continuing presence in the gas phase during protostellar collapse, deuterated molecules may represent the best tracers of the dense, depleted regions in the very last stages prior to the ignition of a protostar (Flower *et al.*, 2004).

### 1.3.2 Cooling in dense molecular clouds

It has long been understood that the most effective cooling mechanism in dense molecular clouds is, in most circumstances, via radiative transitions of molecular species. This in turn is of vital importance in controlling star formation, as collapse can proceed in a stable core only if the gravitational potential energy can be radiated away in this manner (Goldsmith and Langer, 1978; Black, 1987). The situation therefore differs from that in diffuse clouds, where cooling via  $\text{C}^+$  (along with fine structure radiation from atomic oxygen) is dominant. The cooling efficiency for any particular molecule depends on the energy level structure, together with such factors as the collision rate coefficient and transition matrix elements. However, in a typical dense cloud the cooling will always be dominated by the same molecular species, particularly  $\text{H}_2$ , HD and CO. Of these, ortho- $\text{H}_2$  has a large spacing (509K) between the first excited and ground states, and so the cooling rate is negligible for temperatures which are lower than approximately 50K. HD, in contrast, although much less abundant than  $\text{H}_2$ , has a nonzero permanent electric dipole moment and lower energy levels and so it is a (potentially) more effective coolant at low temperatures.

Carbon monoxide has a low rotational constant and transitions which are easily thermalized. This means that a large number of levels are able to contribute to the cooling rate (Goldsmith and Langer (1978) conclude that at least 18 different transitions must be included for cooling rates between 20 and 60K). The CO abundance is usually large

enough for both  $^{13}\text{CO}$  and  $\text{C}^{18}\text{O}$  to contribute to the cooling rate. They are of particular importance in dense clouds, when the effect of radiative trapping limits the contribution of CO itself. For example, Goldsmith and Langer conclude that at a hydrogen density of  $10^4\text{cm}^{-3}$  the two isotopic species can produce 25% of the cooling from CO.

Both ortho- and para- forms of  $\text{H}_2\text{O}$  contribute to cooling, but (at least in the linear regime) the cooling rate from para- $\text{H}_2\text{O}$  is seven times larger than that from ortho- $\text{H}_2\text{O}$ . Neufeld *et al.* (1995) find that water can, in fact, dominate the cooling, particularly at high densities and temperatures.

Further potential coolants include  $\text{H}_2\text{O}$ ,  $\text{O}_2$ ,  $\text{N}_2$  and  $\text{C}_2$ , along with (in the early Universe)  $\text{H}_3^+$ .

Neufeld and Kaufman (1993) provide a detailed description of the methods used to determine the cooling function of any species. They find that the dependence of the cooling rate on temperature depends both on the density and the opacity as follows:

1. low density, optically thin material: the cooling rate is a function of temperature only.
2. high density, optically thin material: the level populations are thermalized, and the cooling rate is inversely proportional to the density.
3. low density, optically thick material : the ‘line emission is optically thick, but effectively thin’; emitted photons are re-emitted until they escape the cloud. As the density is low, every collisional excitation results in cooling as collisional de-excitation can be ignored.
4. high density, optically thick material : as the optical thickness increases, the cooling rate approaches the limit in which it is inversely proportional to it, although in astrophysical situations high-energy transitions will always remain optically thin.

## 1.4 The history of star formation

### 1.4.1 The first stars

The beginning of star formation in the Universe was marked by the appearance of a unique generation of stars - the first stars, often known as population III<sup>7</sup> - and in recent years

---

<sup>7</sup>According to traditional nomenclature, population II stars are old stars such as those which populate elliptical galaxies and the bulges of spirals, and population I stars are young and blue stars such as those

rapid progress has been made in understanding their formation and in determining the properties of these first stars, both observationally and theoretically. As the formation of these stars is critical in determining the evolution of the galaxies in which they form, I will consider these developments in some detail, beginning with the observational data.

The appearance of the first sources of radiation following the epoch of last scattering (marked by the cosmic microwave background) is believed to cause rapidly the reionization of the Universe. One method of determining the age of the epoch of reionization is to study the linear polarization of the CMB, observed today as a result of the presence of large scale structure. Linear polarization results from the Thompson scattering of photons from the background radiation by free electrons, which exist only after the (re-)ionization of the Universe. A net linear polarization is produced if and only if the background radiation field is anisotropic. The CMB radiation incorporates an intrinsic quadrupole anisotropy due to density fluctuations at the time of recombination and so the redshift at which reionization is thus, in principle, derivable from the observed optical depth.

The first limits on the magnitude of the polarization of the CMB were found by the discoverers of the microwave background, Penzias and Wilson (1965). For the next 37 years attempts were made to improve the limits, but the first detection was only reported in 2002 when the DASI team reported a detection at 30GHz (Kovac *et al.*, 2002; Leitch *et al.*, 2005). This detection was then improved by other experiments, and a review is given by Piacentini *et al.* (2006). The Wilkinson Microwave Anisotropy Probe (WMAP) satellite then provided maps of the entire sky between 23 and 94GHz, and detected significant levels of polarized foreground over much of the sky. An optical depth of  $\tau = 0.088^{+0.028}_{-0.034}$ <sup>8</sup> is derived, which corresponds to a maximum likelihood peak for the reionization epoch of  $z_{reion} = 10.9^{+2.7}_{-2.3}$  (Page *et al.*, 2006). However, as with all such measurements, it should be remembered that this analysis assumes that there was a single epoch of ionization instead of a gradual - or local - phase transition from a neutral to an ionized Universe.

An alternative method of constraining the age of the epoch of reionization is to use absorption features seen in the spectra of distant quasars. The results show that absorption due to neutral hydrogen in the intergalactic medium (IGM) increases dramatically with redshift (Becker *et al.*, 2001; Pentericci *et al.*, 2003). In fact, these authors claim the detection of a complete Gunn-Peterson trough (Gunn and Peterson, 1965), with no flux formed in the arms of spiral galaxies.

<sup>8</sup>0.434Gyr after the Big Bang for the standard cosmological model.

detected over a 300Å range on the blue side of the Ly- $\alpha$  emission line in a source at a redshift of  $z = 6.28$ . Such a lack of flux was expected if the light from the quasar passes through a Universe which has not yet been reionized. At first glance, this appears to contradict the results obtained from the cosmic microwave background, and favour a late reionization.

That said, even a small neutral hydrogen fraction in the IGM would be sufficient to account for the observed Gunn-Peterson trough, and it is possible to reconcile the observations by allowing reionization to occur at different rates and times in different regions of the Universe, rather than considering a single, universal epoch of reionization. The CMB results are sensitive to the average reionization across the line of sight, whereas the Gunn-Peterson trough tests only the end of reionization. In any case, it is clear that the first sources of light appeared at redshifts greater than 6.

I have discussed reionization assuming that these first sources of light - and hence the cause of the epoch of reionization - are the first stars themselves, but other sources are possible. In particular, as Barkana and Loeb (2001) comment, quasars are a more efficient means of ionization than stars due to their harder emission spectrum, the efficiency of accretion flows (which can be more than an order of magnitude above the radiative efficiency of a star) and the increased escape fraction of quasar ionizing photons. In order for quasars to contribute to the reionization of the Universe, massive black holes must be able to form directly from gas rather than via stellar evolution. The main obstacle to this process lies in the centrifugal force, but Eisenstein and Loeb (1995) showed that a small fraction of objects have a low enough angular momentum that black holes can form quickly. Even if this was the case, however, the detection of carbon monoxide at  $z > 6$  (see chapter 6) indicates that the most distant galaxies yet observed have already formed stars.

Kashlinsky *et al.* (2005) recently reported observations made with the Spitzer Space Telescope of the cosmic infrared background as it appears in the near-IR. Current theory (see below) suggests that the first stars were massive (with masses likely to be in excess of  $100M_{\odot}$ ) and thus they should have contributed significantly to the diffuse background (Rees, 1978) regardless of the details of their mass function. Indeed, these sources (with much of their emission, which would peak in or near the ultraviolet, and hence shifted into the observer's frame near infrared) could be responsible for much of the observed background excess (Magliocchetti *et al.*, 2003; Santos *et al.*, 2002) observed in the

IR. Intriguingly, it has been suggested that such emission would have a distinguishable anisotropic signature which - if the foreground emission from more recent sources can be removed - would be detectable with current instruments. Kashlinsky *et al.* argue that the observed excess in their data is indeed consistent with the presence of energetic sources at high redshift; this result depends on the reliability of their method for using Spitzer data to remove galaxies at extremely faint flux limits ( $\geq 0.3\mu\text{Jy}$ ).

Until the advent of the James Webb Space Telescope sometime in the next decade with its capability to detect the supernovæ associated directly with the first stars it is unlikely that much observational progress will be made. What, then, of theory? The current state of the art in simulations of early star formation is the self-consistent three-dimensional hydrodynamic simulation of Abel *et al.* (2002). These simulations use the technique of adaptive mesh refinement (AMR, Abel *et al.* (2000)) in order to cope with the physics throughout the large dynamic range involved (including physics across scales separated by up to ten orders of magnitude) in following evolution on both cosmological and stellar scales.

Although the chemistry of the first stars, forming from material enriched only by big bang nucleosynthesis (BBN), is less complicated than that of local star forming regions, Abel *et al.* follow the chemistry of what they consider to be the eight dominant species: H, H<sup>+</sup>, H<sup>-</sup>, He, He<sup>+</sup>, He<sup>2+</sup> and H<sub>2</sub><sup>+</sup>, along with the density of free electrons. This list is probably comprehensive, although there have been suggestions that at high densities H<sub>3</sub><sup>+</sup> may act as a significant coolant<sup>9</sup> and it is important that three-body formation of molecular hydrogen (3H → H<sub>2</sub> + H) is included. This latter reaction is normally ignored, but it becomes important once the gas density reaches  $\sim 10^{10}\text{cm}^{-3}$ .

In the absence of metals, the only effective route for cooling of the gas is via H<sub>2</sub> and it is this relatively poor cooling rate which is responsible for the large size of the protostar produced. In the Abel *et al.* simulations the protostar does indeed grow to large size rapidly; within 10<sup>4</sup> years,  $70M_{\odot}$  of material will have been accreted, assuming that angular momentum does not slow the collapse. Such work, indicating that all first stars may have been massive and relatively isolated, is supported by recent observational evidence that low metallicity stars in the Galactic halo may have been enriched by a single population of massive stars (Wasserburg and Qian, 2000).

---

<sup>9</sup>See the presentation by Glover & Savin at [http://www.int.washington.edu/talks/WorkShops/int\\_06\\_2a](http://www.int.washington.edu/talks/WorkShops/int_06_2a)

### 1.4.2 From population III to the present day

The fate of the massive population III stars will depend on their exact mass. The discussion in this paragraph is largely based on the results of Heger and Woosley (2002). Their results are strictly valid for non-rotating stars, and so some adjustment is expected in reality. However, some indication of the fate of realistic stars can be given. Above an initial mass of  $\sim 40M_{\odot}$ , black holes form by the direct collapse of the star's iron core, while the hydrogen-rich envelope (along with a fraction of the helium shell) escapes in the supernova explosion, enriching the surrounding medium. At the other extreme, if the star's mass upon joining the main sequence is greater than  $\sim 260M_{\odot}$ , complete collapse to a black hole with little or no loss of material is predicted; the release of potential energy as the star collapses is not sufficient to reverse the implosion. Were the first stars to be this massive, they would contribute very little to the enrichment of the interstellar medium, and we should expect a second generation of 'population III-like' massive stars to follow. For stars which have zero age main sequence masses less than  $260M_{\odot}$  but larger than  $\sim 140M_{\odot}$  the so-called pair-instability seems likely to prevent the formation of any dense remnant. Instead, the internal energy in the star's gaseous component is rapidly converted to mass, and the star can then contract rapidly as the particle pairs contribute little to the pressure resisting collapse (Bond *et al.*, 1984). Oxygen and silicon burning then completely disrupt the structure of the star, meaning that these events are likely to be excellent sources of metals for the surrounding interstellar medium.

Could a second generation of stars form in such an environment? O'Shea *et al.* (2005) have carried out simulations in order to investigate this question, and find that the rapid formation of a second generation of stars is possible. Specifically, they find that a protostar would quickly form from primordial material within the large HII regions surrounding a true 'first generation' star, with rapid accretion occurring soon after the appearance of the HII region. As HII regions accompanying the first stars are expected to be extremely large, up to kiloparsecs in diameter (Whalen *et al.*, 2004; Kitayama *et al.*, 2004), O'Shea *et al.* suggest the majority of stars produced from primordial gas may form in this way. The enrichment of the interstellar medium resulting from the dispersal of the diffuse remnants of the supernovæ of such stars will promote star formation by providing additional coolants, particularly atomic carbon and oxygen.

Once star formation has begun, therefore, it is likely to proceed rapidly and quickly

resulting in the formation of stars with significant quantities of elements formed not in BBN, but in previous generations. Both type 1a and type 2 supernovæ contribute their own individual nucleosynthetic signatures to the interstellar medium. For the supernovæ of all but the most massive stars, these signatures are the result of the nuclear reactions that power the star over the course of its lifetime. For extremely massive (and population III) stars, however, the energy of the supernova breaks down atomic nuclei before a second stage of nucleosynthesis occurs in the ejecta. In addition to enrichment of the ISM by supernovæ the complicated mixing processes and mass loss from intermediate mass stars in the later stages of their lives result in mass loss from the star, and this can be an important source of metals. Once the process of mixing the products of such processes into the interstellar medium has begun, the signature of a single supernova is obscured.

It is therefore easiest to follow the history of star formation not in individual stars, but in terms of a universal star formation rate. Recent observations have revealed that the star formation rate of the Universe is now in decline from its peak; Lilly *et al.* (1996) and Cowie *et al.* (1999) suggest that the current universal star formation rate is a factor of 3-15 below that at a redshift of  $z=1$ . The universal average star formation rate earlier than  $z=1$  remains controversial, however. The best known attempt to constrain its evolution was made by Madau *et al.* (1996) who, despite deriving only lower limits on the star formation rate from the Hubble Deep Field, concluded that it declines beyond a redshift of  $1 \leq z \leq 2$ . Steidel *et al.* (1999), in contrast, find no difference between the star formation rate derived for a sample of galaxies at  $z \sim 3$  and that for another sample at  $z \sim 4$ . Their result is shown in figure 1.5. They suggest that there is no obvious peak in star formation activity, and explain the difference between their results and those of Madau *et al.* by differences in the treatment of dust extinction (see Bell (2002) for a review). A recent attempt to resolve the discrepancies was made by Glazebrook *et al.* (2003) who used a sample of star-forming galaxies selected from the Sloan Digital Sky Survey. As with previous observers, their determination of the SFR was based on the rest-frame UV (accessible in the optical at  $z=0$ ) which is believed to have as its source young stars and hence should be proportional to the star formation rate. A double power law parameterization (due originally to Baldry *et al.* (2002)) is used with star formation assumed to begin at a redshift of  $z = 5$ .

$$SFR \propto \begin{cases} (1+z)^\beta & \text{for } z < 1 \\ (1+z)^\alpha & \text{for } 1 \leq z < 5 \\ 0 & \text{for } z \geq 5 \end{cases}$$

Although the observations are not of sufficient quality to constrain a unique fit, evidence from the SDSS supports a range of solutions with  $2 < \beta < 3$  and  $0 < \alpha < 1$ , consistent with a small drop in star formation rate or no drop at all at redshifts beyond 1. These results depend on the assumption of uniform, universal Salpeter IMF (Salpeter, 1955), and fail to distinguish between star formation in different galaxies or galaxy types. It is also possible to use the luminosity of a source in the far infra-red as an indicator of star formation, and this will be discussed in section 6.3.

Support for a constant star formation rate from a redshift of 1 to  $z \sim 3$  is also provided by observations of galaxies which have photometric redshifts determined by observations with the Spitzer Space Telescope; Pérez-González *et al.* (2005) find that at low redshift the star formation rate density is dominated by galaxies which are dim in the infrared, with the contribution from galaxies with  $L_{\text{IR}} > 10^{11}L_{\odot}$  increasing between  $z \sim 0$  up to  $z \sim 2.5$ . Ultraluminous infrared galaxies (ULIRGs) with  $L_{\text{IR}} > 10^{12}L_{\odot}$  are increasingly important at redshifts above 1.3. The presence of these sources in the Spitzer survey is particularly important as (relatively) local ULIRGs are almost invisible in the rest frame UV, due to huge attenuation by the large quantity of dust associated with these objects.

Wherever stars are forming, the process will be governed by the physical processes of gravitational collapse. The best observational studies of star formation, however, come from the Milky Way, and so chapters 2, 3 and 4 present investigations into Milky Way star forming regions. Chapter 2 presents an analysis of the way in which chemical models can be used to constrain one particular physical parameter, the cosmic ray ionization rate. Chapter 3 contains the results of a molecular survey of a particular young star-forming region, L134A, while Chapter 4 presents a novel explanation for existing observational features in accelerated (faster than free fall) collapse. Looking beyond our Galaxy, Chapter 5 presents observations of the nearby starburst, M82, and the results of chemical and (more traditional) population synthesis models are compared. Chapter 6 contains an application of astrochemical models initially developed for the Milky Way to the distant Universe, specifically to the second generation of stars. Chapter 7 is an analysis of the likely sites of star formation, the systems which are seen in the local Universe as massive elliptical galaxies, while Chapter 8 presents a brief outline of the future directions for this work.

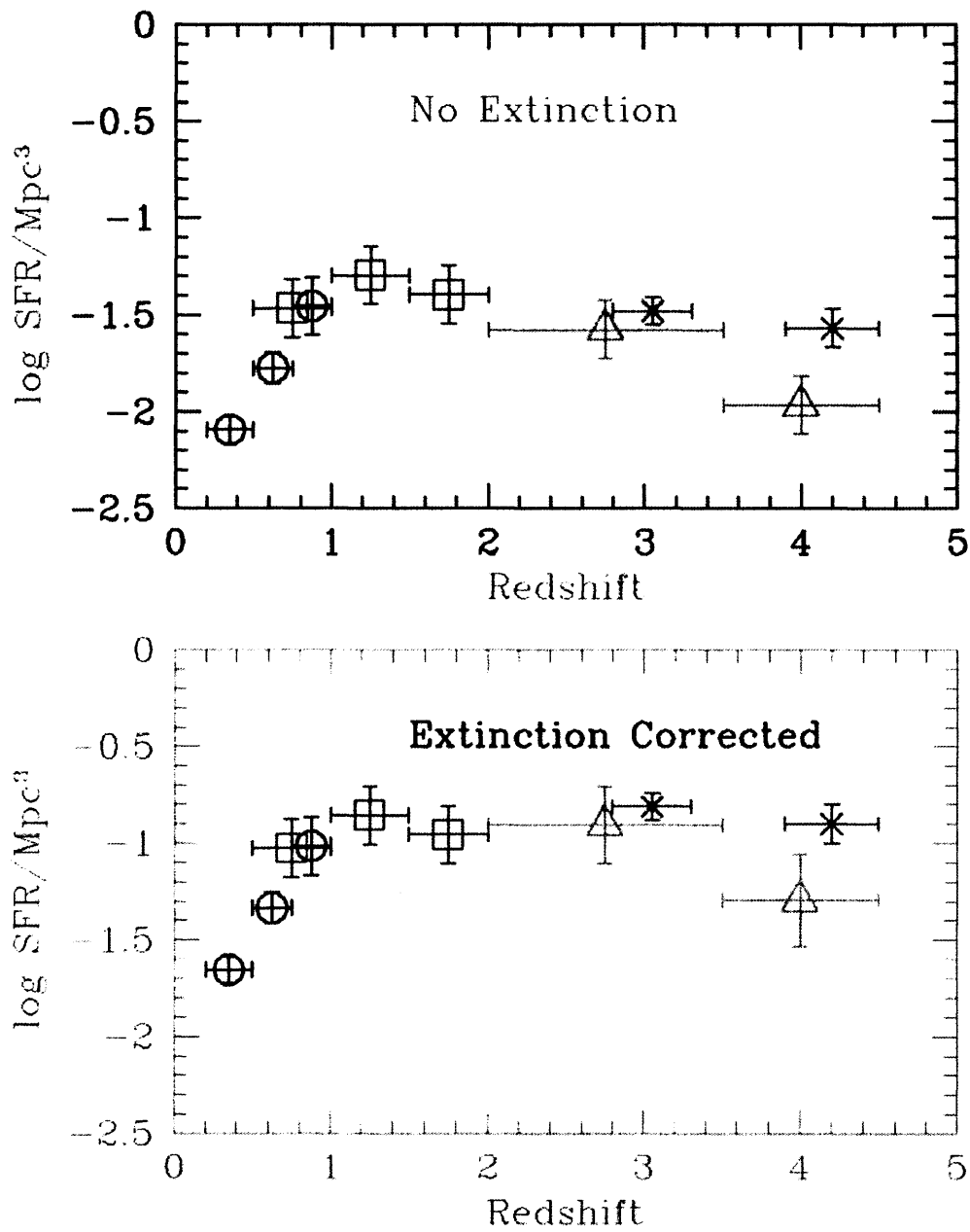


Figure 1.5: The history of UV luminosity density and hence star formation as determined by Steidel *et al.* The raw data is shown in the top figure, while the lower figure includes an attempt to correct for the effect of extinction by interstellar dust.

## 1.5 Definition of common symbols

I have attempted to define symbols as and when they appear. However, it is necessary to give here the definition of several parameters - most of them cosmological - which appear throughout, without further definition. A billion is always  $10^9$  (not the older, British standard,  $10^{12}$ ).  $c$  is the speed of light in a vacuum so that  $c \approx 3 \times 10^8 \text{ ms}^{-1}$ ,  $h$  is the Planck constant and  $k_B$ , unless otherwise stated, is the Boltzmann constant.

$m_e$ ,  $m_p$  and  $m_h$  are the electron, proton and hydrogen masses respectively. Following astronomical convention,  $\odot$  represents solar values so that  $1M_\odot$  is one solar mass and so on.  $z$  is used throughout to represent redshift, while  $Z$  is the overall metallicity.  $k_i$  is used throughout to represent the rate coefficient for reaction  $i$ .

A given observer in an expanding universe will see a nearby observer, a distance  $D$  away, receding at a velocity of  $H(t)D$  where  $H(t)$  is the Hubble constant, parameterized by  $h$  defined such that  $H_0 = 100h \text{ km s}^{-1} \text{ Mpc}^{-1}$ .

The critical density can then be defined as the density needed for the Universe to have zero curvature, given by

$$\rho_c(t) = \frac{3H^2(t)}{8\pi G}. \quad (1.26)$$

The ratio of the total density in a particular component with energy density  $\rho$  to the critical density is then defined as

$$\Omega = \frac{\rho}{\rho_c}. \quad (1.27)$$

## CHAPTER 2

---

# Astrochemical models : Determining the cosmic ray ionization rate

*This chapter is based on Lintott & Rawlings 2006, published in Astronomy & Astrophysics, 448, pp.425-432*

## 2.1 Introduction

In this chapter, I aim to examine the accuracy of the methods which are commonly used to constrain the rate of cosmic-ray induced ionization in the molecular clouds which provide the sites for star formation. Cosmic rays are high energy particles observed across a wide range of energies. The primary component appears to be protons, but atomic nuclei from across the periodic table and electrons and positrons are also seen. The shielding effect of the Earth's atmosphere means that 'primary' cosmic rays can only be observed in space, although fragments do reach the planet's surface as a matter of course. The distribution of cosmic rays on the sky is isotropic (Meyer, 1969), although this is most likely a result of scattering by galactic magnetic fields. This makes determining the source of these high energy particles extremely difficult, but the consensus is that the particles are accelerated to high velocities by the shock waves associated with supernovæ (the basic process is described in Bell (1978)).

In diffuse clouds the ionization fraction is likely to be determined by the exposure of the cloud's material to the interstellar radiation field. Inside a dark cloud, however, the primary mechanism for ionization will be the collision of neutral species with rapidly

moving cosmic ray particles (CRPs). This has important consequences for the cloud, as the level of ionization within a dark cloud may determine whether it is stable against the gravitational collapse which leads to the formation of protostellar objects. This is true if magnetic fields permeate the cloud, in which case the process of collapse is likely to be controlled by the coupling between the ions (which are tied to the magnetic field lines) and the neutral species. This applies to clouds undergoing quasi-static contraction<sup>1</sup> both via ambipolar diffusion (see section 1.1.2) and turbulent dissipation. Ruffle *et al.* (1998) investigated these processes and showed that the apparent stability of low extinction ( $A_v < 3$ ) clumps in the Rosette Molecular Cloud could be explained in terms of photochemically-driven high ionization levels, which in turn inhibit the damping of Alfvén waves which provide turbulent support. In fact, the sharp decline in fractional ionization which occurs at extinctions of  $A_V \approx 2 - 3$  is, according to Ruffle et al., associated with the distinction between starless and star-forming cores.

Aside from their effect on the equilibrium level of ionization, cosmic rays play a very important rôle in the physics of the interstellar medium. For example, they are an important source of heating in dark molecular clouds (Goldsmith and Langer, 1978). These dark clouds are highly opaque to optical and ultraviolet (ionizing) interstellar radiation (see, for example, the study of Alves *et al.* (2001) of the canonical dark cloud: Barnard 68), yet they are known to contain a wide variety of atomic and molecular ions (e.g. Di Francesco *et al.* (2002)). Although dust grain surface chemistry is extremely important in both dark and diffuse clouds (most significantly in the synthesis of H<sub>2</sub>: see section 1.2) the chemistry within dark clouds is driven by gas phase reactions. The most significant of these (particularly for oxygen and nitrogen-bearing species) are ion-neutral reactions. The initial source of this ionization (in the absence of the interstellar radiation field) must be cosmic ray particles; in the case of diffuse media the initiating reaction is



(where, as throughout this section, ‘crp’ stands for ‘cosmic ray particle’).

In dense molecular clouds, however, approximately 97% of impacts of cosmic ray particles on H<sub>2</sub> lead to the formation of H<sub>2</sub><sup>+</sup> (Hartquist and Williams, 1995) via the reaction

---

<sup>1</sup>The term ‘quasi-static contraction’ is usually applied to the collapse of individual, isolated cores such as those believed to be responsible for low-mass star formation.



This is then followed by the rapid reaction



Subsequently, the  $\text{H}_3^+$  ion drives chemical networks based on reactions between ions and neutral molecules (see section 2.2).

As a result of these reactions, nearly every cosmic-ray induced ionization quickly creates a  $\text{H}_3^+$  ion which can then react, typically, with an abundant metal, such as oxygen or nitrogen. The rate coefficient for equation 2.2,  $\zeta$ , is therefore a key parameter in models of dark cloud chemistry. For example, the relevant timescale for a cosmic-ray ionization induced chemistry to reach equilibrium is of the order of the fractional abundance of the reacting metals (approximately  $10^{-4}$ ) divided by  $\zeta$ . A value of  $\zeta = 1.3 \times 10^{-17}\text{s}^{-1}$  is often quoted in the literature as a ‘standard’ value appropriate for star forming regions, although in most cases only an order of magnitude accuracy is appropriate. In some sources, much higher values of  $\zeta$  have been inferred. For example van Dishoeck and Black (1986) derive a minimum value of  $\zeta = 8 \times 10^{-16}\text{s}^{-1}$  in *o* Per. Generally, studies such as that of Federman *et al.* (1996) or van der Tak and van Dishoeck (2000) indicate that  $\zeta = 10^{-16} - 10^{-17}\text{s}^{-1}$  per hydrogen atom.

Assuming for now a ‘standard’ value of  $\zeta \sim 10^{-17}\text{s}^{-1}$ , I note that the typical chemical timescale for a dark cloud is approximately  $10^6$  years. The standard method of deriving an ‘observed’ value of  $\zeta$  from molecular abundance ratios assumes that chemical equilibrium has been achieved. Is this assumption valid? The free-fall collapse timescale of a typical gas cloud is  $3.4 \times 10^7 n^{-0.5}$  years (Spitzer, 1978) where  $n$  is the gas density. For a typical dark cloud density of  $10^3 - 10^4\text{cm}^{-3}$ , a dynamical timescale of  $3.4 \times 10^5 - 10^6$  years is obtained which is approximately the same order as the chemical timescale. It is not clear, therefore, that a star-forming core which is in the process of collapsing, or which has only recently collapsed will have reached chemical equilibrium.

In contrast, the rates of ionization have been clearly established for diffuse clouds, largely via observations of OH and HD (see below). It is tempting, therefore, to assume that the cosmic ray ionization rate for diffuse clouds can be applied to dark clouds and

so avoid the problems discussed above. However, even in diffuse clouds there seems to be very considerable variation in  $\zeta$  from source to source. Thus, in a careful study based on  $\text{H}_3^+$  observations in  $\zeta$  Per, McCall *et al.* (2003) deduce that  $\zeta$  must be as high as  $1.2 \times 10^{-15} \text{s}^{-1}$ . Le Petit *et al.* (2004), however, find that their model (based on the PDR model of Le Bourlot *et al.* (1993)) reproduces the observed abundances of  $\text{H}_3^+$  and other important species, particularly OH, HD and the atomic/ionic balance for species such as carbon and sulphur in this source while using  $\zeta = 2.5 \times 10^{-16}$ .

There seems no *a priori* reason to assume that  $\zeta$  is the same in diffuse and denser dark clouds which may also have ordered magnetic fields in addition to having interiors shielded from external radiation. Most matter in a molecular cloud is essentially sterile, in that stars form only from a small fraction of the mass of a cloud (Leisawitz *et al.*, 1989). Most of this mass exists in regions of low extinction and is effectively in a photon-dominated region (Evans, 1999). Thus, most diffuse clouds are either supported against gravitational collapse, or else are transient objects that are dispersed before collapse and subsequent star formation can occur. This in turn implies that if dark, dense clouds form from diffuse clouds, they may retain some degree of the chemical identity of their precursors. The ionization fraction of a dense core may depend not simply on the current ionization rate, but on the rate at each point in its past. If so, it seems that we cannot simply assume that all ionization in dense clouds is due to impacts of cosmic ray particles.

In this section, I aim to assess the implications of the assumption of chemical equilibrium on the inferred cosmic ray ionization rate in molecular clouds which, as we have seen, may be evolving on timescales which are short compared to the time required for chemical equilibrium to be established.

## 2.2 Estimates of the cosmic ray ionization rate, $\zeta$

The usual methods of estimating the cosmic ray ionization rate employ a technique which is both semi-analytical and semi-empirical. Thus what is, in reality, a complex chemistry with many alternate routes to the formation of many species, is simplified to a small number of primary reactions. The absolute abundances, or abundance ratios, of key tracers are then interpreted through the use of simple analytic expressions in order to obtain a value for  $\zeta$ . In practice, whilst many of the abundances required in the resulting expressions are directly measurable (such as those for CO,  $\text{HCO}^+$  and  $\text{H}_3^+$ ), others are

unobservable (e.g. H<sub>2</sub>O) or else observational data exist only for a small subset of sources. Consequently, the values used as input to the calculations are a combination of observed quantities and the predictions of often complex chemical models, which will in turn have been compared to those abundances which are observable. However, both the derivation of the analytical expressions *and* the abundances obtained from models almost invariably, as discussed above, depend on the assumption of chemical equilibrium. Therefore, for the reasons stated above, it is possible that they may not reliably yield accurate values for  $\zeta$ .

Lepp *et al.* (1987) used the relationship between the abundances of (observable) OH and H<sub>3</sub><sup>+</sup>, together with the equilibrium relationship between  $n$  (H<sub>3</sub><sup>+</sup>) and  $\zeta$  (see equation 2.20) to deduce constraints on  $\zeta$  in dense, dark interstellar clouds. This analysis was fundamentally based on the assumption that the photodissociation of H<sub>2</sub>O by cosmic-ray induced ultraviolet photons is a major (in fact, the dominant) source of OH in dark clouds, with a rate that can be given by  $800\zeta/(1 - \omega)$  s<sup>-1</sup> where  $\omega$  is the grain albedo as suggested by Sternberg *et al.* (1987).

The abundances of most carbon-bearing species in diffuse clouds are not sensitive to  $\zeta$  (Pickles and Williams, 1981), and as discussed above the best estimators of  $\zeta$  come from observations and models of the OH and HD abundances (e.g. van Dishoeck and Black (1986), Federman *et al.* (1996)). The entry into the oxygen chemistry is different in these sources than in dense molecular environments. The source of O<sup>+</sup> is cosmic ray ionization of hydrogen atoms (Wagenblast and Williams, 1996) and resonant charge exchange with oxygen atoms.



This reaction is followed by reaction with H<sub>2</sub> and dissociative recombination,



whilst the HD is formed via the route given by the reactions



Thus the abundances of both OH and HD are, in this reaction scheme, directly proportional to  $\zeta$ . Studies using this reaction network yield values of  $\zeta \sim 10^{-17} - 10^{-16}\text{s}^{-1}$  for the rate of cosmic ray ionization of H atoms in diffuse clouds (Federman *et al.*, 1996); the spread of values being partly due to genuine variations between sources and partly attributable to different assumptions being made for different sources. The latter may derive from differences in the temperatures and the background radiation fields (particularly, the authors note, in the UV) which are only loosely constrained by observations. Federman *et al.* (1996) also comment that any estimate of  $\zeta$  which is based on the chemistry of HD will be acutely sensitive to the elemental abundance of deuterium which is used in the model, and to the inclusion or otherwise of production mechanisms beyond the standard gas phase reactions. For example, the endothermic reaction between oxygen and molecular hydrogen is possible in shocked regions. If reactions such as this become important, then it is obvious that the link between the cosmic ray ionization rate and the OH abundance (used in another of their estimators) becomes weakened.

If localised heating, for example through the action of shocks, is present then the reaction



can occur (Hartquist *et al.*, 1980), in which case these methods overestimate the value of  $\zeta$ .

An alternative estimator which avoids this problem, based on the  $\text{H}_3^+$  abundances, is often used. In diffuse clouds,  $\text{H}_3^+$  is formed by reactions 2.2 and 2.3 and lost through dissociative recombination:



This approach can be undermined by uncertainties in the value of the dissociative recombination rate co-efficient, and the electron density (which can only be determined indirectly).

In diffuse clouds, the main loss channel of simple molecular species is photodissociation and the implied timescales for this process are of the order of 300 years, significantly less than the dynamical timescales. In addition, the chemistry and rate-coefficients are

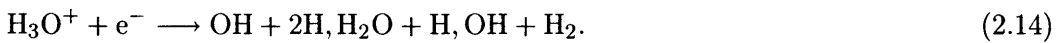
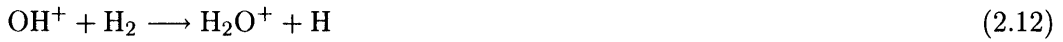
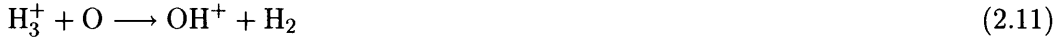
well-defined. For these reasons, the inferred ionization rates are believed to be reasonably robust (Hartquist and Williams, 1995). (Although see the discussion in section 2.1 regarding the rates derived by McCall *et al.* (2003)).

In dark clouds, the reactive species  $\text{H}_3^+$  provides important entries into the ion-neutral chemistry.  $\text{H}_3^+$  is usually more easily detected in its deuterated form,  $\text{H}_2\text{D}^+$ , to which it is linked via the deuterating reaction



This reaction also leads to the deuteration of molecular ions, such as  $\text{DCO}^+$ , which can then be used to constrain the fractional ionization if the deuterium to hydrogen ratio is known (or can be assumed) (Caselli *et al.*, 1998).

As an example, the oxygen chemistry follows a simple route via the following reaction network:



The other major reactions which destroy  $\text{H}_3^+$  are reaction with water



followed by dissociative recombination (equation 2.14) and reaction with CO, which in turn leads to the formation of  $\text{HCO}^+$ :



which (Savage and Ziurys, 2004) is then destroyed through dissociative recombination



reaction with water,



and charge transfer with elements with low ionization potential,



The last of these reactions is particularly important in determining the ionization level of dark clouds. In metal-poor dark clouds, such as those in dwarf galaxies or the early Universe, it is possible for  $\text{HCO}^+$  to be the dominant ion. However, the radiative recombination rates for elemental ions such as  $\text{Na}^+$  and  $\text{Mg}^+$  are very slow. In un-depleted regions, therefore, the reactions shown in equation 2.19 can effectively result in a higher, yet still stable, ionization level.

Williams *et al.* (1998) used observations of  $\text{C}^{18}\text{O}$ ,  $\text{H}^{13}\text{CO}^+$  and  $\text{DCO}^+$  and a steady state chemical model to derive a mean value of  $\zeta = 5 \times 10^{-17} \text{s}^{-1}$  towards 23 low-mass cores. The cores were selected as high extinction spots in nearby dark clouds, and the sample includes sources both with and without associated IRAS sources. The  $[\text{DCO}^+] / [\text{HCO}^+]$  ratio is relatively insensitive to  $\zeta$  but strongly dependent on the electron density (Guelin *et al.*, 1977), and so was used to deduce the ionization fraction. However, in low mass pre-protostellar cores such as these, the ionization can be enhanced not only by cosmic rays, but as a result of the presence of newly-formed stars (which are X-ray sources) and by the penetration of external UV (see section 6.3), if the clouds are inhomogeneous. Bergin *et al.* (1999) also used observations of  $[\text{DCO}^+] / [\text{HCO}^+]$  to infer the fractional ionization within massive dark cores in Orion; in such sources cosmic rays rather than x-rays or UV are believed to be the dominant source of ionization. Both of these studies initially allowed

$\zeta$  to vary within a limited range of  $1 - 15 \times 10^{-17}\text{s}^{-1}$ .  $\zeta$  was then further constrained by the necessity of achieving thermal balance at the temperatures and densities of the sources being considered, recognising that cosmic rays are the dominant source of heating in protostar-less cores.<sup>2</sup> Following this initial discussion, Bergin *et al.* (1999) subsequently adopted a value of  $\zeta = 5 \times 10^{-17}\text{s}^{-1}$  for all nine of their modelled sources.

However, the results of studies which use these techniques are complicated by the fact that the fractional ionization and  $\zeta$  are only partly independent of each other and both also depend on free parameters such as the oxygen and carbon depletion, the abundance of metals with low ionization potential and the density. Caselli *et al.* (1998) performed a detailed study of the ionization fraction,  $X(e^-)$ , and  $\zeta$  in dense cores. They compared simple analytical expressions for these quantities, dependent on two abundance ratios ( $[\text{DCO}^+]/[\text{HCO}^+]$  and  $[\text{HCO}^+]/[\text{C}^{18}\text{O}]$ ) and the free parameters mentioned above, with the predictions of a more elaborate chemical model which was then allowed to evolve until a steady state was reached. They found reasonably good agreement between the two methods, particularly for low cosmic ray ionization rates ( $\zeta < 10^{-17}\text{s}^{-1}$ ). In addition, they also noted that the abundance ratios used do show considerable time-dependence on timescales shorter than  $10^5$  years. As the sources that they modelled are quiescent cores (taken from the survey of Butner *et al.* (1995)) they assume that all are older than this critical timescale, justifying the use of models which make use of chemical equilibrium. Their chemical model also assumed that the physical conditions within each core remained constant, but in a dynamically evolving system the appropriate chemical timescales may be longer and the initial conditions less well constrained.

The steady state abundances of  $\text{HCO}^+$  and  $\text{H}_3^+$  were modelled by van der Tak and van Dishoeck (2000), who further assumed that the abundances of both  $\text{H}_2\text{O}$  and  $\text{O}_2$  are low (due to freeze out), unless  $T > 100\text{K}$  when mantle sublimation occurs. They found that the value of  $\zeta$  inferred from estimators based on the chemistry of  $\text{H}_3^+$  is systematically higher than that inferred from the  $\text{HCO}^+$  abundances. Noting that  $\text{HCO}^+$  traces dense gas (its critical density is  $10^5\text{cm}^{-3}$  (Seaquist *et al.*, 1998)), they speculate that the main cause of the discrepancy is the presence of otherwise undetected intervening clouds which lie along the line of sight. Given that their model considers only the steady-state, we suggest

<sup>2</sup>Field *et al.* (1969) suggest that such heating takes place both directly, via interactions between charged species in the gas and cosmic ray particles, and indirectly, in the form of energy imparted to electrons liberated by ionization of previously neutral species.

that a significant contribution may lie in the non-equilibrium character of the chemistry.

As described above, in contrast to diffuse clouds, the relevant timescale in dark clouds is approximately  $10^6$  years, which may be longer than the dynamical timescale. Moreover, there is increasing evidence to suggest that many of the structures in the interstellar medium are more dynamically active than had been previously believed. Thus, for example, Elmegreen (1999) and Hartmann *et al.* (2001) have suggested that many of the translucent clumps detected in CO are transient. This has prompted the development of plausible magneto-hydrodynamic models of transient structure formation (e.g. Falde and Hartquist (2002)). Garrod *et al.* (2006a) go so far as to represent dark molecular clouds as nothing more than an ensemble of transient clumps, few of which ever reach a density great enough to trigger permanent collapse. These models explain the presence of small, non-gravitationally bound clumps, which are found to have lifetimes of  $\sim 10^5$  years. This timescale is significant as it is less than the time taken for the complete conversion of atomic to molecular hydrogen and for chemical equilibrium to be established. The chemical implications of an initially H-rich chemistry were investigated by Rawlings *et al.* (2002) who identified strong chemical signatures of such a non-equilibrium H<sub>2</sub>:H ratio (see chapter 3). In a cloud of density  $\sim 10^4 \text{ cm}^{-3}$  the dynamical (free-fall), chemical and freeze-out timescales are all comparable ( $\sim \text{few} \times 10^5$  years) so that the temporal and spatial variations of molecular abundances are expected to be sensitive to the parameters of the model (Rawlings, 2003). Ward-Thompson *et al.* (2006) have argued that the typical lifetime of a starless core is of the order of  $10^6$  years, comparable with the chemical timescale and longer than the models suggested above. For any individual core under observation, however, it remains a difficult task to determine an age, and we would expect a significant proportion of any sample to have ages which are significantly shorter than the mean lifetime.

In this chapter, therefore, we suggest that in dynamically evolving regions the origin of the ionization can be ambiguous. Specifically, a significant fraction of the ionization that is inferred for dark clouds may be a ‘fossilised’ remnant remaining from diffuse cloud conditions. In other words, the dark cloud carries chemical signatures of its more diffuse nascent state prior to establishing dark cloud chemical equilibrium. If this is true, then the inferred ionization rates for these objects may be incorrect *unless* it can be shown that the objects are significantly older than the longest relevant chemical timescale.

## 2.3 Chemical indicators of $\zeta$ in dark clouds

As discussed in the previous section, the chemical networks within dark molecular clouds are well-known and, in their early stages, follow a reasonably linear chain of reactions. Without recourse to complex chemical models, it is possible to identify the key formation and destruction channels for those species which are sensitive to the value of  $\zeta$ . This simplification has been used in the determination of  $\zeta$  via the use of simple analytical expressions derived from a knowledge of the relevant chemical species. We investigate the validity of two well-known analytical expressions for  $\zeta$ , given below.

1.  $\zeta_1$  is based on the abundance of  $\text{H}_3^+$  (see e.g. Lepp *et al.* (1987)).  $\text{H}_3^+$  is primarily formed by cosmic ray ionization (2.2) and rapid reaction with  $\text{H}_2$  (2.3). In dense environments it is mainly lost through reactions with  $\text{O}$ (2.11),  $\text{H}_2\text{O}$ (2.15) and  $\text{CO}$  (2.16). Thus in equilibrium

$$\zeta_1 = \frac{n(\text{H}_3^+)}{X(\text{H}_2)} [k_{16}X(\text{CO}) + k_{11}X(\text{O}) + k_{15}X(\text{H}_2\text{O})]. \quad (2.20)$$

2.  $\zeta_2$  is based on the  $\text{HCO}^+$  abundance (see e.g. van der Tak and van Dishoeck (2000)).  $\text{HCO}^+$  is formed by the reaction of  $\text{H}_3^+$  with  $\text{CO}$  (2.16) and primarily lost through dissociative recombination (2.17) and reaction with water (2.18). Thus, after substituting for  $n(\text{H}_3^+)$  from equation 2.20 we obtain

$$\zeta_2 = \frac{n(\text{HCO}^+) [k_{16}X(\text{CO}) + k_{11}X(\text{O}) + k_{15}X(\text{H}_2\text{O})]}{k_{16}X(\text{CO}) X(\text{H}_2)} \times [k_{17}X(e^-) + k_{18}X(\text{H}_2\text{O})]. \quad (2.21)$$

In these expressions, the subscripts of the rate coefficients ( $k_i$ ) refer to the reaction numbers given in the previous section, and the fractional abundance of a species is defined to be the ratio of its number density to the total hydrogen density. For a species X this is given by

$$X_i = \frac{n(X)}{n(H) + 2n(H_2)}. \quad (2.22)$$

## 2.4 The model

The accuracy of both estimators for  $\zeta$  was investigated using a one-point model of the time-dependent chemistry. The model treats protostellar clouds as being of uniform density and temperature, both of which are allowed to change with time in three distinct phases of evolution.

1. *Phase I:* Diffuse cloud conditions (column density,  $n_0 = 100\text{cm}^{-3}$ , temperature,  $T = 100\text{K}$  and initial visual extinction  $A_{v0} = 0.5$ ) apply. The system is allowed to evolve chemically with constant density and temperature until no species' abundance changes by more than 0.1% in an individual time step. At this point we deem equilibrium to have been reached.
2. *Phase II:* The spherically symmetric and homogeneous cloud undergoes free-fall collapse to a specified terminal density of (usually)  $n_{max} = 10^5\text{cm}^{-3}$ . Initially, the collapse is assumed to occur isobarically so that the temperature is inversely proportional to the number density, subject to the constraint that the temperature does not fall below some minimum value (usually  $T_{dark} = 10\text{K}$ ). As the collapse is assumed to be both spherically symmetric and homogeneous, the extinction  $A_v$  is given by

$$A_v = A_{v0} \left( \frac{n}{n_0} \right)^{\frac{2}{3}}. \quad (2.23)$$

3. *Phase III:* Once the terminal density is reached, the cloud is allowed to relax to chemical equilibrium in dark cloud conditions (constant density and temperature,  $T_{dark} = 10\text{K}$ ).

The chemical model includes 87 gas-phase and 36 solid-state chemical species, comprising the most commonly observed species and composed of the elements hydrogen, helium, carbon, nitrogen, oxygen, sulphur and sodium. They are linked through a network of 1265 chemical reactions with rates taken from the UMIST99 ratefile. The elemental abundances used are given in table 2.1.

These values are broadly representative of cosmic abundances, with a depletion factor of 0.5 included for carbon to account for the composition of the dust grains. Recent observations (e.g. Meyer *et al.* (1997)) have suggested that nitrogen and oxygen also

Species	Abundance/ $X(H)$
He	0.1
C	$1.87 \times 10^{-4}$
N	$1.15 \times 10^{-4}$
O	$6.74 \times 10^{-4}$
S	$8.00 \times 10^{-6}$
Na	$2.00 \times 10^{-6}$

Table 2.1: Elemental abundances by number, relative to hydrogen

Reaction	Rate coefficient ( $\text{cm}^3\text{s}^{-1}$ )
$k_2$	$2.08 \times 10^{-9}$
$k_3$	$8.0 \times 10^{-10}$
$k_{15}$	$5.9 \times 10^{-9}$
$k_{16}$	$1.7 \times 10^{-9}$
$k_{17}$	$1.1 \times 10^{-7} \times (300/T)$
$k_{18}$	$2.5 \times 10^{-9}$

Table 2.2: Rate coefficients for key reactions ( $\text{cm}^3\text{s}^{-1}$ )

depleted by 50% in diffuse clouds. However, including this extra depletion results in only minor changes to the results.

Two extremes of metallicity were investigated; high (as in table 2.1) and low (as in table 2.1 but with the abundances of sulphur and sodium - the representative low ionization potential metals - reduced by a factor of 0.01x). These values are consistent with those used by Caselli *et al.* (1998).

The rate coefficients,  $k_i$ , for key reactions (2.2, 2.3, 2.15, 2.16, 2.17 and 2.18) are taken from UMIST ratefiles (Millar *et al.* (1991, 1997)) and are given in table 2.2.

It should be noted, however, that since this study is concerned with the comparison of analytical indicators with modelled abundances (rather than a comparison of model results and observations), both of which depend on the same rate coefficients, the results are not sensitive to the adopted values of  $k_i$ .

Radiation is expected to pass rapidly through such regions of intermediate extinction, which may form part of the structure of the clumps, and in any case the collapse is rapid so that the core as a whole quickly changes from low to high extinction. No attempt

has therefore been made to model the details of the photochemistry, other than through the normal dependence of photochemical reaction rates on extinction. The exception is the assumption that H<sub>2</sub> is self-shielding against photodissociation at all times whilst photoionization of C and photodissociation of CO can only occur in low-extinction (i.e. the diffuse cloud conditions of phase I).

Other than the formation of H<sub>2</sub> (for which  $k_{dust} = 1.6 \times 10^{-17} \text{ cm}^3 \text{s}^{-1}$  as in Rawlings *et al.* (1992)) in the standard model only gas phase chemistry has been considered. However, models in which gas-phase species were allowed to freeze out onto the surface of the grains once the extinction rose above some critical value ( $A_{v,crit} \sim 3$ ) were also studied. As the sources considered are dense and cold (and therefore pre-protostellar) we do not need to consider the effects of surface chemistry; return to the gas phase of species contained in ice mantles is unlikely to be efficient. (The discussion in section 1.2 for details of desorption without heating is unlikely to apply to the species whose abundances directly affect  $\zeta_1$  or  $\zeta_2$ .)

## 2.5 Results

### 2.5.1 Evolution with time

The evolution of selected species for a typical run is shown in figure 2.1. The chemistry starts from primarily atomic abundances appropriate for diffuse cloud conditions. As the cloud collapses and becomes both denser and more opaque to photodissociating radiation, the chemistry adjusts to the molecule-rich and lower ionization state which is characteristic of dark clouds.

In order to assess the validity of the analytical estimators of  $\zeta$  introduced in section 2.3, the logarithmic ratio of the rates inferred from each of the two analytical expressions ( $\zeta_1, \zeta_2$ ) to the ‘true’ value used as an input to the chemical model ( $\zeta_{true}$ ) is calculated.

$$R_i = \log_{10} \left( \frac{\zeta_i}{\zeta_{true}} \right) \quad (2.24)$$

is then plotted as a function of time. Thus, if  $\zeta_i$  were to accurately reflect the real cosmic ray ionization rate, devoid of any contaminating sources of ionization, then  $R_i$  would be zero.

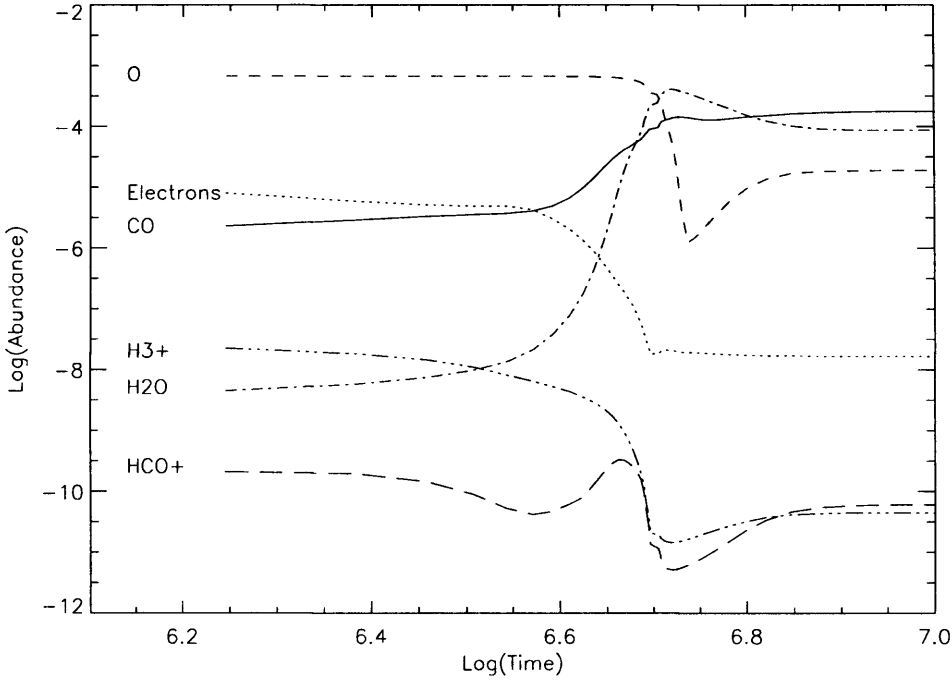


Figure 2.1: The evolution of the fractional abundances, relative to hydrogen, of key species used in the determination of the cosmic ray ionization rate. In this model, the cosmic ray ionization rate is  $\zeta_{true} = 1 \times 10^{-17} \text{ s}^{-1}$ , and the final temperature and density are 10 K and  $10^5 \text{ cm}^{-3}$  respectively.

Collapse ends approximately at  $\text{Log}(\text{time}/\text{years})=6.6$

Results are shown in figure 2.2 for runs of the model which have  $\zeta_{true} = 10^{-18}, 10^{-17}, 10^{-16}, 10^{-15}$  and  $10^{-14}$ .

The first thing to note about these results is that, at late times (in phase III, once dynamical evolution has ceased) the curves all converge to values of  $R_i$  close to zero. This is rather reassuring in the sense that (although the estimators are based on huge simplifications of large chemical networks) the expressions are remarkably accurate indicators of the cosmic ray ionization rate for a wide range of ionization rates *only when the twin assumptions of chemical equilibrium and dynamical steady state are appropriate*.

It is also encouraging that whilst there are clearly very large discrepancies during earlier phases of collapse, the expressions give accurate results almost as soon as the collapse phase is halted, with no notable relaxation period. If it can be determined from observations that a core has finished its collapse, therefore, the cosmic ray ionization rate can be reliably estimated.

However, during the collapse phase (phase II) obvious and significant discrepancies

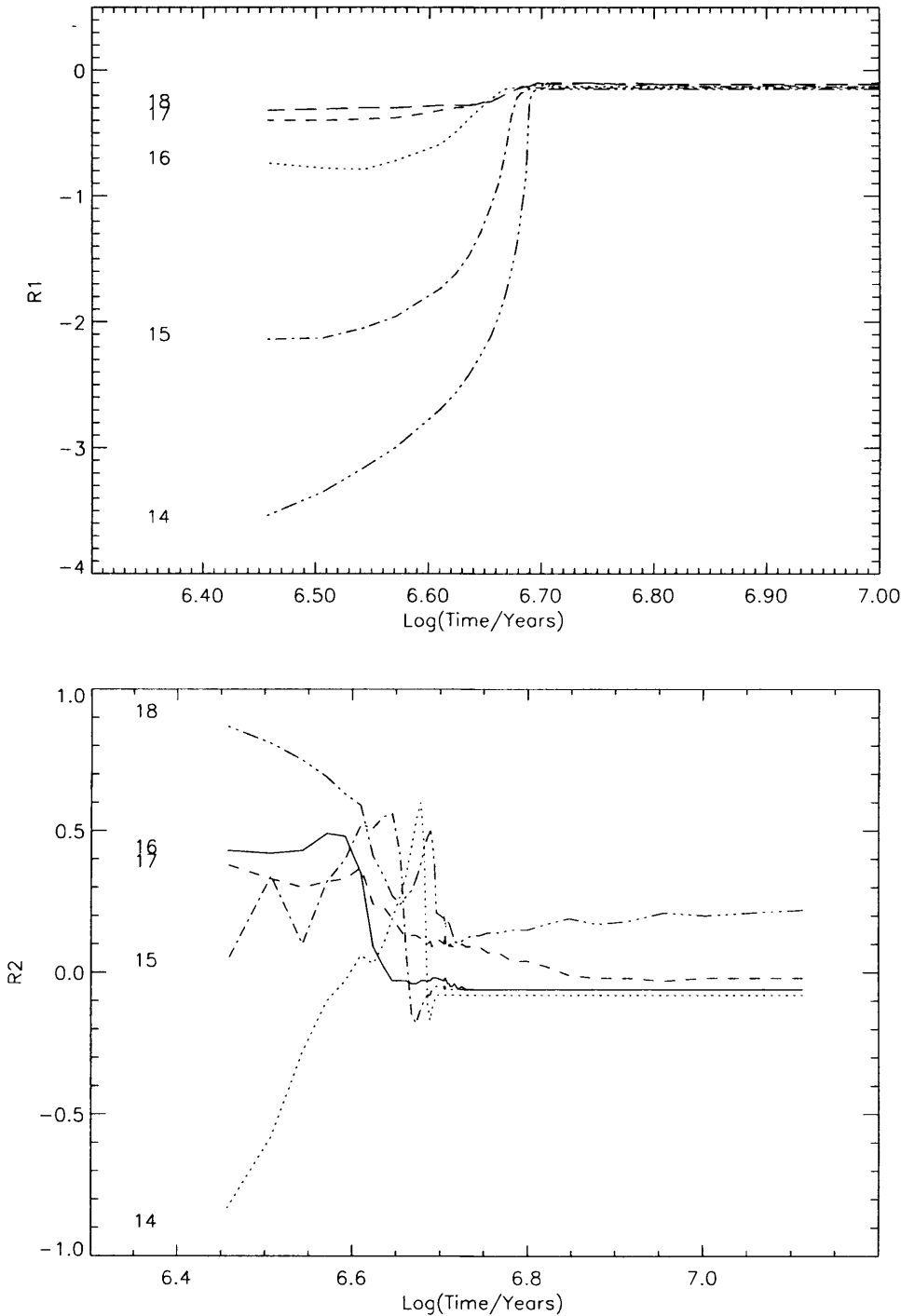


Figure 2.2: The variation of (a)  $R_1$ , and (b)  $R_2$  with time during phases II (collapse) & III (post-collapse) for several values of the cosmic ray ionization rate ( $\zeta_{true}$ ). The labels on each curve correspond to  $-\log(\zeta_{true})$ . Note that  $R_1$  has a much larger range than  $R_2$ .

are present.  $\zeta_1$  consistently underestimates  $\zeta_{true}$ . For the lower ionization rates, this is only by a factor of  $\sim 2 - 3$ , but if  $\zeta_{true}$  were to be as high as  $10^{-16}$  or  $10^{-15}\text{s}^{-1}$  (as in the work of McCall *et al.* (2003) toward  $\zeta$  Per) then the underestimate is much larger. In fact, it can be as large as a factor of  $10^3$ .  $\zeta_2$  is derived incorporating additional reactions in the same network which provides the motivation for  $\zeta_1$ , and thus inherits the underestimates of  $\zeta_1$ . It is also extremely sensitive to the abundances of species such as H<sub>2</sub>O, HCO<sup>+</sup> and especially CO (see equation 2.21). These abundances change dramatically during the collapse phase (and would change more directly if freeze-out was included in the model; see below). The complex structure visible in the lower panel of figure 2.2 is partly attributable to this chemical complexity and is partly a result of inaccuracies in the numerical integration. As with  $\zeta_1$ , the magnitude of the discrepancies are largest in the early stages of collapse. Although  $R_2$  is more inconsistent than  $R_1$  and may over- or underestimate  $\zeta$ ,  $R_2$  spans a smaller range ( $\sim -1$  to 1) than  $R_1$  for the values of  $\zeta_{true}$  investigated here. The smaller values of  $\zeta_{true}$  ( $< 10^{-16}\text{s}^{-1}$ ) are *overestimated* by  $\zeta_2$ , whilst the larger values are *underestimated* by  $\zeta_1$ . From these results it would seem that  $\zeta_2$  would always be  $\geq 10^{-17}\text{s}^{-1}$ , even though  $\zeta_{true}$  may be somewhat smaller.

### 2.5.2 Sensitivity to free parameters

The sensitivity of the results to the various free parameters in the model was investigated. These include the terminal density ( $n_{max}$ ), final temperature ( $T_{dark}$ ), the choice of initial conditions which correspond to diffuse cloud equilibrium or purely atomic abundances, the inclusion of freeze-out, the metallicity and the rate of collapse in phase II.

In models where the final density ( $n_{max}$ ) was varied by up to two orders of magnitude,  $R_1$  was found to be approximately 10% closer to zero for smaller values of  $\zeta_{true}$  whilst  $R_2$  was found to be insensitive to  $n_{max}$ , varying by less than a few percent.

A range of post-collapse temperatures ( $5 < T_{dark} < 20\text{K}$ ) was investigated for a test case with  $\zeta_{true} = 10^{-16}\text{s}^{-1}$ . The effects on  $R_1$  were small ( $\sim 20\%$ ) and are restricted to the early stages of collapse. In these early stages  $R_1$  is larger (closer to zero and hence  $\zeta_1$  is more accurate) whereas the opposite effect is seen in the behaviour of  $R_2$ . The dependence on  $T_{dark}$  is even more marginal and is also restricted to early times. Lower final temperatures result in  $R_2$  being closer to zero and hence more accurate in determining  $\zeta_{true}$ .

It has been shown (Rawlings *et al.*, 2002) that the evolution of the chemistry may be

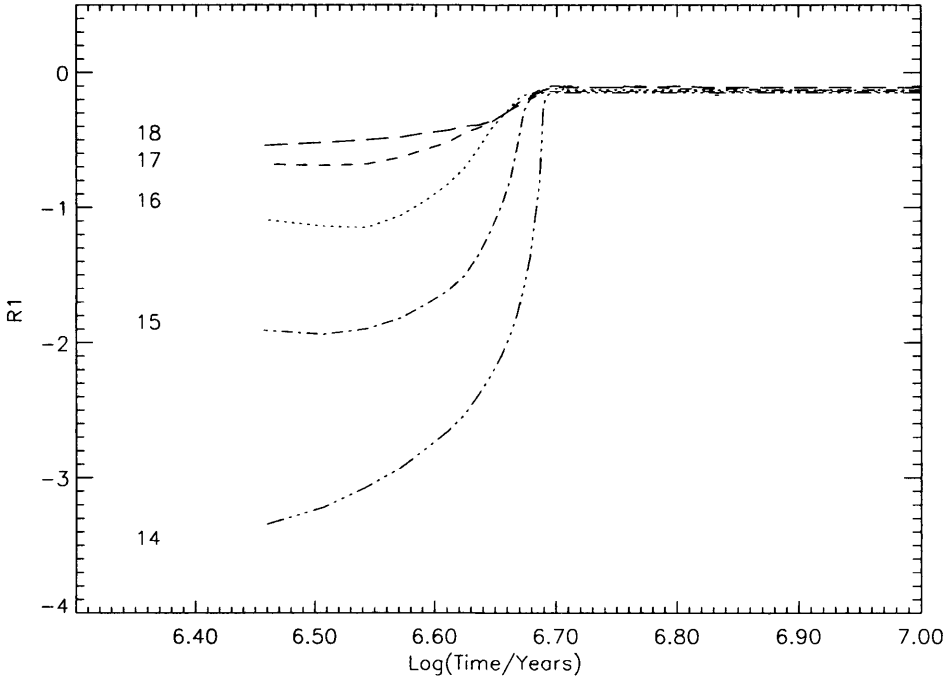


Figure 2.3: Variation of  $R_1$  with time for a model in which the chemical initial conditions (Phase I) are characterized by an atomic gas with no  $\text{H}_2$  present. As before, the labels on each curve correspond to  $-\log(\zeta_{true})$ .

sensitive to the assumed initial conditions, particularly the  $\text{H:H}_2$  ratio. In the standard model it is assumed that the gas is initially characterized by diffuse cloud conditions, with all hydrogen in molecular form. To investigate the possible effects of differing initial conditions on the validity of the  $\zeta$  estimators calculations were also performed with initially atomic gas. In other words,  $\text{H}$ ,  $\text{He}$ ,  $\text{C}^+$ ,  $\text{N}$ ,  $\text{O}$ ,  $\text{S}^+$  and  $\text{Na}^+$  are present with no  $\text{H}_2$  present. This is an extreme case; in reality, even the youngest cores are likely to have some molecular hydrogen present.

$R_2$  is hardly affected by the choice of initial conditions, but some differences are seen in the behaviour of  $R_1$  (figure 2.3). For large values of  $\zeta_{true}$ ,  $\zeta_1$  is larger by a factor of  $\sim 10$ , making it more accurate in the early stages of phase II. For smaller values of  $\zeta_{true}$  ( $< 10^{-15} \text{s}^{-1}$ ) the differences are marginal.

Estimates of  $\zeta$  and the fractional ionization are closely linked (as the fundamental assumption is that all ionization is due to cosmic rays), and the latter will also be affected by the assumptions that are made concerning the metallicity of the gas. Therefore, in addition to the standard model a ‘low metallicity’ model was considered in which the

abundances of the two low ionization potential metals considered in the model (sulphur and sodium) are reduced by a factor of 100 (to  $8 \times 10^{-8}$  and  $2 \times 10^{-8}$  respectively).

The results show a remarkable insensitivity to the metallicity and, as noted above, only a relatively small dependence on the initial conditions. This helps confirm the hypothesis first suggested in section 2.1; that estimators of  $\zeta$  are more sensitive to the dynamical status of the observed sources than any other individual chemical or physical parameter.

As discussed in chapter 4, observational evidence from high-mass star forming regions suggests that accelerated (i.e. faster-than-freefall) collapse may be taking place. In order to investigate how this would affect the determination of the cosmic-ray ionization rate, the rate of change of the density was artificially increased by a factor of two. (A factor of two is sufficient to produce the chemical changes discussed in the later chapter, and the work presented there also shows that there is little difference between a doubling of the rate of collapse and further acceleration.) This also had very minimal effects, further supporting the idea that observed discrepancies originate from near-instantaneous dynamical effects rather than the existence of longer term chemical hysteresis. In other words,  $\zeta_1$  and  $\zeta_2$  are influenced by the current dynamical state of the core, rather than its dynamical history. Whether the core is currently in the process of collapsing is more important than how long ago it began collapsing, for example.

Other factors investigated were the extinction, and the temperature of the cloud prior to collapse, neither of which had a significant effect. In summary, these results show that  $R_1$  and  $R_2$  are insensitive to the various free parameters, and are primarily determined by dynamical activity within the cloud.

The standard model did not include any form of gas-grain interaction apart from the formation of molecular hydrogen on grain surfaces, but the effect of this assumption was investigated via a model in which gas-phase species were allowed to freeze-out once  $A_v > 3.0$  mag. This value is approximately the critical value of the extinction required for ice water bands to be observed in the Taurus molecular cloud Whittet *et al.* (2001). In practice, this means that freeze-out commences during the collapse phase (phase II). No desorption from grains was included in the model. Results are shown for both  $R_1$  and  $R_2$  in figure 2.4.

Two clear conclusions can be drawn from these results. Firstly, if gas-grain processes are in operation - as is likely in the denser regions of the interstellar medium - then the analytical estimators *always* yield inaccurate values for  $\zeta$ , and secondly, the origins of

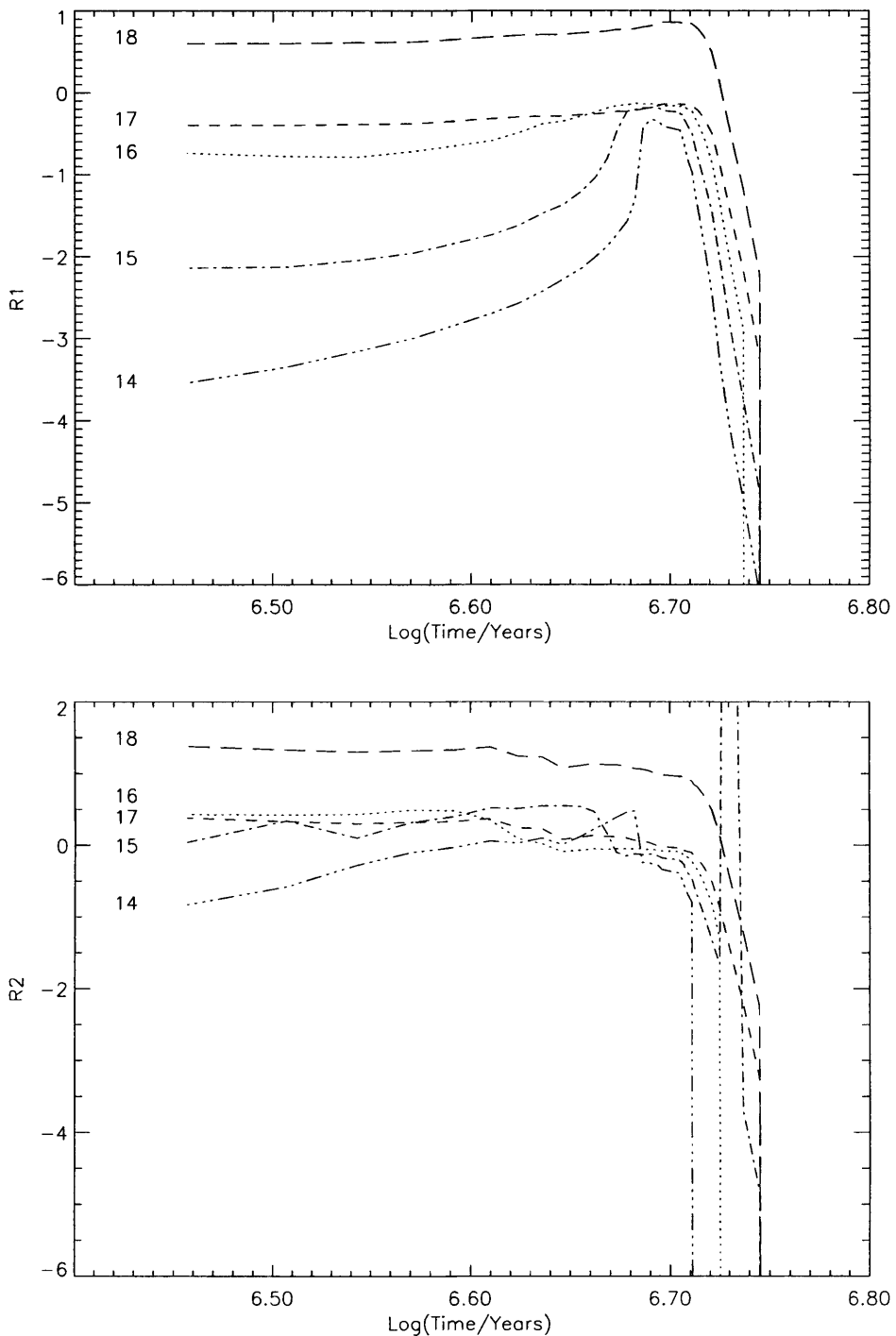


Figure 2.4: Variation of (a)  $R_1$  and (b)  $R_2$  with time for a model in which freeze-out occurs once  $A_v > 3.0$  mag. As before, the labels on each curve correspond to  $-\log(\zeta_{\text{true}})$ , and the same line style has been used for each  $\zeta_{\text{true}}$  in figure 4(b). The large jump in  $R_2$  at  $\text{Log}(\text{time}/\text{years})=6.74$  is an effect of numerical integration.

the discrepancies (deviations of  $R_i$  from 0) are separable; at early times, dynamic effects dominate over the ‘true’ ionization rate whereas at late time freeze-out - and not ionization - dominates changes in the abundances of crucial species. In other words, in the collapse phase the differences have a dynamical origin as in the gas-phase models, whilst in the static, post-collapse phase the differences are entirely a consequence of the freezing-out of molecules onto dust grain surfaces.

## 2.6 Discussion and conclusions

Two related methods of estimating the cosmic ray ionization rate,  $\zeta_{true}$  have been tested for a wide range of parameters. These were based on chemical networks centered on the reactions of  $H_3^+$  (with  $\zeta_2$  using an extended version of the chemical network used for  $\zeta_1$ ). In those cases where gas-grain interactions were ignored, chemical equilibrium is rapidly re-established after the end of collapse, and both analytical expressions give accurate measures of the true cosmic ray ionization rate as soon as dynamical activity has ceased. If freeze-out processes are important, then the analytical expressions are inaccurate at all times.

There are two components to the discrepancies between the analytical expressions for  $\zeta_1$  and  $\zeta_2$  and the true cosmic ray ionization rate  $\zeta_{true}$  (leaving aside the effect of freeze-out). Firstly, one must consider the fact that the analytical expressions are simplifications of a rather complex chemistry, and make allowance only for the dominant chemical pathways, and secondly the assumption of chemical equilibrium may not always hold. As noted in 2.5.1, it is however reassuring to see that - at late times and in the absence of freeze-out onto grains - the simple analytical expressions are reasonably accurate and the contribution from the first of the two problems is small. However, this will not always be the case, and the consequences have been investigated in some detail by Caselli *et al.* (1998) (see their fig. 9). The authors conclude that, even given the equilibrium approximation, the analytical expressions may overestimate  $\zeta$  by a factor of  $\sim 2 - 3$  for cases where  $\zeta_{true} \geq 10^{-17} s^{-1}$ .

In the models considered here, the same set of rate coefficients are used in both the analytical expressions and the full, time-dependent, models. Therefore, as the results are presented as the ratios of these quantities, they are reasonably robust and insensitive to the values of the adopted rate co-efficients.

In all of the cases investigated, however, the analytical expressions were found to be

very inaccurate in regions which are rapidly evolving or dynamically active. Discrepancies of several orders of magnitude are present, especially for the largest values of  $\zeta_{true}$ . Such conditions may, indeed, be common even in dark clouds that have previously been thought of as quiescent; there is an increasing body of evidence that suggests that dark molecular clouds are, not monolithic entities, but ensembles of clumps (and other sub-structure) that are not resolved by single-dish molecular line observations. For example, populations of sub-cores have been seen in two canonical dark cloud sources, TMC-1 (Peng *et al.*, 1998) and L673 (Morata *et al.*, 2003). Moreover, if these cores are not self-gravitating, but are transient entities of varying size, mass and dynamical behaviour. This picture has been supported by recent chemical models (Garrod *et al.*, 2006b) which identify the sub-cores as objects that grow and decay on timescales of  $\sim 10^6$  years.

Some sensitivity to physical parameters was found, in particular to the density reached at the end of the collapse. However, these effects are much smaller than the differences observed in the same core at different stages of its evolution. It can therefore be seen that these methods cannot accurately determine the cosmic ray ionization rate unless collapse can be definitely shown to have been completed. This forms an extremely challenging observational requirement as discussed in section 1.1.2.

Geballe *et al.* (2003) use the observed  $H_3^+$  abundance in several dark clouds to constrain the cosmic ray ionization rate. Oka *et al.* (2005) compare these measurements to their measurements of  $\zeta$  in diffuse clouds. However, the results presented in this section suggest that such a comparison is invalid unless the dark clouds being studied were sufficiently old for the dynamical effects revealed by our models to be unimportant and the dominant sources of ionization in the diffuse clouds were cosmic rays and not photo-ionization.

In their study of massive star forming regions, van der Tak and van Dishoeck (2000) found that the cosmic ray ionization rate derived from observations of  $H_2^+$  was larger than that deduced from observations of  $HCO^+$ . That is to say, models using  $\zeta$  from  $H_3^+$  observations resulted in a significant over-production of  $HCO^+$ . The authors speculated that, whilst the use of  $HCO^+$  probes only the densest molecular gas, contributions from foreground layers (e.g. in photon dominated regions or translucent clouds) may be responsible for the discrepancies. This is a valid explanation, but it should be noted that dynamical activity may help explain the discrepancy; the differences between the values of  $\zeta$  inferred from the  $H_3^+$  and  $HCO^+$  observations (effectively represented in the model presented in this chapter by  $R_1 - R_2$ ) depends on the ‘true’ value of  $\zeta$  and on the dynamical status of

the observed source. The more dynamically active the source, the greater the discrepancy.

In conclusion, it is possible that, if a reasonably full dataset of observations of key molecular tracers is available for any given source, the absolute values of  $\zeta_1$  and  $\zeta_2$  and the difference between  $R_1$  and  $R_2$  (and perhaps other analytical expressions for  $\zeta$ ) could be used to simultaneously constrain the true ionization rate *and* the dynamical status of the source. If it turns out that similar results are obtained for  $\zeta_1$  and  $\zeta_2$  then this is an indication that the observed cores are both dynamically quiescent and chemically ‘old’. If these conditions cannot be satisfied, then the use of chemical models to estimate the cosmic ray ionization rate should be treated with caution.

## CHAPTER 3

---

# L134A: A young H-rich star-forming region?

### 3.1 Introduction

Models of interstellar chemistry typically assume that hydrogen is exclusively in the form of H<sub>2</sub> at all times of interest in the evolution of a molecular cloud. So universal is this assumption that it is not usually stated explicitly. However, the timescale for the conversion of atomic to molecular hydrogen may, in cold conditions, be of the same order as the dynamical timescale for the collapse of some pre-protostellar cores. In such situations, therefore, young cores will be expected to have a H:H<sub>2</sub> ratio which is substantially different from the equilibrium value.

Specifically, Jura (1974) find that, at 100K, the timescale for the conversion of atomic hydrogen to H<sub>2</sub> is (when the removal of H<sub>2</sub> is ignored) given by

$$\tau_{\text{H} \rightarrow \text{H}_2} = 10^9 \times \frac{1 \text{cm}^{-3}}{n_{\text{H}}} \quad (3.1)$$

where  $n_{\text{H}}$  is the total number density of hydrogen nuclei. Hence a typical cloud with density of  $10^{3-4} \text{cm}^{-3}$  will reach an equilibrium ratio of H to H<sub>2</sub> in  $\sim 10^6$  years. It has been suggested (by e.g. Falle and Hartquist (2002)) that many of the clumps seen within giant molecular clouds form due to the action of magneto-hydrodynamic waves in a process which is a generic consequence of the presence of such waves whenever the ratio of the thermal to the magnetic pressures is small. If this model is correct, then a typical clump

would form in approximately  $10^7$  years. If the same mechanism forms dense cores, then the timescale is  $\sim 10^6$  years, suggesting that the equilibrium H:H<sub>2</sub> may not be reached once the core has been formed.

Indeed, it has long been known that atomic hydrogen can be observed within dense interstellar clouds. A recent survey of dark clouds, which used the Arecibo radio telescope, found that a large majority of such clouds in Taurus show HI narrow self-absorption (Li and Goldsmith, 2003) and that this atomic hydrogen is associated with the distribution of such molecules as OH, C<sup>18</sup>O and <sup>13</sup>CO. A more detailed survey of four clouds was made by Goldsmith and Li (2005) who find that the extent of the HI is close to but smaller than that of the <sup>13</sup>CO emission. Using their observations to derive a central density for the cloud, they are able to produce a simple model of the conversion of atomic to molecular hydrogen. For the sources in question (L1544, B227, L1574, CB45), they find that the ages of the clouds derived from the H:H<sub>2</sub> ratio are in the range  $3 - 10 \times 10^6$  years. Although these values are uncertain (depending, for example on the sticking coefficient of atomic hydrogen on the grain surface) it is clear from these observations too that dark clouds may still harbour a significant proportion of atomic hydrogen.

In their models of dark clouds rich in atomic hydrogen, Rawlings *et al.* (2002) (hereinafter RHWF) found that the chemistry of such objects is strongly dependent on the initial H:H<sub>2</sub> abundance ratio, with different chemical pathways being applicable in H-rich and H-poor environments. To give just one example, the reaction



which is not normally considered to be important in dark clouds dominates the formation of OH in H-rich models. Reaction with atomic nitrogen can then rapidly lead to further nitrogen chemistry and enhanced abundances not just of OH, but of NH<sub>3</sub> and HNC. Not all abundances are enhanced, and the formation of HCN and HCS, for example, are expected to be strongly inhibited in gas which is initially rich in atomic as opposed to molecular hydrogen (see section 3.4).

In this chapter we follow up these previous observational (van der Werf *et al.* (1988)) and theoretical (Rawlings *et al.*, 2002) studies which have suggested that one particular dense core - L134A - may be the type of object within which this unusual chemistry is dominant; for an object of its density the dynamical timescale is certainly less than

the timescale for the conversion of an initially diffuse cloud composed of purely atomic hydrogen to H<sub>2</sub>. This assertion, and the chemical model of RWHF are tested by the results of a small targeted molecular survey carried out with the James Clerk Maxwell Telescope (JCMT). The implications of this work may have important consequences in the ongoing debate as to whether protostellar collapse is essentially an isolated, quasi-static or driven, dynamically rapid process involving chemically young and transient structures.

Lynds 134 (L134) is a rather large cloud ( $\sim 1.7\text{pc}$ ) located at a distance of  $\sim 150\text{pc}$ , so that it has an apparent diameter of  $\sim 40$  arcminutes. Despite its large size and its proximity, L134 has not been subject to the same degree of chemical scrutiny as, for example, the star-forming cloud TMC-1. This is possibly because it has a very extended and irregular morphology (see figure 3.1) which has made it difficult to clearly delineate structures and thus constrain the physical parameters. However, one of the most significant chemical features of the cloud is that it exhibits strong absorption of the background galactic H<sub>I</sub> 21-cm emission, which implies the presence of cold atomic hydrogen within the cloud.

Moreover, several other molecular species have been observed within the cloud; the CO emission, for example, correlates well with the H<sub>I</sub> 21-cm absorption. This suggests that the atomic hydrogen co-exists with the molecule-rich gas (Mahoney *et al.*, 1976). These authors derive a CO excitation temperature of  $11.6 \pm 0.9\text{K}$ , a total molecular hydrogen column density (based on their CO column density) of  $N(\text{H}_2) = 3.9 \times 10^{21}\text{cm}^{-2}$  and a H:H<sub>2</sub> ratio of  $\geq 7.7 \times 10^{-3}$ . Tucker *et al.* (1976) find a clear correlation in the source between  $N(\text{CO})$  and total gas column density. Unlike Mahoney *et al.* (1976) who depended on an assumed conversion factor between CO and total gas density, the results of Tucker *et al.* are derived directly from the extinction as measured by star counts. That said, Mahoney *et al.* note that strong CO emission is seen in regions of low extinction ( $A_v \leq 1$ ) which calls into question the interpretation put upon these observations. Furthermore, all of these observations - and the inferences that are drawn from them - are subject to consideration of the low angular resolution of the surveys ( $\sim 2.5$  arcmin).

## 3.2 Observations

The previous studies discussed in the last section describe observations of the entire L134 complex in the CO J=1-0 transition. Focussing on just the L134A core, more recently Lee

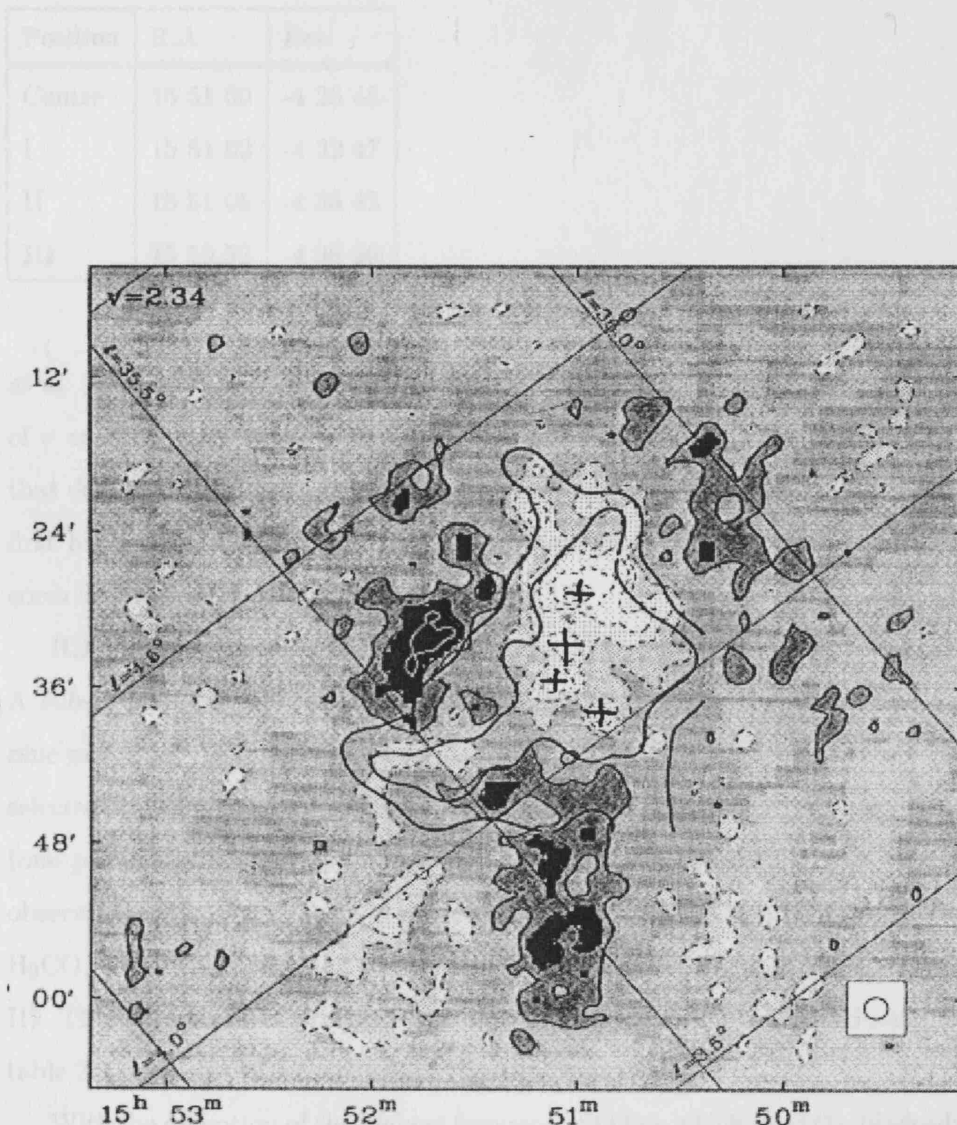


Figure 3.1: HI emission in L134 (from van der Werf *et al.* 1988). The circle in the lower right corresponds to the beam size ( $100''$ ), and the grey scale and contours correspond to main beam brightness temperatures. Grey scale transitions correspond to brightness temperatures of -6, -4.5, -3, -1.5, 1.5 and 3K (darker colours correspond to higher temperatures) and contours are drawn at these levels and at -7.5 and 4.5K. Negative contours are represented by dashed lines. The thick contours correspond to optical extinctions of  $2''$  and  $10''.3$ . Positions observed with the JCMT are marked with a cross. From top to bottom : Centre, Positions I, II and III

Position	R.A.	Dec
Centre	15 51 00	-4 28 48
I	15 51 02	-4 32 47
II	15 51 05	-4 35 42
III	15 50 52	-4 38 20

Table 3.1: All coordinates are B1950.0

*et al.* (2004) successfully detected both CS and DCO<sup>+</sup> in L134A, finding a local velocity of  $v = 2.78 \pm 0.01 \text{ kms}^{-1}$ . Mao and Sun (2005) studied the object in C<sup>18</sup>O, concluding that depletion occurs throughout most of the cloud. In the present paper, we present the first high resolution molecular studies of the region, concentrating on four small, dense cores detected in HI and identified in figure 3.1.

RHWF identified several molecular species as potential traces of the initial H:H<sub>2</sub> ratio. A subset of these were selected and attempts were made to observe the transitions of nine molecules (CN, SO, H<sub>2</sub>CO, C<sup>17</sup>O, HCN, HNC, C<sub>2</sub>H, C<sub>2</sub>S and CS) in four positions, selected from the denser regions of the van der Werf *et al.* (1988) HI map. Ten transitions (one per molecular species except for SO which was observed in two transitions) were observed both at the centre and at one other position (position III). Six species (CN, SO, H<sub>2</sub>CO, C<sup>17</sup>O, HCN and HNC) were also observed at two further positions (position I and II). The four observed positions are shown in figure 3.1, their coordinates are given in table 3.2 and a list of frequencies is given in table 3.2.

With the exception of the highest frequency SO line which used the heterodyne receiver RxB3<sup>1</sup>, all the observations were carried out using the heterodyne receiver RxA3<sup>2</sup> at the JCMT on Mauna Kea, Hawai'i. The half-power beam width is 20" (0.84pc at the distance of L134A) with receiver RxA3 and 14" (0.58pc) for receiver RxB3. Data were obtained on the nights of 2004 August 2,26,30,31, September 24-26, October 3, 5, December 19,21,22 and 2005 January 31, February 8,11,14-16, March 17, 27, April 16, 20. The data were reduced in the standard manner using the SPECX software package (Padman, 1990) and were converted to the  $T_{mb}$  scale using a main beam efficiency calculated, where possible, by observations of planets used as standard sources. The expected brightness temperature from a planetary observation, can be converted into an expected antenna temperature

<sup>1</sup>[http://www.jach.hawaii.edu/JCMT/spectral\\_line/Instrument\\_homes/RxB3/rxbman.html](http://www.jach.hawaii.edu/JCMT/spectral_line/Instrument_homes/RxB3/rxbman.html)

<sup>2</sup>[http://www.jach.hawaii.edu/JCMT/spectral\\_line/Instrument\\_homes/RxA3/a3i-info.html](http://www.jach.hawaii.edu/JCMT/spectral_line/Instrument_homes/RxA3/a3i-info.html)

Molecule	Transition	Frequency/GHz
CN	N=2-1	226.5964
	F=5/2-3/2	
	F=7/2-5/2	
SO	2(1)-1(2)	236.4523
	J=2(1)-1(0)	329.3855
H <sub>2</sub> CO	N=3-2	218.2222
C <sup>17</sup> O	J=2-1	224.7144
HCN	J=3-2	265.8864
HNC	J=3-2	271.9811
C <sub>2</sub> H	N=3-2	262.0415
C <sub>2</sub> S	N=4-1,J=3-2	236.2
CS	J=5-4	244.9356

Table 3.2: Frequencies observed using the James Clerk Maxwell Telescope. Frequencies were taken from the Lovas line list (<http://physics.nist.gov/cgi-bin/micro/table5/start.pl>).

using the theoretical efficiency for a perfect dish of

$$\eta_{\text{Gauss}} = 1 - 2^{-\frac{D^2}{B}} \quad (3.3)$$

where D is the apparent diameter of the planet and B the half-power width of the Gaussian beam. The expected antenna temperature is then  $T_{A,\text{exp}}^* = T_b \eta_{\text{Gauss}}$ , and the efficiency given by

$$\eta_{\text{Gauss}} = \frac{T_A^*}{T_{A,\text{exp}}^*} \quad (3.4)$$

For 2005 March 17,  $\eta_m b = 0.7$ , and where observations of planets were unavailable this was used as a standard efficiency.

### 3.3 Results

#### C<sup>17</sup>O

C<sup>17</sup>O was clearly detected in each of the four positions, at a velocity of 2.75 km s<sup>-1</sup> at the centre, and in positions I and III, and at a velocity of 2.88 km s<sup>-1</sup> in position II. Given

the clear detections, we have assumed that these represent the systematic velocities of the sources. There is a suggestion of fine structure visible in three of the positions, although the detection is marginal and the fine structure lines have not been used in the analysis below. The data are shown in figure 3.2. The apparent variation in linewidths is perhaps significant, and is indicative of the physical complexity of the source alluded to in section 3.1.

## HCN

HCN was not detected in the central position, or at position I or II. There was an extremely marginal detection ( $\sim 2\sigma$ ) at position III, which was modelled by a Gaussian with amplitude 0.064K and a width of  $0.21 \text{ kms}^{-1}$ . The data with the fit is shown in figure 3.3.

## HNC

The HCN to HNC ratio will prove to be an essential diagnostic of the presence of H-rich chemistry. HNC was not detected at either position I or position III. The (marginal) detections at the centre and at position III are shown in figure 3.4. The line at the central position was fitted by a Gaussian model with an amplitude of 0.049K and a width of  $0.32 \text{ kms}^{-1}$ , and that at position II by a Gaussian of amplitude 0.024K and width  $0.25 \text{ kms}^{-1}$ .

## CS and other molecules

No other transitions were successfully detected. These non-detections, when used to derive upper limits on molecular abundances, can be extremely significant, especially when compared with predictions from the modelling. As an example, our modelling (section 3.4.1) suggests that the abundance of CS is strongly time-dependent, and this species is therefore particularly important in distinguishing between (comparatively) early and late evolutionary times. Table 3.3 therefore includes limits on the CS column density obtained from our observations.

### 3.3.1 Deriving column densities and fractional abundances

In order to compare the observations shown in figures 3.2, 3.3 and 3.4 with the results of models, it is necessary to derive column densities and, ultimately, fractional abundances.

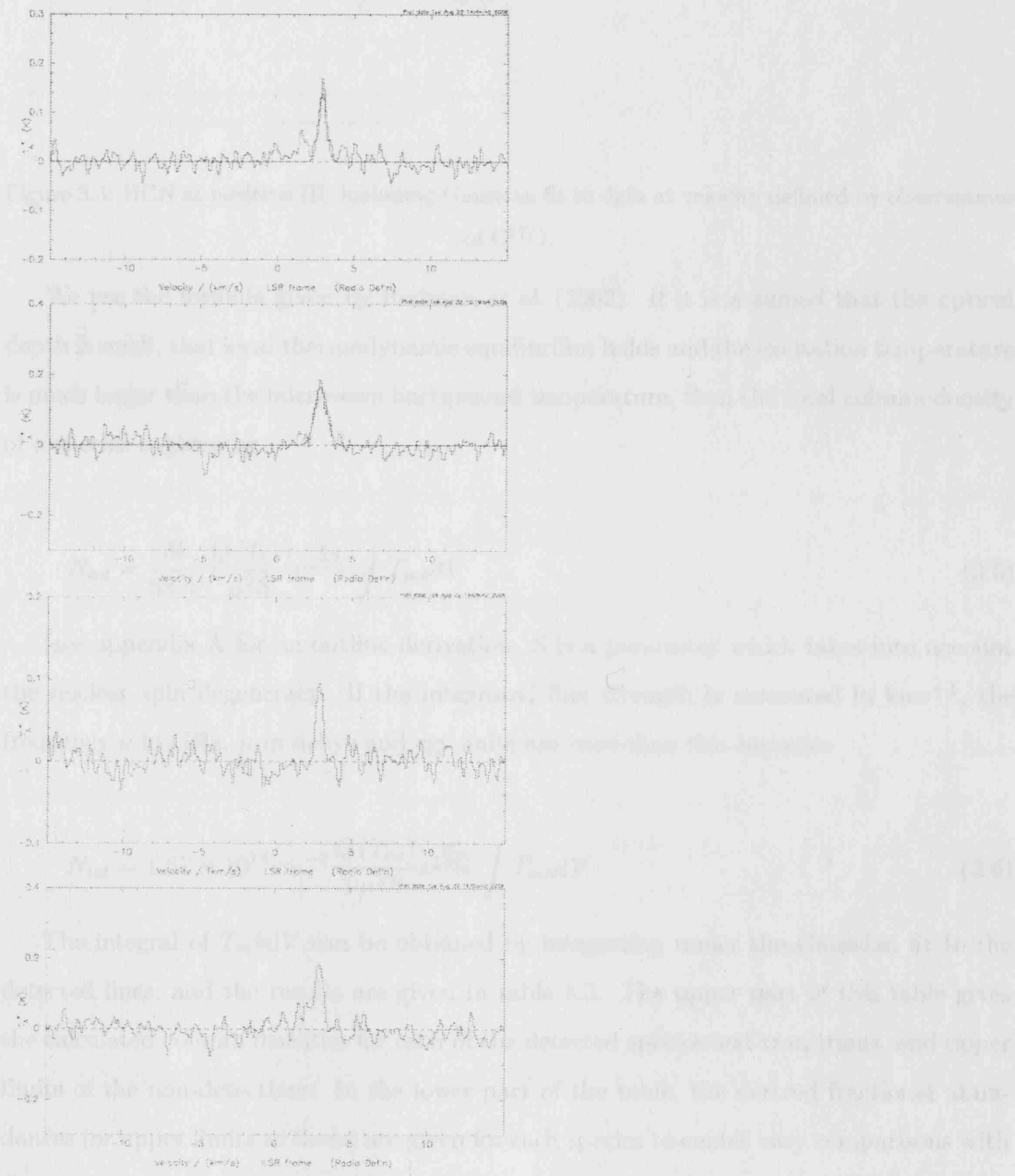


Figure 3.2:  $\text{C}^{17}\text{O}$  at (from top to bottom) centre and positions I, II and III. A polynomial baseline detected in either of the observations was subtracted from each observation.

that of HCN.

In order to derive the total column densities, total column density was integrated along the total column density along the line of sight. This is equivalent to a convolution

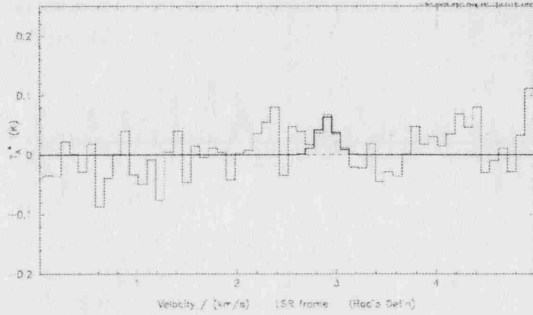


Figure 3.3: HCN at position III, including Gaussian fit to data at velocity defined by observations of C<sup>17</sup>O.

We use the formula given by Redman *et al.* (2002). If it is assumed that the optical depth is small, that local thermodynamic equilibrium holds and the excitation temperature is much larger than the microwave background temperature, then the total column density of a species is given by

$$N_{tot} = \frac{3k}{8\pi^3\nu} \frac{Q(T_{ex})}{\mu^2 S} e^{\frac{E_u}{kT_{ex}}} \int T_{mb} dV \quad (3.5)$$

(see appendix A for an outline derivation. S is a parameter which takes into account the nuclear spin degeneracy. If the integrated line strength is measured in km s<sup>-1</sup>, the frequency  $\nu$  in GHz,  $\mu$  in debye and cgs units are used then this becomes

$$N_{tot} = 1.67 \times 10^{14} \text{ cm}^{-2} \frac{Q(T_{ex})}{\nu \mu^2 S} e^{\frac{E_u}{kT_{ex}}} \int T_{mb} dV \quad (3.6)$$

The integral of  $T_{mb} dV$  can be obtained by integrating under the Gaussian fit to the detected lines, and the results are given in table 3.3. The upper part of this table gives the calculated column densities for each of the detected species and transitions, and upper limits of the non-detections. In the lower part of the table, the derived fractional abundances (or upper limits to them) are given for each species to enable easy comparisons with the model predictions presented below. In each case, the limits were derived by assuming that the line had the same shape as the detected lines of the same species. As CS was not detected in either of the positions at which it was observed, we use a line width equal to that of HCN.

In order to derive these fractional abundances, some assumptions need to be made about the total column densities along the line of sight. This is quite difficult for a source

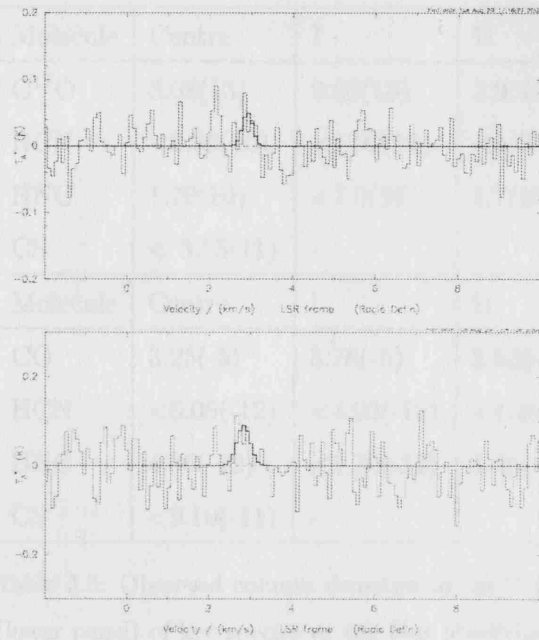


Figure 3.4: HNC at the centre and at position II, including a Gaussian fit to the data at a velocity defined by the observations of C<sup>17</sup>O.

such as L134A which clearly has a very complicated and clumpy structure. We have calculated fractional abundances by assuming that the total column density is given by  $N(H_2) \sim 3.9 \times 10^{21} \text{ cm}^{-2}$ , the value derived by Mahoney *et al.* (1976). This value, however, represents an average value for the whole L134 cloud - not just the L134A core - made from very low resolution (2.5 arcmin) observations. To deduce the total fractional abundance of CO, we have assumed a C<sup>17</sup>O:CO ratio of  $\sim 0.0004$ , reflecting the cosmic ratio of <sup>17</sup>O : <sup>16</sup>O.

### 3.4 Discussion

The most surprising result is that the derived column densities (and hence the fractional abundances) in table 3.3 are extremely low; indeed, they are much lower than those predicted by RHWF regardless of whether the H-rich or H-poor gas models are used. Other than C<sup>17</sup>O, HCN and HNC we have succeed in determining only upper limits from non-detections (and the detections of the latter two molecules are 2- $\sigma$  at best). There are several possible explanations for these results:

1. L134A may not be a singular entity, but may instead contain unresolved - perhaps hierarchical - substructure. This would be consistent with the complex observed

Molecule	Centre	I	II	III
C <sup>17</sup> O	5.08(13)	9.03(13)	3.95(13)	1.02(14)
HCN	<2.36(10)	<1.92(10)	<1.75(10)	5.33 (10)
HNC	1.70(10)	<7.0(9)	1.7(10)	< 1.0(10)
CS	< 3.55(11)	-	-	< 1.46(11)
Molecule	Centre	I	II	III
CO	3.25(-5)	5.78(-5)	2.53(-5)	6.55(-5)
HCN	<6.05(-12)	<4.92(-12)	<4.49(-12)	1.37(-11)
HNC	4.36(-12)	<1.79(-12)	4.36(-12)	<2.56(-12)
CS	<9.10(-11)	-	-	<3.74(-11)

Table 3.3: Observed column densities in  $\text{cm}^{-2}$  (upper panel) and derived fractional abundances (lower panel) of key species at the four observing positions. The format  $a(b)$  indicates a value of  $a \times 10^b$ . See text for description and assumptions.

morphology of the cloud (see figure 3.1). If this were to be the case, then the species and transitions that we have observed may originate from regions that are extremely compact and therefore subject to extreme beam dilution. By contrast, emission from CO, which has a low critical density, of  $\sim 10^3 \text{ cm}^{-3}$  for the J=1-0 transition (Narayanan *et al.*, 2005), is likely to come from both dense (unresolved) clumps and the inter-clump medium, so that its ‘true’ value is observed.

2. The core may be dynamically and chemically very young, whether or not it is rich in atomic hydrogen. If this were the case, then molecular abundances may not have had time to reach their predicted equilibrium values.
3. The total gas volume density inferred from the observations (e.g. Mahoney *et al.* (1976)) is  $\sim 10^4 \text{ cm}^{-3}$ , which is typical for a molecular cloud. This is less than the critical density for many of the transitions observed<sup>3</sup>, and so our assumption of local thermal equilibrium may significantly underestimate the abundances of these species

Of these suggestions, both (1) and (3) may help to explain the non-detections of CS, specifically. This molecule was not detected in either of the two positions in which observations were attempted. However, the data presented by Lee *et al.* (2004), who

<sup>3</sup>For example, the critical density of the CS J=5 → 4 transition is  $8.8 \times 10^6 \text{ cm}^{-3}$  and that for HCN 3 → 2 is  $7.8 \times 10^7 \text{ cm}^{-3}$  (Evans, 1999).

detected the J=3-2 transition, imply a column density of  $3 \times 10^{11} \text{ cm}^{-2}$ . This could imply, as suggested for CO in (1) above, that the CS detected by Lee, Myers and Plume is globally distributed and is in a large envelope surrounding the dense cores rather than in the dense cores themselves. Alternatively, as in (3), the density of the observed cores lies above the effective density required to excite J=3-2 but below that required to excite J=5-4. The critical density is defined as, for a transition between level  $j$  and level  $k$

$$n_{crit} = \frac{A_{jk}}{C_{jk}} \quad (3.7)$$

where  $A_{jk}$  and  $C_{jk}$  are the Einstein coefficients for excitation and deexcitation respectively, so that  $nC_{jk}$  is the rate per molecule of collisional deexcitation in level  $j$ .

Using values taken from Evans (1999), this explanation requires a density between  $8.8 \times 10^6 \text{ cm}^{-2}$  and  $4.6 \times 10^4 \text{ cm}^{-2}$  which is possible given the total gas density found by Mahoney *et al.* (1976).

It is possible to further investigate the possibility that the gas is not in local thermal equilibrium (option (3) above). To do this, the RADEX code described by van Langevelde and van der Tak may be employed.<sup>4</sup> For any particular line, the code assumes that the gas is optically thin, and thus predicts the relative populations of relevant energy levels. This solution allows the calculation of optical depths for transitions of interest, and a new guess at the extinction can then be calculated. The calculation can then be repeated iteratively until a self-consistent set of populations and optical depths are obtained. Using this code indicates that the C<sup>17</sup>O lines are optically thin as expected and that the excitation temperatures of the lines remain approximately equal to the ‘true’ temperature. For HCN and HNC, the code indicates that the excitation temperature in L134A for the 3-2 transitions are  $T_{ex} \sim 5 \text{ K}$ , supporting the suggestion that these lines are not thermalized, and that this may account for the low observed abundances.

Whatever the reason for the low abundances, we should attempt to compare them with the models. Two of the key predictions made for RHWF for H-rich chemistries are that, in a young core rich in H and relatively poor in H<sub>2</sub> then

1. the molecular abundances are generally lower
2. the HCN/HNC ratio is enhanced when compared to the more ‘normal’, H-poor case.

---

<sup>4</sup>RADEX is available online at [www.strw.leidenuniv.nl/~moldata/radex.html](http://www.strw.leidenuniv.nl/~moldata/radex.html) .

The latter difference occurs because the two isomers have different formation rates. HCN forms primarily via the reaction



and

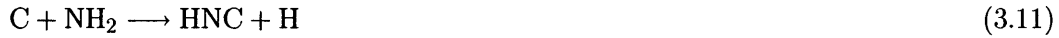


As mentioned above, the presence of large abundances of atomic hydrogen provides an effective loss route for CH, thus inhibiting the formation of other carbon bearing species. As the formation rate is proportional to the abundance of CH<sub>2</sub> and CH<sub>3</sub> HCN behaves like a carbon bearing species, and so is enhanced in H-poor models.

In contrast, nitrogen-bearing species are enhanced in H-rich chemistries. The higher OH abundances (see section 3.1) allow rapid initiation of nitrogen chemistry via the reaction:



NH<sub>2</sub> forms from the dissociative recombination of NH<sub>3</sub><sup>+</sup>, allowing the formation of HNC primarily via



and it is therefore enhanced in chemistries which are rich in atomic hydrogen.

Considering first of all the models presented by RHWF, it is quite clear that a comparison between the observed CO/HCN and CO/HNC ratios and those in the models is largely meaningless. The modelled abundances of CO are comparable to the observed values, but the observed abundances of both HCN and HNC are much lower than the predictions of any of the models. As suggested by the results for CS discussed above, we propose a model in which most of the CO lies in large, low-density clouds within which are embedded the dense cores to which our models can appropriately be applied.

A more useful test of the model lies, therefore, in the abundance ratio between species whose emission is likely to be restricted to the same physical regions. Fitting the observed

HCN:HNC ratio thus provides a stringent test of the models. The oft-mentioned fact that the observed column densities for both HCN and HNC are extremely low supports the conclusion of van der Werf *et al.* (1988) that the objects observed are young cores, which have not yet had time to reach high densities of many molecular species. Table 3.3 shows significant spatial variation in the HCN:HNC ration; the central core and position II have HCN:HNC<1, whereas at position III HCN:HNC>1. We therefore hypothesise that the central core and position II are young, and H-poor, whilst position III is an example of a young H-rich core. The peak of HCN abundance in the models in RHWF occurs in cores with an age of approximately  $\log(t/\text{yrs})=5$ . As expected, their model B (H-poor) is favoured for the centre and position II, whereas model A is ruled out. Although the CS observations are not used in testing the models (for the reasons given above), it is worth noting that each of these models produce low CS abundances.

### 3.4.1 Modelling

If L134A does indeed contain clumpy sub-structure or could be chemically young, or both, then it is necessary to consider the chemistry of less opaque objects at very early times. The model described in RHWF has thus been extended to consider earlier times ( $t < 10^3$  years), higher initial H:H<sub>2</sub> ratios and lower visual extinctions. The model employs a chemistry that is an enhanced version of that described by Rawlings and Yates (2001), and follows the time-dependent chemical evolution of some 117 chemical species and  $\sim 1620$  chemical reactions in a single, static fluid element in a dense ( $n \sim 10^4 \text{ cm}^{-3}$ ) and cold ( $T \sim 10\text{K}$ ) environment. The chemical network was selected to be similar to those used in studies of dark clouds, and cosmic abundances are used. Sodium and sulphur are assumed to be fully ionized, and the H:H<sub>2</sub> is model-dependent. As the young cloud is assumed to have been in a dark, dense state for only a relatively short time, freeze-out and surface chemistry are assumed to be unimportant, with the obvious exception of the conversion of H to H<sub>2</sub>. It was also assumed that the regions of interest lie well inside any PDR boundary layer that may exist, so that photodissociation of both H<sub>2</sub> and CO are suppressed along with the photoionization of atomic carbon. The cosmic ray ionization rate used was  $1.3 \times 10^{-17} \text{ s}^{-1}$ . Chemical rates were derived from the UMIST databases (Millar *et al.*, 1991, 1997).

Calculations were performed for high extinction ( $A_v = 100$ , models A-C) and low extinction ( $A_v = 3$ , models D-F) cases. The initial H:H<sub>2</sub> ratio was 10:1 in models A and D, 1:1 in models B and E, and  $\sim 0$  (ie all hydrogen in molecular form throughout) in

models C and F. Thus model C is broadly representative of the initial conditions usually adopted in chemical models of molecular clouds. Results for selected species at selected times are shown in table 3.4; the modelled fractional abundances of C<sub>2</sub>H and CN are not shown, but are between  $10^{-12} - 10^{-9}$  and  $10^{-9} - 10^{-8}$  respectively over the time interval of  $10^3 - 10^6$  years.

Comparing the results of models A-C with those models D-F it is apparent that the effects of a lower extinction ( $A_v = 3$ ) - of interest if the cloud being studied is very clumpy with much semi-transparent sub-structure - are small, except at late times ( $t \sim 10^5$  years). At these times, in all models, the abundances approach equilibrium values, and are essentially decoupled from the initial conditions. Thus, by the latest times shown, the abundances of HCN, HNC and CS are, as expected, approximately 10 times lower than in the darker clouds which have extinctions of  $A_v \sim 100$ . Comparing models A, B and C we see that the effects of increasing the H:H<sub>2</sub> ratio from 1:1 to 10:1 are marginal, and so the most useful comparison for our purposes is between B and C.

In these models, it can be seen that all of the molecular abundances gradually increase (in fact, all of the selected species show an increase in abundance with time in every model), and that the abundance ratios of HCN, HNC and CS relative to CO do not, as a consequence, change dramatically with time. On the basis of these calculations it would therefore seem that early-time, or low-extinction models, or those models which incorporate very low initial H<sub>2</sub> abundances are not by themselves sufficient to explain the observed abundance ratios.

In contrast, the HCN:HNC ratio does vary with time, and is particularly different at the earliest times in model C. These models thus support the conclusions of RWHF who found that the HCN:HNC ratio is able to discriminate between H-rich and H-poor scenarios at all but the latest times (i.e. discrimination is possible for  $t < 10^6$  years).

The model with extremely low H<sub>2</sub> predicted a HCN:HNC ratio which was consistent with the observed limits both at the centre and at position II, but also predicted an overabundance of CS.

### 3.5 Conclusions

The detections reported in this chapter are extremely marginal and it is clear that a deeper survey of the entire L134 cloud (with much larger spatial extent than these results) would

Model	Species	$10^3$ yr	$10^4$ yr	$10^5$ yr	$10^6$ yr
A	CO	-7.18	-6.02	-5.10	-4.13
	HCN	-12.62	-10.32	-9.03	-7.44
	HNC	-11.78	-9.21	-8.13	-8.08
	CS	-9.37	-7.68	-6.57	-5.76
B	CO	-7.54	-6.37	-5.42	-4.06
	HCN	-12.01	-10.52	-8.97	-7.22
	HNC	-11.52	-9.35	-8.11	-8.12
	CS	-9.39	-7.93	-6.82	-5.77
C	CO	-6.58	-5.54	-4.53	-3.79
	HCN	-9.11	-8.12	-7.20	-7.12
	HNC	-11.38	-9.73	-8.50	-8.02
	CS	-7.56	-6.71	-6.27	-5.61
D	CO	-7.19	-6.03	-5.12	-4.16
	HCN	-12.84	-10.57	-9.76	-8.56
	HNC	-11.80	-9.31	-8.59	-8.97
	CS	-9.39	-7.79	-7.42	-7.29
E	CO	-7.55	-6.38	-5.43	-4.08
	HCN	-12.08	-10.77	-9.82	-8.39
	HNC	-11.54	-9.46	-8.58	-9.12
	CS	-9.42	-8.05	-7.65	-7.31
F	CO	-6.60	-5.56	-4.54	-3.81
	HCN	-9.13	-8.27	-8.00	-8.49
	HNC	-11.41	-9.86	-9.26	-9.71
	CS	-7.60	-6.93	-7.31	-7.49

Table 3.4: Logarithmic fractional abundances of CO, HCN, HNC and CS as a function of time for models A-F. See text for a description of the models

be necessary to clarify the observations and their physical implications.

Despite these limitations, we find that the low absolute abundances and the abundance ratios of HCN:HNC are consistent with the expectations of a model which does not make the usual assumption for the chemical initial conditions, that all hydrogen is in the form of  $H_2$ . However, although these simple ratios are as expected, the individual fractional abundances of HCN and HNC, the abundances relative to CO and the apparent non-detection of CS, CN, SO and several other simple molecules expected to be present in significant abundances, pose severe problems. Several possible resolutions of these problems exist, all of which are not ruled out by the work presented here; either (a) L134A is composed of clumpy sub-structures, or (b) the volume densities of even the dense, molecule rich regions may be below the critical densities for some of the observed transitions (this is almost certainly a factor in the non-detection of CS), or (c) L134A is chemically very young indeed. In reality, the truth probably involves all of these possibilities and, whilst we have support for the hypothesis that the hydrogen rich parts of L134A are chemically young, more extensive observations of low energy transitions are necessary to disentangle the effects described above.

Using the results from a chemical survey of four dense areas of the star-forming cloud L134A, we have found evidence of chemical differentiation between individual dense cores. We note that any attempt to compare observations of such regions with models places a stringent requirement for high-resolution observations, in order to distinguish between neighbouring regions with different chemical compositions. In particular, of the three cores within which detections of multiple molecules have been obtained, we find tantalizing, but not conclusive evidence, that two can be characterised as being chemically young and hydrogen rich cores. This result suggests that the ‘standard’ assumption made (that the dynamical timescale for the formation and evolution of structures within molecular clouds is longer than the timescale for the conversion of atomic to molecular hydrogen) is not necessarily correct in all cases, and should not be assumed in astrochemical models of these objects.

The discussion here has focussed on one set of observations, of one particular star forming core. As discussed in section 3.1, there are other sources which are known to harbour significant quantities of atomic hydrogen, and detailed observation and modelling of these will allow the model to be refined. If significant deviations from equilibrium H: $H_2$  ratios can, in fact, be shown to exist in substantial numbers of young cores, then this

will have important consequences for astrochemical models of such sources. If the initial conditions in models which commonly assume that all the hydrogen is in molecular form are incorrect, then any so-called chemical clocks based on such models may need to be reset due to the changes in chemistry discussed above. Furthermore, if quasi-static models of star forming cores are correct, then the equilibrium H:H<sub>2</sub> density would be expected, regardless of the density of the core. The presence of large abundances of atomic hydrogen may thus provide a means of differentiating between quasi-static and dynamical collapse of such cores.

## CHAPTER 4

---

# Accelerated collapse in regions of high-mass star formation

*This section is based on Lintott et al. 2005, published in the Astrophysical Journal, 620, 795*

### 4.1 Introduction

Molecular lines are effective probes of physical conditions in star forming regions. The abundances of molecules together with their line profiles, give information about the physical state of the gas and its likely evolution during the collapse to form a star (Rawlings *et al.*, 1992). Methods based on observations of molecular lines have been used together with detections of dust continuum emission to probe regions of both low-mass and high-mass star formation (Pirogov *et al.*, 2006). Recent work has shown that the species used to trace dense gas may be significantly depleted in the central parts of dense cores. In low-mass star forming regions, for example, CS and CO do not trace the gas mass in the central cores. Aikawa *et al.* (2001) show a central ‘hole’ in the CO distribution in the prestellar core L1544, with a radius of 4000AU. Their later work (Aikawa *et al.*, 2003b) reproduces a wide variety of observed column densities by including surface chemistry, adding support to the supposition that such depletions are associated with the freeze-out of species such as CO. Bergin *et al.* (2001) find evidence for the gas phase depletion of CO and CS in the dense portions of a dark cloud, IC5146. The abundance reductions for both CO and CS in this object occur at extinctions of  $A_v \sim 12$  mag. Redman *et al.* (2002)

contrast CO J=2-1 measurements toward L1689B with SCUBA column densities, and find that 90% of the CO present in the central 5000AU of the core must have frozen onto the grains. This conclusion is only compatible with the core having existed for longer than a free-fall timescale. Finally, Tafalla *et al.* (2002) carry out a systematic study of five starless cores, and conclude that CO and CS ‘almost vanish’ near the centre of the cores. In all cases these species have a decrease in abundance of 1 or 2 orders of magnitude compared to those in the outer core and the authors interpret this as depletion of the molecules onto dust grains at densities of  $2 - 6 \times 10^4 \text{ cm}^{-3}$ .

Many of the studies cited in the previous paragraph include evidence that  $\text{N}_2\text{H}^+$  is an excellent tracer of the dust continuum emission even in the centre of the cores. A further example is given in the work of Caselli *et al.* (1999) which shows that, in L1544, ‘ $\text{N}_2\text{H}^+$  is concentrated close to the dust emission peak, whereas  $\text{C}^{17}\text{O}$  appears to trace a completely different component of the core’. Recognising the utility of  $\text{N}_2\text{H}^+$ , Caselli *et al.* (2002) and Bergin *et al.* (1999) use  $\text{N}_2\text{H}^+$  to map  $\sim 60$  low-mass cores.

One possible explanation for this behaviour is that the  $\text{N}_2$  molecules that drive the nitrogen chemistry do not freeze out onto dust grains as readily as some other species (Bergin and Langer, 1997). Species derived from  $\text{N}_2$  - including  $\text{N}_2\text{H}^+$  - would then remain present in the gas to higher densities, tracing its mass along with the dust continuum emission. In fact, astrochemical models require the ratio between the binding energies of  $\text{N}_2$  and CO to be between 0.5 and 0.75 in order to reproduce the observations discussed above. However, in recent lab work by Öberg *et al.* (2005) using pure ices this ratio is found to be  $0.923 \pm 0.003$ . In layered ices, a significant fraction of  $\text{N}_2$  does indeed desorb at lower temperatures than CO, in addition to the large fraction which desorbs simultaneously with the CO (suggesting the ices become mixed following mobility of  $\text{N}_2$ ). Hence the fraction of  $\text{N}_2$  which desorbs before CO depends on the morphology of the ice rather than the chemical properties of the species involved. Temperature programmed desorption (TPD) experiments carried out by Bisschop *et al.* (2006) produce similar results, and the authors suggest that the explanation for the observed desorption may lie in the gas phase chemistry. For example, it is possible for dissociative recombination of  $\text{N}_2\text{H}^+$  with electrons to become the dominant destruction mechanism for  $\text{N}_2\text{H}^+$  (Jørgensen *et al.*, 2005). This leads to the production of NH rather than  $\text{N}_2$  (Geppert *et al.*, 2004) so that  $\text{N}_2\text{H}^+$  depletion only occurs at high densities (or, equivalently, at late times).

Regardless of the actual explanation, it is clear that in regions of low-mass star for-

mation CO and  $\text{N}_2\text{H}^+$  behave differently. In high-mass star forming regions, however, the situation is unclear. The epoch most readily accessible to observations is, as discussed in section 1.1.2, the hot core phase. During this phase of the evolution of a protostar, a characteristic chemistry signifies the operation of processes unlike those taking place in quiescent clouds. This chemistry arises from the evaporation of molecules that had been frozen out onto dust grains during the collapse of the prestellar core. These species are released back into the gas phase when the newly formed massive star warms the surrounding gas, causing the ices to sublime.

Recent molecular line observations (Pirogov *et al.*, 2003; Zinchenko *et al.*, 2005; Pirogov *et al.*, 2006) of high-mass star forming cores show differences between the distributions of CS and  $\text{N}_2\text{H}^+$ . In a survey of sources in 35 dense molecular cloud cores<sup>1</sup> believed to be associated with high-mass star formation, Pirogov et al. (2003) find that the CS and dust emission distributions are very similar, and differ significantly in many cases from the  $\text{N}_2\text{H}^+$  distributions. In contrast to the behaviour in the vicinity of low-mass star forming regions, the  $\text{N}_2\text{H}^+$  abundance falls near massive young stellar objects. This drop is seen on scales as large as a parsec in regions in which the temperature does not appear significantly different from the rest of the cloud and to the CS peak. The variation in relative intensity can be as large as one order of magnitude, larger than could be accounted by differences between excitation and opacity, and is seen in approximately one-third of the sources studied by Pirogov *et al.* (2003). A detailed study is expected to reveal significant differences in the majority of the sources (Zinchenko, private correspondance). Zinchenko et al. also discuss the behaviour of other molecules in similar cores. The evidence from these surveys indicates that, in contrast to its behaviour in low-mass star forming regions, in regions of high-mass star formation  $\text{N}_2\text{H}^+$  does not trace the mass.

In this chapter, we propose an explanation for these differences between the behaviours of CS and  $\text{N}_2\text{H}^+$ . Why is there a complete reversal of behavior between regions which are forming high-mass stars (in which CS appears to be a good tracer of core mass) and low-mass stars (in which  $\text{N}_2\text{H}^+$  is the better tracer)? A possible explanation may be found in differences between the dynamical state of the two types of star forming region, and with a detailed computational model of high-mass star formation (presented below) we obtain results which are consistent with observation.

<sup>1</sup>These cores were selected to have embedded stars visible in the infrared, and to have extended emission in either CS or  $\text{NH}_3$ .

## 4.2 Observations

In this section I briefly review the observations upon which this work is based, and which are reported in full elsewhere by the observers (Pirogov *et al.* (2003), Zinchenko *et al.* (1995), Zinchenko *et al.* (1998), Pirogov *et al.* (2006) & Zinchenko *et al.* 2006 in preparation).

$\text{N}_2\text{H}^+$  (1-0) emission was observed in 2000 and 2001 at the Onsala 20m telescope<sup>2</sup> and at the 15m Swedish-ESO submillimetre telescope (SEST)<sup>3</sup>. The CS(2-1) transition has also been observed at SEST and Onsala. The CS(5-4) transition was observed at SEST and, along with  $\text{C}^{34}\text{S}$ , at the NRAO 12m telescope<sup>4</sup>. Thirty-five sources were observed in the Onsala/SEST  $\text{N}_2\text{H}^+$  surveys, and  $\sim 20$  of these were later observed in dust continuum emission at SEST using the SIMBA bolometer array<sup>5</sup> and at the IRAM 30m with the MAMBO array<sup>6</sup>. The CS correlates well with dust emission, whereas CS and  $\text{N}_2\text{H}^+$  are poorly correlated in many cases. Several sources were also mapped in HCN, HNC,  $\text{HCO}^+$ ,  $\text{CH}_3\text{OH}$  and several other species. The gas kinetic temperatures were estimated for S255 and S187. Inferred temperatures for S255 from observations of  $\text{CH}_3\text{C}_2\text{H}$  are  $\sim 35\text{K}$  at both the CS and  $\text{N}_2\text{H}^+$  peaks, somewhat warmer than cold-cloud conditions.

As an example of these observations, figure 4.1 shows  $\text{C}^{34}\text{S}(2-1)$  and  $\text{N}_2\text{H}^+(1-0)$  maps of S255 overlaid on the map of the dust continuum emission at 1.3mm. The  $\text{C}^{34}\text{S}(2-1)$  emission is presumed to be optically thin, and the peak optical depth for  $\text{N}_2\text{H}^+(1-0)$  in S255 is  $\sim 0.5$  (Pirogov *et al.*, 2003). The dust continuum data shows two peaks which are almost equal in their intensity. The  $\text{C}^{34}\text{S}(2-1)$  distribution is similar, although the emission at the southern peak is somewhat stronger than its northern counterpart. The observed  $\text{N}_2\text{H}^+$  distribution is very different and the northern component is much stronger in this

<sup>2</sup>The Onsala 20m telescope is a millimetre wave telescope which was built in 1975 and substantially upgraded in 1992. Its receivers cover a frequency range from 2.2-116 GHz.

<sup>3</sup>SEST operated in the frequency range 70-365GHz from a site at La Silla 2400m above sea level. It was built in 1987 and comprised a 15m dish. SEST is no longer available for use.

<sup>4</sup>The NRAO 12m telescope is located on Kitt Peak in Arizona, and operates with receivers from 68 to 180GHz.

<sup>5</sup>SIMBa is a 37 channel hexagonal bolometer array which operated at 1.2mm. A single element has a half-power beam width of 24" and the pixel sensitivity is  $50\text{-}70\text{mJys}^{-1}$ . It was commissioned in June 2001.

<sup>6</sup>The IRAM 30m telescope, on Pico Veleta, Spain at 2850m above sea level, has heterodyne receivers capable of detecting radiation with frequencies between 80 and 272GHz. Up to four of these receivers can be used at one time. MAMBO is a 37 channel bolometer array (of similar design to SIMBA) operating at 1.2mm. It was replaced in 2001 by the 117 pixel MAMBO-2.

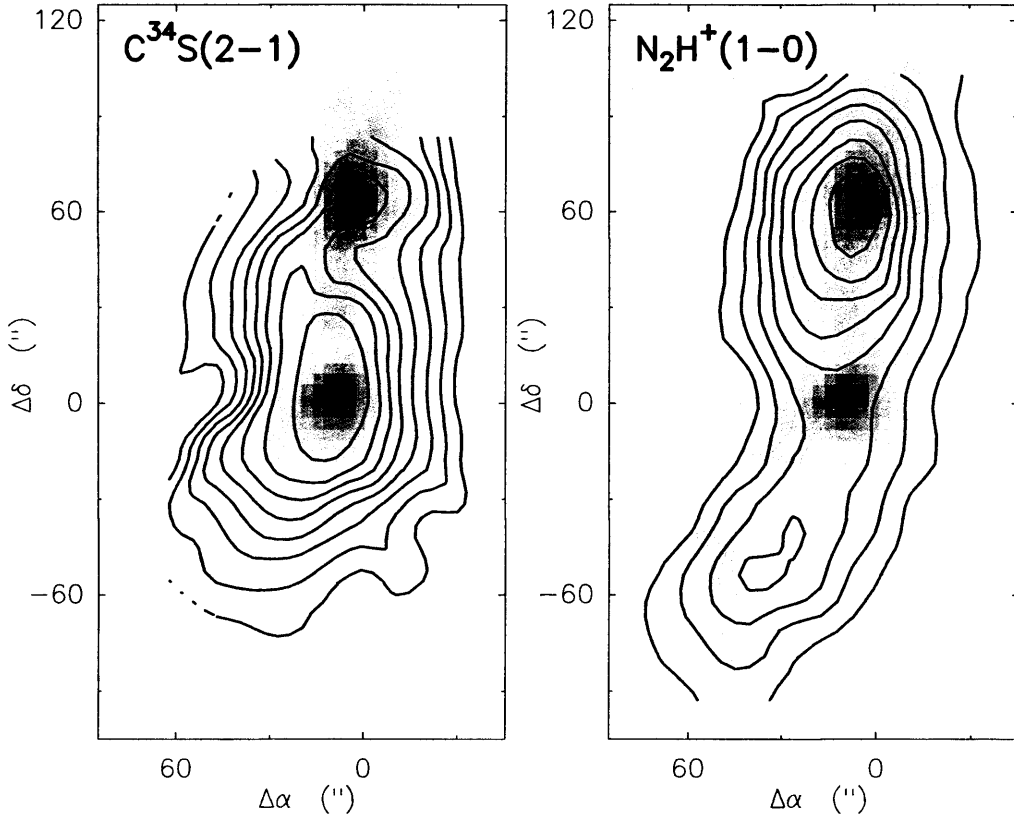


Figure 4.1: Observed contours of  $\text{C}^{34}\text{S}(2-1)$  and  $\text{N}_2\text{H}^+(1-0)$  in S255, overlaid on 1.2mm continuum map obtained from IRAM.  $\text{C}^{34}\text{S}$ , which we presume is optically thin, shows a clear correlation with the dust which is absent in  $\text{N}_2\text{H}^+$ . The model presented in this chapter attempts to account for this observed difference in distribution.

line than the southern one. There is a slight concentration below the southern component (at  $\Delta\delta = -60''$ ) visible in figure 4.1, but it is not significant.

The nature of these two components differs. The southernmost peak in dust distribution is associated with a luminous cluster of infrared sources, whereas an ultracompact HII region (G192.58-0.04) was detected toward the northern component (Kurtz *et al.*, 1994). S255 is extremely red when viewed in the mid-IR. Crowther and Conti (2003) and Mezger *et al.* (1988) derived dust masses and temperatures for both components from 1.3mm and 350 $\mu\text{m}$  observations which were almost identical for both species. Their dust temperatures appear to be very close to the gas kinetic temperature referred to above. Taking this into account, the southern source is believed to be a young high-mass protostellar candidate which is at an earlier stage of evolution than the northern source. It is this younger category of object that the models in this chapter apply to.

Similar observations of the entire sample show that differences between CS(5-4) and

$\text{N}_2\text{H}^+(1-0)$  distributions are common. The CS intensities depend (for a large majority of objects) in an almost linear fashion on the continuum flux; the small deviations which are observed are attributed by Pirogov *et al.* (2006) to differences in excitation conditions. A substantial subset of the cores studied show the anticorrelation between CS and  $\text{N}_2\text{H}^+$  seen in S255 and described above. Can the observed variation between sources be explained by opacity or excitation effects, or does the explanation lie in a difference in chemistry?

If the cores were to have high optical depths in the observed transitions, then one would expect to detect the effect of line saturation, leading to a decreasing of relative line intensities towards the CS and dust emission peaks. This effect is not seen in the CS(5-4) data or in the  $\text{C}^{34}\text{S}$  data described above (although it is seen in CS(2-1) toward some sources). Opacity can not therefore account for differences between sources.

The CS(5-4) lines have a critical density which varies from that of the  $\text{N}_2\text{H}^+(1-0)$  transitions by about an order of magnitude, and this may be expected to affect the observed intensity distributions. Pirogov *et al.* use a low-velocity gradient model to study the excitation of the observed transitions for a wide range of densities and kinetic temperatures. They find that for a large range of densities the intensities may be changed by a factor of  $\sim 3$ , but not by enough to explain the order of magnitude difference between CS: $\text{N}_2\text{H}^+$  ratios in different sources. It is also possible that nearby infrared sources may be able to ‘pump’ the material, overpopulating the upper rotational levels and hence increasing the observed CS(5-4) line intensity and reducing the observed  $\text{N}_2\text{H}^+(1-0)$  intensity. Carroll and Goldsmith (1981) showed, however, that for CS the maximum size of CS which could be affected by infrared pumping (via vibrational transitions) is 0.03pc, and a similar result is found for  $\text{N}_2\text{H}^+$  by Pirogov *et al.*. In the absence of an explanation from excitation, therefore, we must look to chemical or dynamical differences.

### 4.3 Rapid collapse of cores in high-mass star forming regions

While cores in low-mass star forming regions are generally quiescent (Myers and Benson, 1983; Evans *et al.*, 2001), regions of high-mass star formation are dynamically active. It is interesting, therefore, to explore the possibility that additional external pressure arising from this dynamical activity may act on a core and so enhance the rate of collapse above the natural free-fall rate. I do not propose to consider in detail the possible mechanisms

for such an enhanced rate of collapse, concentrating instead on observational signatures of such an accelerated collapse. Briefly, such an enhancement could be due to compression by shocks which are sufficiently weak that they have little effect on the temperature of the dense core. Conventionally, cores associated with low-mass star formation are assumed to be falling at, or slower (see section 1.1.2) than, free fall, and so for convenience this work uses the free-fall collapse law described in Rawlings *et al.* (1992) after Spitzer (1978). The enhancement of collapse rate in high-mass regions is included in the model by allowing the choice of a large value for the inverse time constant in the free-fall collapse equation which relates density and time.

Consider a (cold) sphere of uniform density  $\rho$  at rest at time  $t = 0$ . If a shell of radius  $r(t)$  has a size  $r_0$  at  $t = 0$  then the equation of motion is

$$\frac{d^2r}{dt^2} = -\frac{GM}{r^2} = -\frac{4\pi G\rho_0 r_0^3}{3r^2} \quad (4.1)$$

where  $M$  is the mass enclosed within the initial radius. It is assumed that the mass within a shell stays constant during the collapse (the ‘no shell crossing’ approximation).

Multiplying by  $dr/dt$  and integrating produces

$$\frac{dr}{r_0 dt} = -\left[\frac{8\pi G\rho_0}{3}\left(\frac{r_0}{r} - 1\right)\right]^{\frac{1}{2}}. \quad (4.2)$$

Rearranging to obtain the change in number density,  $n$ , as collapse proceeds from initial density  $n_0$  to final density  $n_f$  is then given for spherical systems by

$$\frac{dn}{dt} = B \left(\frac{n^4}{n_0}\right)^{\frac{1}{3}} \left(24\pi G m_H n_0 \left[\left(\frac{n}{n_0}\right)^{\frac{1}{3}} - 1\right]\right)^{\frac{1}{2}}, \quad (4.3)$$

where  $t, G$ , and  $m_H$  are the time, the gravitational constant and the mass of hydrogen atoms respectively.  $B$  is an arbitrary variable which can be adjusted to take account of collapse faster than or slower than freefall. Values of  $B$  greater than 1 correspond to cores undergoing accelerated collapse (ie collapsing faster than free-fall). This is obviously an approximation; there is no physical reason why rapid collapse should simply be a more rapid version of free-fall, but it is a useful first assumption.

The adoption of this enhanced free-fall description allows the exploration of the qualitative response of the chemistry to this more rapid collapse. The timescale of the collapse

compared to the time-scale of freeze-out is more important for the chemical results than the other details of the collapse history. *The effect of an enhanced collapse rate should be to allow the core to reach high gas densities more rapidly, before the effects of freeze-out come to dominate the chemistry.*

How will this change in behaviour affect the species of interest? The primary formation route for  $\text{N}_2\text{H}^+$  is through the reaction between  $\text{H}_3^+$  and  $\text{N}_2$ , which also produces molecular hydrogen. The  $\text{N}_2\text{H}^+$  molecule is then able to react with species such as  $\text{H}_2\text{O}$ , C, O or CO to form  $\text{N}_2$  and a positive ion. It is easy to see, therefore, that the abundance in the gas phase of these potential removal agents will be critical in determining the abundance of  $\text{N}_2\text{H}^+$  present.

We have already mentioned that, in accelerated collapse, high densities would be reached earlier than would otherwise be the case - before molecules that are important as  $\text{N}_2\text{H}^+$  removal agents are fully depleted in the gas phase. If this is indeed the case, then  $\text{N}_2\text{H}^+$  abundances should be reduced compared to a standard (free-fall) model.

CS is produced through reactions such as the interaction of  $\text{He}^+$  and HCS, or between atomic carbon and diatomic molecules such as SO. In the canonical model with free-fall collapse, molecules such as CS freeze out of the gas phase before being destroyed in further reactions. However, in an accelerated collapse, high gas densities would be reached faster than in the canonical model. The higher gas density would then promote gas-phase chemistry, and this increased rate of reaction would increase the abundance of CS.

In an accelerated collapse model, therefore, the abundance of CS should be enhanced while that of  $\text{N}_2\text{H}^+$  should be reduced (compared to canonical calculations). This prediction can thus be used to test the hypothesis of accelerated collapse. A chemical model based on that of Viti and Williams (1999) is used to describe the formation and chemistry of high-mass stars. Their model is a two-stage calculation: the first stage begins with a fairly diffuse ( $n \sim 300\text{cm}^{-3}$ ) medium with the gas in purely atomic form (apart from a fraction of hydrogen which is in the form of  $\text{H}_2$ ) and undergoes a collapse until the densities typical of hot cores are reached ( $n \sim 10^7\text{cm}^{-3}$ ). During this phase the temperature is held constant at 10K and the collapse follows the single-point evolution prescribed by equation 4.3. During this time, atoms and molecules from the gas are allowed to freeze onto the grains and subsequently hydrogenate where possible. The advantage of this approach is that the composition of the ice is *not* assumed but is self-consistently derived from the interactions of the gas with the dust grains.

Typical atomic abundances appropriate for the solar neighbourhood were adopted. The chemical network is taken from the UMIST rate99 database (Le Teuff *et al.*, 2000). We follow the chemical evolution of 168 species involved in 1857 gas-phase and grain reactions. At the end of stage I,  $\sim 99\%$  of the gas is frozen out.

The second stage follows the chemical evolution of the remnant core after the protostar has been born. For most of the runs described in this chapter, only stage I is used; as all the observed objects have gas temperatures of around 30K the prestellar evolution of the core is of most interest. Several different models were completed in order to explore the effect of a two-phase collapse, in which a collapse was allowed to proceed up to a critical density,  $n_{crit}$  (treated as a free parameter). This early phase was then followed by collapse at an enhanced rate (up to four times the freefall rate, i.e.  $B > 1$  in equation 4.3) until the final density of  $10^7 \text{ cm}^{-3}$  was reached.

For some models, stage II (as described in Viti *et al.* (2004b)) was also added to the calculations. The presence of an infrared source in the center of the core or in its vicinity is simulated by subjecting the core to a time-dependent increase in the gas and dust temperature. The final temperature is 50K, and the temperature rise is followed by partial evaporation of grains according to the prescription of Viti *et al.* (2004b). In these runs, the temperature increase is initiated once a density  $n_T$  is reached. The parameter choices for the calculations are given in table 4.1.

### 4.3.1 Results

As expected, enhancing the collapse rate so that collapse occurs faster than the free-fall rate results in an increase in the CS abundance and accompanying reduction in the abundance of  $\text{N}_2\text{H}^+$ . The shift in each case is about half of one order of magnitude. The results for collapse rate enhancements differ significantly from the results for free-fall, but not dramatically for different size enhancements (factors of 2-4 were tried) or for accelerations triggered at different critical densities. Figure 4.2 shows the ratio of the CS and  $\text{N}_2\text{H}^+$  abundances as a function of time for the cases  $B = 1$  (free fall) and  $B=2-4$  (enhanced collapse rate).

The substantial enhancement seen when the collapse rate is enhanced is not observed when the freeze-out of molecules is artificially removed from the simulation, thus providing support for the hypothesis that the change in abundance observed is associated with the freeze-out of species from the gas phase. In order to ensure that the behaviour of CS and

Run	$n_{crit}$	$B_{new}$	Temp. Rise?	$n_T$
A	$10^5$	1.0	No	N/A
B	$10^5$	2.0	No	N/A
C	$10^5$	3.0	No	N/A
D	$10^5$	4.0	No	N/A
E	$10^5$	2.0	Yes	$10^6$
F	$10^5$	1.0	Yes	$10^4$
G	$10^5$	2.0	Yes	$10^4$
H	$10^6$	3.0	Yes	$10^4$
I	$10^5$	4.0	Yes	$10^4$
J	$10^3$	2.0	No	N/A
K	$10^4$	2.0	No	N/A
L	$10^6$	2.0	No	N/A
M	$10^5$	0.1	Yes	$10^6$

Table 4.1: For each run, collapse occurs under free-fall until number density  $n_{crit}$  is reached, when an acceleration by a factor  $B_{new}$  is applied. For some runs, a temperature increase to 50K was initiated at a density  $n_T$  as described in the main text.

$\text{N}_2\text{H}^+$  seen in the observations could not be replicated simply by allowing the collapse to continue until depletion of species was complete, a run was carried out in which the rate of collapse was decelerated by a factor of ten relative to free-fall. In this case the  $\text{N}_2\text{H}^+$  abundance in the gas phase was found to drop rapidly to zero before depletion could become significantly advanced. The observations thus cannot be explained by an extreme deceleration of the collapse.

The effect of heating the gas to the observed temperatures of 35-50K was also investigated, via models in which the temperature of the core was increased monotonically following a power law. The evaporation of a fraction of any species present in the icy mantle occurs in a single step when the temperature required for a particular desorption event is reached (see section 1.2). Heating was initiated in the final stages of collapse and the results were unsurprisingly insensitive to the density at which the temperature increase was begun. A comparison of figure 4.2 with figure 4.3 reveals that the increase in CS and decrease in  $\text{N}_2\text{H}^+$  abundances are not significantly affected by the incorporation of heating into the simulation.

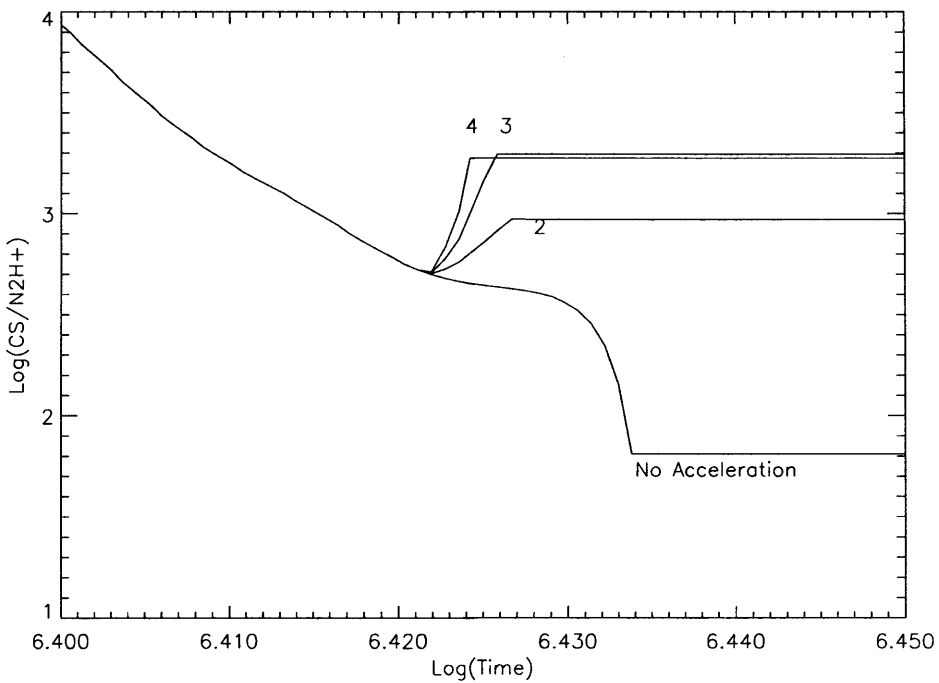


Figure 4.2: Evolution of the ratio of CS to  $\text{N}_2\text{H}^+$  abundances during collapse. Once a critical number density of  $10^5 \text{ cm}^{-3}$  was achieved, three of the four runs (A,B,C & D in Table 1) shown incorporated a collapse accelerated by the factor shown (2, 3 or 4 times the free-fall rate). The acceleration increased the abundance of CS and decreased the  $\text{N}_2\text{H}^+$  abundance by approximately an order of magnitude; we conclude that this provides a possible explanation of the recent observations of high-mass cores.

## 4.4 Discussion and Conclusions

Recent observational data on cores in regions of high-mass star formation show exciting and unexpected results, with the behaviour of some species opposite in character to well established trends in regions of low-mass star formation. I have argued that the enhancement of CS and reduction in the abundance of  $\text{N}_2\text{H}^+$  found in these regions may be related to the high level of dynamic activity in such objects, which could enhance the rate of collapse of cores above the rate dictated by free-fall. Consequently, high gas densities would be achieved before freeze-out had removed the molecules responsible for  $\text{N}_2\text{H}^+$  loss, while the high densities promote CS formation. (Equivalently, the dynamical timescale will become much shorter than the chemical timescale.) Furthermore, using a computational model of the appropriate chemistry, the predicted effects are indeed seen given reasonable choices of parameters. The results are not especially sensitive to the particular enhance-

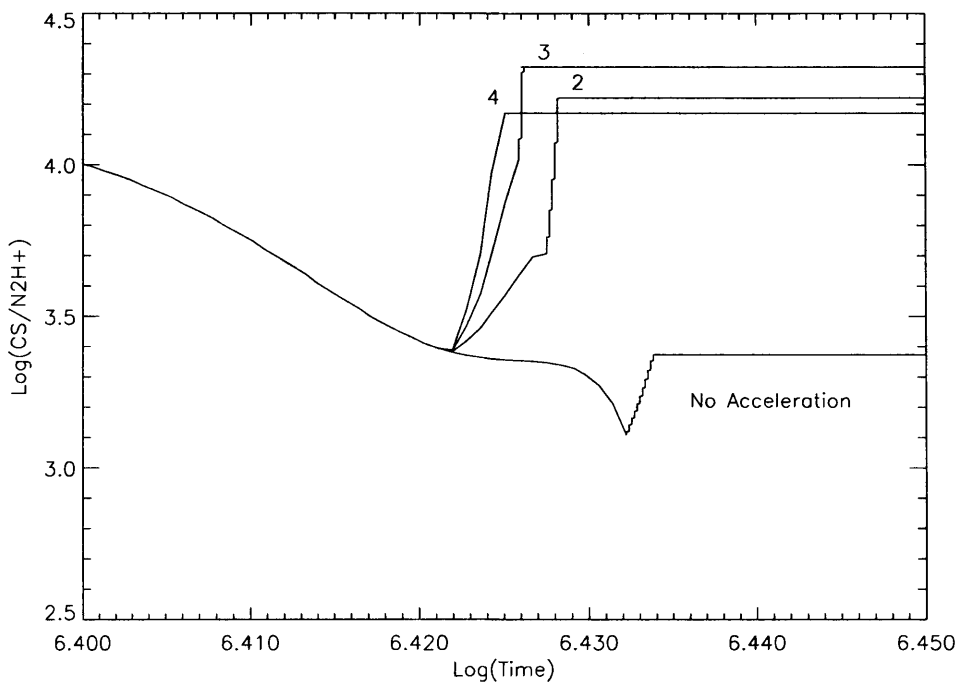


Figure 4.3: Evolution of CS to  $\text{N}_2\text{H}^+$  abundances in runs F,G,H & I incorporating an increase of temperature to a maximum of 50 K, in the later stages of the collapse.

ment rate adopted once above a factor of twice the free-fall rate. The observational results also give some information about variations of other molecules with respect to the chosen high-density tracers. The model presented here also confirms, for example, that HCN is similar to CS in its distribution, as found by Pirogov *et al.* (2006). However, the model further predicts that SO would have a distribution similar to  $\text{N}_2\text{H}^+$ , whereas observations of S255 - the core for which sample observations are shown in section 4.2 - indicate that it is much closer to CS (see table 4.2). As yet, data on the distribution of SO is available only for S255, and so it is not clear whether this result is significant or restricted to this source. As with most molecules, the effect of an accelerated collapse on the SO abundance will be both to increase the rate of production and to prevent the removal of other possible reaction partners from the gas phase. This discrepancy between observation and theory for SO suggests that the classification of molecules into two classes of species, each of which is primarily affected by only one of these two competing effects is over-simplistic for molecules at the center of complex reaction networks. Should further SO observations confirm the S255 results, a detailed analysis of the behaviour of sulphur-bearing species in this model will be necessary.

$\text{N}_2\text{H}^+$ -like	CS-like
$\text{NH}_3$	HCN
$\text{HCO}^+$	OCS
$\text{H}_2\text{S}$	
SO	
$\text{SO}_2$	

Table 4.2: Examples of model predictions of species with abundances which behave like either  $\text{N}_2\text{H}^+$  or CS.

If the accelerated collapse model applies to the cores observed by Pirogov *et al.* (2006), one might expect that the velocity measurements would reveal detectable signatures. In particular, Mardones *et al.* (1997) introduced a parameter known as the normalized velocity. This is the difference between the observed velocities of species which are optically thick or thin:  $\delta V = (V_{\text{thick}} - V_{\text{thin}})/\Delta V_{\text{thin}}$ . Using optically thick CS(2-1) lines (Zinchenko *et al.*, 1995) and optically thin  $\text{N}_2\text{H}^+$  reveals no indication of systematic motions towards the peaks of CS(5-4) emission, as would be expected if the accelerated collapse model is appropriate. However, if the sources consist of a large number of small clumps which are unresolved (as some LVG models suggest) then the low effective depth of CS would lead to nearly symmetric profiles regardless of the internal velocity of the cores. An enhanced line broadening toward the centre of the cores would remain as an indicator of infall, and this has indeed been seen by Pirogov *et al.* (2006) in sources with low  $\text{N}_2\text{H}^+$  abundances.

These observations are encouraging, but it should be noted that the temperatures found in these cores are somewhat warmer than those normally assumed for dense core environments. We have examined the results from computational models in which the initial warming of the hot core (up to temperatures of 30-50K) are included, but the behaviour of key species (CS and  $\text{N}_2\text{H}^+$ ) is not significantly altered. The model investigated is consistent with the rather limited observational data, whereas the free-fall collapse model cannot account for the observed differences in the behaviour of different species. This first investigation of the effect of accelerated collapse on the chemical abundances of species in high-mass star formation regions therefore suggests a possible explanation for the observations, and provides an important route for future observational and theoretical work.

## CHAPTER 5

---

# Extragalactic astrochemistry : sulphur in starbursts

### 5.1 Introduction

The previous three chapters have provided examples of the power of astrochemical models to constrain the physical parameters of star forming regions, to determine their dynamical history and to derive their age. In seeking to apply these astrochemical models beyond the Milky Way, we lose most of this power. With the exceptions of the largest satellites of our own Galaxy, the Large and Small Magellanic Clouds, it is not possible, in the radio and in the sub-mm, to resolve individual star forming regions in external systems. We gain, in contrast, a new set of exotic environments with which to test our models, and a wealth of knowledge about star formation rates and conditions which would be unobtainable in any other way. In chapter 6, I argue that astrochemical modelling could make a valuable contribution to our understanding of the most distant sources in the Universe, but such an investigation presents a formidable challenge both to observers and to theoretical models. The nearest local analogues to these distant galaxies - which appear to be forming stars at a prodigious rate - are the so-called starburst galaxies, and this chapter therefore explores their unique and distinctive chemical signature. This signature forms a rich source of information about these unusual systems, but is also a stepping stone to the early Universe.

Starburst galaxies contain regions - usually, but not always associated with the galaxy's nucleus - which are undergoing 'high' rates of star formation. The exact definition of 'high' remains nebulous, but the observed rates are usually far in excess of the Milky Way value,

and large enough that a significant fraction of the gas available for star formation will be exhausted in a single dynamical timescale (Lehnert and Heckman, 1996). Curiously, Lehnert and Heckman also find that starburst galaxies seem to have a limiting infrared surface brightness of about  $10^{11} L_{\odot} \text{kpc}^2$ , which for a Milky Way-like initial mass function corresponds to a star formation rate per unit area of  $20 M_{\odot} \text{yr}^{-1} \text{kpc}^2$ . This result suggests that starbursts are in some way self-regulating, rather than simply star formation run amok. Such a limit is much lower than that imposed by the free-fall gravitational collapse of a self-gravitating system, and may be due to a balance between collapse and an outflow of hot gas from the starburst region itself (see Dopita (1990) for an early development of this idea).

Whatever the limit is, such rapid star formation requires the accumulation of a large quantity of dense gas in a small volume in a short time. An effective method of achieving this is through the merger of gas rich spiral galaxies. Such an event can result in the majority of the gas in both ‘parent’ systems ending up in the inner 100pc of the resulting merged galaxy (Barnes and Hernquist, 1996). Once the starburst has begun, the massive stars which are formed quickly evolve to supernovæ (Engelbracht *et al.*, 1998), and these supernovæ can produce massive winds, moving material away from the centre of the galaxy (Doane and Mathews, 1993).

The nearest large starbursts to the Milky Way are NGC253, in the Southern hemisphere, and M82, near the celestial north pole. Both are edge-on, barred and are similar in spectrum and in luminosity (Lenc and Tingay, 2006). They are both also strong sources of molecular emissions, and it will be useful to review existing observations in both sources here. The work contained in the rest of the chapter will focus on M82, but NGC253 will serve as a useful comparison.

### 5.1.1 NGC253

This starburst, believed to be younger than that in M82, has proved to be a fruitful target for astrochemists. Of particular interest are the first extragalactic detections of SO<sub>2</sub> and NS by Martín *et al.*. Although it is necessary to make assumptions about the overall extent of the nuclear emission, it seems clear that the abundances of both SO<sub>2</sub> and NO are much larger than those seen in galactic PDRs (Jansen *et al.*, 1995). The only sources that show abundances as large are galactic hot cores (e.g. Nummelin *et al.* (2001)), perhaps when enhanced by the presence of X-ray ionization (see section 6.3). The

rotational temperatures derived from these extragalactic observations are, at  $T_{rot} \sim 10\text{K}$ , much lower than those associated with hot cores in the Milky Way. This is surprisingly low, and Martín *et al.* conclude that the species in question must be subthermally excited and the true temperature of the gas is that seen in NH<sub>3</sub> (Mauersberger *et al.*, 2003).

These observations show the strength of sulphur-bearing molecules in determining the properties of star forming regions, showing enhanced abundances in hot molecular cores. An outline chemistry begins with the freeze-out of much of the available sulphur onto dust grains, where it hydrogenates to form H<sub>2</sub>S. Once the protostar ignites and the icy mantle sublimates, H<sub>2</sub>S can be attacked by protons, and so is able to drive a high temperature chemical network which leads to the formation first of SO and SO<sub>2</sub>, and then to later models such as CS and H<sub>2</sub>CS (Charnley, 1997). This chemistry will be more important in the early Universe, when gas enriched only by the supernovæ of population III stars is expected to be deficient in nitrogen (see chapter 6). Martín *et al.* (2005) thus extended their observations of sulphur-bearing species in NGC253 to include H<sub>2</sub>S, CS, NS, SO, H<sub>2</sub>CS, OCS and SO<sub>2</sub>.

It is clear from these observations of NGC253 that, at least in the local Universe, starburst galaxies have a rich chemistry similar to that seen in galactic hot cores. This source, however, is believed to be a recent starburst, having begun rapid star formation within the last  $\sim 10^7$  years (Tacconi-Garman, 2006). In order to examine how long this chemistry might survive, we will need to consider an older starburst, the nearest of which is M82.

### 5.1.2 Molecules and structure of M82

M82 is a nearby starburst galaxy at a distance of 3.9Mpc and with a luminosity of  $3.7 \times 10^{10} L_\odot$  within the inner 0.25kpc (close to the limit of Lehnert and Heckman (1996)). It has a rich chemistry, the study of which should help to constrain the star formation history of the galaxy. It also contains a large reservoir of molecular gas; Wild *et al.* (1992) report  $M(\text{H}_2) \approx 1 \times 10^8 M_\odot$ . The galaxy is the nearest example of a giant starburst galaxy, with the present burst of nuclear star formation triggered by a tidal interaction with its neighbour, M81,  $2 - 5 \times 10^8$  years ago (Brouillet *et al.*, 1991; Yun *et al.*, 1993). The starburst activity remains vigorous today, with the active starburst region having a diameter of 500pc (O'Connell and Mangano, 1978), and this star forming activity seems

to be propagating outwards (Satyapal *et al.*, 1997). This simple picture cannot explain all the observations, however, and studies of star clusters which lie outside the central regions (e.g. Gallagher and Smith (1999)) reveal older star formation away from the central regions; typical ages for these events, derived from evolutionary synthesis, are  $60 \pm 20$  Myr. Stars forming in such an environment may have a different initial mass function than that seen in the Milky Way, and the data available to resolve this question in M82 is contradictory. O'Connell and Mangano (1978); Satyapal *et al.* (1997) and others find a ‘normal’ mass function, whereas Rieke *et al.* (1993) and Förster Schreiber *et al.* (2003) find a mass function which is deficient in low-mass stars. The picture is clearly on the scale of individual clusters, where Smith and Gallagher (2001) and McCrady *et al.* (2003) (in one of their sample clusters) find a deficiency of low-mass stars.

The most common molecule in the Universe (aside from molecular hydrogen) is carbon monoxide, and this is therefore the first target of choice for observers. In the case of M82, Mao *et al.* (2000) present observations of the CO J=1-0, 2-1, 4-3, 7-6 transitions and the  $^{13}\text{CO}$  1-0, 2-1 and 3-2 transitions toward the nuclear region of the galaxy. They find two ‘hotspots’ on either side of the dynamical centre of the galaxy, with differences in spacing between the two spots varying with transition. Their modelling of the emission as an extended PDR (photon-dominated region) consistently reveals that most of the CO arrives from diffuse gas with a column density of  $5 \times 10^{20} \text{ cm}^{-2} (\text{km s}^{-1})^{-1}$ . Such a result is typical for CO, and explains adequately why species such as HCN or CS, which trace dense regions, are preferred as indicators of star formation. The authors conclude, however, from these observations and modelling, that the molecular gas is embedded within this larger, low-density environment, in the form of warm clouds ( $T_k > 50\text{K}$ ) of intermediate ( $n > 10^4 \text{ cm}^{-3}$ ) density.

Weiβ *et al.* (2001) were the first to detect ammonia ( $\text{NH}_3$ ) in the southwestern ‘lobe’ of the galaxy. They find mean kinetic temperatures of  $T_{kin} \approx 60\text{K}$  which is consistent with the CO observations discussed above. The fractional abundance of ammonia is, however, extremely low at  $X(\text{NH}_3) \approx 5 \times 10^{-10}$  (compared to  $X(\text{NH}_3) \approx 10^{-7}$  for Milky Way dark clouds (Benson and Myers, 1989) and there is also evidence that the abundance decreases closer to the central (that is, the active) regions of the galaxy. The authors interpret this as being due to increased dissociation of ammonia in the centre.

The formyl radical (HCO) is associated with regions in which chemistry is driven by an enhanced UV radiation field (Schilke *et al.*, 2001). This volatile species has a large

photodissociation rate (van Dishoeck, 1988) and therefore a lifetime of only  $\approx 30$  years when exposed to the mean interstellar radiation field. Observers have speculated that the presence of HCO may indicate the sublimation of formaldehyde from ice mantles followed by rapid photodissociation. M82 was the first external galaxy in which HCO was observed, by García-Burillo *et al.* (2002). Their high-resolution map shows a ring of 650pc diameter toward the outer edge of the region of molecular emission. They interpret the high abundance ( $X(\text{HCO}) \sim 4 \times 10^{-10}$ ) of the radical as evidence for a giant PDR region extending throughout the nuclear disk. This may seem paradoxical, but it is suggested (or indeed, required for the model to account for this) that UV fields associated with the strongest HII regions (which all lie in the central  $\sim 400\text{pc}$ ) have dissociated HCO in the central regions of the galaxy.

Fuente *et al.* (2005a) recently expanded the range of molecules associated with PDR chemistry which have been observed in the galaxy with a survey that included radicals (CN, C<sub>2</sub>H), ions (CO<sup>+</sup>, HOC<sup>+</sup>) and hydrocarbons (*c* – C<sub>3</sub>H<sub>2</sub>). Of these species, HOC<sup>+</sup>, in particular, is almost exclusively associated with regions with a high ionizing flux (Usero *et al.*, 2004). Noting that species such as CS, CN and HCN have fractional abundances of  $X \sim 10^{-9}$ , they note that, following Suchkov *et al.* (1993), increasing the cosmic-ray ionization rate to  $\zeta = 4 \times 10^{-15}\text{s}^{-1}$  (from  $\zeta = 5 \times 10^{-17}\text{s}^{-1}$ ) improves the fit between the model and observation. The HCO<sup>+</sup> abundance, however, remains stubbornly low by an order of magnitude.

Similarly, Fuente *et al.* (2006) observed CO<sup>+</sup> in the inner 650pc of the nuclear disk. They find an extremely high [CO<sup>+</sup>]/[HCO<sup>+</sup>] ( $> 0.04$ ) which their PDR model is able to explain. However, the derived column density for CO<sup>+</sup> is anomalously large at  $\sim 1 - 4 \times 10^{13}\text{cm}^{-2}$ . In order to reconcile the PDR model with the observed column density, it is necessary to assume that  $\sim 20$  clouds must lie along the line of sight.

These indications from HCO<sup>+</sup> and CO<sup>+</sup> that the molecular gas in M82 cannot be accounted for solely by a PDR are further strengthened by the observations of Martín *et al.* (2006) who detected methanol (CH<sub>3</sub>OH) in the nucleus of the galaxy. In Milky Way PDRs induced by powerful UV radiation incident on already dense gas, methanol is easily photodissociated by UV radiation (Hartquist, 1995), and so the large fractional abundance in M82 (a few  $\times 10^{-9}$ ) indicates ‘the presence of a significant fraction of dense gas which must necessarily be well-shielded from the radiation field’.<sup>1</sup> Methanol is, apart from water,

---

<sup>1</sup>The most common model of a PDR - in which the UV-rich radiation is present from the beginning -

Molecule	Transition	Frequency/GHz
CS	$5 \rightarrow 4$	244.936
SO	$6(5) \rightarrow 5(4)$	219.949
$\text{SO}_2$	$4(2,2) \rightarrow 3(1,3)$	238.698

Table 5.1: Molecules and transitions observed toward M82 with the JCMT. Frequencies taken from the JPL molecular database.

the most abundant constituent of interstellar ice (Allamandola *et al.*, 1992). Observed abundances are several orders of magnitude larger than those in gas-phase chemical models, which struggle to produce fractional abundances larger than  $10^{-9}$  (Lee *et al.*, 1996). These three facts taken together suggest that, in general, the presence of large abundances of methanol are associated with the evaporation or disruption of icy mantles.

## 5.2 Observations of sulphur-bearing species

In order to add to the variety of species and transitions known in M82, we attempted to observe CS, SO and  $\text{SO}_2$  with the JCMT toward the nuclear region. The lines observed (with frequencies taken from the JPL molecular database<sup>2</sup>) are shown in table 5.2. CS was selected as a common molecule in gas of moderate densities, and as a check on the sulphur abundance in the galaxy. SO and  $\text{SO}_2$  are, at least in the Milky Way, the major repositories of gas phase sulphur when oxygen is present, and as such are excellent tracers of the dense gas associated with star formation, and specifically of hot cores.

None of these transitions had previously been observed toward M82. Henkel and Bally (1985) report a detection of the  $2 \rightarrow 1$  transition of CS toward the galaxy's nucleus, using the 7m offset Cassegrain telescope at Bell Laboratories, Holmdel, New Jersey. The telescope had a half-power beam-width of 1.7 arcmin and a beam efficiency of 90%. Petuchowski and Bennett (1992) attempted to observe both SO ( $3_2 \rightarrow 2_1$ ) and  $\text{SO}_2$  ( $3_1\ 3 \rightarrow 2_0\ 2$  and  $10_1\ 9 \rightarrow 10_0\ 10$ ) toward M82 (and in NGC253) using the NRAO 12-m telescope. No clear detection was made, but the authors report a ‘marginal’ detection of the SO  $3_2 \rightarrow 2_1$  toward M82.

---

provides no route in which methanol can form, rather than being dissociated as in the models discussed in the main text. In either case, the presence of large abundances of the molecule is difficult to explain with a solely PDR model.

<sup>2</sup><http://spec.jpl.nasa.gov/>

For the observations reported here, the RxA3 receiver was used. The half-power beam width for this receiver is 20'', which corresponds to 16.1 kpc at the distance of M82. Observations were carried out on 2005 October 11, 12 and 13, November 13 and 2006 February 9 and 11. A beam efficiency of  $\eta = 70\%$  was assumed throughout the analysis. The total integration time was 2 hours each for the CS and SO transitions, and 2 hours and 10 minutes for SO<sub>2</sub>.

### 5.2.1 Results

CS was detected, and the data is shown in figure 5.1. A Gaussian fit to the data was applied, with amplitude 0.019 K and width 210 km s<sup>-1</sup>. Assuming the line is optically thin (and optical depths of 0.3–3 are typical in galactic sources) and conditions for local thermal equilibrium are satisfied, the column density can then be derived. The general expression relating the line optical depth ( $\tau$ ), the column density in a level ( $N_l$ ) and the excitation temperature  $T_{ex}$  is (Rohlfs and Wilson, 2004):

$$N_l = 93.5 \frac{g_l \nu^3}{g_u A_{ul}} \frac{1}{1 - e^{-\frac{-4.80 \times 10^{-2}}{T_{ex}}}} \int \tau dv \quad (5.1)$$

where  $g_l$  and  $g_u$  are the degeneracies of the lower and upper levels,  $A_{ul}$  is the Einstein coefficient for the transition in question and  $\nu$  is the transition frequency in GHz. In the Rayleigh-Jeans approximation, when  $T_{ex}/\nu \gg 4.80 \times 10^{-2}$  K, then this becomes

$$N_l = 2.07 \times 10^3 \frac{g_l \nu^2 T_{ex}}{g_u A_{ul}} \int \tau dv. \quad (5.2)$$

Now, if  $t \ll 1$  then  $T_{ex}\tau \cong T_{MB}$  allowing direct calculation of the column density in a level without any dependence on the excitation temperature. The total column density can then be found via the partition function,  $Z$ , for a transition between J+1 and J:

$$N_{Tot} = N_l \frac{Z}{2J + 1} \exp\left(\frac{\hbar B_e J(J + 1)}{kT}\right) \quad (5.3)$$

where  $B_e$  is the rotational constant for the molecule in question.

If we assume local thermal equilibrium, so that the excitation temperature is equal to the kinetic temperature found by Weiß *et al.* (2005), 50 K, then the derived total column density (in all states) for CS toward M82 is  $1.09 \times 10^{13} \text{ cm}^{-2}$ . This value compares well with

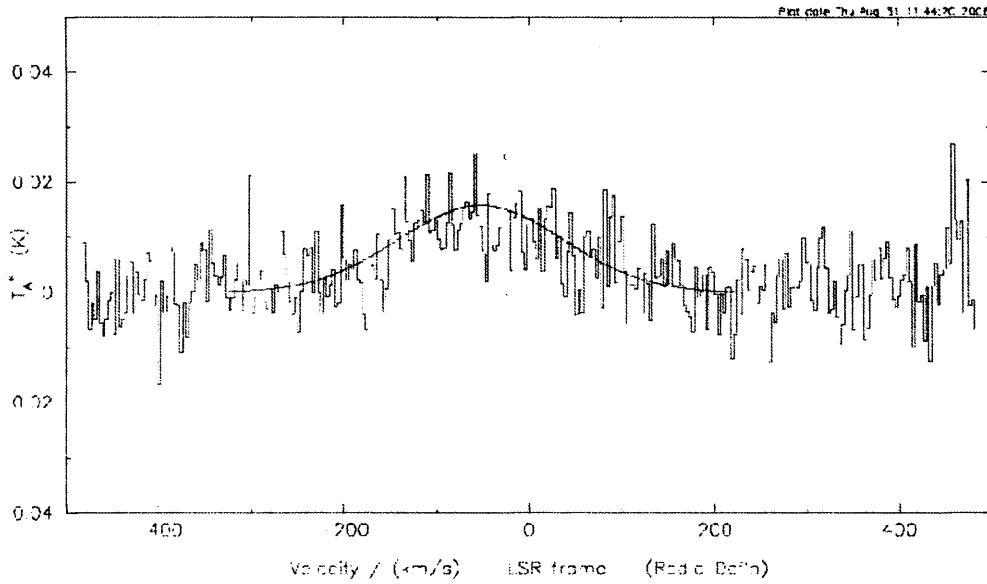


Figure 5.1: CS(5 → 4) toward the nucleus of M82. A Gaussian fit to the data, as described in the text, is shown. A polynomial baseline was subtracted from the data before the model was applied.

the total column density derived by Henkel and Bally (1985) using the 2 → 1 transition, as they obtained  $1.13 \times 10^{13} \text{ cm}^{-2}$ . If we assume, however, that the CS is associated with emission from hot cores (or hot core like chemistry) with typical temperatures of  $T_{ex} = 300 \text{ K}$ , then the value derived from our observations becomes  $4.39 \times 10^{13} \text{ cm}^{-2}$ .

In combination with the CS 2 → 1 data, it is possible to derive an estimate of the rotational temperature for the CS-containing gas. As the column density in the upper level of any transition,  $N_u$  (with degeneracy  $g_u$  and energy  $E_u$ ) is given by

$$\frac{N_u}{g_u} = \frac{N_{Tot}}{Z} e^{-\frac{E_u}{kT_{rot}}} \quad (5.4)$$

when LTE is assumed and the Rayleigh-Jeans approximation ( $h\nu \ll kT$ ) applies. It is therefore possible to derive a rotational temperature from the gradient of a plot of  $\ln N_u/g_u$  against  $E_u$ . Ideally, several transitions would be used, but the two transitions we do have result in an estimate of  $T_{rot} = 38.2 \text{ K}$ .

Neither the SO or the SO<sub>2</sub> transition we looked for were detected. The  $3\sigma$  limits on the *total* column densities are, if  $T_k = 50 \text{ K}$  is assumed,  $7.6 \times 10^{12} \text{ cm}^{-2}$  and  $2.3 \times 10^{13} \text{ cm}^{-2}$  for SO and SO<sub>2</sub> respectively. If a higher temperature ( $T_k = 300 \text{ K}$ ) is assumed, the limits are  $3.1 \times 10^{14} \text{ cm}^{-2}$  and  $1.8 \times 10^{14} \text{ cm}^{-2}$ . These are consistent with the limit derived by Petuchowski and Bennett (1992) which, for SO<sub>2</sub> is (at  $3\sigma$ )  $2.0 \times 10^{13} \text{ cm}^{-2}$ . Assuming

Molecule	Column density/cm <sup>-2</sup>	Source
CS	$1.09 \times 10^{13}$	This chapter
NH <sub>3</sub>	$1.0 \times 10^{13}$	Weiß <i>et al.</i> (2005)
CH <sub>3</sub> OH	$3.49 \times 10^{14}$	Martín <i>et al.</i> (2006)
CH <sub>3</sub> C <sub>2</sub> H	$1.0 \times 10^{14}$	Fuente <i>et al.</i> (2005a)

Table 5.2: Observed column densities for four species in M82. The species were selected from those whose abundances cannot be accounted for by PDR models.

X	CS	NH <sub>3</sub>	CH <sub>3</sub> OH	CH <sub>3</sub> C <sub>2</sub> H
CS	X	0.92	32.02	9.17
NH <sub>3</sub>	X	X	34.90	10.00
CH <sub>3</sub> OH	X	X	X	0.29

Table 5.3: Abundance ratios derived from column densities given in table 5.3. The ratios are given as X/Y; ie the NH<sub>3</sub>/CS ratio is 0.92.

their ‘marginal’ detection is real, they derive a column density of  $7.6 \times 10^{12} \text{ cm}^{-2}$ . The lack of any such detection in our data suggests that the abundances derived from this detection may be over-estimated.

### 5.3 Comparison with models

It is clear from the observations described in section 5.1.2 that a large proportion of the molecular gas contained within the system must be in PDR-like conditions. However, as we remarked before, it is equally obvious that there must also be a substantial contribution from dense gas. In this section, we investigate whether the observed abundances of the species associated with this dense phase might be explained by the application of the hot core model of Viti *et al.* (2004b). As described in section 1.1.2, the hot core phase of (canonically) massive star formation occurs when the newly ignited protostar is able to cause the sublimation of ice from the surface of dust grains in the material making up the protostellar core, producing a rich molecular chemistry for observers. We select four species (CS, NH<sub>3</sub>, CH<sub>3</sub>OH and CH<sub>3</sub>C<sub>2</sub>H<sup>3</sup>), the observed abundances of which are not well explained by extant PDR models. Their column densities are given in table 5.3 and the abundance ratios in table 5.3.

<sup>3</sup>Following convention, we will refer to CH<sub>3</sub>C<sub>2</sub>H as C<sub>2</sub>H<sub>4</sub>.

The models of *Viti et al.* (2004b) introduce a multi-stage depletion of molecules from the surface of the grains; of the species considered here, CS has a ‘CO-like’ desorption history, with fractions desorbing at low temperatures (either directly or from a monomolecular layer on water ice), while NH<sub>3</sub> and CH<sub>3</sub>OH desorb only along with the water ice. CH<sub>3</sub>C<sub>2</sub>H is intermediate between the two cases, desorbing from a layer on water ice but not as a pure species. The timing of these events (see section 1.2) is determined by the size of the newly formed protostar, and initially we considered two models, each with a different protostellar mass. 25M<sub>⊙</sub> and 60M<sub>⊙</sub> were chosen as examples. In fact, although the details of the evaporation do change with the mass of the protostar, the general trends which the abundance ratios follow are not affected, and so the validity of our results is not affected.

Prior to the evaporation of species from the surface of the grains, both models significantly underestimate the value of the C<sub>3</sub>H<sub>4</sub>:CH<sub>3</sub>OH, C<sub>3</sub>H<sub>4</sub>:CS, CH<sub>3</sub>OH:CS, C<sub>3</sub>H<sub>4</sub>:NH<sub>2</sub> and CH<sub>3</sub>OH:NH<sub>3</sub> ratios, and significantly overestimate the NH<sub>3</sub>:CS ratio. The molecular signature of the nucleus of M82 cannot therefore be explained by the early stages of massive star formation.

Once the desorption of molecules from the dust grains is under way, however, it is possible to find a match between the models and observations. Between 10<sup>5</sup> and 10<sup>6</sup> years after the warming of the material surrounding the protostar has begun the model produces ratios of CH<sub>3</sub>OH:CS, of C<sub>3</sub>H<sub>4</sub>:CS and of C<sub>3</sub>H<sub>4</sub>:CH<sub>3</sub>OH which are close to the observed values. The former two cases remain close to the observed value as equilibrium is reached, whereas in the latter case the ratio continues rising, suggesting that this ratio may - if the hot core model proves useful - provide a sensitive chemical clock for the predominant star formation in the galaxy.

The abundance ratios involving nitrogen cannot be explained by the models of *Viti et al.* (2004b). The NH<sub>3</sub>:CS ratio remains above the observed value, and rises as NH<sub>3</sub> desorbs from the dust grains. Both CH<sub>3</sub>OH:NH<sub>3</sub> and C<sub>3</sub>H<sub>4</sub>:NH<sub>2</sub> are underestimated by several orders of magnitude throughout. There is a strong peak in the ratio of C<sub>3</sub>H<sub>4</sub>:NH<sub>3</sub> between two phases of desorption, when C<sub>3</sub>H<sub>4</sub> has desorbed but NH<sub>3</sub> has not, but it is transitory. In all three cases, the models produce too much NH<sub>3</sub> compared with the observations. This is in agreement with observations of *Mauersberger et al.* (2003) toward NGC253 (and two other nearby star forming galaxies, Maffei 2 and IC 342) who find that M82 has an ammonia abundance at least one order of magnitude below the other sources in their survey.

However, the model used up until this point was developed for star formation in the Milky Way. Although a full set of abundances is not available for M82, it is clear from observations which do exist that solar neighbourhood atomic abundance ratios do not necessarily apply. Origlia *et al.* (2004) detail abundances derived both from observations of the galaxies in the near-IR, but also in the galaxy's hot gas, via X-ray spectra obtained with the XMM-Newton and Chandra satellites. The errors in such observations are large, but purely solar abundances cannot account for the observations, particularly in the gaseous phase. It therefore seems likely that, in order to produce models which reproduce the observations of M82, the atomic abundances of species such as carbon or nitrogen may need to be altered.

As an example, we investigated the effect of a reduced nitrogen abundance on the modelled ammonia ratios. The nitrogen abundance was reduced by a factor of between 5 and 50 times. Ideally this factor would be determined by observations, but for now we allow it to vary to investigate the effects. The results are encouraging; the ratio of NH<sub>3</sub>:CS at late times (after desorption is complete) is, as you might expect, reduced. A reduction of the nitrogen abundance by a factor of 10 is sufficient to produce a ratio close to the observations in under 10<sup>6</sup> years. At similar times, in models with reduced nitrogen abundance both C<sub>3</sub>H<sub>4</sub>:NH<sub>3</sub> and CH<sub>3</sub>OH:NH<sub>3</sub> ratios are dramatically increased. An example of the evolution is shown in 5.2. These results suggest that the previously anomalous abundances of four species observed toward the nucleus of M82 could be explained by a hot core chemistry, albeit with a non-solar atomic abundance of nitrogen.

## 5.4 Discussions and conclusions

The results above, although based on a limited set of observations and therefore necessarily tentative, suggest that the 'dense gas ... shielded from the radiation field' which Martín *et al.* (2006) invoke to explain their observations of methanol may have chemistry similar to that seen in the hot cores associated with massive star formation. With the enhanced star formation rate seen in starburst galaxies like M82 and NGC 253, it is not surprising that the signature of hot cores might be visible in extragalactic systems. However, the presence of hot core-like chemistry does not necessarily imply the presence of hot cores.

Requena-Torres *et al.* (2006) observations of complex organic molecules (such as C<sub>2</sub>H<sub>5</sub>OH, HCOOCH<sub>3</sub> and CH<sub>3</sub>COOH) along with CS and CH<sub>3</sub>OH toward the centre of the Milky

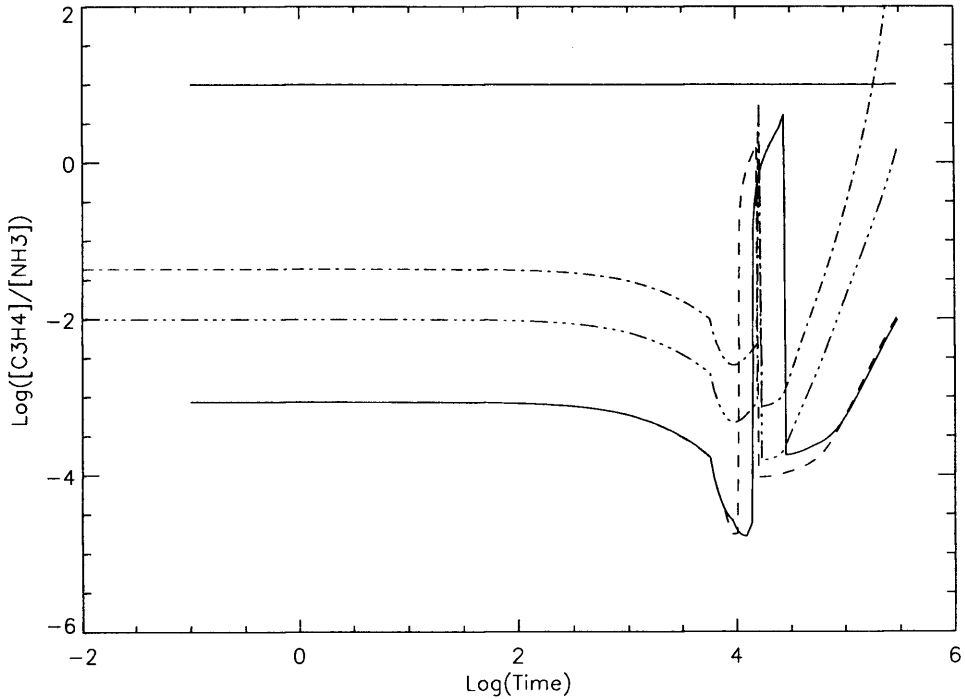


Figure 5.2: Evolution of the  $\text{C}_3\text{H}_4:\text{NH}_3$  ratio with time in years since the beginning of the warming of the gas surrounding the nascent protostar. The straight line represents the observed value of the abundance ratio, and a comparison between models with solar abundances and those in which the nitrogen abundance is  $1/10^{\text{th}}$  and  $1/50^{\text{th}}$  of the solar value. The ‘spike’ in abundance at  $\log t \sim 4$  is due to the desorption of  $\text{C}_3\text{H}_4$  before that of  $\text{NH}_3$ .

Way. One might expect this environment to provide a close, local, analogue to the nucleus of M82, and in common with the results of our modelling reported here, the authors find the ratio of the abundances of the more complex species with that of methanol are similar in Milky Way hot cores and in the galactic centre clouds. The high abundance of these complex molecules suggests that they have indeed been ejected from the icy mantles of dust grains, whether by the presence of newly formed stars or, as Requena-Torres *et al.* suggest, by shocks. If the shocks are periodic, then a high abundance of such molecules can be maintained indefinitely. In this way, a ‘hot core’ signature can be present without the need for associated star formation. However, sustained star formation at a constant rate would also be expected to result in an apparently uniform hot core chemistry, and so it is not yet clear whether the molecules seen in extragalactic sources are part of many individual hot cores or form a single, large, hot core-like region.

An obvious test of this sort of idea would be to examine systems with different star formation rates and histories. If the molecules are indeed associated with true hot cores,

then some dependence of the observed abundances with the star formation rate (derived, for example, from the infrared luminosity) would be expected. The type of models used here could practically be applied to the wealth of observations of NGC253 described in section 5.1.1.

Returning to M82, there are two lessons to be learnt from the models which had a reduced abundance of nitrogen, and which provided the best fit to the observations. First, slightly counterintuitively, it suggests that further study of the sulphur chemistry of the source may be useful. If nitrogen is indeed underabundant compared to the solar value, then sulphur-bearing molecules are expected to show enhanced abundances, and hence will be more important as tracers of star formation.

Second, further work is required to constrain the abundance of nitrogen in the source. One possibility is to use so-called ‘chemical evolution’ models to constrain the abundance of nitrogen from observations that already exist. These models (e.g. Ferreras *et al.* (2005a)) use models of the yields from supernovæ to predict the evolution of the atomic abundance with time for a galaxy with a given star formation history. Although nitrogen is a notoriously difficult element to constrain, having both primary and secondary sources, it is possible to use such a model to predict the nitrogen abundance from observations such as those of Origlia *et al.* (2004), mentioned in the previous section. More directly, observations of further nitrogen bearing species would improve the constraints on the model, or optical spectra could be used to directly obtain the ratio of nitrogen to other atomic species.

In conclusion, it is clear that the complex chemistry of a source such as M82 (at a distance which precludes the resolution of individual emission regions) cannot be accounted for by any single model. Although large proportions of the gas contained in the system must be in a PDR, we have shown that hot core chemistry is able to explain many of the abundance ratios which the PDR models cannot. The fit is particularly good if a model with reduced nitrogen abundance is used, suggesting that models need to take into account the star formation history of a source as well as the environment that exists in the present day.

## CHAPTER 6

---

# Hot cores: Probes of star formation at high-redshift

## 6.1 Introduction

In recent years there has been much debate - informed by both observational data and theoretical models and simulations - about the presence and nature of star formation in the early Universe. This debate exists whether one is considering the global star formation rate (for instance, the evidence seems to point to a greatly enhanced star formation rate earlier in the evolution of the Universe (Calzetti (2001), but see also Bunker *et al.* (2004)) or the history of individual objects. Indeed, individual objects with greatly enhanced star formation rates have been detected in the early Universe; a good example is the quasar at a redshift of  $z = 6.4$ , which was studied by Bertoldi *et al.* (2003). They report a detection of CO and, via the object's far-infrared emission, derive a star formation rate of  $3000M_{\odot}\text{yr}^{-1}$  (see section 6.3.1 for details of deriving star formation rates).

As we have noted in section 1.4.1, the first epoch of star formation must be very different from those that follow. Studies such as those carried out by Abel *et al.* (2002) and Bromm *et al.* (1999) have used simulations to investigate the nature of the first stars, which are expected to have formed at redshifts in excess of 10. Such work indicates that the characteristic mass of these first stars was large, with masses in excess of  $100M_{\odot}$ . This result is a conclusion drawn from simulation, but it can be understood intuitively as an increase in the Jeans mass due to the higher temperature, as cooling is less efficient in the absence of carbon and oxygen. These massive stars must necessarily have a profound

influence on the environment around them; they may be the source of the reionization of the Universe (Barkana and Loeb, 2001) and the metals they produce may seed the interstellar medium for later star formation.

It is possible that the first stars may trigger further star formation directly. O’Shea *et al.* (2005) used a three-dimensional computational model to study the formation of stars within the HII region which surrounds a Population III star. As discussed in section 1.4, such stars will surround themselves with HII regions several kiloparsec in diameter (Kitayama *et al.*, 2004). Following the violent death of the central star, the ionized gas will remain as warm as 1000K even  $10^7$  years after the supernova, creating an environment which, at first glance, is hostile to the formation of further stars. Star formation will be further inhibited by the presence of a hard ultraviolet background created by the first stars themselves. These problems notwithstanding, the work of O’Shea *et al.* (2005) suggests that stars *can* form from primordial gas in such conditions, and that any stars formed in this way - despite having zero initial metallicity - may be smaller than their predecessors. In fact, approximately 10 ‘minihalos’ which may go on to form stars were quickly produced within the simulated HII regions. If these results are confirmed, it would seem that a first, large, generation of primordial stars are succeeded by a second generation, which are smaller but still composed of primordial material. These would presumably be followed by a ‘true’ second generation of stars, formed from gas enriched with metals from the two types of Population III star.

Mixing must occur eventually between the interstellar medium and the ejecta from supernovæ, but the timescale on which this process occurs and many of the details remain obscure. However, it is clear that substantial mixing must have occurred within the first billion years after the Big Bang, as significant quantities of molecular gas are observed in the most distant individual objects yet seen. The most abundant molecule, as in the Milky Way (excluding, as ever,  $H_2$ ), is carbon monoxide; I have already mentioned the CO detection at  $z \sim 6$ . It is also possible to detect other molecules at great distances; HCN and  $HCO^+$ , for example, have been seen in the quasar APM08279 at a redshift of  $z = 3.91$  (Wagg *et al.*, 2005; García-Burillo *et al.*, 2006). In fact, the anomalously large ratio of HCN/ $HCO^+$  luminosities in this object suggests that such observations can provide both information about the sources being studied, and a stringent new test for chemical models which until now have been applied only to the local neighbourhood. The next section will consider how such models may be adapted to cope with more exotic environments.

## 6.2 Modelling high-mass star formation in the early Universe

*This section is based on Lintott et al. 2005, published in the Monthly Notices of the Royal Astronomical Society, 360, 1527.*

### 6.2.1 How to observe distant star formation

If objects at redshifts of  $z > 6$  have such rates of star formation which are hundreds, or even thousands of times the Milky Way rate, then this star formation should betray its presence in the familiar observational signatures of strong infrared emission and the presence of a typical chemistry. The presence of molecular ‘signatures’ are often distinct and robust indicators of star-forming activity in our own Galaxy. In this section models of Milky Way star formation are adapted in order to investigate the visibility and utility of such signatures in systems at high redshift.

The distant systems within which molecular emission has been seen are, without exception, extremely luminous in the infrared. Indeed, they are often classified as Luminous Infrared Galaxies (LIRGs) or Ultra-Luminous Infrared Galaxies (ULIRGs)<sup>1</sup>. As I will discuss in more detail in section 6.3.1, such high luminosities in the infrared are usually associated with extensive star forming activity. In fact, if taken at face value, then these infrared luminosities indicate a star formation rate equal to  $10^2$  or  $10^3$  times the Milky Way value of  $\sim 1 M_{\odot} \text{yr}^{-1}$ . The work in this chapter is thus based upon the fundamental assumption that as these distant systems are forming stars at such an accelerated rate, then models of star formation developed for the Milky Way should (when suitably adapted) be of use in predicting - and accounting for observable - molecular abundances despite the large distances. This assumption will be explored and tested in more detail later, but for now we should consider which models are likely to be most useful in identifying star formation.

As discussed in section 1.4, the evolution of the initial mass function, or IMF, is not well constrained between the epoch of the massive first stars and the present day. For most purposes, it is usual to assume that a Milky Way IMF is appropriate, except in the

---

<sup>1</sup>The commonly accepted definition of a ULIRG is a system which has an intergrated luminosity between 8 and  $1000 \mu\text{m}$  of in excess of  $10^{12} L_{\odot}$ . Systems with a luminosity between  $10^{11}$  and  $10^{12} L_{\odot}$  are classified as LIRGs.

very early Universe. Within the Milky Way, the richest sources of radiation associated with molecules are the ‘hot cores’ phase during the formation of massive stars, and so it is this phase of star formation that we have taken as the basis for our models of high-redshift star-formation. Hot cores are particularly associated with the formation of massive stars, and this is also an advantage. If the IMF in distant systems does differ from that in the Milky Way, then it is likely to favour the formation of more massive stars. The reasons for this are twofold. Firstly, the primary cooling mechanism for gas at high temperature is radiation from atomic carbon and nitrogen, and this will obviously be less efficient in low-metallicity gas. As with the first stars, inefficient cooling should lead to less fragmentation and hence more massive stars. Secondly, it may be that systems which are forming stars at such rapid rates will necessarily form stars in clusters, favouring massive star formation.

Although the sequence of events that leads to the formation of a hot core is fully discussed in section 1.1.2, it will be useful to summarise here. The hot core phase is a short-lived episode in the evolution of a high mass protostar (although recent work by Bottinelli *et al.* (2004) has shown that low-mass stars too may pass through a similar stage of evolution). During the initial collapse of the forming star, as the temperature is typically approximately 10K, many molecular species which are present in the gas phase ‘freeze out’ on to the surface of dust grains. This process has a profound influence on the chemical evolution of the core. Initially, potential reactants and coolants are removed from the gas phase material, and the grain surfaces themselves subsequently provide sites for further chemical evolution, producing more complex species than would be possible if only gas phase chemistry were present. Once the newly-formed star has begun to radiate, it heats the surrounding dust to a temperature of (typically) 300K. The ice mantle on the grains therefore sublimates, and the newly formed (generally more complex) molecules appear in the gas phase, where they radiate strongly in the warm gas. This molecular ‘soup’ is the signature of the hot core phase, and it is this period in the protostar’s evolution with which we are concerned in this chapter.

Despite much interest in star formation at high redshift, prior to this work there had been no detailed study of the application of chemical models of the type used in studies of nearby star forming regions to observations of distant star-forming galaxies. The question addressed here is whether or not the molecular emission associated with hot cores will be detectable in distant (i.e. high redshift) systems.

## 6.2.2 Methodology

### 6.2.2.1 Initial Abundances

In adapting extant chemical models to reflect the situation at high redshift, the selection of initial abundances for atomic species is crucial. In seeking to study the formation of a second generation of stars, models predicting the yield from the massive first generation are used rather than a simplistic model of low metallicity which maintains solar abundance ratios. These yields will depend critically on the mass of progenitor; a particularly important example is the case of zero-metallicity stars with masses in the range  $40 - 140M_{\odot}$ . Heger *et al.* (2003) suggest that such stars will form black holes via the direct collapse of the core (rather than by the more normal process of ‘fallback’, in which material is ejected from the core before collapsing to the centre and only then forming a dense remnant). In this case, there may be little mixing of the nucleosynthetic products with the surrounding medium. However, if the star has a helium core mass of about  $65M_{\odot}$  (corresponding to an initial mass of approximately  $140M_{\odot}$ ), the situation is different. The conditions in these stars at the end of the helium burning phase produce large numbers of electrons and positron pairs, which then annihilate. This has the net effect of converting the internal energy of the gas into radiation, allowing the star to contract rapidly (Barkat *et al.*, 1967). Explosive oxygen and silicon burning ensues, providing enough energy to reverse the collapse; the net result of such a pair-production supernova is not a black hole or neutron star, but the complete dispersal of the material into the surrounding medium. Stars which are larger still, with helium core masses of greater than  $\sim 135M_{\odot}$  (an initial mass of greater than  $\sim 260M_{\odot}$ )<sup>2</sup>, will once more collapse to a massive black hole (Fryer *et al.*, 2001).

As simulations cannot yet distinguish between these possibilities and so the strict divisions between categories remain uncertain, three different models of the yields from zero-metallicity stars are used in this initial study, allowing a contrast to be made between predictions for the widest possible range of masses. Chieffi and Limongi (2002) (hereinafter CL02) have performed calculations using the FRANEC code (Chieffi *et al.*, 1998) to predict the results of a set of zero metallicity stars which have initial masses between 15 and  $80M_{\odot}$ . Taking advantage of the relative simplicity of zero-metallicity stars compared to their present-day equivalents, the code includes the evolution of the star from

---

<sup>2</sup>These values are appropriate strictly only for non-rotating stars.

before it joins the main sequence until the onset of the supernova explosion, following the abundance of 179 separate isotopes. Each of these will be sensitive to different parameters; an example is the dependence of the abundance of intermediate-mass elements on the carbon left by core helium burning (Weaver and Woosley, 1993). The evolution during the explosion itself is followed by assuming that the pressure inside the shock front, which moves outward through the envelope of the star, is (almost) constant and dominated by the radiation pressure. This assumption, along with a set explosion energy of  $1.2 \times 10^{51}$  erg, allows the variation of temperature and density to be calculated and the evolution of the chemical network to be followed.

Having produced a set of predicted yields, it is possible to perform a detailed comparison between their models and the ‘average’ observation obtained by Norris *et al.* (2001) from five low-metallicity stars in the Milky Way. These observations are complementary to those of high-redshift systems, as old stars in the Milky Way are assumed to have formed from near-primordial gas. Systematic searches for such stars have therefore been undertaken, resulting in well over 100 stars which are known to have metallicities<sup>3</sup> of less than 1/1000th the solar value (Norris, 1999). Each of the stars in the Norris *et al.* (2001) sample has  $[\text{Fe}/\text{H}] < -3.5$ .

The best fit to these data found by CL02 was a model of a Population III progenitor with an initial mass of  $80M_{\odot}$ , and this model was therefore used as the starting point for the models described in this chapter. As we do not expect stars to form solely from the remnant of a supernova, and in the absence of any detailed predictions of the process by which the mixing with the interstellar medium occurs a simple procedure was adopted. Specific values of the carbon abundance as a fraction,  $f$ , of the local abundance taken from Sofia and Meyer (2001) were adopted. The abundance ratio of the other species, X/C (for any atomic species, X), was then matched to the model chosen from CL02.

The models of Umeda and Nomoto (2002) (hereinafter UN02) use a separate set of codes to model the evolution of the progenitors of pair instability supernovæ, which they define as those with initial masses between 150 and  $270M_{\odot}$ . They find, however, that pair-instability supernovæ are unable to reproduce the  $[\text{Zn}/\text{Fe}]$  ratio observed in Milky Way low metallicity stars. It is still interesting to consider the molecular chemistry of star formation from gas enriched in this way, both as an independent test and because it is difficult to distinguish between low metallicity stars which are truly second generation

---

<sup>3</sup>Metallicity is defined here, following Norris *et al.* (2001), as  $[\text{Fe}/\text{H}] = \log(N_{\text{Fe}}/N_{\text{H}})_{\text{star}} - \log(N_{\text{Fe}}/N_{\text{H}})_{\odot}$

Model	CL02	UN02	HW02	Solar
Stellar Mass/ $M_{\odot}$	80	150	200	N/A
C	1.0000	1.0000	1.0000	1.0000
O	3.212	8.3887	10.833	2.719
N	4.240(-7)	0.0023	1.1155(-5)	0.293
S	0.05375	0.2874	1.0895	0.172
Mg	0.1293	0.4373	0.8504	0.232

Table 6.1: Abundances relative to carbon, obtained from the modelled yields of population III stars due to Chieffi and Limongi (2002), Umeda and Nomoto (2002) & Heger and Woosley (2002). CL02 assume a progenitor of  $80 M_{\odot}$ , whereas UN02 model a larger star with a mass of  $150 M_{\odot}$ . HW02 use a model which produces a total yield of  $80 M_{\odot}$ . These abundances provide the initial conditions for the results presented in section 6.2.3. The largest difference is the near-absence of nitrogen in the CL02 and HW02 models. Solar abundances are photospheric, taken from Grevesse and Sauval (1998), and are shown for purposes of comparison. We define  $1.2(15) = 1.2 \times 10^{15}$

stars, and those enriched by several separate supernova events. Hence, the model for  $150M_{\odot}$  is included in this study.

The third set of abundances was taken from the models of Heger and Woosley (2002) (hereinafter HW02) of a star with a  $80M_{\odot}$  helium core, corresponding to a total mass of  $200M_{\odot}$ . They use the KEPLER code (Weaver *et al.*, 1976; Heger *et al.*, 2003) to follow the evolution of 304 isotopes both before and during the explosion. The abundances relative to carbon used for each of the three models are shown in table 6.1. Three different models were included in order to (a) investigate the sensitivity of the results to the choice of enrichment model and (b) investigate the possibility that future observations of subsequent star formation could distinguish between different models of star formation.

It should be noted that the nitrogen abundances constitute the largest differences between the three models. The synthesis of primary nitrogen is not considered in detail by current supernova models. For instance, HW02 evolve only helium cores, thereby neglecting the (significant) production of nitrogen which takes place during the earlier phases of stellar evolution. Furthermore, the nitrogen yields are highly sensitive to the poorly understood phenomena of rotation and convective overshoot (when material sinking through the convective zone of the star's interior is carried into the radiative zone). Nitrogen is mostly a secondary element, produced as a byproduct of the CNO cycle, as illustrated by

the high abundance ratio found in the Sun (Renzini and Voli, 1981)<sup>4</sup>.

### 6.2.2.2 Chemical and dynamical model

A chemical model based on that described in Viti and Williams (1999) was used to describe the chemical evolution of regions of high mass star formation. The model is essentially a two-stage calculation, beginning with a diffuse ( $\sim 300\text{cm}^{-3}$ ) medium<sup>5</sup> in purely atomic form (apart from a fraction of hydrogen which we assume is already incorporated into H<sub>2</sub>) which then undergoes a collapse which is assumed to be under free-fall. The dynamical and chemical equations are solved simultaneously during this phase, and the free-fall collapse law described in Rawlings *et al.* (1992) is used. The change in central gas number density,  $n$ , as collapse proceeds from initial density  $n_0$  to final density  $n_f$  is then given by (see section 4.3 for the derivation):

$$\frac{dn}{dt} = B \left( \frac{n^4}{n_0} \right)^{\frac{1}{3}} \left( 24\pi G m_{\text{H}} n_0 \left[ \left( \frac{n}{n_0} \right)^{\frac{1}{3}} - 1 \right] \right)^{\frac{1}{2}}. \quad (6.1)$$

It should be noted that no attempt is made to include the internal structure of the core in the calculations. The free-fall collapse of a sphere is homologous and so a uniform density and temperature are used throughout. Although undoubtably an approximation, this allows the chemistry to be followed during collapse, instead of requiring a static solution. During the initial collapse phase the temperature is 10K, and so during this first phase of protostellar evolution, all species except hydrogen and helium freeze on to the grains and, where possible, hydrogenate. At the end of this stage, approximately 99% of molecules have frozen on to the grains (Caselli *et al.*, 1998).

Once a critical density at which the protostar is assumed to ignite (chosen to represent the observed density of hot cores) is reached, the collapse stops and the temperature increases to 300K. The system is allowed to continue evolving chemically despite the halt applied to the dynamical evolution (this is obviously a first-order approximation; any such sudden halt would, in reality, result in the disruption of the core by massive shocks). For massive stars, the increase in temperature due to the ignition of the protostar occurs extremely rapidly, and hence the model in this chapter uses an instantaneous increase in

---

<sup>4</sup>There is some evidence of a primary component. See van Zee *et al.* (1998) and references therein for a discussion.

<sup>5</sup>The results are insensitive to the choice of initial density.

temperature rather than a more sophisticated model.

The chemical network was derived from the UMIST rate 99 database (Le Teuff *et al.*, 2000) and follows the chemical evolution of 168 species involved in 1857 gas-phase and grain reactions. This subset of the full UMIST database was selected to include a full reaction network for all species detected in Milky Way star forming regions.

### 6.2.2.3 Dust properties & extinction

As discussed in section 6.2.2.1, in adjusting this basic model of star formation to suit the early Universe, the effects of the differences in the metallicity of the material which makes up the star forming region between low and high redshift systems has been taken into account. It is also necessary to allow for the presumably lower density of dust in the early Universe. The formation and evolution of dust in such an environment is poorly understood. We know neither the chemical nature of the dust, nor the dust grain size distribution, and the appropriate interstellar extinction curve is thus poorly constrained. It is clear from the nature of the chemical signature of hot cores that these issues may prove to be critical, but in the absence of data which might allow more informed decisions, the simple assumption that the dust mass scales with overall metallicity and that the size distribution produces an interstellar extinction curve similar to that seen in the Milky Way (and discussed in section 1.2) has been made. The presence of SCUBA galaxies is an indication that substantial quantities of dust did indeed form in the early Universe.

Another important difference between star formation at a redshift of  $z \sim 6$  and  $z = 0$  could be the evolution of the cosmic microwave background, or CMB. The evolution of the temperature of its blackbody spectrum is given by  $T = T_0(1 + z)$  and the well-known Planck formula then gives the intensity for a particular wavelength at a given redshift:

$$B_\nu(T) = \frac{2h}{c^2} \frac{\nu^3}{e^{\frac{h\nu}{kT}} - 1}. \quad (6.2)$$

The important wavelengths in this context are those which would participate in the dissociation of molecules, and these are in the ultraviolet. Even at a redshift as large as  $z \sim 10$ , the order of magnitude increases in CMB temperature are accompanied by an insignificant increase in intensity at these wavelengths. In addition, it should be noted that at  $z=6$  the temperature of the CMB would be about 20K, and this may begin to affect the freeze-out of species necessary for the formation of hot-core chemistries discussed here.

However, as long as the cores being considered remain optically thick, then the effect should be minimal.

In local hot cores, the extinction is usually estimated to be between a few hundred and a few thousand visual magnitudes (see, for example, van der Tak *et al.* (2000)). The extinction of the core will obviously be reduced in a high redshift system if the dusty component of its material is less dense here. If the accompanying drop in visual extinction is severe enough, then, as the cloud becomes optically thin, photodissociation will be able to destroy the molecules which are associated with a hot core chemistry and which we would like to use as signatures of star formation. We have already adopted a model in which the amount of dust is proportional to the metallicity, and we would like to be able to model the formation of stars at extremely low metallicities, perhaps down to one-thousanth of the solar values. At these low dust densities, it is necessary to assume that the diameter of the core is increased by a factor of 10 (to 0.3pc). Assuming that cores are larger than their Milky Way counterparts in this way produces an extinction of 10 to 15 magnitudes, which is large enough to prevent the photodissociation of hot core molecules.

The survival of the molecules within the cores is, nonetheless, uncertain. However, the detection of CO at a redshift of 6.42 by Walter *et al.* (2003) provides evidence that molecules can and do survive at these early epochs. It should also be noted that the change in the spectrum of the CMB will alter the excitation of molecular species (Redman *et al.*, 2004*b*).

### 6.2.3 Results

#### 6.2.3.1 Single hot core

The results of the initial runs, expressed as final column densities (i.e. those once chemical equilibrium in the hot core phase has been reached), are shown in tables 6.2, 6.3 and 6.4. The final column densities have been chosen as these represent the predictions for the hot core phase. The tables reveal differences between the models, regardless of the overall metallicity adopted. In particular, the UN02 models (which use the yield from a  $150M_{\odot}$  zero-metallicity progenitor) yield much higher predicted column densities for sulphur-bearing species such as CS, H<sub>2</sub>CS and SO<sub>2</sub>. As an example, figure 6.1 shows the ratio between the abundances of SO and HCN in hot cores formed from gas with solar abundance ratios, and with a low metallicity model.

Species	SN,1/100	SN,1/500	SN,1/1000	*
CO	6.5(15)	1.8(15)	1.1(15)	1.1(15)
H <sub>2</sub> CS	6.9(14)	1.1(14)	3.4(13)	3.7(13)
CH <sub>3</sub> OH	1.1(12)	3.1(10)	9.6(9)	9.4(9)
H <sub>2</sub> CO	2.9(14)	9.3(13)	4.2(13)	4.4(13)
SO <sub>2</sub>	7.1(14)	2.1(12)	3.7(11)	4.3(11)
H <sub>2</sub> S	1.5(9)	2.3(9)	3.9(9)	4.1(9)
CS	1.2(15)	5.7(14)	3.1(14)	3.1(14)
SO	7.9(14)	7.8(12)	2.7(12)	2.8(12)
CH <sub>3</sub> CN	3.1(9)	1.9(9)	1.2(9)	1.2(9)
HC <sub>3</sub> N	2.5(12)	3.6(11)	1.1(11)	1.1(11)

Table 6.2: Calculated column densities (in  $\text{cm}^{-2}$ ) for a variety of species. The first three columns have a carbon abundance set to 1/100<sup>th</sup>, 1/500<sup>th</sup> and 1/1000<sup>th</sup> of solar, and the other species set so that their ratio with carbon matches that predicted by a model for a zero metallicity star which yields  $80\text{M}_\odot$ . This model is from CL02. The results in the fourth column show the effect of using 1/1000<sup>th</sup> local abundances but with no change either to the diameter or to the extinction compared to standard models appropriate to the Milky Way.

Species	SN,1/100	SN,1/500	SN,1/1000	*
CO	6.0(15)	3.5(15)	2.2(15)	1.289(17)
H <sub>2</sub> CO	1.0(14)	3.2(13)	6.2(12)	8.565(9)
H <sub>2</sub> S	9.6(9)	5.4(9)	7.6(9)	1.652(6)
CS	2.7(15)	1.9(15)	1.1(15)	1.796(16)
H <sub>2</sub> CS	1.8(15)	5.4(14)	1.3(14)	2.190(15)
SO	1.1(15)	4.0(12)	2.7(12)	1.574(9)
SO <sub>2</sub>	1.1(15)	6.7(11)	2.1(11)	1.316(13)
CH <sub>3</sub> OH	1.3(12)	9.7(10)	2.4(10)	7.353(12)
HC <sub>3</sub> N	4.4(12)	3.6(12)	2.5(12)	1.165(12)
CH <sub>3</sub> CN	4.7(9)	4.3(10)	7.8(10)	8.383(12)

Table 6.3: As table 6.2, except for yields from a 150 solar mass supernova as calculated by UN02

Species	SN,1/100	SN,1/500	SN,1/1000
CO	1.4(16)	3.3(15)	1.8(15)
H <sub>2</sub> CO	3.1(12)	5.4(11)	6.1(10)
H <sub>2</sub> S	7.6(11)	2.5(11)	1.6(11)
CS	3.3(15)	3.2(15)	2.1(15)
H <sub>2</sub> CS	4.1(15)	1.3(15)	3.1(14)
SO	1.4(16)	7.8(14)	2.2(14)
SO <sub>2</sub>	9.3(15)	1.3(14)	1.9(13)
CH <sub>3</sub> OH	4.7(12)	9.2(10)	2.4(10)
HC <sub>3</sub> N	5.0(7)	3.2(8)	2.6(9)
CH <sub>3</sub> CN	1.9(6)	2.9(7)	7.8(7)

Table 6.4: As table 6.2, except for yields from models by HW02.

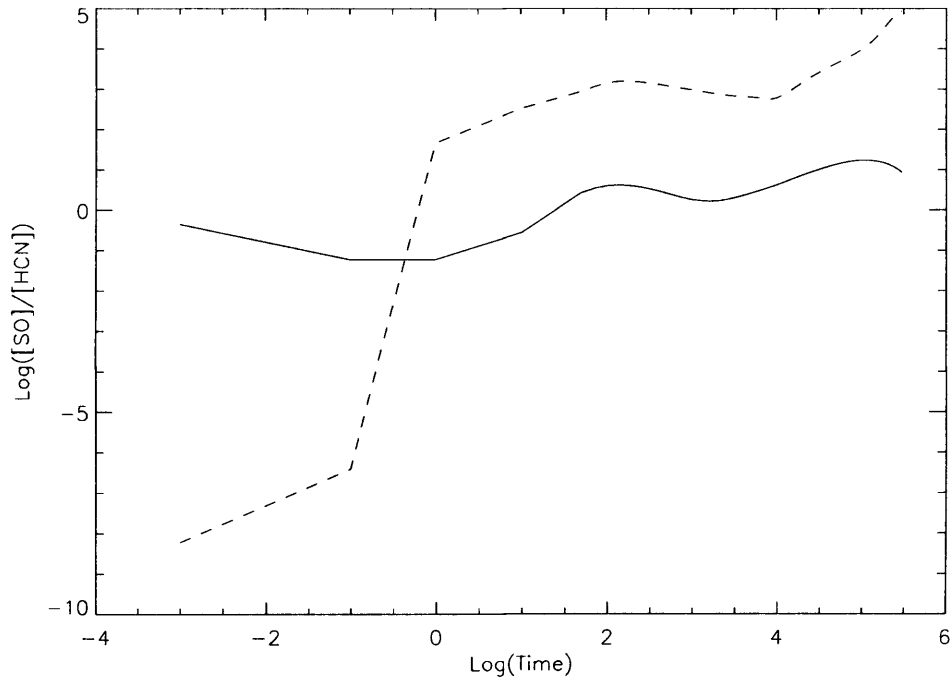


Figure 6.1: The ratio between the abundances between SO and HCN in a hot core formed from gas with Milky Way abundances (solid line) and in gas enriched only by the ejecta from a population III star (using the models of CL02) (dashed line). The enhanced importance of sulphur-bearing species is clearly seen.

The effects of the changes to the core size (and hence to the extinction) discussed above are clearly shown in table 6.2. Although the general trend is for the predicted column density to be reduced in the ‘high redshift’ cores when compared with the Milky Way models, the effect is small and for some species the net effect of the reduction in extinction when coupled with the increase in size is an increase in column density.

Chieffi & Limongi have recently published new calculations for the yields of smaller stars with zero or low metallicity (Chieffi and Limongi, 2004). Using these yields - appropriate for the supernovæ of zero metallicity stars with masses of  $30M_{\odot}$  - produces column densities for most species which are approximately an order of magnitude larger than those presented in table 6.2. A further enhancement in column density is found if the primordial material is enriched with the remnant of a supernova associated with a star with extremely low metallicity ( $10^{-4}Z_{\odot}$ ), rather than zero metallicity. If a picture of triggered star formation similar to that suggested by O’Shea *et al.* (2005) and discussed above is correct, then it may be that such low metallicity stars appear early on in the history of the Universe. If so, these results indicate that substantial abundances of many molecules will accompany the formation of all but the first generations of stars, regardless of the details of the star formation history.

### 6.2.3.2 Observing multiple hot cores

Will these molecular abundances correspond to detectable signals from high redshift galaxies? In order to answer this question it is necessary to estimate the number of hot cores in a system which might be forming a second generation of stars for us to observe.

Lumsden *et al.* (2002) combine a mid-infrared survey from the Midcourse Space eXperiment (MSX) satellite with ground-based near-infrared photometry (from the 2MASS survey) to provide an unbiased survey of the Milky Way galactic plane, and detect 3000 massive young stellar objects. Making a reasonable adjustment for the incompleteness of their survey<sup>6</sup> one obtains a conservative estimate of approximately  $10^4$  hot cores in the Milky Way, which has a star formation rate of around  $1M_{\odot}\text{yr}^{-1}$  (Noh and Scalo, 1990). Bertoldi *et al.* (2003) estimate from far-infrared luminosity that QSOs of the type considered here may have a star formation rate as high as  $3000M_{\odot}\text{yr}^{-1}$ . If we assume that the number of hot cores is proportional to the overall star formation rate, this might suggest

---

<sup>6</sup>They use a ‘crude analysis’ to suggest that their survey is 50% complete at 10kpc, and this neglects any young stellar objects hidden behind regions of high extinction.

that there could be  $10^7 - 10^8$  hot cores in such a system.

Is it realistic to expect this many hot cores at high redshifts? We have already seen (in chapter 5) that the chemistry of starbursts shares many of the properties with that of Milky Way hot cores. Carilli *et al.* (2002) report a detection of CO in the host galaxy of a quasar at a redshift of  $z=4.69$  using the Very Large Array (VLA). Taking beam dilution effects into account,  $1.4 \times 10^7$  hot cores are necessary at a redshift of  $z = 4.69$  in order to produce a signal of the same strength as this detection of CO. This calculation assumes that the observations were of transitions in molecules with a column density at least equal to that of CO in the Carilli *et al.* source. This analysis does not depend on an identification of CO in this source as CO contained in hot cores; the extant observations are merely used as a guide to what constitutes a detectable abundance.

Alternatively, Bertoldi *et al.* (2003) report the detection of CO in a quasar host at a redshift of  $z=6.42$ . They do not see extended emission in observations with a resolution of 1.5 arcseconds. We repeat the calculation at this redshift, assuming a source size of 1.5 arcseconds (the worst-case scenario, as smaller sources would require fewer hot cores), and find that one requires  $2.5 \times 10^8$  hot cores to provide the same level of signal. Assuming a source size of 0.3 arcsec, the size of the source considered by Carilli *et al.*,  $1.01 \times 10^7$  hot cores are sufficient.

When so many hot cores are present in a high redshift source, therefore, many molecular species reach significant column densities. Once again, there are differences between the three models regardless of the overall metallicity adopted. In particular, while the UN02  $150M_\odot$  models have much higher predicted column densities for sulphur-bearing species such as CS, H<sub>2</sub>CS and SO<sub>2</sub>, other species such as CH<sub>3</sub>CN and CH<sub>3</sub>OH are more sensitive to the overall metallicity than the choice of model for the initial abundances. This result suggests that, given detections (or limits on the abundance) of several species, it may be possible to independently constrain the overall metallicity and the mass of the first stars.

#### 6.2.4 Conclusions

Enhanced levels of star formation expected in systems incorporating quasars at high redshifts provide an opportunity to investigate both the nature of the first generation of stars and that of subsequent star formation. Systems containing as many as  $10^7$  hot cores should produce a signal at the same level as existing detections of molecular CO. Furthermore,

detailed chemical modelling of such galaxies suggests that a variety of molecular species which have transitions which are accessible to facilities such as the Very Large Array will have sufficient column density to be detectable as far away as  $z \sim 6$ . A good example is SO, for which molecule the J=5-4 transition is detectable by the current instrumentation available at the VLA for redshifts in the range  $4.50 > z > 3.40$  and the J=8-7 transition for the range  $7.66 > z > 5.93$ .

By considering the change in the model predictions produced by altering the initial abundances, it has been shown that this type of analysis (accompanied by observations) could distinguish between competing models for the first generation of stars. The yields from the supernovæ which must end the lives of the first stars are used to form the input to the model for the formation of the next generation. For example, comparing the behaviour of SO with that of CO in each model has the potential to distinguish between CL02 and UN02 models of nucleosynthesis, and hence between zero-metallicity stars of different masses.

The importance of this work is not limited to searches specifically aimed at the formation of the second generation of stars. Indeed, this should be regarded as a ‘worst-case’ scenario for the high-redshift astrochemist. Later star formation would only further enhance the proportion of metals available for molecule formation, increasing the chance of success. The runs using yields from Chieffi and Limongi (2004) suggest that the prediction of significant (and observable) column densities holds even if the first generation of stars are not as massive as simulations predict. Nor should we be limited in choice of targets; for example, Lyman-break galaxies<sup>7</sup> may prove to be worth investigation, but more detailed models of chemical enrichment (similar to that in Matteucci and Calura (2005)) are needed to make specific predictions (see chapter 8).

In conclusion, we predict that observational searches for the multiple molecular species associated with the hot core stage of high-mass star formation at high redshift would be likely to succeed, given the prediction of extremely high star formation rates in objects in this redshift range. This preliminary work also demonstrates that the use of sophisticated chemical models could be used in association with observations of this nature to provide constraints on models for the first stars. In the foreseeable future, facilities such as the Atacama Large Millimetre Array and the Square Kilometre Array will provide a huge

<sup>7</sup>Lyman-break galaxies are selected by comparing the flux through broad-band filters in the ultra-violet, green and red. Star-forming galaxies at redshifts in excess of  $z \sim 2.5$  will be faint in the UV filter.

increase in our capacity to carry out this kind of analysis, but this work also shows that important results could be obtained with existing facilities.

## 6.3 Star formation in the presence of active galactic nuclei

*This section is based on Lintott & Viti 2006, published in Astrophysical Journal Letters, 646, 37.*

### 6.3.1 Introduction

Recent work (Gao and Solomon, 2004; Wu *et al.*, 2005) indicates that there exists a strong correlation between the luminosity of molecular lines - particularly the HCN J=1-0 transition - and the star formation rate which is derived from the infrared luminosity. Impressively, these relations apply to individual star-forming regions in the Milky Way and also to external systems, spanning some ten orders of magnitude in luminosity.

These relations are important because they provide independent paths to deriving the star formation rate (SFR) for the systems being studied. The SFR is related to the infrared luminosity of a system by

$$\dot{M}_{\text{SFR}} \approx 2 \times 10^{-10} (L_{\text{IR}}/L_{\odot}) M_{\odot} \text{yr}^{-1} \quad (6.3)$$

which assumes that the observed infrared emission is primarily the result of dust heating by hot (O, B and A) young stars (Kennicutt, 1998). As HCN is primarily excited by collisions with molecular hydrogen rather than radiative excitation (Stutzki *et al.*, 1988; Paglione *et al.*, 1997), it is a tracer of dense gas. The more dense gas in a system, the greater the potential for star formation from the gas, and so it is logical to expect a correlation between the luminosity of a system in HCN emission and the star formation rate. In fact, Gao and Solomon find that

$$\log L_{\text{IR}} = 1.00 (\pm 0.05) \log L_{\text{HCN}} + 2.9 \quad (6.4)$$

which, combined with equation 6.3, gives the relation

$$\dot{M}_{\text{SFR}} \approx 1.8 \times 10^{-7} (L_{\text{HCN}}/\text{Kkm s}^{-1} \text{pc}^2) M_{\odot} \text{yr}^{-1}. \quad (6.5)$$

Gao and Solomon state that, as this is a linear relation, ‘the HCN emission is a direct tracer of the SFR in all galaxies’. Wu *et al.* (2005) extend the same relation to our own Galaxy, plotting Milky Way star forming regions on the same axis and obtaining a remarkably good correlation.

However, the three highest redshift systems in the sample used by Gao & Solomon (at  $z \sim 2$ ) do not follow the established trend, but have luminosities in HCN lower than would be expected given their infrared luminosities (which, remember, are proportional to their star formation rates). There is also weak evidence that such deviations from the local trend continue at higher redshifts still; a detection of the HCN J=5-4 line in the quasar APM08279+5255 at a redshift of  $z = 3.91$  has been reported, with  $L_{FIR}/L_{HCN}$  similar to that seen in the sources at  $z \sim 2$  (Wagg *et al.*, 2005). This result does, however, depend on the conversion from the luminosity of the J=5-4 transition to that of the J=1-0 line, which depends on the details of the radiative transfer model used to fit the CO lines observed in the same source. Limits on HCN luminosities obtained for the most distant systems examined, at redshifts of  $z \sim 6$  (Carilli *et al.*, 2002), indicate that these systems too do not fit the low-redshift relation. It is important to note that, as these systems are at high-redshift, it is possible that gravitational lensing may cause magnification of these systems. For the systems studied by Gao & Solomon, however, it has been possible from observations to constrain the magnification and recover the unaltered luminosities. The effect is, for these systems, less than an order of magnitude in size.

The conventional explanation for these discrepancies is to attribute the observed infrared excess to the presence within the observed systems, of an active nucleus. The  $z \sim 2$  systems are, indeed, quasar hosts, presenting us with the problem of distinguishing infrared radiation associated with star formation, and that due to the AGN; remember that the relationship between infrared luminosity and star formation rate given above depends critically on the assumption that the only source of infrared luminosity is dust irradiated by newly formed hot stars. If the contribution of the AGN to the infrared luminosity is significant, then the star formation rate derived from it will be artificially inflated, and the molecular luminosity will provide a more accurate (and lower) SFR.

A possible solution is to use detailed observations and modelling to distinguish the two contributions to the infrared luminosity, by fitting possible components to the spectral energy distribution (SED). Such work has been completed for one of the sources in Gao & Solomon’s study, the Cloverleaf quasar (Weiβ *et al.*, 2005). This work has shown

that, in addition to the AGN, there does indeed exist a warm dust component which has a temperature which suggests that it must be associated with star-forming activity. However, it is not trivial to move from such a result to a luminosity which is free of contamination from AGN, and so in the next section, we test the hypothesis that hidden AGN activity may be responsible for the deviation of the high-redshift sources from the local relationship between infrared and HCN luminosity. By using chemical models of high-mass star formation, we find that, contrary to the conventional view, AGN activity should be accompanied by an *increase* in the relative abundance of HCN. Furthermore, we find that models of star formation taking place in near-primordial gas (first introduced in section 6.2), enriched only by the ejecta from the supernovæ of Population III stars, can account for the observed (lower than expected) abundance of HCN; hence the star formation rates derived from infrared luminosity are consistent with those derived from molecular observations. There is no lack of HCN at high redshift. Finally, we show that this model could easily be tested with observations of further molecular species.

### 6.3.2 The effect of Active Galactic Nuclei

The work presented in the first half of this chapter used a time-dependent chemical model to simulate the formation of massive stars, in order to predict the expected emission from a variety of molecular species in high redshift systems. In this section, we make use of the same model to explore the effect of active galactic nuclei on high redshift star forming systems. A model with initial atomic abundance ratios selected from recent calculations of the yield from a zero-metallicity supernova (Chieffi and Limongi, 2004) and an overall metallicity equal to 1/100<sup>th</sup> of the solar value was used. The initial collapse of a protostellar clump was then modelled, including chemical reactions both in the gas and on the surfaces of dust grains. Once a critical density is reached, it was assumed that the high-mass protostar will ignite, causing chemical species which are trapped in the icy grain mantles to sublime. The newly released molecules radiate strongly in the warm gas; the protostar has reached the ‘hot core’ stage (see section 1.1.2 for details of the evolution of a forming star).

The main effect of the presence of an AGN in the centre of a star forming system will be an increase in the flux of X-rays to which the collapsing protostellar material is exposed, and this in turn will lead to an increased ionization of species in the gas phase. Lepp and Dalgarno (1996) used chemical models with increased ionization to model chemistry

driven by X-rays in diffuse interstellar clouds and low mass star forming regions, and we follow their example here.

Lepp and Dalgarno were inspired not by the flux from AGN, but by the presence of a hard X-ray source within the Milky Way. Specifically, they considered the behaviour of  $\text{HCO}^+$  and several nitrogen-bearing compounds, including photo-dissociation from ultraviolet photons, produced by the excitation of both atomic and molecular hydrogen (and helium) by electrons liberated in X-ray ionization. In the low density sources which they model, they find that the abundances of many molecules (including HCN, CO and  $\text{HCO}^+$ ) increase with ionization. At very high ionization rates, however, photodissociation dominates and the abundances of most species drop rapidly.

In the high-density environments within which massive stars form, photodissociation should play a much less important role, but the ionization fraction is still of crucial importance in driving the chemistry of star-forming regions. The most significant gas phase reactions within dark clouds, particularly for oxygen and nitrogen bearing species, are reactions between ions and neutral species. The increase in x-ray ionization is simulated by increasing the ‘standard’ ( $1.0 \times 10^{17} \text{s}^{-1}$ ) cosmic ray ionization rate used by the models by a factor,  $\zeta$ , of between 2 and 1000. The effects of such a change on the abundance of HCN are shown in Figure 6.2.

The primary formation route for HCN in the benchmark (i.e. ‘standard’ ionization, or  $\zeta = 1$ ) model is via the reaction between  $\text{H}_2$  and CN. The latter species is formed from atomic nitrogen reacting with  $\text{C}_2$ . In the models with enhanced ionization ( $\zeta > 1$ ), by contrast, the increased ionization results in a greater density of free electrons, which (as in the low-mass star formation model) results in greater excitation of species and an increase in the density of ultraviolet photons. The increased probability of photodissociation of species increases the abundance of atomic nitrogen, which in turn promotes the formation of first CN and, following on, HCN. In addition, the increased ionization promotes the formation of HCN from the dissociative recombination of  $\text{HCNH}^+$ . This is in fact the dominant formation route for HCN in the early stages of protostellar collapse in the models which have enhanced ionization. Note that the reactions that take place on the surface of the grains do not affect the abundance of HCN in the model, as there is no significant formation or destruction of this species on the grains. However, if the process of freeze-out were to be less efficient (perhaps because dust density is reduced, as expected in sources in the early Universe), then HCN would reach higher abundances, forming via

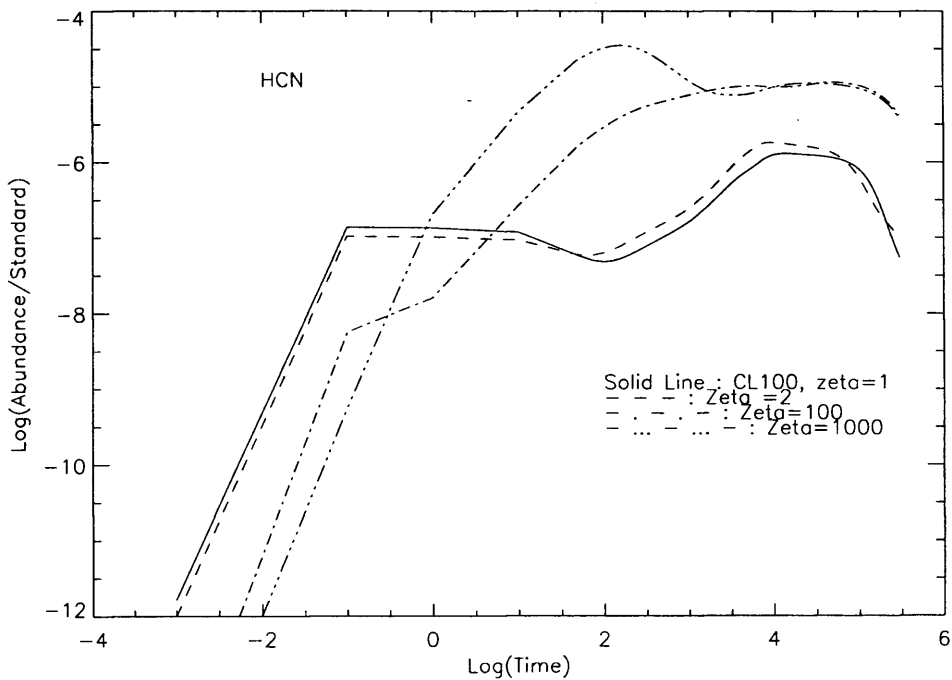


Figure 6.2: Change in abundance for HCN relative to a ‘benchmark’ model with only cosmic ray ionization and Milky Way metallicity and atomic abundances. The solid line represents a model with only cosmic ray ionization and abundances from Chieffi and Limongi (2004), standardized to 1/100th solar. The time elapsed since the ignition of the protostar and consequent sublimation of species from grain mantles is shown on the x-axis.

gas phase reactions during the collapse. Any ‘lack’ of HCN cannot therefore be explained by reducing the efficiency of molecular freeze-out.

As it is not easy to constrain the exact effect of the AGN on the ionization rate, a range of values for  $\zeta$  was used. Models with a  $\zeta$  of 100 result in an increase in the relative abundance of HCN at all but very early times. Runs in which a  $\zeta$  of 1000 was used initially produce a higher fractional abundance of HCN than those with a  $\zeta$  of 100, although the final abundance is the same in both models. This result echoes that of Lepp and Dalgarno in low-mass star forming regions, although they find that, in such objects, the abundance of HCN (in common with all of the species in their model) declines at ionization rates as high as those explored in this model. In collapsing cores, the increased density during collapse and the resulting freeze-out of molecules prevents dissociation as expected.

Our models show clearly that an increase in HCN abundance is likely to accompany AGN activity. The magnitude of the increase in relative abundance can, even for a relatively modest increase in the ionization rate, be as large as two orders of magnitude.

The far-IR excess - the difference between the luminosity of the observed source and that predicted if the low redshift IR/HCN luminosity relation holds - seen in the most distant sources included in the work of Gao & Solomon is approximately an order of magnitude. A typical source with  $\log(L_{\text{HCN}}) \sim 9.5$  has  $\log(L_{\text{IR}}) \sim 13.5$  while the low-redshift relation would have predicted  $\log(L_{\text{IR}}) \sim 12.5$ . Note that the physics of the AGN itself is not modelled, only its probable effects on the chemistry of surrounding star formation regions, and further research is necessary in order to investigate the relationship between the increases in ionization and infrared luminosity. For example, it is not possible to conclude from the work presented here whether an AGN which increases the observed infrared luminosity by an order of magnitude corresponds to  $\zeta = 2$  or  $\zeta = 1000$ . However, it seems likely that the consequent increase in HCN abundance from the presence of an AGN powerful enough to cause an order of magnitude increase in infrared luminosity is sufficient to ensure that the deviation from the observed trend cannot be explained by the presence of an active galactic nucleus.

Enhancements of HCN in nearby AGN are actually observed in nearby galaxies (Kohno *et al.*, 2001), and the use of HCN/HCO<sup>+</sup> and HCN/CO ratios as diagnostics for AGN activity has been suggested by previous authors. Kohno *et al.* report what they describe as ‘extremely strong’ HCN emission in three of the seven nearby Seyfert galaxies in their sample, and suggest that this is the result of x-ray driven chemistry.

In addition, the preliminary results from the models detailed in this chapter suggest that other species, in particular CS and SO<sub>2</sub>, may be worth investigating as they are less sensitive than HCN to an increase in the ionization rate.

### 6.3.3 Infrared excess or nitrogen under-abundance?

If the activity associated with the presence of AGN is not responsible, what could be causing the deviation of high redshift systems from the relation between molecular and infrared luminosities? This relationship, it should be remembered, is found to hold for a large variety of systems across some ten orders of magnitude in infrared luminosity. In section 6.2 of this chapter it was suggested that the molecular gas in systems with rapid rates of star formation could be predominantly in the form of hot cores. Furthermore, we noted that gas enriched only by large zero-metallicity (population III) stars is predicted to be under-abundant in nitrogen compared to the metallicity of the solar neighbourhood. Hot cores formed from such gas should therefore have lower abundances

Reaction	Rate coefficient/cm <sup>3</sup> s <sup>-1</sup>
H + HNC → HCN + H	$6.2 \times 10^{-10} \exp^{-\frac{12500}{T}}$
N + CH <sub>2</sub> → HCN + H	$7.89 \times 10^{-11} \left(\frac{T}{300K}\right)^{0.17}$
H <sub>2</sub> + CN → HCN + H	$4.04 \times 10^{-13} \left(\frac{T}{300K}\right)^{2.87} \exp^{-\frac{820}{T}}$
N + HCO → HCN + O	$1.70 \times 10^{-10}$
<b>HCNH<sup>+</sup> + e<sup>-</sup> → HCN + H</b>	$9.0 \times 10^{-8} \left(\frac{T}{300K}\right)^{-0.5}$
<b>H + H<sub>2</sub>CN → HCN + H<sub>2</sub></b>	$1.0 \times 10^{-10} \left(\frac{T}{300K}\right)^{0.5}$
H <sub>3</sub> <sup>+</sup> + HCN → HCNH <sup>+</sup> + H <sub>2</sub>	$8.1 \times 10^{-9}$
H <sup>+</sup> + HCN → HCN <sup>+</sup> + H	$1.05 \times 10^{-8} \left(\frac{T}{300K}\right)^{-0.13}$
H <sub>3</sub> O <sup>+</sup> + HCN → HCNH <sup>+</sup> + H <sub>2</sub> O	$4.0 \times 10^{-9}$
<b>HCN + Photon + → CN + H</b>	$1.3 \times 10^{-9} \exp(-2.1A_v) \text{ s}^{-1}$

Table 6.5: Major formation and destruction reactions of HCN. All those which account for 10% of the formation or destruction rate at any point in both benchmark and enhanced ionization models have been included. Those in bold are important only in models with enhanced ionization (although note the final reaction is important only in the very early stages). Rates are taken from the UMIST99 rate file.  $T$  is the temperature and  $A_v$  is the extinction.

of nitrogen-bearing compounds such as HCN than would otherwise be expected. In this section, we investigate whether the molecular abundances derived from models described in section 6.3.2 are consistent with existing detections of HCN in high-redshift galaxies, and thus test the hypothesis that deviations from standard  $L_{IR}/L_{HCN}$  ratios are due, not to an excess of infrared luminosity, but to an under-abundance of HCN in star-forming regions incorporating a substantial fraction of near-primordial gas.

Two sources which have been observed using the Very Large Array and included in the sample of Gao and Solomon are considered. The first is the Cloverleaf quasar (H1413) at a redshift of  $z = 2.56$ , which was observed by Solomon *et al.* (2003), and the second is J1409 at a redshift of  $z = 2.58$ , observed by Carilli *et al.* (2005). Unfortunately, both of these sources have significant optical depths in the molecular transitions which have so far been observed, making accurate calculation of the column density difficult. However, the column density can still be derived following the method of Nguyen *et al.* (1992).

It is assumed that the population fraction can be described in terms of the partition function,  $Q$ , which is a function of a single excitation temperature,  $T_{ex}$ . The optical depth,  $\tau$ , is then related to the total column density  $N_{tot}$  by the relation

$$\frac{N_{\text{tot}}}{\Delta V} = \frac{3kQ(T_{ex})\tau J_\nu(T_{ex})}{8\pi^3\nu\mu_0^2 J_u e^{-\frac{E_u}{kT_{ex}}}} \quad (6.6)$$

where  $J_u$  and  $E_u$  are respectively the rotational quantum number and the energy of the upper level of the transition which has frequency  $\nu$ ,  $\Delta V$  is the line width and  $\mu_0$  is the permanent dipole moment.  $J_\nu$  is the Planck function in units of temperature:

$$J_\nu(T) = \frac{\hbar\nu}{k} \frac{1}{e^{\frac{\hbar\nu}{kT}} - 1}. \quad (6.7)$$

The optical depth,  $\tau$ , is also related to the main beam brightness temperature,  $T_{\text{MB}}$  by

$$T_{\text{MB}} = \phi [J_\nu(T_{ex}) - J_\nu(T_{\text{BG}})] (1 - e^{-\tau}), \quad (6.8)$$

where  $\phi$  is the beam filling factor and  $T_{\text{BG}}$  is the temperature of the cosmic background, equal to 2.73K at  $z = 0$ . If we make assumptions about the beam filling factor and the excitation temperature, therefore, it is possible to derive an estimate of the column density from the detection of a single line.

As discussed above, the spectral energy distribution of the Cloverleaf has been studied in detail, resulting in the detection of a warm dust component with  $T_d = 50\text{K}$ . Using this as a general indication of the temperature in the source, we will therefore assume a temperature of  $T_{ex} = 50\text{K}$  for both sources. In order to arrive at an estimate for the beam filling factor it was assumed that the only source of HCN emission arises from hot cores which have radii of 0.3 parsec (larger than their Milky Way analogues for the reasons discussed in section 6.2.2.3).

The early Universe model as described above predicts the contribution of each individual hot core to the column density and, thus, given the number of hot cores in the source, the overall column density. The observed luminosities for the Cloverleaf and for J1409 in  $\text{Kkm s}^{-1}\text{pc}^2$  are  $L_{\text{HCN}} = 3.2 \pm 0.5 \times 10^9$  and  $L_{\text{HCN}} = 6.7 \pm 2.2 \times 10^9$  respectively.

If approximately  $10^7$  hot cores are present in each of these sources, then the model is consistent with observations. The column densities derived for the two sources are then  $1.8 \times 10^{17}\text{cm}^{-2}$  (for the Cloverleaf) and  $3.8 \times 10^{16}\text{cm}^{-2}$  (for J1409). In section 6.2, we made use of the estimate that the Milky Way contains  $10^5$  hot cores, and asserted that

the number of hot cores scaled with the star formation rate. As both of these sources have star formation rates (determined from the infrared luminosities) greater than two orders of magnitude above that in the Milky Way, a population of  $10^7$  hot cores seems to lie within realistic limits. It should be noted, however, that so far we have assumed that the observed molecular gas is entirely in the form of hot cores, and so the values derived above for the predicted column densities are upper limits. It is nonetheless clear from figure 6.2 that the relative abundance of HCN produced by all of the low metallicity models is at least a factor of  $10^4$  below that expected in hot cores formed from gas with the atomic abundance ratios observed in the solar neighbourhood. Even if the number of hot cores in these rapidly star forming systems is - despite their much larger rates of star formation - the same as that in the Milky Way, hot cores with solar abundance ratios would result in a luminosity of HCN greatly in excess of the observed value. The identification of the molecular gas in these systems with hot cores can be valid only if the metallicity is less than that of the solar neighbourhood.

Thus, there is no discrepancy between the star formation rate as derived from the infrared luminosity, and the observed luminosity of HCN, if one accepts that stars are forming from near-primordial gas at redshifts of  $z = 2 - 4$ .

#### 6.3.4 Conclusions

We have argued that the observed differences between  $L_{IR}/L_{HCN}$  in systems at low and high redshifts cannot be due to the presence of AGN enhancement of the infrared luminosity. Such activity, the modelling presented here shows, would increase the abundance of HCN in the observed systems as well as the infrared luminosity. Detailed chemical models of such systems show promise in distinguishing between AGN enhanced and purely star-forming activity, through the changes observed in the ratio of the abundances of HCN and the species which are not enhanced by AGN. Examples of such species may include both CS and SO<sub>2</sub>, both of which are observed to be enhanced in galactic hot cores (Hatchell *et al.*, 1998), and (as discussed in the first half of this chapter) are expected to be favoured in nitrogen-deficient gas.

We explain the observations instead by proposing the hypothesis that stars are forming from near-primordial material, which would be deficient in nitrogen compared with solar neighbourhood abundances. Jimenez and Haiman (2006) discuss four observational constraints on the nature of star formation at redshifts between 3 and 4. Specifically

they consider the following observational results, all of which require the presence of more ultraviolet radiation than would be emitted by ‘normal’ stellar populations. The results are:

1. Significant ultraviolet emission seen in Lyman break galaxies at wavelengths shorter than 912Å (Steidel *et al.*, 2001). This can be explained by the presence of ongoing formation of massive stars in addition to the standard initial mass function (IMF).
2. Strong Lyman- $\alpha$  emission is seen from extended ‘blobs’ which have little or no associated ionizing continuum (Matsuda *et al.*, 2004).
3. A population of galaxies which have unusually strong Lyman- $\alpha$  emission lines exists (Malhotra and Rhoads, 2002).
4. A strong HeII emission line at 1640Å is seen in the composite spectrum of Lyman break galaxies (Shapley *et al.*, 2003).

Each of the last three of these problems can be solved by an increase in the number of energetic (i.e. ionizing) photons, large enough that a bias in the IMF is insufficient to account for it. Metal-free stars will have reduced opacity due to the lack of carbon, nitrogen and oxygen (Bromm *et al.*, 2001), which leads to increased temperature and hence an increase in the flux of ultraviolet flux. Jimenez & Haiman therefore propose that a significant fraction of star formation at redshifts of  $z \sim 4$  is occurring in primordial gas, enriched only by Big Bang nucleosynthesis. These results imply that the mixing of metals is inefficient within galaxies, and thus solar abundance ratios may not have been reached in a substantial fraction of gas which makes up galaxies at  $z = 2$ .

Such models present a challenge to existing models of chemical enrichment, which assume that the first population II stars form at much higher redshifts. Simulations (e.g. Abel *et al.* (2002)) which suggest that population III stars will be massive assume that such stars will form at redshifts much greater than 4. It may be that the predictions of the yields from such stars may need to be revised. These results, if borne out by further observations do, however, suggest that star formation from near-primordial gas (as proposed in this section) at redshifts of  $z = 2 - 3$  may be realistic. Such a result would suggest that the mixing of gas enriched by metals with existing primordial matter, a process which has not to date been modeled in detail on galactic scales, may not be

efficient. Alternatively, it may indicate the infall of fresh supplies of primordial (or near-primordial) gas on to galaxies which are already undergoing enhanced star formation. If this latter possibility is correct, then one may expect to see a difference in the  $L_{IR} : L_{HCN}$  ratios of galaxies in dense environments and those in the field, which presumably would accumulate infalling gas at different rates.

## CHAPTER 7

---

# Massive elliptical galaxies : From cores to haloes

*This section is based on Lintott, Ferreras & Lahav 2006, astro-ph/0512175, accepted by the Astrophysical Journal.*

## 7.1 Introduction

New large galaxy surveys such as the 2dF Galaxy Redshift Survey (Colless *et al.*, 2001) and the Sloan Digital Sky Survey (SDSS) (York *et al.*, 2000) have transformed the way in which astronomers are able to study the statistics of galaxy populations, and of their distributions. The work presented in this chapter focuses on a sample of elliptical galaxies derived from the early-type <sup>1</sup> sample first selected by Bernardi *et al.* (2003a), hereinafter B03.

### 7.1.1 Dark matter in the Universe

Astronomers are well used to the idea that the visible matter makes up only a proportion of the Universe. Not long after the Royal Astronomical Society adopted ‘Quicquid nitet notandum’<sup>2</sup> as its motto, the announcement of invisible companions perturbing the movements of Sirius and Procyon (Bessel (1844)) led to an expansion of the astronomer’s remit.

<sup>1</sup>Early-type galaxies may include both ellipticals and S0. Although we deal here with massive ellipticals, it should be understood that we are strictly referring to early-type systems.

<sup>2</sup>‘Whatever shines, let it be noted.’

This particular form of dark matter was quickly disposed of (Sirius B was discovered by Alvan Clark in 1862) but in the first half of the twentieth century more resilient forms of dark matter appeared in astronomical theory. Analyses of the velocities of nearby stars (Oort, 1932) and of individual galaxies within rich galaxy clusters (Zwicky, 1933) indicated for the first time that the quantity of luminous matter observed was not sufficient in itself to account for the behaviour of matter on large scales. Although the former paper received more attention at the time, it is the latter result which has become the canonical predecessor of modern dark matter theories. The beginning of the ‘modern era’ in studies of dark matter is dated by Trimble (1987) to 1974, when Ostriker *et al.* (1974) and Einasto *et al.* (1974) found that, for both spiral and elliptical galaxies, mass increased (approximately linearly) with radius out to at least 100kpc from the centres of the galaxies. From here, developments in both theory and observation rapidly established that dark matter must have played an essential part in the evolution of structure in the Universe.

How much dark matter is there in the Universe? Fukugita *et al.* (1998) analyse the ‘baryon budget’ of the Universe at the present day, and conclude that a value of  $0.007 \leq \Omega_b \leq 0.041$  is appropriate, with a ‘best guess’ of  $\Omega_b \sim 0.021$ . These figures assume a value for the Hubble Constant of  $H_0 = 70\text{km}\text{s}^{-1}\text{Mpc}^{-1}$ . Although this result depends to some extent upon a series of assumptions about the Universe as observed (for example, that there does not exist a substantial population of hitherto undetected ‘dark galaxies’), it can be checked by comparison with the independent predictions of Big Bang nucleosynthesis theories; perhaps surprisingly, it is easier to account for all possible locations of baryons when the Universe is 1 second old than it is when it is 13.7 billion years old. Modern models of the formation of light elements, expected at redshifts of  $z \sim 10^9$ , are able to predict the mean baryon density in terms of the primaeval abundances (see Copi *et al.* (1995) for a recent review, along with Hata *et al.* (1997)). The best constraints come from rarer nuclei such as  ${}^3\text{He}$ ,  ${}^7\text{Li}$  and particularly deuterium. Despite the extreme conditions being modelled, the results of these calculations agree with the baryon density quoted above to within  $1\sigma$ .

Until the last decade, it was nonetheless believed possible that a major component of the dark matter could be in the form of massive compact halo objects (MACHOs<sup>3</sup>) which were believed to reside in galactic halos. Surveys of stars in the Magellenic Clouds, which aimed to detect the short-lived microlensing events associated with the passage of

---

<sup>3</sup>The alternative almost inevitably became known as weakly interacting massive particles or WIMPs.

a Milky Way MACHO in front of a background star, were successful in detecting several such objects. Alcock *et al.* (2000), for example, report  $\sim 15$  microlensing events in almost 6 years of observations. They conclude that (for maximum likelihood values) 20% of the Milky Way halo is composed of MACHOs with masses of between  $0.15$  and  $0.9M_{\odot}$ .

It is also possible to constrain the matter and baryon densities from observations of the cosmic microwave background. Using only the three-year WMAP data, the best fit models of the CMB power spectrum give  $\Omega_m h^2 = 0.127^{+0.007}_{-0.013}$  and  $\Omega_b h^2 = 0.0223^{+0.0007}_{-0.0009}$  assuming that the Universe is flat (Spergel *et al.*, 2006). However, even if the constraint of a flat Universe is relaxed, it is still clear from the CMB alone that non-baryonic matter must be a significant component of the Universe; the closed universe model which best fits the WMAP3 data has  $\Omega_m = 0.415$  and so  $\Omega_m > \Omega_b$ .<sup>4</sup> Taken together, these three sets of results support the conclusion that there must be a significant non-baryonic component to the dark matter.

If not composed of baryons, therefore, what is the dark matter? The most attractive candidate particle species was, for many years, the neutrino. Unlike many dark matter candidates (see below), neutrinos are known to exist in great numbers. That the neutrino has mass was first established unequivocally by observations of neutrinos produced as a by-product of fusion reactions in the Sun (Ahmad *et al.*, 2002). While it is difficult to measure the absolute value of the rest mass of any of the three neutrino ‘flavours’<sup>5</sup> the difference in masses can be constrained in the laboratory (see Valle (2005)). Experiments that analyse the weak decay of tritium do, however, place an upper limit on the mass of the lightest neutrino of  $m_{\nu_e} \leq 2.3$  eV at 95% confidence (Kraus *et al.*, 2004). Although beyond the scope of the work presented here, it should be noted that currently cosmological measurements (from BBN and CMB observations) are competitive with present and planned experiments in placing limits on the overall neutrino mass scale. For example, Goobar *et al.* (2006) use the three-year WMAP data together with the SDSS and results from observations of type Ia supernovæ and the Lyman- $\alpha$  forest to constrain the sum of the masses of all three neutrino species, and find that  $\Sigma m_{\nu} \leq 0.62$  eV (at 95% confidence). The contribution of neutrinos to the matter density of the Universe is given by Hannestad

<sup>4</sup>Along with  $\Omega_{\Lambda} = 0.630$  and  $H_0 = 55 \text{ km s}^{-1} \text{ Mpc}^{-1}$ . Although the  $\chi^2$  value of this model indicates a better fit to the CMB than the flat model, the value of  $H_0$  it demands is incompatible with other observations such as those of the HST key project (Freedman *et al.*, 2001).

<sup>5</sup>In order of increasing mass, the electron, muon and tau neutrino.

*et al.* (2006) as

$$\Omega_\nu h^2 = N_\nu \frac{m_\nu}{92.5\text{eV}} \quad (7.1)$$

where  $N_\nu$  is the number of neutrinos with mass  $m_\nu$ .

However, a much stronger limit on the contribution of neutrinos can be derived, relying on the fact that neutrinos become non-relativistic relatively late in the history of the Universe. Neutrinos are hot dark matter in that they are relativistic when they decouple from the primordial radiation, and would therefore ‘free-stream’ (that is to say, be unaffected by surrounding regions of high or low density). The net result would be to smooth out early fluctuations, delaying the formation of large scale structure. The detection and analysis of the anisotropies in the CMB reveal that a Universe in which neutrinos were the most significant component of the dark matter, would have insufficient power on small scales to account for the observed structure. A form of cold dark matter (CDM) is therefore necessary.

There exist at least two more exotic candidates for the elusive dark matter particles, in the form of the axion and the neutralino (Sadoulet, 1999). Briefly, the presence of the former type of particle (produced out of thermal equilibrium) is invoked in order to prevent the violation of charge-parity (CP) symmetry in the otherwise well-founded theory of quantumchromodynamics (QCD). The neutralino is a theoretical eigenstate of a combination of the theoretical supersymmetric counterparts of the Z boson (the zino), the photon (the photino) and the (theoretical) neutral higgs particle (the higgsino). Both the axion and neutralino are expected to be both weakly interacting and non-relativistic in the early Universe. As yet, however, there has been no detection of any candidate particle, either cosmologically or in the laboratory.

### 7.1.2 Galaxy formation in a CDM Universe

The theory of galaxy formation in a universe dominated by cold dark matter was first set out in a seminal paper by Blumenthal *et al.* (1984) (hereinafter BFPR) which considers the monolithic collapse (sometimes known as ‘spherical collapse’) of isolated dark matter concentrations (‘halos’). According to this picture, once the cosmological model is determined and the choice of amplitude of fluctuation made, then the redshift at which a halo collapses is determined only by its mass. For example, assuming ‘concordance’ cosmol-

ogy (see the definition below), a halo of mass  $3 \times 10^{10} M_{\odot}$  corresponds to a  $2\sigma$  fluctuation collapsing at a redshift of  $z=5$ .

As discussed in the previous section, the density of dark matter is greater than that of the baryons ( $\Omega_m > \Omega_b$ ). The distribution of baryonic matter is therefore assumed to follow the (dominant) dark matter distribution until the radius of the collapsing halo reaches the virial radius (when the potential energy  $U$  and the kinetic energy  $K$  are related by  $U = -2K$ ). This ‘top down’ picture of structure formation is contrasted with a ‘bottom up’ picture of galaxy formation, in which small dark haloes merge to form large structures. First proposed by White and Rees (1978), such a model is particularly favoured by semi-analytic simulations such as those of Springel *et al.* (2005).

Following the realisation in the late 1980s (particularly after the detection, initially by the COBE satellite, of anisotropy in the cosmic microwave background (Smoot *et al.*, 1992)) that the pure CDM model produced excess power on small scales, it became clear that so-called ‘gastrophysics’ (the physics which governs the evolution of galaxies themselves) associated with baryonic matter was important in the formation of the structure seen in cosmological simulations (Ostriker, 1993). However, the equations which govern the dynamics of the gas from which structures form are highly nonlinear, and hence present difficulties to simulators wishing to validate their results by including detailed descriptions of the physics. Nonetheless, the results of semi-analytic simulations are impressive, producing mock catalogues which reproduce the distributions observed by both 2dF and Sloan surveys (see, for example, Springel *et al.* (2006), particularly figure 1 which shows a direct comparison between the surveys and simulations).

There have been many attempts to discriminate, through observation, between these two pictures of the formation of galaxies outlined above: monolithic (or spherical) collapse, and hierarchical merging. Simulation results notwithstanding, the small scatter of the observed colour-magnitude relation and its evolution with redshift provides evidence that massive ellipticals were already in place at a redshift of  $z \approx 1 - 2$  with little subsequent merging (e.g. Stanford *et al.* (1998) and references therein). The observed relation is best explained by a single burst of star formation. As more massive (and hence more luminous) galaxies are believed to retain the ejecta from supernovæ more effectively, succeeding generations of stars (within the same burst) would have a higher metallicity, resulting in a redder galaxy.<sup>6</sup> At the very least, such correlations indicate that recent

---

<sup>6</sup>Higher metallicity enhances cooling and hence fragmentation, leading the formation of less massive

mergers were not accompanied by the burst of star formation which is the normal result of galaxy mergers (Hopkins *et al.*, 2006). Mergers between systems which have already been denuded of their gas (and which do not, as a result, trigger further star formation) will not affect the observed colour-magnitude relation (Franx and Illingworth, 1990).

In contrast to the observed relation for massive ellipticals, less massive ellipticals present features which are characteristic of recent star formation; a good example is the near-ultraviolet/optical colour-magnitude relation studied by Ferreras and Silk (2000a). They find that the slope of the near ultra-violet/optical colour-magnitude relation is incompatible with monolithic star formation in the cluster Abell 851 at  $z=0.41$ . In fact, some of the early type galaxies in this cluster may have formed  $> 10\%$  of their stars since  $z=0.5$ .

This ‘inverted hierarchy’ or ‘downsizing’ effect (the term was coined by Cowie *et al.* (1996) who used it to describe the ‘remarkably smooth downward evolution in the maximum luminosity of rapidly star-forming galaxies’) illustrates the complexity of galaxy formation and evolution, compared to the simple picture of assembly of dark matter halos. In this chapter, I use the predictions of a BFPR-like spherical collapse scenario as a benchmark, which can then be explored and challenged by further comparisons with observations and detailed simulations.

A new aspect of the analysis presented here is the estimation of the stellar mass of each of the B03 ellipticals, which allows a distinction to be made between baryonic and total mass. The calculations of BFPR are also updated for a Universe with ‘concordance cosmology’. I use throughout a matter density  $\Omega_m = 0.3$ , dark energy density  $\Omega_\Lambda = 0.7$ , Hubble constant  $h = 0.7$ , and amplitude of fluctuations  $\sigma_8 = 0.9$ . An Einstein-de Sitter (EdS) model is used for contrast with  $\Omega_m = 1.0$ ,  $\Omega_\Lambda = 0.0$ , Hubble constant  $h = 0.7$  and  $\sigma_8 = 0.9$ <sup>7</sup>. It should be noted that WMAP 3-year data taken alone prefers lower values for both  $\Omega_m$  and  $\sigma_8$ , but weak lensing results support the higher values used here (Spergel *et al.*, 2006). Despite the attention BFPR has received, the relatively simple generalization of their work to  $\Lambda$ CDM has not previously appeared in the literature. This work also, to the best of my knowledge, is the first attempt to incorporate data for individual galaxies (as opposed to schematic data) in the parameter space used by BFPR. Another important stars.

<sup>7</sup> $\sigma_8$  is the normalization of the matter power spectrum, chosen to be that smoothed on a scale of  $8h^{-1}$  Mpc.

parameter in this form of analysis is the cosmological baryon fraction. For simplicity, throughout this chapter we use a value of 1/6 unless otherwise stated<sup>8</sup>.

Although the cosmological baryon ratio is well constrained, the baryonic contribution to the mass distribution is less well-known on galactic scales. Klypin *et al.* (2002) model the mass profile of the Milky Way within its virial radius ( $\approx 250$  kpc) and find that a substantial ‘feedback’ mechanism which removes baryons from the galactic centre must have operated at some time in the past. Do similar processes occur in massive elliptical galaxies? Are their cores<sup>9</sup> dominated by baryonic or dark matter? Romanowsky *et al.* (2003) and Dekel *et al.* (2005) have reached conflicting conclusions to this last important question, based on the analysis of planetary nebulae out to five times the effective radius,  $R_e$ . By using the central velocity dispersion and stellar mass in the core - within  $R_e$  - the work presented here seeks to answer the same question without introducing possible bias associated with planetary nebulae. The results show that the cores of the galaxies are baryon dominated, at least within this central region.

By making the straightforward assumption that the total mass of the galaxy is proportional to the mass of the galactic ‘core’, it is possible to investigate the regime within which the benchmark model of spherical collapse discussed above is consistent with modern data. The profile of the undisturbed dark matter halo is also recovered from present-day observationally determined parameters via the procedure of adiabatic contraction, which allows the comparison of the derived concentration of the mass profile with both simulations and observations. Defining  $\alpha = M_{\text{tot}}/M_{\text{dyn}} (< R_e)$  – the total mass of the collapsing halo divided by the dynamical mass within the half-mass, or effective, radius  $R_e$  – a strong constraint is obtained so that that  $\alpha \geq 10$ .  $\alpha \approx 20$  provides a good fit to the data.

The outline of this chapter is as follows: we first present the B03 sample and a volume-limited sample of over 2000 galaxies selected from it. I then describe the derivation of stellar masses of these ellipticals from the SDSS colours, and also derive dynamical masses. In order to extend the Faber-Jackson relation to these data, I present the relations between luminosity, velocity dispersion and stellar and dynamical mass, and then comment on the acceleration of stars in the ellipticals and the connection between this derived property and theories of modified Newtonian gravity (MOND). The extended benchmark spherical collapse model is then used to compare the observations with the level of rms fluctuations

---

<sup>8</sup>As discussed above, WMAP-3 alone gives  $\Omega_m = 0.24^{+0.03}_{-0.04}$  and  $\Omega_b = 0.042^{+0.003}_{-0.005}$ .

<sup>9</sup>Throughout this chapter, we use the term ‘core’ to refer to the innermost part of a galaxy, within  $1R_e$ .

expected on the cooling diagram. Finally, I present a new reconstruction method, based on adiabatic contraction, which recovers the initial halo parameters from present-day observations of the galactic core.

## 7.2 The sample

Galaxies were selected from the sample of B03, who in turn extracted their sample from the SDSS.<sup>10</sup> The Sloan survey is fully described in York *et al.* (2000), and provides imaging and spectroscopic surveys over a large area of the sky. It uses a telescope of 2.5m primary diameter to image the sky in five optical bands ( $u'$  with design effective wavelength 3550Å,  $g'$ , 4770Å,  $r'$ , 6230Å,  $i'$ , 7620Å and  $z'$ , 9130Å). Follow-up spectroscopy is then obtained for a sub-sample of objects which are selected from the images. As of the fourth data release (Adelman-McCarthy *et al.*, 2006) the survey comprised photometry for 180 million objects, together with  $\sim 8 \times 10^5$  follow-up spectra. For the work presented here, the data as presented in B03 are used (i.e. the Data Release 1 standard). The exception is the photometric data set, where DR4 has been used in order to avoid many of the problems with photometry identified in earlier releases (see Stoughton *et al.* (2002) §4 for details).

The sample of B03 comprises almost 9,000 early-type galaxies, with spectroscopic redshifts in the range  $0.01 \leq z \leq 0.3$  (in the heliocentric reference frame). These galaxies were selected via the following criteria:

1. Concentration index  $\frac{r_{90}}{r_{50}} > 2.5$  in  $i^*$ .
2. The likelihood of the de Vaucouleurs' model is at least 1.03 times that of the exponential model when fitted to the observed light profile.
3. Spectra with PCA classification numbers (Connolly *et al.*, 1995)  $a < -0.1$ .

<sup>10</sup>Funding for the creation and distribution of the SDSS Archive has been provided by the Alfred P. Sloan Foundation, the Participating Institutions, the National Aeronautics and Space Administration, the National Science Foundation, the U.S. Department of Energy, the Japanese Monbukagakusho, and the Max Planck Society. The SDSS Web site is <http://www.sdss.org/>. The SDSS is managed by the Astrophysical Research Consortium (ARC) for the Participating Institutions. The Participating Institutions are The University of Chicago, Fermilab, the Institute for Advanced Study, the Japan Participation Group, The Johns Hopkins University, the Korean Scientist Group, Los Alamos National Laboratory, the Max-Planck-Institute for Astronomy (MPIA), the Max-Planck-Institute for Astrophysics (MPA), New Mexico State University, University of Pittsburgh, University of Portsmouth, Princeton University, the United States Naval Observatory, and the University of Washington.

4. Spectra without masked regions (ie those spectra not flagged as low quality by the SDSS pipeline).
5. Signal-to-noise ratio greater than 10.
6. Redshift less than 0.3.

As the photometry of each of the spectral bands is used in the subsequent analysis, it is important to note that these criteria do not include selection by colour.

The sample as contained in B03 is magnitude rather than volume limited, and so the sample was further restricted in order to rectify this. Selecting only those galaxies with  $M_{\text{star}}(R_e) < 7.94 \times 10^{10} M_\odot$  (for  $M_{\text{star}}(R_e)$  as defined in the next section) produces a volume-limited sample of 2040 galaxies with  $z < 0.1$  that appears to be free of selection effects. The mass function of this subset is shown in figure 7.1. Unless otherwise stated, it is this sample to which all subsequent results refer.

### 7.3 Stellar Mass

For massive elliptical galaxies with little gas content, the baryonic mass is (by definition) approximately equal to the stellar mass, at least within the effective (or half-mass) radius,  $R_e$ . For a simple model of such a galaxy with a profile of the type described by Hernquist (1990), the scale and effective radii are related by

$$r_s = 0.551 R_e. \quad (7.2)$$

The stellar mass content within  $R_e$  was computed by comparing the available SDSS photometry with that calculated for systems with a wide range of star formation histories (SFHs). Assuming an exponentially decaying star formation rate, each SFH is uniquely defined by three parameters:

1. Stellar metallicity, which was assumed to be constant with time. In other words, the timescale upon which star formation takes place is assumed to be less than the lifetime of the stars being formed. For galaxies forming stars at the rapid rates expected in the early Universe, the lifetime of the starburst is likely to be short relative to the lifetime of even the massive stars produced by it. Ratios of elemental abundance were taken to be equal to their local (solar neighbourhood) values.

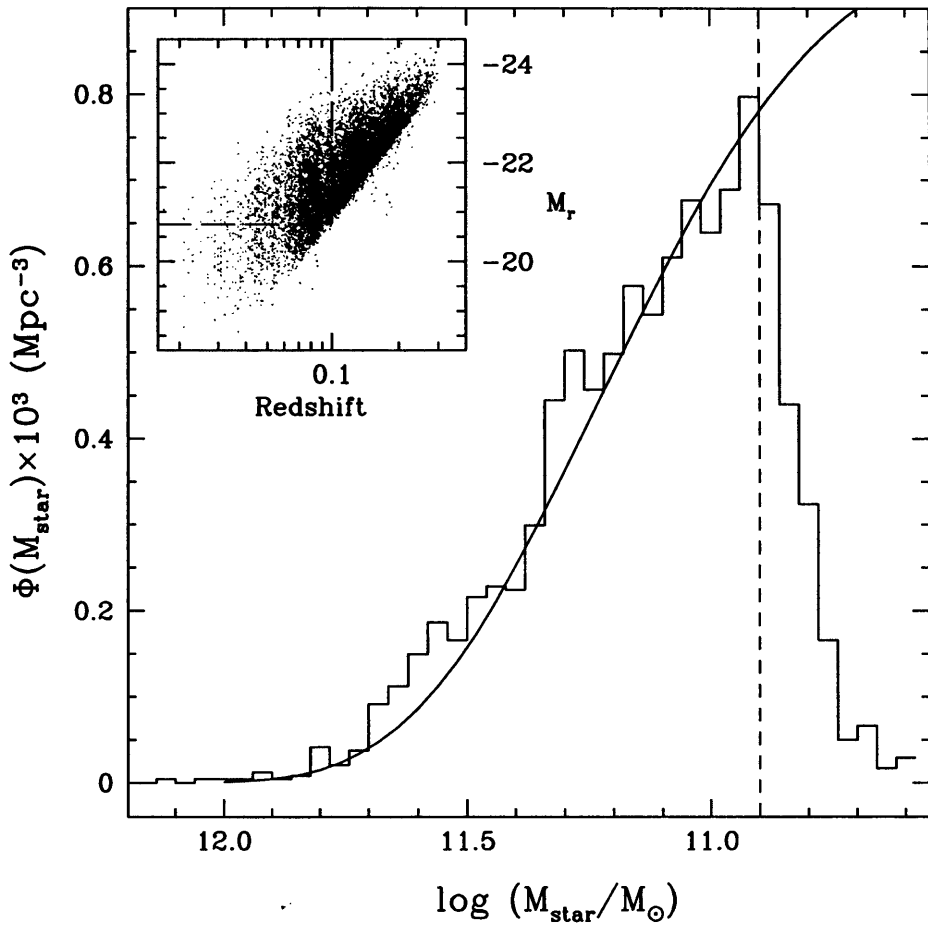


Figure 7.1: Stellar mass function (MF) of our volume-limited sample of early-type galaxies extracted from Bernardi et al. (2003). As shown in the insert (in which we plot the full sample of  $\sim 8700$  galaxies), we initially make cuts in redshift and absolute magnitude, plotting the MF for the remaining galaxies as the jagged line. In order to check that these cuts produce a useful sample, we compare the result with the luminosity function derived for all SDSS early-type systems (type  $0 < T < 1$ ) obtained independently by Nakamura et al (2003). For the purposes of this comparison, we assume a characteristic  $M_{\text{star}}/L_r = 4$  (see figure 7.5). Our sample is complete for systems with stellar masses greater than  $7.94 \times 10^{10} M_\odot$  (dashed line), and so we make a final cut at this mass to leave our final sample of 2040 galaxies.

2. Star formation timescale
3. Formation redshift  $10 > z_F > 2$

Depending on the choice of parameters, therefore, a model such as this can represent both a short, sharp burst of star formation and a more extended episode. For every choice of star formation history, the resulting synthetic stellar populations are calculated using the models described in Bruzual and Charlot (2003), and these are used to generate a simulated composite spectrum. The models compute the spectral evolution of stellar populations between  $1 \times 10^5$  and  $2 \times 10^{10}$  years after protostellar ignition to a resolution of 3Å. They take into account stellar evolution theory and, particularly, observations of thermally pulsing stars on the asymptotic giant branch of the Hertzsprung-Russell diagram. Their model reproduces in detail the typical spectra of Sloan galaxies.

The mass function of the stars within each galaxy must also be selected. Salpeter (1955) introduced a version of the IMF, which has proved remarkably successful in fitting observations. It described the number (or, equivalently, the density) of stars per interval of the logarithmic mass as

$$\xi(m) = \frac{dN}{d \log(m)} = \ln(10) m \xi(m). \quad (7.3)$$

Salpeter suggested that the IMF was well described by a power-law of the form  $\xi(m) \propto m^{-\alpha}$ , with  $\alpha \simeq 2.35$  for stars with  $m \geq 1M_\odot$ . Scalo (1986) and, more recently, Kroupa (2001) suggest for  $\alpha \sim 2.7$ , the difference being due to the inclusion of observationally unresolved binaries. In this chapter (unless otherwise stated), I use the refined version of Chabrier (2003), which includes a fit to the low-mass part of the distribution. Chabrier gives three functional forms of the mass function, the simplest of which is

$$\xi(m) = \frac{dn}{dm} = Am^{-\alpha} \quad (7.4)$$

where  $A = 0.019 M_\odot^{-1} \text{pc}^{-3}$  and

$$\alpha = \begin{cases} 1.55 & m \leq 1.0M_\odot \\ 2.70 & m > 1.0M_\odot \end{cases}$$

Photometry from four of the SDSS passbands was used, and the modelled flux in each of three colours ( $g-r$ ,  $r-i$ ,  $i-z$ ) was compared with the observations for each source. The best fit was then used to determine a stellar mass-to-light ratio. The stellar mass content of each source could then be estimated from the absolute  $r$ -band magnitude, given in the Sloan data release.

It seems initially that the use of the full spectral energy distribution instead of the few colours considered in this work would produce a more accurate estimate of the stellar mass content. However, the results shown in figure 7.2 indicate that the stellar mass to light ratio in the  $r$  band for these early-type galaxies does not alter much with respect to allowed SFH. All photospectropic observables suggest that local early-type galaxies have old and passively evolving stellar populations (Bernardi *et al.*, 2003b), which results in a weak dependence of the mass to light ratio on age or metallicity. (See the right-hand panel of figure 7.5.) The largest systematic error in the stellar mass is due to the choice of the initial mass function (IMF), which amounts to a factor of 0.1-0.2 dex in  $\log(M/L)$  for a range of standard IMFs.

As discussed above, following the initial work by Salpeter (1955), observations have forced the extension of the mass function to small masses, below the hydrogen-burning limit. Bruzual & Charlot (2003), upon whose models this work is based, note that the results obtained using two recent mass functions, the Chabrier and Kroupa IMFs (Kroupa, 2001) are ‘very similar’.

## 7.4 Dynamical Mass

It is also possible to use the projected size and central velocity dispersion of the galaxies, along with a simple model of the dynamics of early-type systems, to estimate the total (i.e. baryonic and dark matter combined) matter content within  $R_e$ . Assuming that the velocity dispersion and the anisotropy of the velocity distribution do not vary with radius, one can solve Jeans’ equation relating velocity and mass distributions in the form

$$\frac{d(\nu \bar{v}_r^2)}{dr} + \frac{v}{r} [2\bar{v}_r^2 - (\bar{v}_\theta^2 + \bar{v}_\phi^2)] = -\nu \frac{d\Phi}{dr} \quad (7.5)$$

Defining the anisotropy,  $\beta$  as

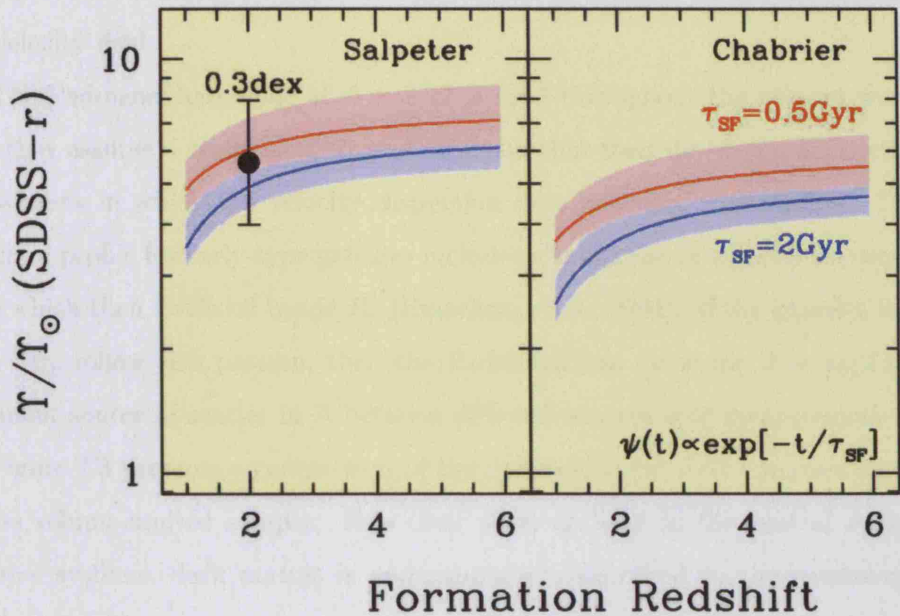


Figure 7.2: Figure by Ignacio Ferreras, demonstrating the effect of altering model parameters on the derived mass to r-band light ratio. The left hand panel uses the Salpeter IMF, that on the right the Chabrier mass function. Red curves represent a short burst of star formation, lasting 0.5Gyr whereas the blue curves represent a 2Gyr burst of star formation. As it is the r-band luminosity which is ultimately used to estimate the stellar mass content, these results show the maximum variation which should be expected in the stellar mass derived for these systems.

$$\beta \equiv 1 - \frac{\bar{v}_\theta^2}{\bar{v}_\phi^2} \geq 0 \quad (7.6)$$

equation 7.5 can be written as (Binney and Tremaine, 1987)

$$\frac{1}{\nu} \frac{d(\nu \bar{v}_r^2)}{dr} + 2 \frac{\beta \bar{v}_r^2}{r} = - \frac{d\Phi}{dr}. \quad (7.7)$$

A similar method is used by Padmanabhan *et al.* (2004) to perform a careful analysis of the profiles of massive galaxies and they find that

$$M_{\text{dyn}} (< R_e) = A \frac{\sigma^2 R_e}{G} \quad (7.8)$$

where  $R_e$  is the effective (or projected half-light) radius,  $\sigma$  the velocity dispersion as measured at the centre and  $A$  is a constant which depends weakly on the anisotropy of the velocity field.

The Padmanabhan value of  $A \approx 2.72$  is used throughout the present work, but note that they assume a systematic error of 30% and that their derivation is strictly valid only for systems in which the velocity dispersion does not vary with radius. The expected standard profile for early-type galaxies includes a sharp rise in velocity dispersion at small radii which then levels off inside  $R_e$  (Emsellem *et al.*, 2004). If the galaxies in the sample used here follow this pattern, then the Padmanabhan value for  $A$  is appropriate. The dominant source of scatter in  $A$  between different sources is in measurement errors.

Figure 7.3 presents a comparison of the dynamical and stellar masses for the galaxies in the volume-limited sample. It is clear that, at least in the central regions ('cores') of these systems, dark matter is underabundant compared to the cosmological baryon fraction. In other words, the core region is baryon-dominated, in agreement with recent modelling by Mamon and Lokas (2005) who suggest that the dark matter component becomes important only at  $\sim 3 - 5R_e$ . This result, although initially surprising, is also comparable to the results of Loewenstein and White (1999) who use the observed relation between x-ray temperature and stellar velocity dispersion (the so-called T-sigma relation) to find a nearly constant mass-to-light ratio within six half light radii. It should be noted, however, that they use an unrealistic model for anisotropy in their sources. Nonetheless, they conclude that the 'theory of hierarchical halo formation ... badly fails to reproduce the observed T-sigma relation' unless a majority of baryons is expelled from 'typical' systems (those with  $L \sim L_*$ ).

Romanowsky *et al.* (2003) measure the velocity dispersion,  $\sigma$ , through observations of bright planetary nebulae in three local elliptical galaxies (all of which are less massive than those in the sample considered here). They derive a mass to light ratio within  $5R_e$  which is compatible with that expected from a purely stellar population. In other words, there is no need for a dark matter component in explaining their results. They also use a more sophisticated orbit modelling approach for one of the galaxies (NGC3379). This method allows for anisotropies which vary arbitrarily with radius, and fits both the planetary nebulae velocity dispersion as well as the stellar brightest distribution and stellar kinematics. The result is a mass to light ratio at  $5R_e$  which is compatible with only a small contribution from dark matter. Dekel *et al.* (2005) explained this result - without

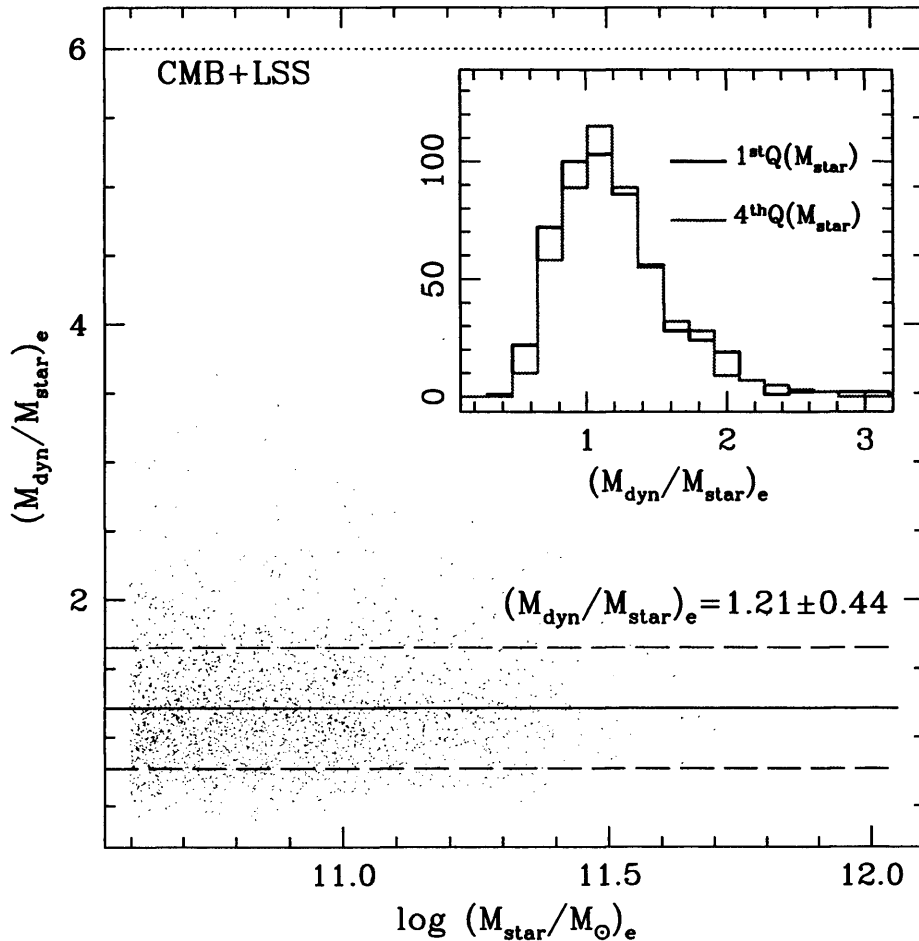


Figure 7.3: Ratio of dynamical to stellar mass measured within  $R_e$ . The solid and dashed lines give the mean and RMS of our  $z < 0.1$  sample. The dotted line labelled CMB+LSS gives the prediction of the cosmological ratio. The inset shows a histogram of the first and fourth quartiles in stellar mass (i.e.  $\log(M_{\text{star}}/M_{\odot}) < 10.72$  and  $> 11.02$ , respectively).

invoking a ‘naked’ stellar population - by suggesting that ‘the stellar orbits in the outer regions … are very elongated’. In the view of Dekel *et al.*, therefore, planetary nebulae are not unbiased tracers of the underlying distribution. The results in this chapter, which are directly applicable only to the innermost  $R_e$ , suggest that results similar to those obtained by Romanowsky *et al.* (2003) should be expected even in large ellipticals (and, indeed, in large samples of ellipticals). Realistic assumptions (á la Dekel *et al.*) about the velocity structure of the cores of these systems do not provide an explanation of the deviation observed within the core from the cosmological baryon fraction.

## 7.5 Scaling relations

Figure 7.4 shows the scaling relations which relate the (*r*-band) luminosity, stellar and dynamical masses to the velocity dispersion. The bottom panel therefore shows the well known Faber-Jackson relation (Faber and Jackson, 1976)

Notice that the truncation imposed by the choice of a volume-limited sample results in a constraint (the cut is made along the dashed, horizontal, line) nearly aligned with the correlation. Hence, a strong bias is expected if this reduced sample is used for the fits (see, for example, appendix B in Lynden-Bell *et al.* (1988) for a nice illustration of this problem, which results in a bias towards low values of the ordinate). In order to avoid this problem, the complete sample is used for the fits presented in this figure.

In order to reduce the effect of outlying data points in the calculation of the best-fitting parameters, all of the fits in this section use a robust M-estimator based on the minimisation of the mean absolute deviation (Press *et al.*, 1992). Instead of finding the minimum of

$$\chi^2(a, b) = \sum_{i=1}^N \left( \frac{y_i - a - bx_i}{\sigma_i} \right)^2 \quad (7.9)$$

we minimise:

$$MAD = \sum_{i=1}^N |y_i - a - bx_i|. \quad (7.10)$$

This is particularly important here, as standard least-squares methods were found to be very sensitive to outliers in the sample. Given the uncertainties in the determination

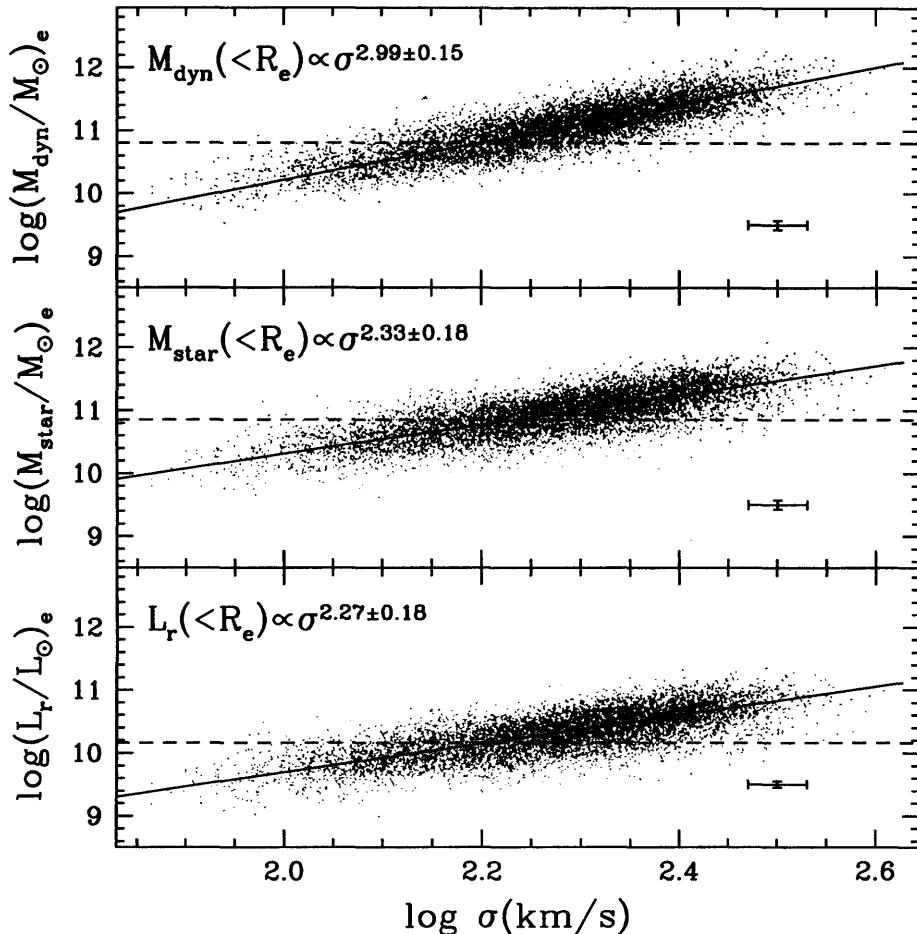


Figure 7.4: Correlations between velocity dispersion and luminosity (bottom), stellar mass (middle) and dynamical mass (top), all measured within  $R_e$ . Characteristic error bars are shown in each panel. The solid lines are fits to the data, with all points equally weighted. The truncation of our volume-limited sample is shown as a dashed line. Given that the truncation and the fit are nearly aligned, we have used the complete sample for the fits shown in this figure.

of the appropriate errors in both velocity dispersion and radius, all points have been equally weighted rather than taking into account differences in their quoted errors. A ‘bootstrap’ method was then used to determine the uncertainty in the slope, with the same fitting technique being applied to 1000 subsamples of 500 galaxies each. Crucially, these subsamples were selected from the larger sample with replacement. The predicted slopes from each of these runs were then used to determine the quoted uncertainties (Efron and Gong, 1983).

The Faber-Jackson relation is believed to appear in the data as a direct consequence of the dynamics of the systems being studied. Early-type galaxies are hot dynamical systems whose support against gravitational collapse comes mostly from the velocity dispersion of the constituent stars. Hence, a correlation is to be expected between the central velocity dispersion and the total mass of the system. The different slopes evident in figure 7.4 for the stellar and dynamical mass estimates can be attributed to stellar population effects, to structural differences in the distributions of stars and dark matter, or to a significant additional correlation between the dark matter fractional contribution and total galaxy mass. This latter effect - essentially just the observation that larger galaxies seem to have more dark matter - has been commonly invoked to explain the tilt of the so-called ‘fundamental plane’.

The fundamental plane, first noted by Djorgovski and Davis (1987) (who named it) and Dressler *et al.* (1987) relates three parameters via a relationship which is linear in log-space. The parameters are the radius,  $r$ , the velocity dispersion,  $\sigma$  and the luminosity or surface brightness. Expressed as

$$R_e \propto \sigma^a I_e^{-b} \quad (7.11)$$

the virial theorem can be used for homogeneous systems to derive this relation with  $a = 2$  and  $b = 1$  (Faber *et al.*, 1987).<sup>11</sup>

Observed values of  $a$  and  $b$  differ from this simple prediction, leading to a ‘tilt’ in the fundamental plane. Explanations of such a tilt have ranged from variance in stellar populations to changing distributions of dark and baryonic matter. Guzman *et al.* (1993) explain the tilt in terms of a ratio between half-mass and effective radius which is a decreasing function of galaxy mass. Ferreras and Silk (2000b), in contrast, suggest that differences

---

<sup>11</sup>Details of derivation

in the efficiencies of both star formation and outflow from the galaxy are required in order to account for the observations. Finally, Trujillo *et al.* (2004) chose to attribute the tilt to ‘three quarters structural nonhomology, one quarter stellar population’.

Figure 7.5 shows the correlation between velocity dispersion and the mass to light ratio (for both stellar and dynamical, or total, mass). Early-type galaxies in the local, present-day Universe are dominated by stars that are older than about 7-8 Gyr, which implies that the contribution of stellar populations to the tilt of the fundamental plane cannot be too large, as previously suggested by Dressler *et al.* (1987). Nevertheless, figure 7.5 reveals a remarkable difference between stellar and dynamical mass-to-light ratios. The slope of the dynamical mass-to-light ratio is sufficient to explain the tilt of the fundamental plane, despite the fact that equation 7.8 assumes that all galaxies in the sample are homologous. Hence the observed slope is recovered without the need to invoke structural non-homology. Recent estimates using observations of 18 strongly gravitationally lensed quasars (Ferreras *et al.*, 2005b) suggest that main cause of the tilt lies in the distribution of dark matter, a view supported by the results in this chapter.

## 7.6 Acceleration

The analysis so far has been conducted within the framework of Newtonian dynamics, and we have seen that the cores (defined as within  $R_e$ ) of massive early-type elliptical galaxies are dominated by baryons, rather than by dark matter. However, the appearance of discrepancies between observations and models using only baryonic matter can be explained either by the presence of non-baryonic dark matter or by modifications to the theory of gravity. Indeed, as Sanders and McGaugh (2002) note, ‘it is a simple matter to claim that Newton’s law of gravity fails on galactic scales and then to cook up a recipe that explains a particular aspect of the observations’. Finding a credible theory which explains various aspects of astronomical observation (and, ideally, is an extrapolation of existing theory) is more difficult, but the most successful of such attempts is the Modified Newtonian Dynamics (MOND) proposed by Milgrom (1983). The most obvious modification - a change in the strength of the gravitational attraction on large scales - is incompatible with the observed Tully-Fisher relation between velocity and luminosity (Tully and Fisher, 1977). Instead, the model of Milgrom includes a modification to gravity at low acceleration such that the rotation curves of isolated masses are flat.

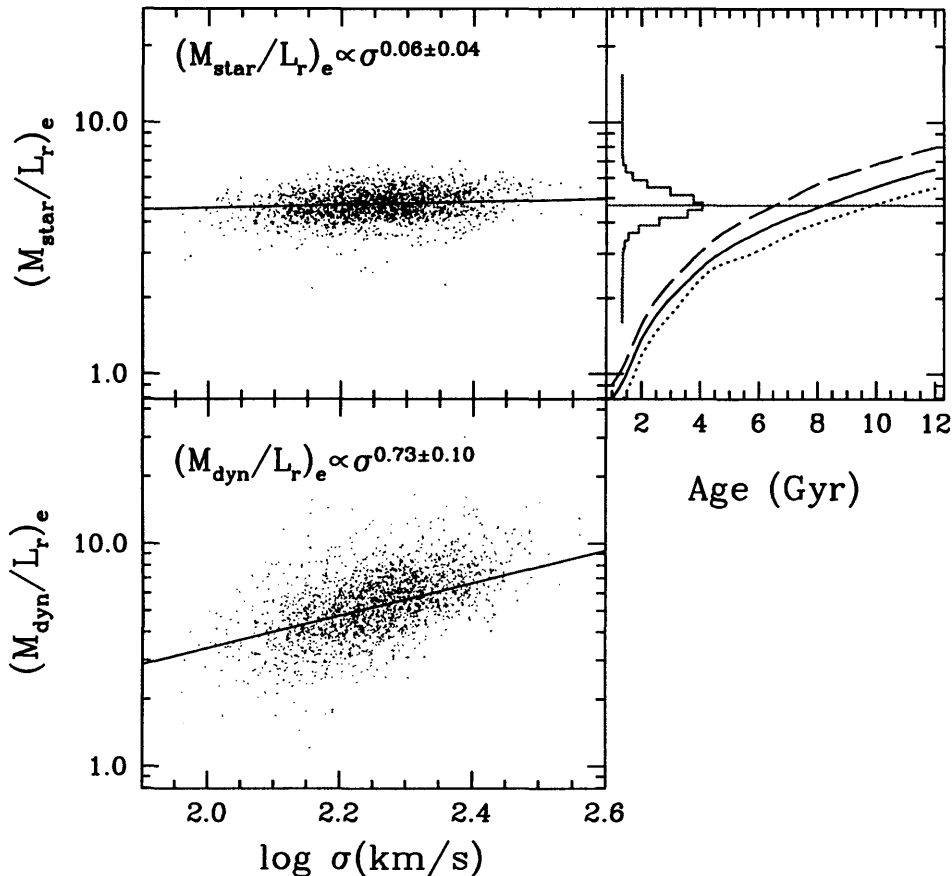


Figure 7.5: Stellar (top) and dynamical mass-to-light ratios as a function of velocity dispersion for our volume-limited sample, after cuts have been applied. The straight lines are fits to the data, and the corresponding power law indices are labelled in each panel. The panel on the right shows the predictions for simple stellar populations from the models of Bruzual & Charlot (2003) as a function of age. The dashed, solid and dotted lines correspond to metallicities 2, 1 and 1/2 times solar. The histogram refers to the data (left panel), with the average given as a horizontal line.

It is intriguing in this context to see an inverse correlation between the Newtonian mass-to-light ratio and the centripetal acceleration ( $a = v^2/r$ ) at the outermost measured radial point in spiral galaxies, at least for  $a < 10^{-8}$  cms $^{-2}$  (Sanders and McGaugh, 2002). The results from this work are shown in figure 7.6 as circles. Such low accelerations are not expected in the cores of massive ellipticals, which have smaller radii than the outermost parts of spiral galaxies. (Typical effective radii of a few kpc compared to  $\sim 10$  pc for the radius of a large spiral.) Nevertheless, it is interesting to look for any such correlation in the sample of ellipticals, and thus figure 7.6 includes as dots the ratio  $M_{\text{dyn}}/L_K$ , plotted against the acceleration. The acceleration is defined for the ellipticals in this sample as  $a = v^2/R_e = 3\sigma^2/R_e$ . No obvious correlation is seen, and there is no continuity in relation between the spirals and the elliptical systems. As expected, the ellipticals have accelerations which are  $\sim 10$  times larger than the limits which MOND requires in order for departures from Newtonian dynamics to become apparent (see figure 7.6). If indeed ellipticals are immersed in large dark halos, similar measurements of acceleration at large radii would be important in distinguishing between MOND and true dark matter models.

## 7.7 Spherical collapse in a $\Lambda$ CDM Universe

Returning to a conventional, dark matter dominated Universe, there is renewed interest in spherical collapse models as part of a picture of galaxy formation which is more complicated and varied than the simple hierarchical merging of dark matter halos (and indeed, is more complex than simple spherical (also known as monolithic) collapse). How, then, do the predictions of this simple model compare to data from modern galaxy surveys such as the SDSS, and how do the predictions of the model change when used with a cosmological model which incorporates a non-zero cosmological constant?

There have been many attempts to study spherical collapse in  $\Lambda$ CDM models. To give two examples, Lahav *et al.* (1991) considered the growth of perturbations, concluding that the presence of a cosmological constant produces objects with a smaller final radius while Wang and Steinhardt (1998) derived limits on  $\Lambda$  from the abundance of clusters. Here I will follow the analysis of BFPR more closely, using plots of velocity dispersion against mass and of baryon density against temperature to compare model predictions with data.

In order to check whether a simple spherical collapse model is compatible with the observed properties of massive galaxies, figure 7.7 shows the correlation between total mass

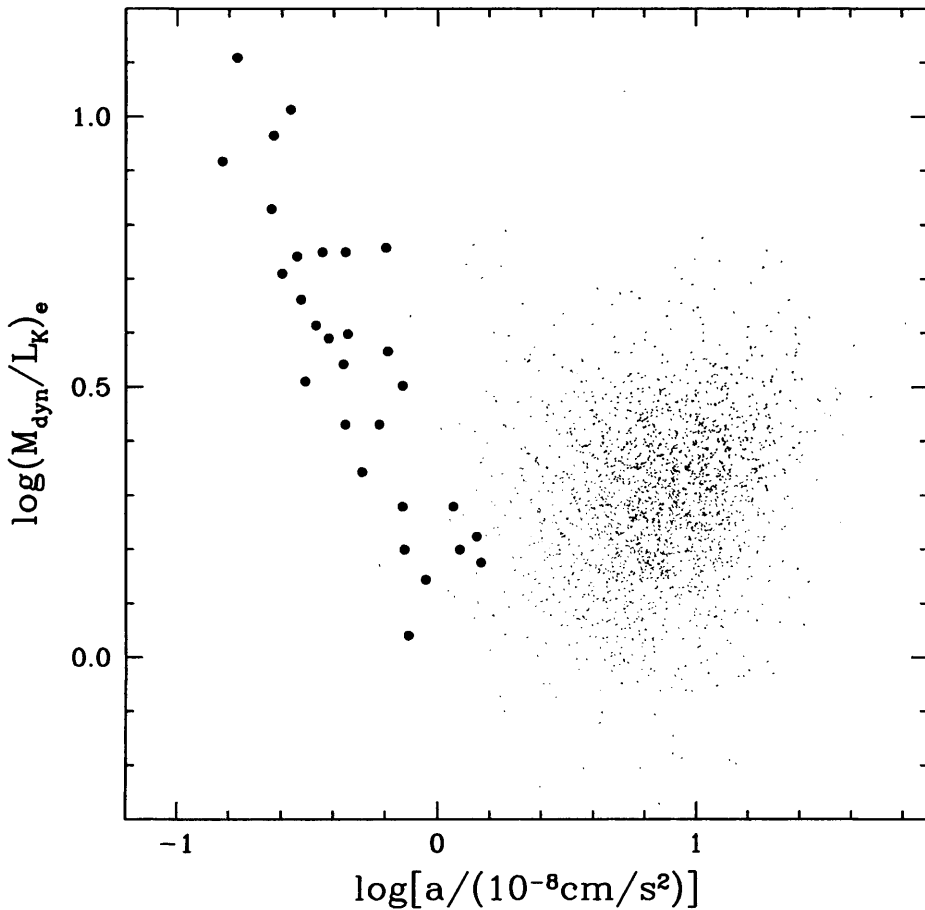


Figure 7.6: Comparison of the acceleration of early-type and late-type galaxies. We plot the dynamical  $M/L_K$  as a function of acceleration (defined as  $a = v^2/R_e = 3\sigma^2/R_e$ ). In order to generate  $K$  band  $M/L$  ratios, we use  $r - K = 2.4$ , typical of early-type systems. The late-type data (circles) come from Sanders & McGaugh(2002). Notice that early-type galaxies fall outside of the low-acceleration regime required by MOND to give a significant departure from Newtonian dynamics.

(i.e. the mass including the halo) and the central velocity dispersion. The lines shown in the figure represent the theoretical mass and velocity dispersion of systems produced by the spherical collapse of dark matter haloes. The collapse of a spherical, ‘top-hat’, perturbation is described by

$$\frac{d^2r}{dt^2} = H_0^2 \Omega_\Lambda r - \frac{GM(< r)}{r^2} \quad (7.12)$$

where  $r$  is the radius in a fixed coordinate frame, within which is enclosed a mass,  $M(< r)$  and where the initial velocity field is given only by the Hubble flow. The cosmological constant has been assumed to be scale invariant. If the mass described by such an equation is gravitationally bound, it will initially expand before reaching a maximum radius and then collapsing. Linear theory predicts that the over-density at which the ‘top-hat’ collapses to a point is  $\delta_{\text{linear}} = 1.686$  (Peebles, 1980). This expression is strictly appropriate only in an Einstein-de Sitter universe, but the value of the constant used is only slightly sensitive to the choice of cosmology. Thus, for a ‘top-hat’ fluctuation to be on the point of collapsing at a redshift,  $z$ , then its density extrapolated to the present day must satisfy:

$$\delta_c(z) = \frac{1.686}{D(z)} \quad (7.13)$$

where  $D(z)$  is the growth factor from linear theory.

Collapse of these fluctuations to a single point is prevented by violent relaxation (sometimes known as ‘phase mixing’) which produces a state of virial equilibrium. Bryan and Norman (1998) use the virial theorem to obtain the final over-density (relative to the critical density at the collapse redshift), given by the following formula which is valid for universes in which  $\Omega_m + \Omega_\Lambda = 1$  and is accurate to 1%:

$$\Delta_c = 18\pi^2 + 82d - 39d^2 \quad (7.14)$$

where  $d = \Omega_m^z - 1$  and

$$\Omega_m^z = \frac{\Omega_m(1+z)^3}{\Omega_m(1+z)^3 + \Omega_\Lambda + \Omega_k(1+z)^2}. \quad (7.15)$$

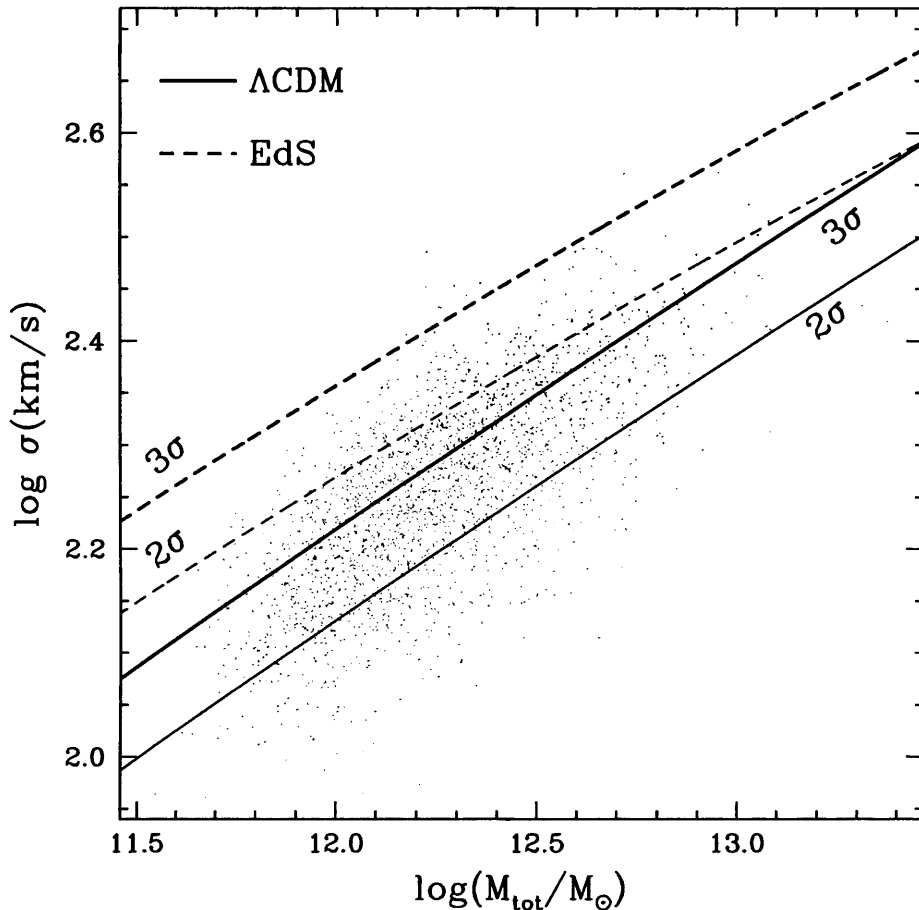


Figure 7.7: A comparison of the spherical collapse model with our sample of massive early-type galaxies for both EdS (dashed lines) and  $\Lambda$ CDM cosmologies. (EdS parameters :  $\Omega_m = 1.0, \Omega_\Lambda = 0.0, h = 0.7, \sigma_8 = 0.9$ ,  $\Lambda$ CDM parameters :  $\Omega_m = 0.3, \Omega_\Lambda = 0.7, h = 0.7, \sigma_8 = 0.9$ ). In obtaining  $M_{\text{tot}}$  we have assumed  $\alpha = 20$  (see text for details). The  $M_{\text{tot}}$  obtained are consistent with a formation process from 2- or 3-sigma perturbations in a  $\Lambda$ CDM cosmology.

A halo will, therefore, collapse at a redshift determined only by its total mass and by the cosmological model adopted. For the massive galaxies contained in our sample, once the collapse has stopped we may assume that the systems are virialized. Via the virial theorem its radius will then be given by (Barkana and Loeb, 2001)

$$r_{\text{vir}} = 0.784 \left( \frac{M_{\text{tot}}}{10^8 h^{-1} M_{\odot}} \right)^{\frac{1}{3}} \left[ \frac{\Omega_m}{\Omega_m^z} \frac{\Delta_c}{18\pi^2} \right]^{-\frac{1}{3}} \left( \frac{1+z}{10} \right)^{-1} h^{-1} \text{kpc} \quad (7.16)$$

and the circular velocity will be

$$v_c = \sqrt{\frac{GM}{r_{\text{vir}}}} = 23.4 \left( \frac{M_{\text{tot}}}{10^8 h^{-1} M_{\odot}} \right)^{\frac{1}{3}} \left[ \frac{\Omega_m}{\Omega_m^z} \frac{\Delta_c}{18\pi^2} \right]^{\frac{1}{6}} \left( \frac{1+z}{10} \right)^{\frac{1}{2}} \text{km s}^{-1}. \quad (7.17)$$

A halo of a particular mass will thus collapse later in a Universe which has a non-zero cosmological constant, and it is this which leads to the differences seen in figure 7.7 between Einstein-de Sitter and  $\Lambda$ CDM models. The EdS calculations match those initially presented by BFPR, but the paper on which this chapter is based was the first time that the diagram has been updated to include a modern cosmological model and data for individual galaxies.

In order to compare these theoretical predictions with the data, it is necessary to convert the dynamical mass within the core (see section 7.4) defined by equation 7.8 to a total mass. A naive solution would be to assume that  $R_e$  is both the half-mass as well as the half-light radius, so that  $M_{\text{tot}} \approx 2M_{\text{dyn}} (< R_e)$ . This approach, however, ignores variations in the mass to light ratio between systems, and the profile of the velocity dispersion used to derive the dynamical mass. Instead, I take the *ansatz* that the total mass of the galaxy is proportional to the dynamical mass within  $R_e$ :

$$M_{\text{tot}} = \alpha M_{\text{dyn}} (< R_e) \quad (7.18)$$

There will presumably exist a scatter in  $\alpha$ , the constant of proportionality, in the population of galaxies, and it is indeed reasonable to expect  $\alpha$  to be a function of the total mass of the galaxy. As this function is unknown, I use the approximation of a single value of  $\alpha$  for all the galaxies in the sample. In this way it is possible to consider for which values of  $\alpha$  the spherical collapse model is a good fit to data. Consider the example of  $\alpha = 2$ ,

which corresponds to the model proposed in the previous paragraph. The slope of the data is initially encouraging, being in good agreement with the theoretical prediction. However, for a given mass, the predicted velocity dispersions are so large that the galaxies correspond to 4-sigma fluctuations in an EdS universe and 7-sigma fluctuations in  $\Lambda$ CDM. These are extremely unlikely fluctuations, and the choice of  $\alpha = 2$  is therefore not compatible with the observed number density of massive galaxies.

In order to produce a rough estimate for the level of fluctuations that actually correspond to the observed population of massive galaxies, it is possible to use the morphologically segregated luminosity functions (LFs) from the SDSS (Nakamura *et al.*, 2003). Integrating the LF of early-type systems (E and S0 galaxies) from  $L_*$  to some bright upper limit<sup>12</sup>, one obtains a comoving number density of ellipticals similar to those in our sample (see figure 7.1). The SDSS luminosity function results give  $n(\text{E/S0}) = 0.11 \times 10^{-2} h^3 \text{Mpc}^{-3}$ . A similar integral for the LF of *all* galaxies in the sample with luminosities in the range  $0.005 < L/L_* < 20$  gives the comoving number density  $n(\text{all}) = 9.02 \times 10^{-2} h^3 \text{Mpc}^{-3}$ . The ratio of the two number densities ( $n(\text{E/S0})/n(\text{all}) = 0.012$ ) corresponds to a Gaussian fluctuation between 2- and 3-sigma. Hence a spherical collapse model which requires 2- to 3-sigma fluctuations to produce the galaxies in the sample is compatible with observations. A choice of  $\alpha = 20$  produces a good correlation between the data and the predicted M- $\sigma$  relation for 3-sigma fluctuations given a  $\Lambda$ CDM cosmology.

## 7.8 The evolution of the dark matter profile

This simple approach gives interesting results, but in order to progress further it is essential to consider the matter profiles of the systems being studied. To investigate the distributions of total and stellar mass within the spherical collapse framework, it is necessary to take into account the evolution of the dissipationless dark matter as the baryons dissipate energy and sink towards the centre of the halo. The procedure of adiabatic contraction of the dark matter halo, normally credited to Blumenthal *et al.* (1986)<sup>13</sup>, is used. It is assumed that the dark matter has an *initial* density profile of the form given by Navarro *et al.* (1997) (hereinafter NFW), given by

<sup>12</sup>  $20L_*$  is used but the choice is essentially unimportant given the exponential cutoff of the LF.

<sup>13</sup> Barnes and White (1984) and Ryden and Gunn (1987) seem to have developed the same idea independently.

$$\frac{\rho(r)}{\rho_c} = \frac{\delta_c}{\frac{r}{r_s} \left(1 + \frac{r}{r_s}\right)^2} \quad (7.19)$$

where  $\delta_c$  is a characteristic density and  $r$  is the radius.

The concentration is defined as  $c = r_{\text{vir}}/r_s$  where  $r_{\text{vir}}$  is the virial radius (which is usually considered to represent the ‘edge’ of the halo) and  $r_s$  is the scale radius associated with the profile. This method is strictly valid, as with much of the analysis presented in this chapter, only for halo particles moving on circular orbits. Perhaps because of this limitation, simulations by Gnedin *et al.* (2004) et al. show that the predicted density profile from adiabatic contraction is more dense than that found in N-body simulations. However, the deviation is small (Sellwood and McGaugh, 2005) and the method is used here as a first approximation.

The initial mass profile and the final dark matter and baryonic profiles are related by two equations:

$$r [M_g(< r) + M_h(< r)] = r_i M_i(< r_i), \quad (7.20)$$

and

$$M_h(< r) = (1 - f_{\text{cool}}) M_i(< r_i). \quad (7.21)$$

In these equations  $M_i(< r)$  is the initial mass within a radius,  $r$ ,  $M_g(< r)$  and  $M_h(< r)$  are the final baryonic and dark matter profiles respectively.  $f_{\text{cool}}$  is the fraction of the system’s mass contained in the baryons which cool to form the galaxy (or other central concentration), and is related to  $\alpha$  via the relation

$$f_{\text{cool}} = \frac{2M_{\text{star}}(< R_e)}{\alpha M_{\text{dyn}}(< R_e)} \quad (7.22)$$

where the stellar mass within  $R_e$  is assumed to be half the cooled baryonic mass (Padmanabhan *et al.*, 2004). For  $\alpha = 20$  (as discussed in the previous section) and the mean ratio of  $M_{\text{star}}(< R_e)$  to  $M_{\text{dyn}}(< R_e)$  found in section 7.4,  $f_{\text{cool}} = 0.08$ . This sort of argument can be used to place limits on  $\alpha$  by requiring  $f_{\text{cool}} < 1/6$  (where  $1/6$  is the cosmological baryon fraction). This corresponds to a requirement for  $\alpha > 10$ .

It is interesting to note that the choice of  $\alpha = 20$ , originally motivated by the requirement to match data with 2- or 3-sigma perturbations, produces a value for the stellar mass to total mass ratio which is approximately half the cosmological baryon fraction. Models with large  $\alpha$  are also consistent with the large mass to light ratios found by studies of such massive ellipticals in x-rays (Griffiths *et al.*, 1996).

The baryons are assumed to have a density profile of the form given by Hernquist (1990)

$$\rho(r) = \frac{M}{2\pi r} \frac{a}{(r+a)^3}. \quad (7.23)$$

In this special case the adiabatic contraction problem can be solved analytically (Kee-ton, 2001). Each initial radius  $r_i$  is found to map to a final radius  $r$  which are related by

$$f_{cool}r^3 + (r+a)^2 [(1-f_{cool})r - r_i] m_i (< r_i) = 0, \quad (7.24)$$

where  $a = 0.551R_e$  is the scale radius of the Hernquist profile, and

$$m_i(r_i) = M_i(< r_i) / M_{\text{tot}}. \quad (7.25)$$

A halo of mass  $M_{\text{tot}}$  will, in the spherical collapse picture considered here, collapse at a redshift determined only by the cosmology and the amplitude of perturbations. The virial radius is then given by equation 7.16. After choosing a value for  $\alpha$ ,  $f_{cool}$  can then be calculated by equation 7.22 using the observed value of  $M_{\text{star}}(< R_e) / M_{\text{dyn}}(< R_e)$  for each galaxy. For any concentration,  $c$ , the total mass inside the initial radius ( $r_i$ ) that will evolve into a final radius  $r = R_e$  is then calculated. The adiabatic contraction prescription implies that this mass is equal to the final mass observed within  $R_e$ . Finally, the concentration that best satisfies  $M_{\text{dyn}}(< R_e) = M_i(< r_i)$  can be determined.

### 7.8.1 Results

Figure 7.8 shows the histogram of the calculated concentration of the *initial* DM halos for the volume-limited sample, for 2- and 3-sigma perturbations and for  $\alpha$  of 10 and 20. The figure overlays a Gaussian distribution corresponding to the results. The fit is excellent,

and it is clear that the simplistic model of spherical collapse and adiabatic contraction results in a log-normal distribution of concentrations.

This result is remarkable, as a similar distribution is also seen in more detailed N-body simulations (Bullock *et al.*, 2001). Furthermore, the dispersion of the distributions shown in figure 7.8 is  $\sigma(\log c) \sim 0.2 - 0.25$ , in agreement with the simulations which give  $\sigma(\log c) \sim 0.18$ . However, these simulations also give absolute values for the concentration which are higher than those presented here even for 2-sigma fluctuations ( $\langle c_{\text{Sim}} \rangle = 6.5$  for  $\alpha=20$ ).

Hierarchical models give concentrations which are around 4 only for objects which have recently undergone major mergers or for large systems which have galaxy cluster masses. The mean concentration for galaxies with mass  $M_{\text{vir}} \sim 1.5 \times 10^{12} h^{-1} M_{\odot}$  is typically 13.1 (Wechsler *et al.*, 2002).

As figure 7.8 shows, our model does reproduce large values of  $c$  (which match simulations) for models which have small values of  $\alpha$  and 2-sigma fluctuations. However, as discussed above, a value of  $\alpha < 10$  would shift the data points shown in figure 7.7 to the left, away from the predictions for 2- and 3-sigma fluctuations. I therefore conclude that our ‘benchmark’ model predicts a mean concentration which is lower than that found in simulations.

These results are reminiscent of those of Collister and Lahav (2005) who studied the concentration of galaxy clusters and groups in the 2dF galaxy redshift survey. They found concentrations from data which were a factor of  $\sim 2$  lower than the predictions of dark matter simulations (such as those of Kravtsov *et al.* (2004)), albeit on larger scales than those considered here. Furthermore, Trujillo *et al.* (2005) present weak evidence for a change in concentration of massive elliptical galaxies (as derived from the size-mass relation) with redshift, and Borch *et al.* (2006) find that the mass contained in ‘red’ galaxies has substantially increased since  $z=1$ . These results may be testable by the sort of analysis used here; further studies with larger samples should enable the testing of their results with the methods discussed here.

### 7.8.2 Galaxy formation and cooling

In order to consider the baryonic component of the galaxies, it is convenient to plot baryon number density against temperature, following BFPR once more. Defining number density (at the present day) as

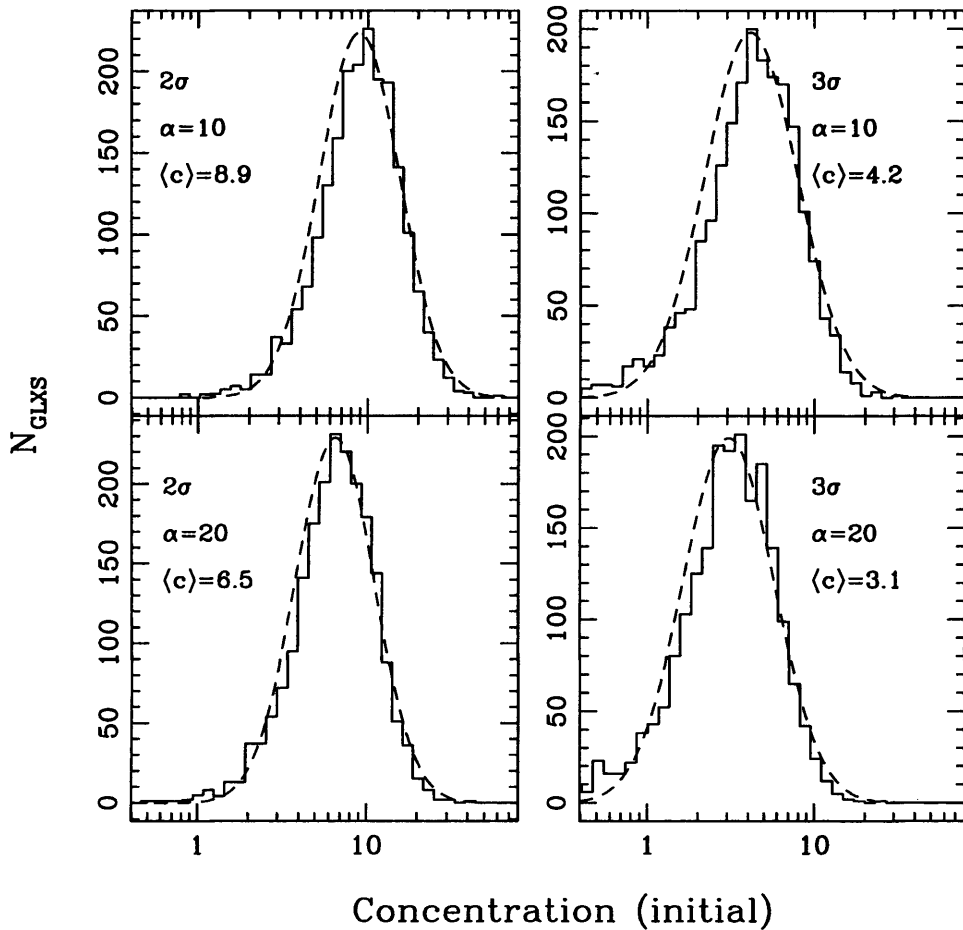


Figure 7.8: Concentration of the (NFW) dark matter halos before adiabatic contraction. The benchmark spherical collapse model, assuming LCDM and either 2- or 3-sigma perturbations is used.  $\alpha = M_{\text{tot}}/M_{\text{dyn}}(< R_e)$  is either 20 or 10 as indicated. In all cases an approximately log-normal distribution of concentration is recovered. A higher order perturbation (3- instead of 2-sigma) or larger  $\alpha$  reduces the mean value of the concentration.

$$n_b = \frac{3M_{\text{star}}(< R_e)}{4\pi R_e^3 \mu m_H} \quad (7.26)$$

and temperature as

$$T = \frac{\mu m_H \sigma^2}{k_B}, \quad (7.27)$$

where  $\mu m_H$  is the mean atomic weight (and  $\mu = 0.6$  for a primordial mix of hydrogen and helium), and  $k_B$  is the Boltzmann constant, data and theory can be compared in a space in which temperature and density are plotted against each other. The results are shown in figure 7.9.

The sample is shown in two different ways: the black dots represent the actual baryon densities (i.e. as observed after adiabatic contraction has taken place), computed within the half-light radius using equation 7.26. The grey dots represent the baryon densities expected from haloes before adiabatic contraction takes place, defined as the density which corresponds to a baryon mass  $M_{\text{bar}} = \langle f_{\text{cool}} \rangle M_{\text{tot}}$  confined within a radius of  $R_{\text{vir}}$ . The grey and black lines are the predictions of the spherical collapse model (for a  $\Lambda$ CDM cosmology), and are shown for 2- and 3-sigma fluctuations both before and after adiabatic contraction. These models require a translation to be made from total to baryonic mass, for which the average value of  $f_{\text{cool}}$  obtained from the sample is used ( $\langle f_{\text{cool}} \rangle = 0.083$ ). For the ‘before AC’ lines (grey) this mass is used with the virial radius defined by equation 7.16. Incidentally, the early-type galaxies indicated in the original cooling diagram in BFPR appear in the region of parameter space occupied here by galaxies before AC. This is the first time that individual galaxies have been plotted in this space; previous work has used ‘schematic’ data. In order to produce the (black) curves labelled ‘after AC’ it was also necessary to assume a ratio between the virial radius and the initial radius ( $r_i$ ) (which is mapped on to  $R_e$ ). The sample used here gives  $r_i \sim 0.1R_{\text{vir}}$  (see figure 7.10).

It is also possible to incorporate into this space an indication of the cooling timescale for objects of different temperatures and densities. The cooling curves shown trace  $t_{\text{dyn}} = t_{\text{cool}}$  where the dynamical timescale is given by

$$t_{\text{dyn}} = \sqrt{\frac{3\pi}{32G\rho}} \quad (7.28)$$

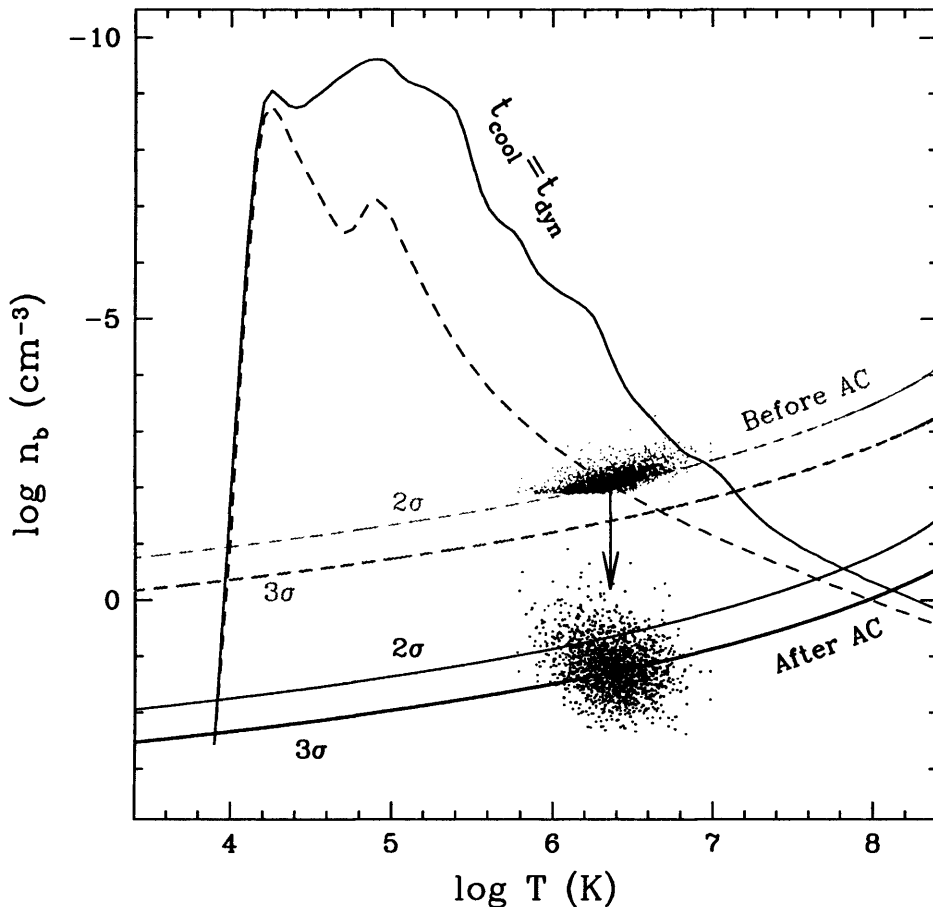


Figure 7.9: Galaxy formation à la BFPR. Our sample galaxies are shown in a density-temperature diagram. The black dots represent the observed sample, whereas the grey dots “extrapolate” the sample to the time of turnaround, before adiabatic contraction ensued. The grey and black lines are predictions for the collapse of uniform spheres corresponding to  $2$  and  $3\sigma$  fluctuations, and are also shown before and after adiabatic contraction (AC). See text for details on the cooling curve; the dashed line corresponds to zero metallicity, the solid line to solar.

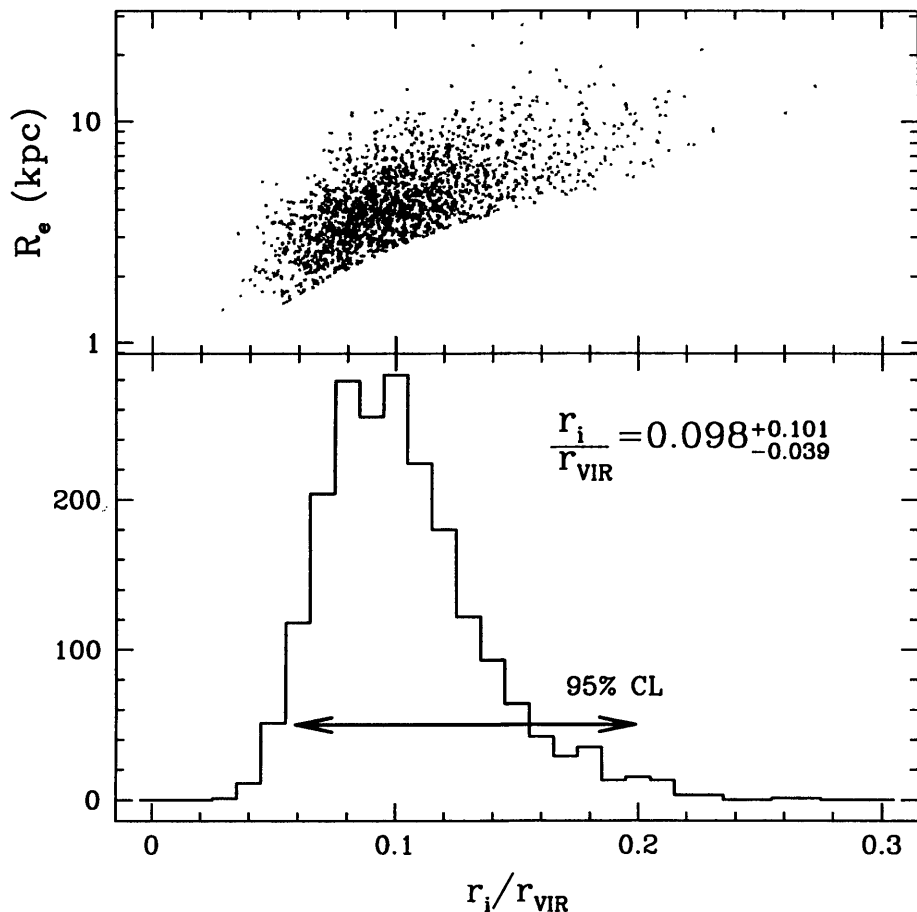


Figure 7.10: Comparison of the virial radius  $r_{\text{vir}}$  and the initial radius used in the adiabatic contraction procedure. For each galaxy  $r_i$  is chosen such that the mass within  $r_i$  before contraction corresponds to the dynamical mass within  $R_e$  after contraction. The top panel shows the correlation with the effective radius,  $R_e$ . In larger galaxies, more of the halo is contracted into  $R_e$ .

where  $\rho$  is the total density of both baryonic and dark matter, and the cooling timescale is

$$t_{\text{cool}} = \frac{3k_B T}{n\Lambda_{\text{net}}} \quad (7.29)$$

where  $n$  is the number density of nuclei and  $\Lambda_{\text{net}}$  is the net cooling rate for solar (or zero) metallicity taken from Sutherland and Dopita (1993). As expected, after contraction the galaxies lie in the region of the plot where  $t_{\text{cool}} < t_{\text{dyn}}$ . Although the approach is simplistic, assuming as it does that galaxies are uniform spheres rather than using radial profiles, it is intriguing that 2-sigma fluctuations for massive galaxies lie on the cooling curve for zero metallicity systems, and that adiabatic contraction promotes the cooling of these systems. This result may be followed up with simulation results.

## 7.9 Conclusions

The sample of early-type galaxies selected by Bernardi *et al.* (2003a) from the Sloan Digital Sky Survey has been used to investigate the distributions of baryonic and dark matter within these systems. For the work presented in this chapter, the sample was further restricted to be volume-limited, containing only massive galaxies at  $z < 0.1$ . Using photometry from Sloan data release 4 and the synthetic stellar populations of Bruzual and Charlot (2003) the mass in stars was calculated for each system.

The well-known Faber-Jackson relation between luminosity and observed velocity dispersion was recovered, and a tight correlation between stellar mass and velocity dispersion - which could be thought of as the ‘baryonic Faber-Jackson relation’ - was found. A slope of  $M_{\text{star}} (< R_e) \propto \sigma^{2.33 \pm 0.18}$  (in appropriate units) was found, and is less steep than that found in previous work (Thomas *et al.*, 2005).

In addition to determining the stellar mass, it is possible to determine a dynamical mass via knowledge of the velocity dispersion and the radius of the system. A comparison of the two estimates of mass reveals that dark matter is underabundant in the centre of such galaxies when compared to the cosmological baryon fraction. However, the results are in good agreement with observers who have claimed that the inner regions of massive ellipticals are baryon dominated.

In order to examine whether this large data set is sufficient to discriminate between galaxy formation via monolithic collapse and via the merging of small dark matter haloes,

the data were compared to a simple model of spherical collapse. It was necessary to assume that the total mass of the systems is proportional with the mass within the baryon-rich core (within  $R_e$ ), but given such an assumption  $\alpha = 20$  (where  $\alpha = M_{\text{tot}}/M_{\text{dyn}} (< R_e)$ ), the data were found to be consistent with simple monolithic collapse of 3-sigma perturbations, assuming  $\Lambda$ CDM cosmology.

Interestingly, this choice of  $\alpha$  also produces a value for the fraction of the mass which lies in the form of cooled baryons which is consistent with other work. A choice of 20 seems large, but corresponds to the stellar mass contributing half of the cosmological baryon fraction. Given the other possible reservoirs of baryons in these systems, this is a reasonable result.

Having motivated the choice of  $\alpha$ , the adiabatic contraction method was used to calculate the response of the dark matter to the presence of the observed baryons. Assuming that the dark matter has an initial profile of the well-known NFW form, the resulting distribution of initial concentration is shown in figure 7.8. The mean concentration is lower than that found in dissipation-less N-body simulations.

In summary, the B03 sample of early-type galaxies is a powerful resource for studying the distribution of matter within these objects. However, despite this excellent data set, it is not possible to rule out spherical collapse as a mode of formation for massive ellipticals. The central regions of the galaxies, which are baryon-dominated, must represent only a small fraction of the total mass of the system.

## CHAPTER 8

---

### Summary and Future work

The conclusions of the last chapter show the importance of baryonic matter, even in large systems such as the elliptical galaxies considered there. The work also illustrated that any conclusions drawn as to the structure and evolution of such a system depend on being able to extrapolate from observations of the light received from such a system to the distribution of the mass. The light, of course, comes from stars, which serves as a reminder that the understanding of the formation of these stars is fundamental even to apparently far-removed subjects.

This understanding is naturally furthest developed for the formation of stars within the Milky Way, where observational evidence is richest. The interpretation of these data requires the development of sophisticated models of the physical and chemical evolution of such regions, and chapter 2 investigates the effectiveness of these models in constraining one particular fundamental parameter, the ionization rate due to cosmic rays. We showed that the results obtained from molecular observations are sensitive not only to the true ionization rate, but also to the dynamical state of the core. This reflects a more general theme in the work presented in this thesis, in that it is essential to model the chemical network applicable to any particular situation rather than simply extrapolating from models which assume equilibrium. That said, the estimators used to determine the cosmic ray ionization rate are shown to be accurate once equilibrium is achieved. In chapter 3, I investigate another common assumption made in astrochemical modelling. Specifically, via observations made with the JCMT we attempt to show that the process of converting atomic to molecular hydrogen is incomplete in one particular pre-stellar core, L134a. The

---

low abundances of the molecular species observed confirm the hypothesis that the core is indeed young, and tentative evidence in support of a non-equilibrium H:H<sub>2</sub> ratio is found. Here too, therefore, it is shown to be necessary to understand (or to be able to constrain) the evolutionary state of a pre-stellar core before models may be successfully applied. In chapter 4, we investigate the effect on the chemical signatures of star formation of an accelerated collapse, faster than freefall. This provides an explanation for existing observations which indicate anomalous behaviour of CS and N<sub>2</sub>H<sup>+</sup>, and we are able to predict the behaviour of other species.

With the recent rapid increase in observational capabilities, it has become possible to observe many molecular species in systems beyond the Milky Way. Carbon monoxide, for example, has been detected in the most distant systems known. The richest extragalactic chemistries, however, belong to starburst galaxies such as NGC253 and M82, the latter of which is the subject of chapter 5. Sulfur bearing species were observed toward the nuclear region of this galaxy and, along with observations of other species drawn from the literature, compared with hot core models. We find that models of the hot core stage of massive star formation are able to account for the observed abundances of molecules such as methanol (CH<sub>3</sub>OH) which cannot be explained by the previously applied PDR models. These models assume that solar atomic abundance ratios are appropriate, but reducing the nitrogen abundance also allows us to fit the ammonia (NH<sub>3</sub>) abundance. This illustrates the possibility that observations of molecules in regions which are currently forming stars may be able to constrain the nucleosynthetic history of these systems.

Hot cores are also the basis of the model which, in chapter 6, is applied to the distant universe. In these models, gas enriched only by the ejecta of the supernovæ of the first generation of stars is used, and the resulting unusual chemical signature of star formation is investigated. We find that significant abundances of several molecular species (in addition to the aforementioned CO) should be detected in distant systems, but that the best tracers of star forming activity at these high redshifts are not necessarily the same as in the low-redshift Universe. This point is well made by the explanation of deviations from the established relation between molecular and infra-red luminosities (both of which are believed to be proportional to the star formation rate) of systems at redshifts of  $z \sim 2$  by a reduced nitrogen abundance. This in turn suggests an inefficient mixing of the products of nucleosynthesis, which leads to the formation of stars from primordial, or near-primordial material, much later than would otherwise be possible.

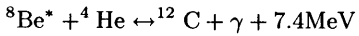
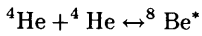
The common thread running through this work is the attempt to use simple models to understand the vast wealth of observational data now available to astronomers. Without the careful application of these models, and an understanding of the relevant assumptions (whether they apply to the chemical composition or the dynamical state of the systems under study) few conclusions can be drawn. On the other hand, it is clear that observational techniques developed for and tested on the Milky Way can have application far beyond our own Galaxy.

## 8.1 Future Work

Having established in chapters 5 and 6 that existing astrochemical models based on those of Viti *et al.* (2004b) can provide insight into systems beyond our own galaxy, it is appropriate to look at how the model can be employed beyond the work presented in this thesis. Potential extention of the work included in each individual chapter are discussed in the conclusions to each section, but one can consider a general program of extention of astrochemical models. Back in the very early Universe, the type of modelling considered here could usefully contribute to the debate as to the nature of the first (population III) stars. As noted before, simulations (Abel *et al.*, 2002) suggest that their mass was in excess of  $100M_{\odot}$ , whereas observations of low metallicity stars in the Milky Way, such as those of Frebel *et al.* (2005) can be accounted for by the yields from a smaller (approximately  $25M_{\odot}$ ) first generation of stars. An obvious extention of the high redshift models, therefore, would be to consider gas enriched by the supernovæ of such relatively small zero metallicity stars. Another way of resolving the discrepancies might be to expand the model beyond a simplistic dichotomy of population III and ‘normal stars’. For example, recent models of extremely low metallicity stars which include the effect of rotation for the first time (Meynet *et al.*, 2006), predict enhanced abundances for carbon, oxygen and crucially nitrogen compared to non-rotating models. The inclusion of rotation is particularly important as stars with extremely low metallicities experience a much stronger internal mixing than their solar metallicity counterparts. This leads to the efficient mixing of the products of the  $3\text{-}\alpha$  reaction<sup>1</sup> with the hydrogen burning shell, and hence to a greater en-

---

<sup>1</sup>The triple- $\alpha$  process is the predominant form of helium burning in old stars, and takes the form:



hancement in heavy metals of the stellar surface during the dredge-up phase, and finally to a large mass loss through the action of the stellar winds. These winds are particularly rich in nitrogen, the presence of which we have already seen has dramatic effects on the chemistry of star forming regions. By using these abundances in the chemical code, therefore, it may be possible to place the first constraints on the importance of an intermediate generation of stars in providing a source of metallicity for later generations, for example by examining the predicted abundance ratio of  $\text{HCO}^+$  to HCN.

These are relatively minor changes to the code, but the scope of future high redshift astrochemistry is much wider. For example, it should be possible to produce a more sophisticated chemical model than that used by Abel *et al.* to model the formation of the first stars. Their model obviously includes a treatment of both the dynamics and the chemistry, and this restricts the size of the chemical network which can be used. In the early Universe, when the only atoms available are the products of big bang nucleosynthesis, the restricted network of approximately 20 reactions is usually sufficient. However, there have been suggestions that molecules not included in this framework may have important roles to play; for example, Kamaya and Silk (2003) suggested that HD and LiH may, in the right conditions, contribute significantly to the cooling rate of primordial gas. Given the evolution of density and temperature found by the full simulation, a one-zone chemical model similar to those described in this work could then be used to estimate molecular abundances. The validity of reduced chemical networks used for the first stars could then be estimated.

The work contained within this thesis (with the sole exception of the modelling of M82 in chapter 5) restricts itself to one of two extremes; either solar metallicity or the Universe as it was shortly after the epoch of the first stars. There exists a long tradition of ‘chemical evolution’ models, which predict the abundance with redshift of any atomic species based on an assumed star formation history. The input to such a model are similar to that used in chapter 7 to study massive elliptical galaxies; a star formation history (usually defined via an exponential function) and an initial mass function for the stars which are produced. A suite of stellar evolution models (such as those by Bruzual and Charlot (2003)) are then used to predict the contribution of the stars to the enrichment of the gas. These models are ideally suited to working alongside an astrochemical code, in order to produce a molecular evolution history for any particular source, and to predict which molecules it may be profitable to search for at any given redshift. The atomic species which best

constrain the chemical evolution models are typically metals such as iron, whereas as we have seen the astrochemical models are sensitive to such parameters as the nitrogen or sulphur abundances. In systems where both molecular and atomic abundances have been derived from observations, therefore, then the two methods can be used in tandem to derive the star formation rate, for example. This kind of approach would be of great use, for example, in investigating whether M82 really does have a reduced nitrogen abundance as suggested in section 5.4.

## 8.2 Observations

The models developed here only have value in so far as they can be compared with observations. Luckily, the opportunities for observations of molecular species, even in distant systems, are legion. In addition to the JCMT, which was used for the observations presented in chapters 3 and 5 and is described there, in millimeter wavelengths the Institut de Radioastronomie Millimétrique (IRAM) is invaluable. The IRAM facilities consist of a single dish with a 30m diameter (at the Pico Veleta Observatory in Spain, 2900m above sea level), and an interferometer combining six dishes each of 15m in diameter (at the Plateau de Bure in France). The large collecting area of the 30m telescope in particular makes it ideal for extragalactic chemistry in the frequency range accessible (from 80-276GHz), and we intend to use it to extend the range of species which have been identified toward M82.

The next few years will also see first light at the Atacama Large Millimetre/Submillimetre Array (ALMA). Situated over 5000 metres above sea level at the Llano de Chajnantor in the Atacama desert, the moveable array will ultimately consist of 64 12-metre dishes with the maximum baseline available larger than 12km. The high resolution afforded by such large baselines together with the massive collecting area will allow ALMA to make observations of ‘normal’ (Milky Way-like) galaxies at redshifts of 1-2 with the same detail that is possible in nearby galaxies presently. Instead of using local starburst galaxies as a stepping stone between Milky Way star formation and the early Universe, it will be possible to study LIRGs and ULIRGs - the most active star forming systems - in detail. Closer to home, the Magellenic Clouds will provide a detailed view of star formation in an environment with a very different background radiation field, dust content and metallicity. All of these possibilities suggest that the development of the kind of astrochemical model discussed above, capable of predicting molecular abundances at a range of redshifts and

environments, will be necessary.

What of the more distant Universe? At redshifts of greater than 4 transitions which, in the Milky Way, lie in the sub-mm region of the spectrum begin to be accessible with the Very Large Array, which has already been used to search for HCN in high-redshift star forming galaxies. Having argued in chapter 6 that HCN is not the most natural star formation tracer at these redshifts, I would suggest that it would be of interest to use the VLA to look for sulphur-bearing molecules such as SO or SO<sub>2</sub> in the early Universe. Detections of molecules such as these would confirm the presence of rapid star formation in these sources, and also provide valuable constraints for chemical evolution models. With the identification of a host of star forming galaxies at redshifts of  $z \sim 5$  (e.g. Bremer and Lehnert (2005)) there will be no shortage of targets for study, even at these extreme redshifts. With the advent of new facilities to add to those already available, wherever in the Universe we look, and whatever questions we would like to answer, the understanding of star formation which is provided by astrochemistry will undoubtedly prove to be invaluable.

## APPENDIX A

---

### Deriving column densities

Deriving column densities requires either knowledge of or assumptions to be made about the radiative transfer of material in the cloud. The equation of transfer in terms of the Einstein coefficients for spontaneous emission ( $A_{21}$ ), absorption ( $B_{12}$ ) and stimulated emission ( $B_{21}$ ) is, for the transition between upper (2) and lower (1) levels is

$$\frac{dI_\nu}{ds} = -\frac{h\nu_0}{c} (N_1 B_{12} - N_2 B_{21}) I_\nu \psi(\nu) + \frac{h\nu_0}{4\pi} N_2 A_{21} \psi(\nu) \quad (\text{A.1})$$

where  $N_1$  and  $N_2$  are the column densities of molecules in the lower and upper states respectively,  $I_\nu$  is the intensity of the radiation at frequency  $\nu$ ,  $\nu_0$  is the rest frequency of the transition and  $\psi(\nu)$  is a function which represents the line shape.

The opacity,  $\kappa_\nu$  and the emissivity,  $\epsilon_\nu$  are defined so that

$$dI_{\nu-} = -\kappa_\nu I_\nu ds \quad (\text{A.2})$$

$$dI_{\nu+} = \epsilon_\nu ds \quad (\text{A.3})$$

where  $s$  is the distance parameter increasing away from the observer. It is then clear from these definitions that

$$\frac{dI_\nu}{ds} = -\kappa_\nu I_\nu + \epsilon_\nu \quad (\text{A.4})$$

and, comparing this with equation A.1 gives the opacity in terms of the Einstein coefficients:

$$\kappa_\nu = \frac{h\nu_0}{c} (N_1 B_{12} - N_2 B_{21}) \psi(\nu). \quad (\text{A.5})$$

However, the Einstein coefficients  $B_{12}$  and  $B_{21}$  are not independent. In a system in which the number of photons emitted is equal to the number absorbed then if  $\bar{U}$  is the average energy density of the radiation field defined by

$$\bar{U} = \frac{4\pi\bar{I}}{c} \quad (\text{A.6})$$

then

$$N_2 A_{21} + N_2 B_{21} \bar{U} = N_1 B_{12} \bar{U} \quad (\text{A.7})$$

and so

$$\bar{U} = \frac{A_{21}}{\frac{N_1}{N_2} B_{12} - B_{21}}. \quad (\text{A.8})$$

If we now make the assumption of local thermal equilibrium<sup>1</sup> then the population of states  $N_2/N_1$  is given by the Boltzman distribution and  $\bar{U}$  is given by the Planck formula. Therefore, if  $g_i$  is the degeneracy of level  $i$ ,

$$\bar{U} = \frac{A_{21}}{\frac{g_1}{g_2} e^{\frac{h\nu_0}{kT}} B_{12} - B_{21}} = \frac{8\pi h\nu_0^3}{c^3} \frac{1}{e^{\frac{h\nu}{kT}} - 1} \quad (\text{A.9})$$

and

$$A_{21} = \frac{8\pi h\nu_0^3}{c^3} B_{21}, \quad (\text{A.10})$$

$$g_1 B_{12} = g_2 B_{21}. \quad (\text{A.11})$$

Hence we can write the opacity (from equation A.5 independently of all but one Einstein coefficient:

---

<sup>1</sup>formal definition

$$\kappa_\nu = \frac{h\nu_0}{c} B_{12} N_1 \left( 1 - \frac{g_1}{g_2} \frac{N_2}{N_1} \right) \psi(\nu) \quad (\text{A.12})$$

where the factor in brackets is necessary because stimulated emission has been included in the analysis.

Similarly the emissivity in terms of an Einstein coefficient is

$$\epsilon_\nu = \frac{h\nu_0}{4\pi} N_2 A_{21} \psi(\nu) \quad (\text{A.13})$$

and the ratio of opacity to emissivity is independent of the Einstein coefficients:

$$\frac{\epsilon_\nu}{\kappa_\nu} = \frac{2h\nu_0^3}{c^2} \frac{1}{\frac{g_2}{g_1} \frac{N_1}{N_2} - 1}. \quad (\text{A.14})$$

In LTE  $dI_\nu/ds = 0$ , and so

$$\frac{N_2}{N_1} = \frac{g_2}{g_1} e^{-\frac{h\nu_0}{kT}} \quad (\text{A.15})$$

and

$$\kappa_\nu = \frac{c^2}{8\pi v_0^2} \frac{1}{g_1} \frac{g_2}{g_1} N_1 A_{21} \left[ 1 - e^{-\frac{h\nu_0}{kT}} \right] \psi(\nu). \quad (\text{A.16})$$

From this expression one may obtain a general relation between line optical depth, column density in a level, and excitation temperature  $T_{ex}$ .

$$N_i = 93.5 \frac{g_1 \nu^3}{g_2 A_{21}} \frac{1}{1 - e^{-\frac{-4.80 \times 10^{-2} \nu}{T_{ex}}}} \int \tau dv. \quad (\text{A.17})$$

For an optically thin line, the integral of the optical depth is equal to the integrated line intensity which can be determined from observations.

The usual quantity of interest is the total column density, derived from the sum over all energy levels. This can be extremely complicated as it depends on the population of each and every state. However, for a simple molecule such as CO in LTE it is possible to solve the problem simply. For a level  $J$ , the degeneracy in CO is given by  $2J+1$ . The fraction of the total population in a particular state is then given by

$$\frac{n(J)}{n(\text{total})} = \frac{(2J+1)}{Z} e^{-\frac{\hbar B_e J(J+1)}{kT}} \quad (\text{A.18})$$

where  $B_e$  is the rotation constant and  $Z$  is the partition function:

$$Z = \sum_{J=0}^{\infty} (2J+1) e^{-\frac{\hbar B_e J(J+1)}{kT}}. \quad (\text{A.19})$$

# Bibliography

Abel, T., Bryan, G. L. and Norman, M. L., 2000, *ApJ*, **540**, 39

Abel, T., Bryan, G. L. and Norman, M. L., 2002, *Science*, **295**, 93

Adams, W. S., 1941, *PASP*, **53**, 73

Adams, W. S., 1949, *ApJ*, **109**, 354

Adelman-McCarthy, J. K., Agüeros, M. A., Allam, S. S., Anderson, K. S. J., Anderson, S. F., Annis, J., Bahcall, N. A., Baldry, I. K., Barentine, J. C., Berlind, A., Bernardi, M., Blanton, M. R., Boroski, W. N., Brewington, H. J., Brinchmann, J., Brinkmann, J., Brunner, R. J., Budavári, T., Carey, L. N., Carr, M. A., Castander, F. J., Connolly, A. J., Csabai, I., Czarapata, P. C., Dalcanton, J. J., Doi, M., Dong, F., Eisenstein, D. J., Evans, M. L., Fan, X., Finkbeiner, D. P., Friedman, S. D., Frieman, J. A., Fukugita, M., Gillespie, B., Glazebrook, K., Gray, J., Grebel, E. K., Gunn, J. E., Gurbani, V. K., de Haas, E., Hall, P. B., Harris, F. H., Harvanek, M., Hawley, S. L., Hayes, J., Hendry, J. S., Hennessy, G. S., Hindsley, R. B., Hirata, C. M., Hogan, C. J., Hogg, D. W., Holmgren, D. J., Holtzman, J. A., Ichikawa, S.-i., Ivezić, Ž., Jester, S., Johnston, D. E., Jorgensen, A. M., Jurić, M., Kent, S. M., Kleinman, S. J., Knapp, G. R., Kniazev, A. Y., Kron, R. G., Krzesinski, J., Kuropatkin, N., Lamb, D. Q., Lampeitl, H., Lee, B. C., Leger, R. F., Lin, H., Long, D. C., Loveday, J., Lupton, R. H., Margon, B., Martínez-Delgado, D., Mandelbaum, R., Matsubara, T., McGehee, P. M., McKay, T. A., Meiksin, A., Munn, J. A., Nakajima, R., Nash, T., Neilson, E. H., Newberg, H. J., Newman, P. R., Nichol, R. C., Nicinski, T., Nieto-Santisteban, M., Nitta, A., O'Mullane, W., Okamura, S., Owen, R., Padmanabhan, N., Pauls, G., Peoples, J. J., Pier, J. R., Pope, A. C., Pourbaix, D., Quinn, T. R., Richards, G. T., Richmond, M. W., Rockosi, C. M., Schlegel, D. J., Schneider, D. P., Schroeder, J., Scranton, R., Seljak, U., Sheldon, E., Shimasaku, K., Smith, J. A., Smolčić, V., Snedden, S. A., Stoughton, C., Strauss, M. A.,

- SubbaRao, M., Szalay, A. S., Szapudi, I., Szkody, P., Tegmark, M., Thakar, A. R., Tucker, D. L., Uomoto, A., Vanden Berk, D. E., Vandenberg, J., Vogeley, M. S., Voges, W., Vogt, N. P., Walkowicz, L. M., Weinberg, D. H., West, A. A., White, S. D. M., Xu, Y., Yanny, B., Yocom, D. R., York, D. G., Zehavi, I., Zibetti, S. and Zucker, D. B., 2006, *ApJS*, **162**, 38
- Ahmad, Q. R., Allen, R. C., Andersen, T. C., D. Anglin, J., Barton, J. C., Beier, E. W., Bercovitch, M., Bigu, J., Biller, S. D., Black, R. A., Blevis, I., Boardman, R. J., Boger, J., Bonvin, E., Boulay, M. G., Bowler, M. G., Bowles, T. J., Brice, S. J., Browne, M. C., Bullard, T. V., Bühl, G., Cameron, J., Chan, Y. D., Chen, H. H., Chen, M., Chen, X. and Cleveland, B. T., 2002, *Phys. Rev. Lett.*, **89**(1), 011301
- Aikawa, Y., Ohashi, N. and Herbst, E., 2003a, *ApJ*, **593**, 906
- Aikawa, Y., Ohashi, N. and Herbst, E., 2003b, *ApJ*, **593**, 906
- Aikawa, Y., Ohashi, N., Inutsuka, S.-i., Herbst, E. and Takakuwa, S., 2001, *ApJ*, **552**, 639
- Alcock, C., Allsman, R. A., Alves, D. R., Axelrod, T. S., Becker, A. C., Bennett, D. P., Cook, K. H., Dalal, N., Drake, A. J., Freeman, K. C., Geha, M., Griest, K., Lehner, M. J., Marshall, S. L., Minniti, D., Nelson, C. A., Peterson, B. A., Popowski, P., Pratt, M. R., Quinn, P. J., Stubbs, C. W., Sutherland, W., Tomaney, A. B., Vandehei, T. and Welch, D., 2000, *ApJ*, **542**, 281
- Allamandola, L. J., Sandford, S. A., Tielens, A. G. G. M. and Herbst, T. M., 1992, *ApJ*, **399**, 134
- Allamandola, L. J., Tielens, A. G. G. M. and Barker, J. R., 1985, *ApJL*, **290**, L25
- Alves, J. F., Lada, C. J. and Lada, E. A., 2001, *Nature*, **409**, 159
- Andre, P., Ward-Thompson, D. and Barsony, M., 1993, *ApJ*, **406**, 122
- Andre, P., Ward-Thompson, D. and Barsony, M., 2000, *Protostars and Planets IV*, 59
- Bacmann, A., Lefloch, B., Ceccarelli, C., Steinacker, J., Castets, A. and Loinard, L., 2003, *ApJL*, **585**, L55
- Baldry, I. K., Glazebrook, K., Baugh, C. M., Bland-Hawthorn, J., Bridges, T., Cannon, R., Cole, S., Colless, M., Collins, C., Couch, W., Dalton, G., De Propris, R., Driver,

- S. P., Efstathiou, G., Ellis, R. S., Frenk, C. S., Hawkins, E., Jackson, C., Lahav, O., Lewis, I., Lumsden, S., Maddox, S., Madgwick, D. S., Norberg, P., Peacock, J. A., Peterson, B. A., Sutherland, W. and Taylor, K., 2002, *ApJ*, **569**, 582
- Ballesteros-Paredes, J., Vázquez-Semadeni, E. and Scalo, J., 1999, *ApJ*, **515**, 286
- Balsara, D., Ward-Thompson, D. and Crutcher, R. M., 2001, *MNRAS*, **327**, 715
- Barkana, R. and Loeb, A., 2001, *PhR*, **349**, 125
- Barkat, Z., Rakavy, G. and Sack, N., 1967, *PRL*, **18**, 379
- Barnes, J. and White, S. D. M., 1984, *MNRAS*, **211**, 753
- Barnes, J. E. and Hernquist, L., 1996, *ApJ*, **471**, 115
- Bates, D. R. and Spitzer, L. J., 1951, *ApJ*, **113**, 441
- Becker, R. H., Fan, X., White, R. L., Strauss, M. A., Narayanan, V. K., Lupton, R. H., Gunn, J. E., Annis, J., Bahcall, N. A., Brinkmann, J., Connolly, A. J., Csabai, I., Czarapata, P. C., Doi, M., Heckman, T. M., Hennessy, G. S., Ivezić, Ž., Knapp, G. R., Lamb, D. Q., McKay, T. A., Munn, J. A., Nash, T., Nichol, R., Pier, J. R., Richards, G. T., Schneider, D. P., Stoughton, C., Szalay, A. S., Thakar, A. R. and York, D. G., 2001, *AJ*, **122**, 2850
- Beichman, C. A., Myers, P. C., Emerson, J. P., Harris, S., Mathieu, R., Benson, P. J. and Jennings, R. E., 1986, *ApJ*, **307**, 337
- Bell, A. R., 1978, *MNRAS*, **182**, 147
- Bell, E. F., 2002, *ApJ*, **577**, 150
- Benson, P. J. and Myers, P. C., 1989, *ApJS*, **71**, 89
- Bergin, E. A., Ciardi, D. R., Lada, C. J., Alves, J. and Lada, E. A., 2001, *ApJ*, **557**, 209
- Bergin, E. A. and Langer, W. D., 1997, *ApJ*, **486**, 316
- Bergin, E. A., Plume, R., Williams, J. P. and Myers, P. C., 1999, *ApJ*, **512**, 724
- Berlind, A. A., Quillen, A. C., Pogge, R. W. and Sellgren, K., 1997, *AJ*, **114**, 107

- Bernardi, M., Sheth, R. K., Annis, J., Burles, S., Eisenstein, D. J., Finkbeiner, D. P., Hogg, D. W., Lupton, R. H., Schlegel, D. J., SubbaRao, M., Bahcall, N. A., Blakeslee, J. P., Brinkmann, J., Castander, F. J., Connolly, A. J., Csabai, I., Doi, M., Fukugita, M., Frieman, J., Heckman, T., Hennessy, G. S., Ivezić, Ž., Knapp, G. R., Lamb, D. Q., McKay, T., Munn, J. A., Nichol, R., Okamura, S., Schneider, D. P., Thakar, A. R. and York, D. G., 2003a, *AJ*, **125**, 1817
- Bernardi, M., Sheth, R. K., Annis, J., Burles, S., Finkbeiner, D. P., Lupton, R. H., Schlegel, D. J., SubbaRao, M., Bahcall, N. A., Blakeslee, J. P., Brinkmann, J., Castander, F. J., Connolly, A. J., Csabai, I., Doi, M., Fukugita, M., Frieman, J., Heckman, T., Hennessy, G. S., Ivezić, Ž., Knapp, G. R., Lamb, D. Q., McKay, T., Munn, J. A., Nichol, R., Okamura, S., Schneider, D. P., Thakar, A. R. and York, D. G., 2003b, *AJ*, **125**, 1882
- Bertoldi, F., Cox, P., Neri, R., Carilli, C. L., Walter, F., Omont, A., Beelen, A., Henkel, C., Fan, X., Strauss, M. A. and Menten, K. M., 2003, *A&A*, **409**, L47
- Bessel, F. W., 1844, *MNRAS*, **6**, 136
- Binney, J. and Tremaine, S., 1987, *Galactic Dynamics* (Princeton University Press, Princeton)
- Bisschop, S. E., Fraser, H. J., Öberg, K. I., van Dishoeck, E. F. and Schlemmer, S., 2006, *A&A*, **449**, 1297
- Black, J. H., 1987, in D. J. Hollenbach and H. A. Thronson, Jr. (eds.), *ASSL Vol. 134: Interstellar Processes*, pp. 731–744
- Blain, A. W., Smail, I., Ivison, R. J., Kneib, J.-P. and Frayer, D. T., 2002, *PhR*, **369**, 111
- Blumenthal, G. R., Faber, S. M., Flores, R. and Primack, J. R., 1986, *ApJ*, **301**, 27
- Blumenthal, G. R., Faber, S. M., Primack, J. R. and Rees, M. J., 1984, *Nature*, **311**, 517
- Bond, J. R., Arnett, W. D. and Carr, B. J., 1984, *ApJ*, **280**, 825
- Bonnell, I. A., Bate, M. R., Clarke, C. J. and Pringle, J. E., 2001, *MNRAS*, **323**, 785
- Bonnell, I. A., Bate, M. R. and Zinnecker, H., 1998, *MNRAS*, **298**, 93
- Bonnor, W. B., 1956, *MNRAS*, **116**, 351

- Borch, A., Meisenheimer, K., Bell, E. F., Rix, H.-W., Wolf, C., Dye, S., Kleinheinrich, M., Kovacs, Z. and Wisotzki, L., 2006, *A&A*, **453**, 869
- Bottinelli, S., Ceccarelli, C., Neri, R., Williams, J. P., Caux, E., Cazaux, S., Lefloch, B., Maret, S. and Tielens, A. G. G. M., 2004, *ApJL*, **617**, L69
- Boulanger, F. and Perault, M., 1988, *ApJ*, **330**, 964
- Bourke, T. L., Hyland, A. R., Robinson, G., James, S. D. and Wright, C. M., 1995, *MNRAS*, **276**, 1067
- Bowey, J. E. and Adamson, A. J., 2002, *MNRAS*, **334**, 94
- Bremer, M. N. and Lehnert, M. D., 2005, in S. Hüttmeister, E. Manthey, D. Bomans and K. Weis (eds.), *AIP Conf. Proc. 783: The Evolution of Starbursts*, pp. 374–380
- Bromm, V., Coppi, P. S. and Larson, R. B., 1999, *ApJL*, **527**, L5
- Bromm, V., Kudritzki, R. P. and Loeb, A., 2001, *ApJ*, **552**, 464
- Brouillet, N., Baudry, A., Combes, F., Kaufman, M. and Bash, F., 1991, *A&A*, **242**, 35
- Bruzual, G. and Charlot, S., 2003, *MNRAS*, **344**, 1000
- Bryan, G. L. and Norman, M. L., 1998, *ApJ*, **495**, 80
- Bullock, J. S., Kolatt, T. S., Sigad, Y., Somerville, R. S., Kravtsov, A. V., Klypin, A. A., Primack, J. R. and Dekel, A., 2001, *MNRAS*, **321**, 559
- Bunker, A. J., Stanway, E. R., Ellis, R. S. and McMahon, R. G., 2004, *MNRAS*, **355**, 374
- Butler, R. P., Wright, J. T., Marcy, G. W., Fischer, D. A., Vogt, S. S., Tinney, C. G., Jones, H. R. A., Carter, B. D., Johnson, J. A., McCarthy, C. and Penny, A. J., 2006, *ApJ*, **646**, 505
- Butner, H. M., Lada, E. A. and Loren, R. B., 1995, *ApJ*, **448**, 207
- Calzetti, D., 2001, *New Astronomy Review*, **45**, 601
- Cardelli, J. A., Clayton, G. C. and Mathis, J. S., 1989, *ApJ*, **345**, 245
- Carilli, C. L., Kohno, K., Kawabe, R., Ohta, K., Henkel, C., Menten, K. M., Yun, M. S., Petric, A. and Tutui, Y., 2002, *AJ*, **123**, 1838

- Carilli, C. L., Solomon, P., Vanden Bout, P., Walter, F., Beelen, A., Cox, P., Bertoldi, F., Menten, K. M., Isaak, K. G., Chandler, C. J. and Omont, A., 2005, *ApJ*, **618**, 586
- Carroll, T. J. and Goldsmith, P. F., 1981, *ApJ*, **245**, 891
- Caselli, P., Benson, P. J., Myers, P. C. and Tafalla, M., 2002, *ApJ*, **572**, 238
- Caselli, P., Walmsley, C. M., Tafalla, M., Dore, L. and Myers, P. C., 1999, *ApJL*, **523**, L165
- Caselli, P., Walmsley, C. M., Terzieva, R. and Herbst, E., 1998, *ApJ*, **499**, 234
- Ceccarelli, C., Castets, A., Caux, E., Hollenbach, D., Loinard, L., Molinari, S. and Tielens, A. G. G. M., 2000, *A&A*, **355**, 1129
- Chabrier, G., 2003, *PASP*, **115**, 763
- Charnley, S. B., 1997, *ApJ*, **481**, 396
- Cheung, A. C., Rank, D. M., Townes, C. H., Thornton, D. D. and Welch, W. J., 1968, *Physical Review Letters*, **21**, 1701
- Cheung, A. C., Rank, D. M., Townes, C. H., Thornton, D. D. and Welch, W. J., 1969, *Nature*, **221**, 626
- Chieffi, A. and Limongi, M., 2002, *ApJ*, **577**, 281
- Chieffi, A. and Limongi, M., 2004, *ApJ*, **608**, 405
- Chieffi, A., Limongi, M. and Straniero, O., 1998, *ApJ*, **502**, 737
- Churchwell, E., 2002, *ARA&A*, **40**, 27
- Clerke, A. M., 1902, *A popular history of astronomy during the nineteenth century* (A. & C. Black)
- Colless, M., Dalton, G., Maddox, S., Sutherland, W., Norberg, P., Cole, S., Bland-Hawthorn, J., Bridges, T., Cannon, R., Collins, C., Couch, W., Cross, N., Deeley, K., De Propris, R., Driver, S. P., Efstathiou, G., Ellis, R. S., Frenk, C. S., Glazebrook, K., Jackson, C., Lahav, O., Lewis, I., Lumsden, S., Madgwick, D., Peacock, J. A., Peterson, B. A., Price, I., Seaborne, M. and Taylor, K., 2001, *MNRAS*, **328**, 1039

- Collings, M. P., Anderson, M. A., Chen, R., Dever, J. W., Viti, S., Williams, D. A. and McCoustra, M. R. S., 2004, *MNRAS*, **354**, 1133
- Collings, M. P., Dever, J. W., Fraser, H. J., McCoustra, M. R. S. and Williams, D. A., 2003, *ApJ*, **583**, 1058
- Collister, A. A. and Lahav, O., 2005, *MNRAS*, **361**, 415
- Combes, F., 1991, *ARAA*, **29**, 195
- Connolly, A. J., Szalay, A. S., Bershady, M. A., Kinney, A. L. and Calzetti, D., 1995, *AJ*, **110**, 1071
- Copi, C. J., Schramm, D. N. and Turner, M. S., 1995, *Science*, **267**, 192
- Cowie, L. L., Songaila, A. and Barger, A. J., 1999, *AJ*, **118**, 603
- Cowie, L. L., Songaila, A., Hu, E. M. and Cohen, J. G., 1996, *AJ*, **112**, 839
- Crapsi, A., Caselli, P., Walmsley, C. M., Tafalla, M., Lee, C. W., Bourke, T. L. and Myers, P. C., 2004, *A&A*, **420**, 957
- Crowther, P. A. and Conti, P. S., 2003, *MNRAS*, **343**, 143
- Dalgarno, A. and Lepp, S., 1984, *ApJL*, **287**, L47
- De Buizer, J. M., Osorio, M. and Calvet, N., 2005, *ApJ*, **635**, 452
- Dekel, A., Stoehr, F., Mamon, G. A., Cox, T. J., Novak, G. S. and Primack, J. R., 2005, *Nature*, **437**, 707
- Desert, F.-X., Jenniskens, P. and Dennefeld, M., 1995, *A&A*, **303**, 223
- Di Francesco, J., Hogerheijde, M. R., Welch, W. J. and Bergin, E. A., 2002, *AJ*, **124**, 2749
- Djorgovski, S. and Davis, M., 1987, *ApJ*, **313**, 59
- Doane, J. S. and Mathews, W. G., 1993, *ApJ*, **419**, 573
- Dopita, M. A., 1990, in H. A. Thronson, Jr. and J. M. Shull (eds.), *ASSL Vol. 161: The Interstellar Medium in Galaxies*, pp. 437–472
- Doty, S. D., Schöier, F. L. and van Dishoeck, E. F., 2004, *A&A*, **418**, 1021

- Draine, B. T., 2003, *ARAA*, **41**, 241
- Draine, B. T. and Li, A., 2001, *ApJ*, **551**, 807
- Dressler, A., Lynden-Bell, D., Burstein, D., Davies, R. L., Faber, S. M., Terlevich, R. and Wegner, G., 1987, *ApJ*, **313**, 42
- Ebert, R., 1955, *Zeitschrift fur Astrophysik*, **37**, 217
- Efron, B. and Gong, G., 1983, *American Statistician*, **37**, 36
- Einasto, J., Kaasik, A. and Saar, E., 1974, *Nature*, **250**, 309
- Eisenstein, D. J. and Loeb, A., 1995, *ApJ*, **443**, 11
- Elmegreen, B. G., 1985, in D. C. Black and M. S. Matthews (eds.), *Protostars and Planets II*, pp. 33–58
- Elmegreen, B. G., 1999, *ApJ*, **527**, 266
- Elmegreen, B. G., 2000, *ApJ*, **530**, 277
- Elmegreen, B. G. and Lada, C. J., 1977, *ApJ*, **214**, 725
- Emsellem, E., Cappellari, M., Peletier, R. F., McDermid, R. M., Bacon, R., Bureau, M., Copin, Y., Davies, R. L., Krajnović, D., Kuntschner, H., Miller, B. W. and de Zeeuw, P. T., 2004, *MNRAS*, **352**, 721
- Engelbracht, C. W., Rieke, M. J., Rieke, G. H., Kelly, D. M. and Achtermann, J. M., 1998, *ApJ*, **505**, 639
- Evans, N. J., 1999, *ARAA*, **37**, 311
- Evans, N. J., Rawlings, J. M. C., Shirley, Y. L. and Mundy, L. G., 2001, *ApJ*, **557**, 193
- Faber, S. M., Dressler, A., Davies, R. L., Burstein, D. and Lynden-Bell, D., 1987, in S. M. Faber (ed.), *Nearly Normal Galaxies. From the Planck Time to the Present*, pp. 175–183
- Faber, S. M. and Jackson, R. E., 1976, *ApJ*, **204**, 668
- Falle, S. A. E. G. and Hartquist, T. W., 2002, *MNRAS*, **329**, 195
- Federman, S. R., Weber, J. and Lambert, D. L., 1996, *ApJ*, **463**, 181

- Ferreras, I., Lisker, T., Carollo, C. M., Lilly, S. J. and Mobasher, B., 2005a, *ApJ*, **635**, 243
- Ferreras, I., Saha, P. and Williams, L. L. R., 2005b, *ApJL*, **623**, L5
- Ferreras, I. and Silk, J., 2000a, *ApJL*, **541**, L37
- Ferreras, I. and Silk, J., 2000b, *MNRAS*, **316**, 786
- Field, G. B., Goldsmith, D. W. and Habing, H. J., 1969, *ApJL*, **155**, L149+
- Finkbeiner, D. P., Padmanabhan, N., Schlegel, D. J., Carr, M. A., Gunn, J. E., Rockosi, C. M., Sekiguchi, M., Lupton, R. H., Knapp, G. R., Ivezić, Ž., Blanton, M. R., Hogg, D. W., Adelman-McCarthy, J. K., Annis, J., Hayes, J., Kinney, E., Long, D. C., Seljak, U., Strauss, M. A., Yanny, B., Agüeros, M. A., Allam, S. S., Anderson, S. F., Bahcall, N. A., Baldry, I. K., Bernardi, M., Boroski, W. N., Briggs, J. W., Brinkmann, J., Brunner, R. J., Budavári, T., Castander, F. J., Covey, K. R., Csabai, I., Doi, M., Dong, F., Eisenstein, D. J., Fan, X., Friedman, S. D., Fukugita, M., Gillespie, B., Grebel, E. K., Gurbani, V. K., de Haas, E., Harris, F. H., Hendry, J. S., Hennessy, G. S., Jester, S., Johnston, D. E., Jorgensen, A. M., Jurić, M., Kent, S. M., Kniazev, A. Y., Krzesiński, J., Leger, R. F., Lin, H., Loveday, J., Mannery, E., Martínez-Delgado, D., McGehee, P. M., Meiksin, A., Munn, J. A., Neilsen, Jr., E. H., Newman, P. R., Nitta, A., Pauls, G., Quinn, T. R., Rafikov, R. R., Richards, G. T., Richmond, M. W., Schneider, D. P., Schroeder, J., Shimasaku, K., Siegmund, W. A., Smith, J. A., Snedden, S. A., Stebbins, A., Szalay, A. S., Szokoly, G. P., Tegmark, M., Tucker, D. L., Uomoto, A., Vanden Berk, D. E., Weinberg, D. H., West, A. A., Yasuda, N., Yocom, D. R., York, D. G. and Zehavi, I., 2004, *AJ*, **128**, 2577
- Fitzpatrick, E. L., 1999, *PASP*, **111**, 63
- Flower, D. R., Pineau des Forets, G. and Walmsley, C. M., 2004, *A&A*, **427**, 887
- Förster Schreiber, N. M., Genzel, R., Lutz, D. and Sternberg, A., 2003, *ApJ*, **599**, 193
- Franx, M. and Illingworth, G., 1990, *ApJL*, **359**, L41
- Fraser, H. J., Collings, M. P., McCoustra, M. R. S. and Williams, D. A., 2001, *MNRAS*, **327**, 1165

- Frebel, A., Aoki, W., Christlieb, N., Ando, H., Asplund, M., Barklem, P. S., Beers, T. C., Eriksson, K., Fechner, C., Fujimoto, M. Y., Honda, S., Kajino, T., Minezaki, T., Nomoto, K., Norris, J. E., Ryan, S. G., Takada-Hidai, M., Tsangarides, S. and Yoshii, Y., 2005, *Nature*, **434**, 871
- Freedman, W. L., Madore, B. F., Gibson, B. K., Ferrarese, L., Kelson, D. D., Sakai, S., Mould, J. R., Kennicutt, Jr., R. C., Ford, H. C., Graham, J. A., Huchra, J. P., Hughes, S. M. G., Illingworth, G. D., Macri, L. M. and Stetson, P. B., 2001, *ApJ*, **553**, 47
- Fryer, C. L., Woosley, S. E. and Heger, A., 2001, *ApJ*, **550**, 372
- Fuente, A., García-Burillo, S., Gerin, M., Rizzo, J. R., Usero, A., Teyssier, D., Roueff, E. and Le Bourlot, J., 2006, *ApJL*, **641**, L105
- Fuente, A., García-Burillo, S., Gerin, M., Teyssier, D., Usero, A., Rizzo, J. R. and de Vicente, P., 2005a, *ApJL*, **619**, L155
- Fuente, A., Rizzo, J. R., Caselli, P., Bachiller, R. and Henkel, C., 2005b, *A&A*, **433**, 535
- Fukugita, M., Hogan, C. J. and Peebles, P. J. E., 1998, *ApJ*, **503**, 518
- Gallagher, J. S. and Smith, L. J., 1999, *MNRAS*, **304**, 540
- Gao, Y. and Solomon, P. M., 2004, *ApJ*, **606**, 271
- García-Burillo, S., Graciá-Carpio, J., Guélin, M., Neri, R., Cox, P., Planesas, P., Solomon, P. M., Tacconi, L. J. and Vanden Bout, P. A., 2006, *ApJL*, **645**, L17
- García-Burillo, S., Martín-Pintado, J., Fuente, A., Usero, A. and Neri, R., 2002, *ApJL*, **575**, L55
- Garrod, R. T., Williams, D. A. and Rawlings, J. M. C., 2006a, *ApJ*, **638**, 827
- Garrod, R. T., Williams, D. A. and Rawlings, J. M. C., 2006b, *ApJ*, **638**, 827
- Geballe, T. R., McCall, B. J. and Oka, T., 2003, in C. L. Curry and M. Fich (eds.), *SFChem 2002: Chemistry as a Diagnostic of Star Formation, proceedings of a conference held August 21-23, 2002 at University of Waterloo, Waterloo, Ontario, Canada N2L 3G1. Edited by Charles L. Curry and Michel Fich. NRC Press, Ottawa, Canada, 2003, p. 46.*, pp. 46–+

- Geppert, W. D., Thomas, R., Semaniak, J., Ehlerding, A., Millar, T. J., Österdahl, F., af Ugglas, M., Djurić, N., Paál, A. and Larsson, M., 2004, *ApJ*, **609**, 459
- Gibb, E. L., Whittet, D. C. B., Schutte, W. A., Boogert, A. C. A., Chiar, J. E., Ehrenfreund, P., Gerakines, P. A., Keane, J. V., Tielens, A. G. G. M., van Dishoeck, E. F. and Kerkhof, O., 2000, *ApJ*, **536**, 347
- Glazebrook, K., Baldry, I. K., Blanton, M. R., Brinkmann, J., Connolly, A., Csabai, I., Fukugita, M., Ivezić, Ž., Loveday, J., Meiksin, A., Nichol, R., Peng, E., Schneider, D. P., SubbaRao, M., Tremonti, C. and York, D. G., 2003, *ApJ*, **587**, 55
- Gnedin, O. Y., Kravtsov, A. V., Klypin, A. A. and Nagai, D., 2004, *ApJ*, **616**, 16
- Goldreich, P. and Kwan, J., 1974, *ApJ*, **189**, 441
- Goldsmith, P. F. and Langer, W. D., 1978, *ApJ*, **222**, 881
- Goldsmith, P. F. and Li, D., 2005, *ApJ*, **622**, 938
- Goobar, A., Hannestad, S., Mörtsell, E. and Tu, H., 2006, *Journal of Cosmology and Astro-Particle Physics*, **6**, 19
- Gould, R. J. and Salpeter, E. E., 1963, *ApJ*, **138**, 393
- Greenberg, J., 1968, *Stars and Stellar Systems* (ed. B.M. Middlehurst & L.H. Aller, Chicago University Press)
- Grevesse, N. and Sauval, A. J., 1998, *Space Science Reviews*, **85**, 161
- Griffiths, R. E., Casertano, S., Im, M. and Ratnatunga, K. U., 1996, *MNRAS*, **282**, 1159
- Guelin, M., Langer, W. D., Snell, R. L. and Wootten, H. A., 1977, *ApJL*, **217**, L165
- Gunn, J. E. and Peterson, B. A., 1965, *ApJ*, **142**, 1633
- Guzman, R., Lucey, J. R. and Bower, R. G., 1993, *MNRAS*, **265**, 731
- Hannestad, S., Tu, H. and Wong, Y. Y., 2006, *Journal of Cosmology and Astro-Particle Physics*, **6**, 25
- Hartmann, L., Ballesteros-Paredes, J. and Bergin, E. A., 2001, *ApJ*, **562**, 852
- Hartquist, T. W., 1995, *Ap&SS*, **233**, 97

- Hartquist, T. W., Dalgarno, A. and Oppenheimer, M., 1980, *ApJ*, **236**, 182
- Hartquist, T. W. and Williams, D. A., 1995, *The Chemically Controlled Cosmos, Astronomical Molecules from the Big Bang to Exploding Stars* (The Chemically Controlled Cosmos, Astronomical Molecules from the Big Bang to Exploding Stars, ISBN 0521419832, Cambridge University Press, —c1995)
- Hasegawa, T. I. and Herbst, E., 1993, *MNRAS*, **261**, 83
- Hata, N., Steigman, G., Bludman, S. and Langacker, P., 1997, *PhR v.D*, **55**, 540
- Hatchell, J., Thompson, M. A., Millar, T. J. and MacDonald, G. H., 1998, *A&A*, **338**, 713
- Hatchell, J. and Viti, S., 2002, *A&A*, **381**, L33
- Heger, A., Fryer, C. L., Woosley, S. E., Langer, N. and Hartmann, D. H., 2003, *ApJ*, **591**, 288
- Heger, A. and Woosley, S. E., 2002, *ApJ*, **567**, 532
- Heger, M. L., 1918, *Lick Observatory Bulletin*, **10**, 146
- Henkel, C. and Bally, J., 1985, *A&A*, **150**, L25
- Herbst, E., 1995, *ARPC*, **46**, 27
- Herbst, E. and Klemperer, W., 1973, *ApJ*, **185**, 505
- Hernquist, L., 1990, *ApJ*, **356**, 359
- Hirota, T., Ikeda, M. and Yamamoto, S., 2003, *ApJ*, **594**, 859
- Hofner, P., Delgado, H., Whitney, B., Churchwell, E. and Linz, H., 2002, *ApJL*, **579**, L95
- Hopkins, P. F., Hernquist, L., Cox, T. J., Di Matteo, T., Robertson, B. and Springel, V., 2006, *ApJS*, **163**, 1
- Jansen, D. J., Spaans, M., Hogerheijde, M. R. and van Dishoeck, E. F., 1995, *A&A*, **303**, 541
- Jeans, J. H., 1928, *Astronomy and cosmogony* (Cambridge [Eng.] The University press, 1928.)

- Jimenez, R. and Haiman, Z., 2006, *Nature*, **440**, 501
- Jones, A. P., Tielens, A. G. G. M., Hollenbach, D. J. and McKee, C. F., 1994, *ApJ*, **433**, 797
- Jørgensen, J. K., Schöier, F. L. and van Dishoeck, E. F., 2005, *A&A*, **435**, 177
- Jura, M., 1974, *ApJ*, **191**, 375
- Kamaya, H. and Silk, J., 2003, *MNRAS*, **339**, 1256
- Kashlinsky, A., Arendt, R. G., Mather, J. and Moseley, S. H., 2005, *Nature*, **438**, 45
- Keel, W. C. and White, III, R. E., 2001a, *AJ*, **121**, 1442
- Keel, W. C. and White, III, R. E., 2001b, *AJ*, **122**, 1369
- Keeton, C. R., 2001, *ApJ*, **561**, 46
- Kennicutt, Jr., R. C., 1998, *ARA&A*, **36**, 189
- Kenyon, S. J., Hartmann, L. W., Strom, K. M. and Strom, S. E., 1990, *AJ*, **99**, 869
- Kerr, T. H., Hibbins, R. E., Fossey, S. J., Miles, J. R. and Sarre, P. J., 1998, *ApJ*, **495**, 941
- Kim, W.-T. and Ostriker, E. C., 2001, *ApJ*, **559**, 70
- Kirk, J. M., Ward-Thompson, D. and André, P., 2005, *MNRAS*, **360**, 1506
- Kitayama, T., Yoshida, N., Susa, H. and Umemura, M., 2004, *ApJ*, **613**, 631
- Klessen, R. S., Heitsch, F. and Mac Low, M.-M., 2000, *ApJ*, **535**, 887
- Klypin, A., Zhao, H. and Somerville, R. S., 2002, *ApJ*, **573**, 597
- Kohno, K., Matsushita, S., Vila-Vilaró, B., Okumura, S. K., Shibatsuka, T., Okiura, M., Ishizuki, S. and Kawabe, R., 2001, in J. H. Knapen, J. E. Beckman, I. Shlosman and T. J. Mahoney (eds.), *ASP Conf. Ser. 249: The Central Kiloparsec of Starbursts and AGN: The La Palma Connection*, pp. 672–+
- Kolmogorov, A., 1941, *Dokl. Akad. Nauk SSSR*, **30**

- Kovac, J. M., Leitch, E. M., Pryke, C., Carlstrom, J. E., Halverson, N. W. and Holzapfel, W. L., 2002, *Nature*, **420**, 772
- Kraus, C., Bonn, J., Bornschein, L., Flatt, B., Kovalik, A., Müller, B., Otten, E., Thümmler, T., Schall, J. and C., W., 2004, *European Physical Journal C*, **33**, s805
- Kravtsov, A. V., Berlind, A. A., Wechsler, R. H., Klypin, A. A., Gottlöber, S., Allgood, B. and Primack, J. R., 2004, *ApJ*, **609**, 35
- Kroupa, P., 2001, *MNRAS*, **322**, 231
- Krumholz, M. R., McKee, C. F. and Klein, R. I., 2005, *Nature*, **438**, 332
- Kurtz, S., Churchwell, E. and Wood, D. O. S., 1994, *ApJS*, **91**, 659
- Lada, C. J., 1987, in M. Peimbert and J. Jugaku (eds.), *IAU Symp. 115: Star Forming Regions*, pp. 1–17
- Lahav, O., Lilje, P. B., Primack, J. R. and Rees, M. J., 1991, *MNRAS*, **251**, 128
- Larson, R. B., 1992, *MNRAS*, **256**, 641
- Larson, R. B., 2001, in H. Zinnecker and R. Mathieu (eds.), *IAU Symposium*, pp. 93–+
- Le Bourlot, J., Pineau Des Forets, G., Roueff, E. and Flower, D. R., 1993, *A&A*, **267**, 233
- Le Petit, F., Roueff, E. and Herbst, E., 2004, *A&A*, **417**, 993
- Le Teuff, Y. H., Millar, T. J. and Markwick, A. J., 2000, *A&As*, **146**, 157
- Lee, C. W., Myers, P. C. and Plume, R., 2004, *ApJS*, **153**, 523
- Lee, H.-H., Bettens, R. P. A. and Herbst, E., 1996, *AAPS*, **119**, 111
- Lehnert, M. D. and Heckman, T. M., 1996, *ApJ*, **472**, 546
- Leisawitz, D., Bash, F. N. and Thaddeus, P., 1989, *ApJS*, **70**, 731
- Leitch, E. M., Kovac, J. M., Halverson, N. W., Carlstrom, J. E., Pryke, C. and Smith, M. W. E., 2005, *ApJ*, **624**, 10
- Lenc, E. and Tingay, S. J., 2006, *AJ*, **132**, 1333
- Lepp, S. and Dalgarno, A., 1996, *A&A*, **306**, L21

- Lepp, S., Dalgarno, A. and Sternberg, A., 1987, *ApJ*, **321**, 383
- Li, A. and Draine, B. T., 2001, *ApJ*, **554**, 778
- Li, D. and Goldsmith, P. F., 2003, *ApJ*, **585**, 823
- Lilly, S. J., Le Fevre, O., Hammer, F. and Crampton, D., 1996, *ApJL*, **460**, L1+
- Linsky, J. L., 2003, *Space Science Reviews*, **106**, 49
- Loeffler, M. J., Baratta, G. A., Palumbo, M. E., Strazzulla, G. and Baragiola, R. A., 2005, *A&A*, **435**, 587
- Loewenstein, M. and White, R. E., 1999, *ApJ*, **518**, 50
- Lumsden, S. L., Hoare, M. G., Oudmaijer, R. D. and Richards, D., 2002, *MNRAS*, **336**, 621
- Lutz, D., Feuchtgruber, H., Genzel, R., Kunze, D., Rigopoulou, D., Spoon, H. W. W., Wright, C. M., Egami, E., Katterloher, R., Sturm, E., Wieprecht, E., Sternberg, A., Moorwood, A. F. M. and de Graauw, T., 1996, *A&A*, **315**, L269
- Lynden-Bell, D., Faber, S. M., Burstein, D., Davies, R. L., Dressler, A., Terlevich, R. J. and Wegner, G., 1988, *ApJ*, **326**, 19
- Mac Low, M.-M. and Klessen, R. S., 2004, *Reviews of Modern Physics*, **76**, 125
- Madau, P., Ferguson, H. C., Dickinson, M. E., Giavalisco, M., Steidel, C. C. and Fruchter, A., 1996, *MNRAS*, **283**, 1388
- Magliocchetti, M., Salvaterra, R. and Ferrara, A., 2003, *MNRAS*, **342**, L25
- Mahoney, M. J., McCutcheon, W. H. and Shuter, W. L. H., 1976, *AJ*, **81**, 508
- Malhotra, S. and Rhoads, J. E., 2002, *ApJL*, **565**, L71
- Mamon, G. A. and Lokas, E. L., 2005, *MNRAS*, **363**, 705
- Mao, R. Q., Henkel, C., Schulz, A., Zielinsky, M., Mauersberger, R., Störzer, H., Wilson, T. L. and Gensheimer, P., 2000, *A&A*, **358**, 433
- Mao, X.-J. and Sun, X.-X., 2005, *Chinese Journal of Astronomy and Astrophysics*, **5**, 144

- Mardones, D., Myers, P. C., Tafalla, M., Wilner, D. J., Bachiller, R. and Garay, G., 1997, *ApJ*, **489**, 719
- Maret, S., Ceccarelli, C., Caux, E., Tielens, A. G. G. M., Jörgensen, J. K., van Dishoeck, E., Bacmann, A., Castets, A., Lefloch, B., Loinard, L., Parise, B. and Schöier, F. L., 2004, *A&A*, **416**, 577
- Martín, S., Martín-Pintado, J. and Mauersberger, R., 2006, *A&A*, **450**, L13
- Martín, S., Martín-Pintado, J., Mauersberger, R., Henkel, C. and García-Burillo, S., 2005, *ApJ*, **620**, 210
- Matsuda, Y., Yamada, T., Hayashino, T., Tamura, H., Yamauchi, R., Ajiki, M., Fujita, S. S., Murayama, T., Nagao, T., Ohta, K., Okamura, S., Ouchi, M., Shimasaku, K., Shioya, Y. and Taniguchi, Y., 2004, *AJ*, **128**, 569
- Matteucci, F. and Calura, F., 2005, *MNRAS*, **360**, 447
- Mauersberger, R., Henkel, C., Weiß, A., Peck, A. B. and Hagiwara, Y., 2003, *A&A*, **403**, 561
- McCall, B. J., Huneycutt, A. J., Saykally, R. J., Geballe, T. R., Djuric, N., Dunn, G. H., Semaniak, J., Novotny, O., Al-Khalili, A., Ehlerding, A., Hellberg, F., Kalhori, S., Neau, A., Thomas, R., Österdahl, F. and Larsson, M., 2003, *Nature*, **422**, 500
- McCrady, N., Gilbert, A. M. and Graham, J. R., 2003, *ApJ*, **596**, 240
- McKee, C. F., 1989, *ApJ*, **345**, 782
- McKee, C. F. and Tan, J. C., 2003, *ApJ*, **585**, 850
- McKellar, A., 1941, *PASP*, **53**, 233
- Meyer, D. M., Cardelli, J. A. and Sofia, U. J., 1997, *ApJL*, **490**, L103+
- Meyer, P., 1969, *ARAA*, **7**, 1
- Meynet, G., Ekström, S. and Maeder, A., 2006, *A&A*, **447**, 623
- Mezger, P. G., Chini, R., Kreysa, E., Wink, J. E. and Salter, C. J., 1988, *A&A*, **191**, 44
- Milgrom, M., 1983, *ApJ*, **270**, 365

- Millar, T. J., Bennett, A., Rawlings, J. M. C., Brown, P. D. and Charnley, S. B., 1991, *A&As*, **87**, 585
- Millar, T. J., Farquhar, P. R. A. and Willacy, K., 1997, *A&As*, **121**, 139
- Morata, O., Girart, J. M. and Estalella, R., 2003, *A&A*, **397**, 181
- Morgan, H. L. and Edmunds, M. G., 2003, *MNRAS*, **343**, 427
- Moseley, H., 1980, *ApJ*, **238**, 892
- Motte, F., André, P., Ward-Thompson, D. and Bontemps, S., 2001, *A&A*, **372**, L41
- Mouschovias, T. C., Tassis, K. and Kunz, M. W., 2006, *ApJ*, **646**, 1043
- Myers, P. C. and Benson, P. J., 1983, *ApJ*, **266**, 309
- Nakamura, O., Fukugita, M., Yasuda, N., Loveday, J., Brinkmann, J., Schneider, D. P., Shimasaku, K. and SubbaRao, M., 2003, *AJ*, **125**, 1682
- Narayanan, D., Groppi, C., Kulesa, C. and Walker, C., 2005, *ApJ*, **630**
- Navarro, J., Frenck, C. and White, S., 1997, *ApJ*, **490**, 493
- Neufeld, D. A. and Kaufman, M. J., 1993, *ApJ*, **418**, 263
- Neufeld, D. A., Lepp, S. and Melnick, G. J., 1995, *ApJS*, **100**, 132
- Ng, C. S. and Bhattacharjee, A., 1996, *ApJ*, **465**, 845
- Nguyen, Q.-R., Jackson, J. M., Henkel, C., Truong, B. and Mauersberger, R., 1992, *ApJ*, **399**, 521
- Noh, H.-R. and Scalo, J., 1990, *ApJ*, **352**, 605
- Norris, J. E., 1999, in B. K. Gibson, R. S. Axelrod and M. E. Putman (eds.), *ASP Conf. Ser. 165: The Third Stromlo Symposium: The Galactic Halo*, pp. 213–+
- Norris, J. E., Ryan, S. G. and Beers, T. C., 2001, *ApJ*, **561**, 1034
- Nummelin, A., Whittet, D. C. B., Gibb, E. L., Gerakines, P. A. and Chiar, J. E., 2001, *ApJ*, **558**, 185

- Öberg, K. I., van Broekhuizen, F., Fraser, H. J., Bisschop, S. E., van Dishoeck, E. F. and Schlemmer, S., 2005, *ApJL*, **621**, L33
- O'Connell, R. W. and Mangano, J. J., 1978, *ApJ*, **221**, 62
- Oka, T., Geballe, T. R., Goto, M., Usuda, T. and McCall, B. J., 2005, *ApJ*, **632**, 882
- Onishi, T., Mizuno, A., Kawamura, A., Ogawa, H. and Fukui, Y., 1996, *ApJ*, **465**, 815
- Oort, J. H., 1932, *Bulletin of the Astronomical Institutes of the Netherlands*, **6**, 249
- Origlia, L., Ranalli, P., Comastri, A. and Maiolino, R., 2004, *ApJ*, **606**, 862
- O'Shea, B. W., Abel, T., Whalen, D. and Norman, M. L., 2005, *ApJL*, **628**, L5
- Ostriker, J. P., 1993, *ARA&A*, **31**, 689
- Ostriker, J. P., Peebles, P. J. E. and Yahil, A., 1974, *ApJL*, **193**, L1
- Padman, R., 1990, *SPECX users manual* (University of Cambridge)
- Padmanabhan, N., Seljak, U., Strauss, M. A., Blanton, M. R., Kauffmann, G., Schlegel, D. J., Tremonti, C., Bahcall, N. A., Bernardi, M., Brinkmann, J., Fukugita, M. and Ivezić, Ž., 2004, *New Astronomy*, **9**, 329
- Page, L., Hinshaw, G., Komatsu, E., Nolta, M. R., Spergel, D. N., Bennett, C. L., Barnes, C., Bean, R., Dore', O., Halpern, M., Hill, R. S., Jarosik, N., Kogut, A., Limon, M., Meyer, S. S., Odegard, N., Peiris, H. V., Tucker, G. S., Verde, L., Weiland, J. L., Wollack, E. and Wright, E. L., 2006, *ArXiv Astrophysics e-prints*
- Paglione, T. A. D., Jackson, J. M. and Ishizuki, S., 1997, *ApJ*, **484**, 656
- Parise, B., Castets, A., Herbst, E., Caux, E., Ceccarelli, C., Mukhopadhyay, I. and Tielens, A. G. G. M., 2004, *A&A*, **416**, 159
- Peebles, P. J. E., 1980, *The large-scale structure of the universe* (Research supported by the National Science Foundation. Princeton, N.J., Princeton University Press, 1980. 435 p.)
- Peng, R., Langer, W. D., Velusamy, T., Kuiper, T. B. H. and Levin, S., 1998, *ApJ*, **497**, 842

- Pentericci, L., Rix, H.-W., Prada, F., Fan, X., Strauss, M. A., Schneider, D. P., Grebel, E. K., Harbeck, D., Brinkmann, J. and Narayanan, V. K., 2003, *A&A*, **410**, 75
- Penzias, A. A. and Wilson, R. W., 1965, *ApJ*, **142**, 419
- Pérez-González, P. G., Rieke, G. H., Egami, E., Alonso-Herrero, A., Dole, H., Papovich, C., Blaylock, M., Jones, J., Rieke, M., Rigby, J., Barmby, P., Fazio, G. G., Huang, J. and Martin, C., 2005, *ApJ*, **630**, 82
- Petuchowski, S. J. and Bennett, C. L., 1992, *ApJ*, **391**, 137
- Phillips, T. G. and Vastel, C., 2003, in C. L. Curry and M. Fich (eds.), *SFChem 2002: Chemistry as a Diagnostic of Star Formation, proceedings of a conference held August 21-23, 2002 at University of Waterloo, Waterloo, Ontario, Canada N2L 3G1. Edited by Charles L. Curry and Michel Fich. NRC Press, Ottawa, Canada, 2003, p. 3.*, pp. 3-+
- Piacentini, F., Ade, P. A. R., Bock, J. J., Bond, J. R., Borrill, J., Boscaleri, A., Cabella, P., Contaldi, C. R., Crill, B. P., de Bernardis, P., De Gasperis, G., de Oliveira-Costa, A., De Troia, G., di Stefano, G., Hivon, E., Jaffe, A. H., Kisner, T. S., Jones, W. C., Lange, A. E., Masi, S., Mauskopf, P. D., MacTavish, C. J., Melchiorri, A., Montroy, T. E., Natoli, P., Netterfield, C. B., Pascale, E., Pogosyan, D., Polenta, G., Prunet, S., Ricciardi, S., Romeo, G., Ruhl, J. E., Santini, P., Tegmark, M., Veneziani, M. and Vittorio, N., 2006, *ApJ*, **647**, 833
- Pickles, J. B. and Williams, D. A., 1981, *MNRAS*, **197**, 429
- Pirogov, L., Zinchenko, I., Caselli, P. and Johansson, L., 2006, *Astronomy and Astrophysics*
- Pirogov, L., Zinchenko, I., Caselli, P., Johansson, L. E. B. and Myers, P. C., 2003, *A&A*, **405**, 639
- Pitman, K. M., Clayton, G. C. and Gordon, K. D., 2000, *PASP*, **112**, 537
- Porter, D. H., Pouquet, A. and Woodward, P. R., 1992, *Physical Review Letters*, **68**, 3156
- Press, W. H., Teukolsky, S. A., Vetterling, W. T. and Flannery, B. P., 1992, *Numerical recipes in C. The art of scientific computing* (Cambridge: University Press, —c1992, 2nd ed.)

- Rawlings, J., 2003, *Ap&SS*, **285**, 777
- Rawlings, J. M. C., Hartquist, T. W., Menten, K. M. and Williams, D. A., 1992, *MNRAS*, **255**, 471
- Rawlings, J. M. C., Hartquist, T. W., Williams, D. A. and Falle, S. A. E. G., 2002, *A&A*, **391**, 681
- Rawlings, J. M. C. and Yates, J. A., 2001, *MNRAS*, **326**, 1423
- Redman, M. P., Keto, E. and Rawlings, J. M. C., 2005, in *Protostars and Planets V*, pp. 8558–+
- Redman, M. P., Keto, E., Rawlings, J. M. C. and Williams, D. A., 2004a, *MNRAS*, **352**, 1365
- Redman, M. P., Rawlings, J. M. C., Nutter, D. J., Ward-Thompson, D. and Williams, D. A., 2002, *MNRAS*, **337**, L17
- Redman, M. P., Rawlings, J. M. C., Yates, J. A. and Williams, D. A., 2004b, *MNRAS*, **352**, 243
- Rees, M. J., 1978, *Nature*, **275**, 35
- Renzini, A. and Voli, M., 1981, *A&A*, **94**, 175
- Requena-Torres, M. A., Martín-Pintado, J., Rodríguez-Franco, A., Martín, S., Rodríguez-Fernández, N. J. and de Vicente, P., 2006, *A&A*, **455**, 971
- Rieke, G. H., Loken, K., Rieke, M. J. and Tamblyn, P., 1993, *ApJ*, **412**, 99
- Roberts, H., 2005, in D. C. Lis, G. A. Blake and E. Herbst (eds.), *IAU Symposium*, pp. 27–36
- Roberts, H., Herbst, E. and Millar, T. J., 2003, *ApJL*, **591**, L41
- Rohlfs, K. and Wilson, T. L., 2004, *Tools of radio astronomy* (Tools of radio astronomy, 4th rev. and enl. ed., by K. Rohlfs and T.L. Wilson. Berlin: Springer, 2004)
- Romanowsky, A. J., Douglas, N. G., Arnaboldi, M., Kuijken, K., Merrifield, M. R., Napolitano, N. R., Capaccioli, M. and Freeman, K. C., 2003, *Science*, **301**, 1696

- Rosenthal, D., Bertoldi, F. and Drapatz, S., 2000, *A&A*, **356**, 705
- Roueff, E., Tiné, S., Coudert, L. H., Pineau des Forêts, G., Falgarone, E. and Gerin, M., 2000, *A&A*, **354**, L63
- Ruffle, D. P., Hartquist, T. W., Rawlings, J. M. C. and Williams, D. A., 1998, *A&A*, **334**, 678
- Ryden, B. S. and Gunn, J. E., 1987, *ApJ*, **318**, 15
- Sadoulet, B., 1999, *Rev. Mod. Phys.*, **71**(2), S197
- Salpeter, E. E., 1955, *ApJ*, **121**, 161
- Sanders, R. H. and McGaugh, S. S., 2002, *ARA&A*, **40**, 263
- Santos, M. R., Bromm, V. and Kamionkowski, M., 2002, *MNRAS*, **336**, 1082
- Satyapal, S., Watson, D. M., Pipher, J. L., Forrest, W. J., Greenhouse, M. A., Smith, H. A., Fischer, J. and Woodward, C. E., 1997, *ApJ*, **483**, 148
- Savage, C. and Ziurys, L. M., 2004, *ApJ*, **616**, 966
- Scalo, J. M., 1986, *Fundamentals of Cosmic Physics*, **11**, 1
- Schilke, P., Pineau des Forêts, G., Walmsley, C. M. and Martín-Pintado, J., 2001, *A&A*, **372**, 291
- Schutte, W. A., Tielens, A. G. G. M., Whittet, D. C. B., Boogert, A., Ehrenfreund, P., de Graauw, T., Prusti, T., van Dishoeck, E. F. and Wesselius, P., 1996, *A&A*, **315**, L333
- Scott, A. and Duley, W. W., 1996, *ApJS*, **105**, 401
- Seaquist, E. R., Frayer, D. T. and Bell, M. B., 1998, *ApJ*, **507**, 745
- Sellwood, J. A. and McGaugh, S. S., 2005, *ApJ*, **634**, 70
- Shapley, A. E., Steidel, C. C., Pettini, M. and Adelberger, K. L., 2003, *ApJ*, **588**, 65
- Shu, F. H., 1977, *ApJ*, **214**, 488
- Shu, F. H., 1983, *ApJ*, **273**, 202
- Smail, I., Ivison, R. J. and Blain, A. W., 1997, *ApJL*, **490**, L5+

- Smith, C. H., Wright, C. M., Aitken, D. K., Roche, P. F. and Hough, J. H., 2000, *MNRAS*, **312**, 327
- Smith, L. J. and Gallagher, J. S., 2001, *MNRAS*, **326**, 1027
- Smoot, G. F., Bennett, C. L., Kogut, A., Wright, E. L., Aymon, J., Boggess, N. W., Cheng, E. S., de Amici, G., Gulkis, S., Hauser, M. G., Hinshaw, G., Jackson, P. D., Janssen, M., Kaita, E., Kelsall, T., Keegstra, P., Lineweaver, C., Loewenstein, K., Lubin, P., Mather, J., Meyer, S. S., Moseley, S. H., Murdock, T., Rokke, L., Silverberg, R. F., Tenorio, L., Weiss, R. and Wilkinson, D. T., 1992, *ApJL*, **396**, L1
- Snyder, L. E., Buhl, D., Zuckerman, B. and Palmer, P., 1969, *Physical Review Letters*, **22**, 679
- Sofia, U. J. and Meyer, D. M., 2001, *ApJL*, **554**, L221
- Solomon, P., Vanden Bout, P., Carilli, C. and Guelin, M., 2003, *Nature*, **426**, 636
- Spergel, D. N., Bean, R., Dore', O., Nolta, M. R., Bennett, C. L., Hinshaw, G., Jarosik, N., Komatsu, E., Page, L., Peiris, H. V., Verde, L., Barnes, C., Halpern, M., Hill, R. S., Kogut, A., Limon, M., Meyer, S. S., Odegard, N., Tucker, G. S., Weiland, J. L., Wollack, E. and Wright, E. L., 2006, *ArXiv Astrophysics e-prints*
- Spitzer, L., 1978, *Physical processes in the interstellar medium* (New York Wiley-Interscience, 1978. 333 p.)
- Springel, V., Frenk, C. S. and White, S. D. M., 2006, *Nature*, **440**, 1137
- Springel, V., White, S. D. M., Jenkins, A., Frenk, C. S., Yoshida, N., Gao, L., Navarro, J., Thacker, R., Croton, D., Helly, J., Peacock, J. A., Cole, S., Thomas, P., Couchman, H., Evrard, A., Colberg, J. and Pearce, F., 2005, *Nature*, **435**, 629
- Stanford, S. A., Eisenhardt, P. R. and Dickinson, M., 1998, *ApJ*, **492**, 461
- Stecher, T. P. and Donn, B., 1965, *ApJ*, **142**, 1681
- Steidel, C. C., Adelberger, K. L., Giavalisco, M., Dickinson, M. and Pettini, M., 1999, *ApJ*, **519**, 1
- Steidel, C. C., Pettini, M. and Adelberger, K. L., 2001, *ApJ*, **546**, 665

- Sternberg, A., Dalgarno, A. and Lepp, S., 1987, *ApJ*, **320**, 676
- Stoughton, C., Lupton, R. H., Bernardi, M., Blanton, M. R., Burles, S., Castander, F. J., Connolly, A. J., Eisenstein, D. J., Frieman, J. A., Hennessy, G. S., Hindsley, R. B., Ivezić, Ž., Kent, S., Kunszt, P. Z., Lee, B. C., Meiksin, A., Munn, J. A., Newberg, H. J., Nichol, R. C., Nicinski, T., Pier, J. R., Richards, G. T., Richmond, M. W., Schlegel, D. J., Smith, J. A., Strauss, M. A., SubbaRao, M., Szalay, A. S., Thakar, A. R., Tucker, D. L., Vanden Berk, D. E., Yanny, B., Adelman, J. K., Anderson, J. E., Anderson, S. F., Annis, J., Bahcall, N. A., Bakken, J. A., Bartelmann, M., Bastian, S., Bauer, A., Berman, E., Böhringer, H., Boroski, W. N., Bracker, S., Briegel, C., Briggs, J. W., Brinkmann, J., Brunner, R., Carey, L., Carr, M. A., Chen, B., Christian, D., Colestock, P. L., Crocker, J. H., Csabai, I., Czarapata, P. C., Dalcanton, J., Davidsen, A. F., Davis, J. E., Dehnen, W., Dodelson, S., Doi, M., Dombeck, T., Donahue, M., Ellman, N., Elms, B. R., Evans, M. L., Eyer, L., Fan, X., Federwitz, G. R., Friedman, S., Fukugita, M., Gal, R., Gillespie, B., Glazebrook, K., Gray, J., Grebel, E. K., Greenawalt, B., Greene, G., Gunn, J. E., de Haas, E., Haiman, Z., Haldeman, M., Hall, P. B., Hamabe, M., Hansen, B., Harris, F. H., Harris, H., Harvanek, M., Hawley, S. L., Hayes, J. J. E., Heckman, T. M., Helmi, A., Henden, A., Hogan, C. J., Hogg, D. W., Holmgren, D. J., Holtzman, J., Huang, C.-H., Hull, C., Ichikawa, S.-I., Ichikawa, T., Johnston, D. E., Kauffmann, G., Kim, R. S. J., Kimball, T., Kinney, E., Klaene, M., Kleinman, S. J., Klypin, A., Knapp, G. R., Korienek, J., Krolik, J., Kron, R. G., Krzesiński, J., Lamb, D. Q., Leger, R. F., Limmongkol, S., Lindenmeyer, C., Long, D. C., Loomis, C., Loveday, J., MacKinnon, B., Mannery, E. J., Mantsch, P. M., Margon, B., McGehee, P., McKay, T. A., McLean, B., Menou, K., Merelli, A., Mo, H. J., Monet, D. G., Nakamura, O., Narayanan, V. K., Nash, T., Neilsen, E. H., Newman, P. R., Nitta, A., Odenkirchen, M., Okada, N., Okamura, S., Ostriker, J. P., Owen, R., Pauls, A. G., Peoples, J., Peterson, R. S., Petravick, D., Pope, A., Pordes, R., Postman, M., Prosapio, A., Quinn, T. R., Rechenmacher, R., Rivetta, C. H., Rix, H.-W., Rockosi, C. M., Rosner, R., Ruthmansdorfer, K., Sandford, D., Schneider, D. P., Scranton, R., Sekiguchi, M., Sergey, G., Sheth, R., Shimasaku, K., Smee, S., Snedden, S. A., Stebbins, A., Stubbs, C., Szapudi, I., Szkody, P., Szokoly, G. P., Tabachnik, S., Tsvetanov, Z., Uomoto, A., Vogeley, M. S., Voges, W., Waddell, P., Walterbos, R., Wang, S.-i., Watanabe, M., Weinberg, D. H., White, R. L., White, S. D. M., Wilhite,

- B., Wolfe, D., Yasuda, N., York, D. G., Zehavi, I. and Zheng, W., 2002, *AJ*, **123**, 485
- Stutzki, J., Genzel, R., Harris, A. I., Herman, J. and Jaffe, D. T., 1988, *ApJL*, **330**, L125
- Suchkov, A., Allen, R. J. and Heckman, T. M., 1993, *ApJ*, **413**, 542
- Sugerman, B. E. K., Ercolano, B., Barlow, M. J., Tielens, A. G. G. M., Clayton, G. C., Zijlstra, A. A., Meixner, M., Speck, A., Gledhill, T. M., Panagia, N., Cohen, M., Gordon, K. D., Meyer, M., Fabbri, J., Bowey, J. E., Welch, D. L., Regan, M. W. and Kennicutt, R. C., 2006, *Science*, **313**, 196
- Sutherland, R. S. and Dopita, M. A., 1993, *ApJS*, **88**, 253
- Swings, P. and Rosenfeld, L., 1937, *ApJ*, **86**, 483
- Tacconi-Garman, L. E., 2006, *New Astronomy Review*, **49**, 569
- Tafalla, M., Myers, P. C., Caselli, P., Walmsley, C. M. and Comito, C., 2002, *ApJ*, **569**, 815
- Testi, L., Palla, F. and Natta, A., 1999, *A&A*, **342**, 515
- Thomas, D., Maraston, C., Bender, R. and de Oliveira, C. M., 2005, *ApJ*, **621**, 673
- Trimble, V., 1987, *ARA&A*, **25**, 425
- Trujillo, I., Burkert, A. and Bell, E. F., 2004, *ApJL*, **600**, L39
- Trujillo, I., Forster Schreiber, N. M., Rudnick, G., Barden, M., Franx, M., Rix, H.-W., Caldwell, J. A. R., McIntosh, D. H., Toft, S., Haussler, B., Zirm, A., van Dokkum, P. G., Labbe, I., Moorwood, A., Rottgering, H., van der Wel, A., van der Werf, P. and van Starkenburg, L., 2005, *ArXiv Astrophysics e-prints*
- Trumpler, R. J., 1930, *PASP*, **42**, 214
- Tucker, K. D., Dickman, R. L., Encenaz, P. J. and Kutner, M. L., 1976, *ApJ*, **210**, 679
- Tully, R. B. and Fisher, J. R., 1977, *A&A*, **54**, 661
- Umeda, H. and Nomoto, K., 2002, *ApJ*, **565**, 385
- Usero, A., García-Burillo, S., Fuente, A., Martín-Pintado, J. and Rodríguez-Fernández, N. J., 2004, *A&A*, **419**, 897

- Valle, J. W. F., 2005, in K. Choi, J. E. Kim and D. Son (eds.), *AIP Conf. Proc. 805: Particles, Strings, and Cosmology*, pp. 128–134
- van der Tak, F. F. S., Schilke, P., Müller, H. S. P., Lis, D. C., Phillips, T. G., Gerin, M. and Roueff, E., 2002, *A&A*, **388**, L53
- van der Tak, F. F. S. and van Dishoeck, E. F., 2000, *A&A*, **358**, L79
- van der Tak, F. F. S., van Dishoeck, E. F., Evans, N. J. and Blake, G. A., 2000, *ApJ*, **537**, 283
- van der Werf, P. P., Goss, W. M. and van den Bout, P. A., 1988, *A&A*, **201**, 311
- van Dishoeck, E. F., 1988, in T. J. Millar and D. A. Williams (eds.), *ASSL Vol. 146: Rate Coefficients in Astrochemistry*, pp. 49–+
- van Dishoeck, E. F. and Black, J. H., 1986, *ApJS*, **62**, 109
- van Dishoeck, E. F. and Blake, G. A., 1998, *ARA&A*, **36**, 317
- Van Loo, S., Falle, S. A. E. G. and Hartquist, T. W., 2006, *MNRAS*, **370**, 975
- van Zee, L., Salzer, J. J. and Haynes, M. P., 1998, *ApJL*, **497**, L1+
- Vázquez-Semadeni, E., Ballesteros-Paredes, J. and Klessen, R. S., 2003, *ApJL*, **585**, L131
- Vazquez-Semadeni, E., Passot, T. and Pouquet, A., 1996, *ApJ*, **473**, 881
- Vidali, G., Roser, J., Manicò, G. and Pirronello, V., 2005, in D. C. Lis, G. A. Blake and E. Herbst (eds.), *IAU Symposium*, pp. 139–+
- Viti, S., Collings, M. P., Dever, J. W., McCoustra, M. R. S. and Williams, D. A., 2004a, *MNRAS*, **354**, 1141
- Viti, S., Collings, M. P., Dever, J. W., McCoustra, M. R. S. and Williams, D. A., 2004b, *MNRAS*, **354**, 1141
- Viti, S. and Williams, D. A., 1999, *MNRAS*, **305**, 755
- Wagenblast, R. and Williams, D. A., 1996, *Ap&SS*, **236**, 257
- Wagg, J., Wilner, D. J., Neri, R., Downes, D. and Wiklind, T., 2005, *ApJL*, **634**, L13

- Walmsley, C. M., Flower, D. R. and Pineau des Forets, G., 2004, *A&A*, **418**, 1035
- Walter, F., Bertoldi, F., Carilli, C., Cox, P., Lo, K. Y., Neri, R., Fan, X., Omont, A., Strauss, M. A. and Menten, K. M., 2003, *Nature*, **424**, 406
- Wang, L. and Steinhardt, P. J., 1998, *ApJ*, **508**, 483
- Wang, Y., Evans, II, N. J., Zhou, S. and Clemens, D. P., 1995, *ApJ*, **454**, 217
- Ward-Thompson, D., Andre, P., R.F., C., Johnstone, D., Onishi, T. and Wilson, C., 2006, in B. e. a. Reipurth (ed.), *Protostars and Planets V*
- Ward-Thompson, D. and Buckley, H. D., 2001, *MNRAS*, **327**, 955
- Ward-Thompson, D., Scott, P. F., Hills, R. E. and Andre, P., 1994, *MNRAS*, **268**, 276
- Weskett, T. J., Eales, S. A., Gear, W. K., Puchnarewicz, E. M., Lilly, S., Flores, H., Webb, T., Clements, D., Stevens, J. A. and Thuan, T. X., 2003, *MNRAS*, **341**, 1217
- Wasserburg, G. J. and Qian, Y.-Z., 2000, *ApJL*, **529**, L21
- Watson, W. D., 1978, *ARAA*, **16**, 585
- Weaver, T. A. and Woosley, S. E., 1993, *PhR*, **227**, 65
- Weaver, T. A., Zimmerman, G. B. and Woosley, S. E., 1976, *BAAS*, **8**, 558
- Wechsler, R. H., Bullock, J. S., Primack, J. R., Kravtsov, A. V. and Dekel, A., 2002, *ApJ*, **568**, 52
- Weinreb, S., Barrett, A. H., Meeks, M. L. and Henry, J. C., 1963, *Nature*, **200**, 829
- Weiβ, A., Downes, D., Henkel, C. and Walter, F., 2005, *A&A*, **429**, L25
- Weiβ, A., Neininger, N., Henkel, C., Stutzki, J. and Klein, U., 2001, *ApJL*, **554**, L143
- Whalen, D., Abel, T. and Norman, M. L., 2004, *ApJ*, **610**, 14
- White, S. D. M. and Rees, M. J., 1978, *MNRAS*, **183**, 341
- Whittet, D. C. B., Gerakines, P. A., Hough, J. H. and Shenoy, S. S., 2001, *ApJ*, **547**, 872
- Whittet, D. C. B., Martin, P. G., Fitzpatrick, E. L. and Massa, D., 1993, *ApJ*, **408**, 573

- Whittet, D. C. B., Schutte, W. A., Tielens, A. G. G. M., Boogert, A. C. A., de Graauw, T., Ehrenfreund, P., Gerakines, P. A., Helmich, F. P., Prusti, T. and van Dishoeck, E. F., 1996, *A&A*, **315**, L357
- Wild, W., Harris, A. I., Eckart, A., Genzel, R., Graf, U. U., Jackson, J. M., Russell, A. P. G. and Stutzki, J., 1992, *A&A*, **265**, 447
- Willacy, K., Rawlings, J. M. C. and Williams, D. A., 1994, *MNRAS*, **269**, 921
- Williams, J. P., Bergin, E. A., Caselli, P., Myers, P. C. and Plume, R., 1998, *ApJ*, **503**, 689
- Wolfire, M. G., Hollenbach, D., McKee, C. F., Tielens, A. G. G. M. and Bakes, E. L. O., 1995, *ApJ*, **443**, 152
- Wootten, A., Loren, R. B. and Bally, J., 1984, *ApJ*, **277**, 189
- Wu, J., Evans, II, N. J., Gao, Y., Solomon, P. M., Shirley, Y. L. and Vanden Bout, P. A., 2005, *ApJL*, **635**, L173
- York, D. G., Adelman, J., Anderson, J. E., Anderson, S. F., Annis, J., Bahcall, N. A., Bakken, J. A., Barkhouser, R., Bastian, S., Berman, E., Boroski, W. N., Bracker, S., Briegel, C., Briggs, J. W., Brinkmann, J., Brunner, R., Burles, S., Carey, L., Carr, M. A., Castander, F. J., Chen, B., Colestock, P. L., Connolly, A. J., Crocker, J. H., Csabai, I., Czarapata, P. C., Davis, J. E., Doi, M., Dombeck, T., Eisenstein, D., Ellman, N., Elms, B. R., Evans, M. L., Fan, X., Federwitz, G. R., Fischetti, L., Friedman, S., Frieman, J. A., Fukugita, M., Gillespie, B., Gunn, J. E., Gurbani, V. K., de Haas, E., Haldeman, M., Harris, F. H., Hayes, J., Heckman, T. M., Hennessy, G. S., Hindsley, R. B., Holm, S., Holmgren, D. J., Huang, C.-h., Hull, C., Husby, D., Ichikawa, S.-I., Ichikawa, T., Ivezić, Ž., Kent, S., Kim, R. S. J., Kinney, E., Klaene, M., Kleinman, A. N., Kleinman, S., Knapp, G. R., Korienek, J., Kron, R. G., Kunszt, P. Z., Lamb, D. Q., Lee, B., Leger, R. F., Limmongkol, S., Lindenmeyer, C., Long, D. C., Loomis, C., Loveday, J., Lucinio, R., Lupton, R. H., MacKinnon, B., Mannery, E. J., Mantsch, P. M., Margon, B., McGehee, P., McKay, T. A., Meiksin, A., Merelli, A., Monet, D. G., Munn, J. A., Narayanan, V. K., Nash, T., Neilsen, E., Neswold, R., Newberg, H. J., Nichol, R. C., Nicinski, T., Nonino, M., Okada, N., Okamura, S., Ostriker, J. P., Owen, R., Pauls, A. G., Peoples, J., Peterson, R. L., Petravick, D., Pier, J. R., Pope, A.,

- Pordes, R., Prosapio, A., Rechenmacher, R., Quinn, T. R., Richards, G. T., Richmond, M. W., Rivetta, C. H., Rockosi, C. M., Ruthmansdorfer, K., Sandford, D., Schlegel, D. J., Schneider, D. P., Sekiguchi, M., Sergey, G., Shimasaku, K., Siegmund, W. A., Smee, S., Smith, J. A., Snedden, S., Stone, R., Stoughton, C., Strauss, M. A., Stubbs, C., SubbaRao, M., Szalay, A. S., Szapudi, I., Szokoly, G. P., Thakar, A. R., Tremonti, C., Tucker, D. L., Uomoto, A., Vanden Berk, D., Vogeley, M. S., Waddell, P., Wang, S.-i., Watanabe, M., Weinberg, D. H., Yanny, B. and Yasuda, N., 2000, *AJ*, **120**, 1579
- Yun, M. S., Ho, P. T. P. and Lo, K. Y., 1993, *ApJL*, **411**, L17
- Zinchenko, I., Mattila, K. and Toriseva, M., 1995, *A&As*, **111**, 95
- Zinchenko, I., Pirogov, L., Caselli, P., Johansson, L. E. B., Malafeev, S. and Turner, B., 2005, in D. C. Lis, G. A. Blake and E. Herbst (eds.), *IAU Symposium*, pp. 115–+
- Zinchenko, I., Pirogov, L. and Toriseva, M., 1998, *A&As*, **133**, 337
- Zinnecker, H., 1982, *New York Academy Sciences Annals*, **395**, 226
- Zuckerman, B. and Palmer, P., 1974, *ARAA*, **12**, 279
- Zwicky, F., 1933, *Helvetica Physica Acta*, **6**, 110